ORGANOTIN(IV) COMPLEXES OF DRUGS: DNA INTERACTION AND *IN VITRO* CYTOTOXIC STUDIES

PH. D. THESIS

by

RANJANA KUMARI

DEPARTMENT OF CHEMISTRY
INDIAN INSTITUTE OF TECHNOLOGY ROORKEE
ROORKEE - 247667 (INDIA)
MAY, 2018

ORGANOTIN(IV) COMPLEXES OF DRUGS: DNA INTERACTION AND *IN VITRO* CYTOTOXIC STUDIES

A THESIS

Submitted in partial fulfilment of the requirements for the award of the degree

of

DOCTOR OF PHILOSOPHY

in

CHEMISTRY

by

RANJANA KUMARI

DEPARTMENT OF CHEMISTRY
INDIAN INSTITUTE OF TECHNOLOGY RORKEE
ROORKEE – 247667 (INDIA)
MAY, 2018

INDIAN INSTITUTE OF TECHNOLOGY ROORKEE
ROORKEE

CANDIDATE'S DECLARATION

I hereby certify that the work which is being presented in the thesis entitled "**ORGANOTIN(IV) COMPLEXES OF DRUGS: DNA INTERACTION AND *IN VITRO* CYTOTOXIC STUDIES"** in partial fulfilment of the requirements for the award of Degree of Doctor of Philosophy and submitted in the Department of Chemistry of the Indian Institute of Technology Roorkee, Roorkee is an authentic record of my own work carried out during a period from January, 2013 to May, 2018 under the supervision of Dr. (Mrs.) Mala Nath, Professor, Department of Chemistry, Indian Institute of Technology Roorkee, Roorkee.

The matter presented in the thesis has not been submitted by me for the award of any other degree of this or any other Institution.

(RANJANA KUMARI)

This is to certify that above statement made by the candidate is correct to the best of my knowledge.

(Mala Nath)
Supervisor

Dated:

ABSTRACT

Organometallic compounds served as potential antitumour, antimicrobial and antimalarial agents, which revealed the metal-specific modes of action. A variety of medicinal and biological applications of organometallics due to their structural diversity and chemical tunability have emerged as a new field of research called bioorganometallic chemistry. Few interesting features of organometallic compounds which make them fit to use in biological system compared to organic compounds include; (1) a variety of coordination numbers of metal in metal complexes, provide them high structural diversity, (2) the prediction of ligand exchange reactions in the metal complexes makes them important candidates for combinatorial synthetic strategies and high biological activities, (3) the characteristic properties of metals *viz.* catalytic properties, Lewis acidities, redox activities, ability to access radical, radioactivity, magnetic and spectroscopic properties, allow the tailored functions in metal complexes. All the features described above are very important to design the new pharmacophores, which could not be acquired by mere organic synthesis.

Organotin compounds found widespread applications in the field of industrial, agricultural, synthetic and biological fields. The biocidal uses of organotin compounds as acaricide, fungicide and in agriculture, as preservatives of wood and for the protection of textiles, cordage fibers, paper, leather and electrical equipment etc. revealed their high toxicity towards living cells. A significant research has been carried out to investigate the biological or pharmaceutical role of organotin compounds, which prove them potential apoptotic inducer, antiviral, anticancer, antibacterial, antifungal, antineoplastic and anti-tuberculosis agent. During last few decades organotin compounds occupy an important place in cancer chemotherapy reports, which place them among the most reliable compounds to replace the platinum based antitumour drugs in order to avoid the serious side effects and to overcome the drug resistance related to platinum based drugs.

In order to understand the distribution of the species of a particular compound in a system under study, it is must to account the data related to various equilibria established and stability constant calculated for the particular species involved. Inside the living systems organotins can interact with proteins, nucleic acids, carbohydrates and lipids biomolecules through heteroatoms like N, P, O, and S, thus the discussion of their equilibria and formation of the different species of

biologically active ligands with organotins is of considerable importance. However, the study in this regard with commercially available drugs are quite rare, thus we carried out the potentiometric study of MESNA (sodium 2-mercaptoethanesulphonate) with organotin(IV) chloride.

Many researchers adopted the idea of syntheses of the organotin complexes with commercially available drugs in order to achieve the desired features. In this way the metal can stabilize the drug which in turn may help the metal complex in transportation in order to reach their potential target and avoid needless side reactions. In this view a number of organotin(IV) complexes with commercially available drugs have been synthesized and many of them exhibited improved biological activities. Further, the non-steroidal anti-inflammatory drugs (NSAIDs) have been found quite effective against various types of cancers *viz.* breast, esophageal, stomach, prostate, bladder, ovarian, lung and colorectal cancers and successfully used in combination therapies with antitumour drugs. Thus, we chose to synthesize the organotin-drug complexes, study their various possible mode of binding with DNA, and further investigate their biological activities. In order to achieve the desired objective the thesis has been divided into seven chapters which are described in detail herein.

First Chapter highlights the importance of organotin(IV) complexes in various fields including commercial, agricultural, synthetic and biological uses. The critical discussion on the mode of action of organotin(IV) complexes inside the biological system and their DNA binding properties has been presented. A huge literature survey based on organotin complexes having antimicrobial and antitumour activities has been exemplified. Further, the importance of potentiometric study of these complexes has been highlighted with various examples.

Second Chapter describes the purity and make of different chemicals used in the current study. This chapter also includes the specification of various instruments used during the experimental work. The details of the methods and procedures which were used in common in all Chapters have also been discussed in this section.

Third Chapter includes the potentiometric study of interaction of $[Me_2Sn(IV)]^{2+}$ and $[Me_3Sn(IV)]^{+}$ with a prodrug, sodium 2-mercaptoethane sulfonate (MESNA) abbreviated as (HL) in aqueous solution (I = 0.1 M KNO_3, 298 K). The concentration distribution of various species formed in the solution was studied with a change in pH (~3–11). A strong coordination of MESNA with metal through S atom of thiol group has been elucidated. In $Me_2Sn(IV)$ – HL system, the

species $[Me_2Sn(L)]^+$ (53.1–75.6%) is predominating at acidic pH (3.73 ± 0.02), and the species $[Me_2Sn(L)_2OH]^-$ (29.4–38.5%) is predominating at basic pH (10.32 ± 0.08). Whereas for $[Me_3Sn(IV)]^+$ system, $[Me_3SnL]$ (37.0–57.4%) is the major species at pH 7.65 ± 0.03 and $[Me_3Sn(OH)]$ (49.9–67.2%) and $[Me_3Sn(L)(OH)]^-$ (30.2–46.5%) are the major species at pH 11.05 ± 0.01. However, at physiological pH (7.01 ± 0.32), in both (1:1) and (1:2) $Me_2Sn(IV)$ – HL systems, the species $[Me_2Sn(L)(OH)]$ (67.2–89.9%) is predominating whereas for $Me_3Sn(IV)$ – HL (1:1) and (1:2) systems, $[Me_3Sn(OH)]$ (53.5%) and $[Me_3SnL]$ (56.8%) are the respective predominated species. In order to characterize the possible geometry of the proposed complex species, multinuclear (^1H, ^{13}C and ^{119}Sn) NMR studies were carried out at different pHs. No polymeric species were detected in the experimental pH range.

Fourth Chapter discussed the synthesis of the diorganotin(IV) complexes (**1-4)** of MESNA (sodium 2-mercaptoethanesulfonate $HSCH_2CH_2SO_3Na$) and a mixed ligand complex of dibutyltin(IV), 1,10-phenanthroline and MESNA (**5**). All the complexes were characterized thoroughly with the help of analytical and various spectroscopic techniques *viz.* FTIR, NMR (^1H, ^{13}C, and ^{119}Sn NMR) spectroscopy and ESI MS spectrometery. Various spectrophotometric studies were carried out to decipher the binding mode of MESNA and its diorganotin complexes **1-5** with calf thymus DNA (CT DNA) and thus, to calculate the binding constant (K_b). Absorption spectrophotometric study confirmed the interaction is through partial intercalation of all the complexes including MESNA, inside the DNA helix and calculated binding constant (K_b) is in the order of 10^3 M^{-1}. A series of emission spectrophotometric experiments support the results obtained through the absorption spectrophotometric studies. Circular dichroic (CD) spectroscopic analysis and viscosity measurement of CT DNA further complemented the fact that the partial intercalation plays a major role in the interaction of the studied complexes with CT DNA. All the studies corroborated that complex **2** bound to CT DNA with maximum affinity followed by complex **5** among all the complexes. Involvement of hydroxyl radicals as an active species in the cleavage activity of pBR322 plasmid DNA is proved by carrying out agarose gel electrophoresis. The cytotoxicity of the complexes was evaluated with MTT assay against DU145 (prostate cancer), HCT-15 (colon adenocarcinoma) and HeLa (cervical cancer) cell lines. Complexes **4** and **5** demonstrated remarkable cytotoxicity *in vitro*, even more than 5-fluorouracil, against prostate cancer cell lines, which possesses intrinsic and acquired resistance to *cis*-platin. Complex **5** displayed highest cytotoxicity against all the cell lines *viz*. DU145, HCT-15 and HeLa with IC_{50}

values 7.15±0.7 μM, 0.83±0.1 μM and 1.85±0.4 μM, respectively. The cause of cell death was further investigated through acridine orange/ethidium bromide staining of cell lines and DNA fragmentation assay which revealed that the other processes along with the apoptosis plays role in cell death.

Fifth Chapter deals with the syntheses of tri- and diorganotin(IV) derivatives of non-steroidal anti-inflammatory drug (NSAID), sulindac (**Sul**), **1-7** *viz.* $[Me_3Sn(Sul)]$, $[Ph_3Sn(Sul)]$, $[Bu_3Sn(Sul)]$, $[Ph_2Sn(Sul)_2]$, $[Me_2SnCl(Sul)]_2$, $[Bu_2Sn(Sul)_2]$ and $[Oct_2Sn(Sul)_2]$. The complexes have been characterized by analytical and spectroscopic (FTIR, ^1H, ^{13}C, ^{119}Sn NMR and ESI MS) techniques. Crystal structure of **3** indicates trigonal bipyramidal geometry around tin atom in solid state, where axial positions were occupied by O atoms of carboxylate and sulphoxide groups. Carboxylate oxygen is coordinating to Sn atom in a monodentate fashion. Dissociation of the coordinate bond between Sn and O (sulphoxide group) resulted in tetrahedral structure of the complex as witnessed from solution study in NMR. Similar structures were proposed for complexes **1** and **2.** Optimized geometry and electronic structures of complexes obtained from DFT calculations reveals that Sn atom in complexes **4** and **6** are hexa-coordinated with highly distorted octahedral geometry, whereas **5** is penta-coordinated with distorted trigonal bipyramidal geometry and **7** is tetra-coordinated with monodentate carboxylates. Probable mode of DNA binding with ligand (**Sul**) and complexes **1–7** has been revealed via various biophysical techniques (UV–visible spectroscopy, fluorometry and circular dichroism). Intrinsic binding constants (K_b) obtained from UV–visible spectroscopy for **Sul** and complexes **1 – 7** are $3.69 \times 10^4\ M^{-1}$, and $7.3 \times 10^3\ M^{-1}$, $1.14 \times 10^4\ M^{-1}$, $1.47 \times 10^4\ M^{-1}$, $1.55 \times 10^4\ M^{-1}$, $1.49 \times 10^4\ M^{-1}$, $2.02 \times 10^4\ M^{-1}$, $1.17 \times 10^4\ M^{-1}$, respectively. The quenching constants (K_{sv}) using flourometric titrations, calculated from competitive binding of ethidium bromide (EB) *vs* **Sul**/complexes (**1–7**) with CT DNA, also corresponds to the above results. Circular-dichroism (CD) spectroscopic patterns of CT DNA with **Sul** and complexes **1–7** have been investigated. All the above results revealed that the complexes bind with DNA through partial intercalative mode. pBR322 Plasmid fragmentation has also been studied by gel electrophoresis, which shows the fragmentation of circular DNA by increase in nicked form and also with the appearance of linear form with increasing concentration of drug or complexes. Further, *in vitro* cytotoxicity of **Sul** and synthesized complexes against HCT-15 (colon adenocarcinoma), MCF-7 (mammary cancer), HeLa (cervical cancer), and LNCaP (androgen-sensitive prostate adenocarcinoma) cancer cell lines have been determined, which indicated a low

to moderate cytotoxicity of these complexes toward MCF-7, HeLa and LNCaP cancer cell lines. However, all the complexes demonstrated good *in vitro* antitumour activity towards the HCT-15.

Sixth Chapter encompasses the synthesis and characterization of organotin(IV) derivatives of non steroidal anti-inflammatory drug Ibuprofen (IBF) *viz.* [(Me_3Sn)(IBF)] (**1**), [(Bu_3Sn)(IBF)] (**2**), [Ph_3Sn(IBF)] (**3**), [(Me_2Sn(IBF))$_2$O]$_2$ (**4**) and [$Bu_2Sn(IBF)_2$] (**5**). The crystal structure of complexes **3**, [Ph_3Sn(IBF)], gives the clearity about the structure of triorganotin complexes. Triorganotin complexes are characterized with highly distorted tetrahedral (td) geometry with anisobidentate mode of co-ordination of the carboxylate group with tin atom. Moreover, the DFT calculation and other studies varified a dimer distannoxane type of structure for complex **4**, [(Me_2Sn(IBF))$_2$O]$_2$. Complex **5** was found to exhibit a highly distorted octahedral geometry around tin atom. To investigate the DNA binding profile of the synthesized complexes, UV-visible and fluorescence titrations were performed, which revealed an intercalative type of binding with DNA for IBF and complex **5** and external binding in case of the complexes **1** and **2.** Plasmid DNA fragmentation studies indicate that the complexes and IBF cleaved the pBR322 plasmid potentially. Further, the IBF and complexes **1**-**5** were screened *in vitro* for cytotoxicity against human cancer cell lines *viz.* DU145 (prostate cancer), HCT-15 (colon adenocarcinoma) and Caco-2 (colorectal adenocarcinoma) through MTT reduction assay and the cause of cell death was investigated through acridine orange/ethidium bromide staining of cells and DNA fragmentation assay. Complex **4** displayed the maximum cytotoxicity against prostate and colon cancer cell lines, with IC_{50} values 3.97±0.81 μM and 2.188±0.67 μM, respectively, while complex **3** was found highly regressive against colorectal cancer (IC_{50} = 1.21±0.84 μM) cell lines.

Seventh Chapter encloses the synthesis and characterization of trimethyltin(IV) (**1**) and tributyltin(IV) (**2**) complexes of an anticoagulant drug warfarin (WR). The full geometry optimization and simple harmonic frequency calculations in gaseous phase by DFT indicated that both the complexes have distorted tetrahedral geometry around tin centre. The synthesized complexes have been investigated for their DNA binding profile (mode and extent of binding with CT DNA) through UV-visible and fluorescence spectrophotometric titrations, which revealed a partial intercalation of complexes inside the base pairs of DNA, and the binding constant (K_b) calculated through UV-visible titration study was found to be in the order of 10^4 M^{-1}. The partial intercalation of the complexes inside the DNA has also been confirmed through a decrease in the viscosity of CT DNA with the increasing complex concentration. Both the complexes were found

to be potential plasmid cleaving agent which has been confirmed though gel electrophoresis of pBR322 plasmid with increasing the complexes concentrations. Both the organotin(IV) complexes have been found to exhibit a greater potential towards DNA binding and fragmentation in comparison to that of WR. Complexes and WR were screened *in vitro* for anti-tumor activity against HCT-15 (colon adenocarcinoma), MCF-7 (mammary cancer), HeLa (cervical cancer), and LNCaP (androgen-sensitive prostate adenocarcinoma) cell lines of human origin, which exhibited a good activity of complexes against prostate cancer cell line.

Chapter 8 concludes the various studies described in different Chapters along with their scope in future.

ACKNOWLEDGEMENTS

With sincere reverence, I am grateful to the great and gracious Almighty who blessed me with spiritual support and fortitude at each and every step of this work. This has been a truly life-changing experience for me, which would not have been possible without the benediction of Almighty God and blessing of my parents.

I owe my wholehearted gratitude to my supervisor, **Prof. (Mrs.) Mala Nath** who has always guided me during the research, not only for her tremendous academic support but also for her amicable and positive disposition. Her meticulous guidance, scholarly inputs, consistent encouragement and constructive criticism have helped me to complete this thesis in a well-organised manner. I appreciate all her contributions of time to clarify my doubts despite her busy schedules and moral boosting inspiration to bring the present work to final conclusions. I consider it as a great opportunity to do my doctoral programme under her guidance and to learn from her research expertise.

I am thankful to **Prof. M. R. Mourya**, the present *Head* and **Prof. Anil Kumar**, *Ex-Head* of Department of Chemistry, Indian Institute of Technology, Roorkee, for providing the instrumentation facilities and support to carry out the research work without any obstruction. I extend my sincere thanks to members of my SRC committee, **Prof. U. P. Singh**, **Dr. Kaushik Ghosh** and **Dr. A. K. Sharma** to evaluate my work and provide relevant suggestions during SRC meetings.

I also wish to express my heartfelt thanks to **Dr. Partha Roy** and **Somesh Banerjee** for completing the necessary cytotoxic activities and related biological activities required for the completion of this thesis. I extend my thanks to **Prof. (Mrs.) Ritu Bharthwal**, former *Head* of NMR facility in Institute Instrumentation Centre, IIT Roorkee for providing NMR and other instrumentation facility.

I would like to thank **Mr. D. C. Meena, Sh. Madan Pal, Mr. Pankaj, Mr. Charan Singh** and **Mr. Anuj Arjun** for providing technical assistance during the work. I wish to extend my sincere thanks to all office staff for their co-operation in every small work.

I thank my senior colleagues **Dr. Monika, Dr. Nagmani, Dr. Mridula** and **Mr. Sundeep** for their valuable guidance and support during throughout the research period. My junior colleagues, **Ramesh, Ankur, Pooja, Vishakha** and **Shubham** have extended their support in a very special

way. All their encouragement, personal, scholarly as well miscellaneous interactions are appreciable which made this path very delightful and worth remembering. I also acknowledge my pals **Nivedita, Manisha, Neha, Rosy** and **Neetu** who were always with me in all joys and difficult times with their moral support, love and affection. We enjoyed this times together in the hostel which will be cherished in my memories. I also admire the role of my friends **Rashmi** and **Harshit** for making this journey adorable. My special thanks are extended to the **Nivedita** and **Manisha** for beautifying the whole journey together.

Finally, but by no means least, thanks go to my mother, **Smt. Urmila Devi** and father, **Sh. Nek Ram** for almost unbelievable support and love, care and everlasting belief in me. They are the most important people in my world and I dedicate this thesis to them, which wouldn't be sufficient to mention the endless efforts they have made to build this platform where I am standing today. I love to express my abounding sentiments to my loving elder sister **Dr. Bandana,** brother **Naresh and** bhabhi **Yagasheela** for their unconditional love, care and holding me all through in such a high spirit. My sister always boosted my morale with her ever buoyant expression and nurtures my enthusiasm for research. I owe her for her love, care and selfless effort, which always pushed me forward. My little, sweet nieces **Anwesha, Kavya** and **Riyanshi** illuminated my world with their smiles and always acted as stress-buster during the research work.

I am in the dearth of words to express my appreciation to my loving husband **Sushil Kumar Thakur,** whose unfathomable patience, perseverance, and belief in me supported me all through my pursuits. His never-ending love, understanding and care in a very special manner in all odds endowed me the courage to complete this work successfully. I also adore the support and love of **Sh. S. K. Thakur** (father-in-law), **Smt. Rama Thakur** (mother-in-law), **Manish** (brother-in-law), and **Kamlesh** (sister-in-law), kept me crossing through all hurdles in this journey of the pursuit of Ph. D. thesis.

Thanks are also due, to the **Ministry of Human Resource Development** (MHRD), New Delhi, India for providing Junior Research Fellowship (JRF) and Senior Research Fellowship (SRF) during the period of research.

Roorkee RANJANA KUMARI

May, 2018

LIST OF ABBREVIATIONS

MESNA	Sodium 2-mercaptoethanesulfonate
Sul	2-[5-fluoro-1-[(4-methanesulfinylphenyl)methylidene]-2-methyl-1H-inden-3-yl]acetic acid (Sulindac)
IBF	2-(4-(2-methylpropyl)phenyl)propanoic acid (Ibuprofen)
WR	4-hydroxy-3-(3-oxo-1-phenylbutyl)coumarin (Warfarin)
PVC	Ploy(vinyl chloride)
NMR	Nuclear Magnetic Resonance
FTIR	Fourier Transform Infra Red
ESI MS	Electrospray ionization mass spectroscopy
DFT	Density Functional Theory
DNA	Deoxyribonucleic acid
RNA	Ribonucleic acid
MTT	3-(4,5-dimethylthiazol-2-yl)-2,5-diphenyltetrazolium bromide
ROS	Reactive oxygen species
EB	Ethidium bromide
AO	Acridine orange
Oh	Octahedral
TBP	Trigonal bipyramidal
td	Tetrahedral
SP	Square planner
TOF	Time-of-flight
EDTA	Ethylenediaminetetraacetic acid
ATP	Adenosine-5’-triphospate
5-FU	5-fluorouracil
TMS	Tetramethyl silane
IC_{50}	Concentration of Compound at 50% growth inhibition
ID	Infectious dose
Bu	butyl
Ph	phenyl
Me	methyl
Oct	octyl

DMSO	Dimethyl sulphoxide
DMSO-d_6	Hexadeuteriodimethyl sulphoxide
$CDCl_3$	Deuterated chloform
L	Litre
M	Molarity
PBS	Phosphate buffer saline
MP	Melting point
min	Minute
h	Hour
ppm	Part per million
MHz	Mega hertz
mol	Mole
viz.	videcilet
UV	Ultra-violet
Eq./Eqs.	Equation/Equations
g	Gram
e.g.	Example
i.e.	that is
n.d.	Not determined
cm	Centimeter
Phen	1,10-phenanthroline
νs	Symmetric stretching
νas	asymmetric stretching
v/v	Volume/volume
SEM	Standard error of mean
SD	Standard deviation
TAE	Buffer (tris base + acetic acid + EDTA)
TBE	Buffer (tris base + boric acid + EDTA)
Fig.	Figure
b.p	Boiling point
I	Ionic strength
BSA	Bovine serum albumin
ZOI	Zone of inhibition
TPTH	Triphenyltin hydroxide

CT DNA	Calf thymus DNA
A/T/G/C	Adenine/thymine/guanine/cytosine
D_2O	Deuterium oxide
V	Volt

LIST OF FIGURES

Fig. 4.9. Emission spectra of complexes (100 μM): **2** (A), **3** (B), **4** (C), **5** (D) in the absence and presence of CT DNA ($1.3–13\times10^{-5}$ M) in Tris-HCl/NaCl (5:50 mM) buffer, pH =7.2 at 25 °C. Arrow indicates the increase in intensity with increasing concentration of DNA.

Fig. 4.10. Fluorescence quenching titration spectra of EB–CT DNA ([DNA]/[EB] = 5.3) with successive addition of ($2–35\times10^{-5}$ M) MESNA (A), **1** (B); **2** (C), **3** (D), **4** (E), **5** (F), in Tris-HCl/NaCl (5:50 mM) buffer, pH = 7.2 at 25 °C [Excitation λ_{max} at 515 nm]. Inset is showing linear Stern-Volmer plots and arrow indicates the decrease in intensity with increasing concentration of MESNA/Complexes.

Fig. 4.11. Stern-Volmer plots obtained from fluorescence quenching of complexes (100 μM) **2** (A); **3** (B); **4** (C); **5** (D) by KI (0–20 mM), in the presence and absence of CT DNA (100 μM) in Tris-HCl/NaCl (5:50 mM) buffer, pH = 7.2 at 25 °C.

Fig. 4.12. CD spectra of CT DNA in the absence and presence of MESNA (A), **1** (B); **2** (C), **3** (D), **4** (E), **5** (F), ([MESNA] or [Complex]/[CT DNA], [r = 0.08-0.25]) in Tris-HCl/NaCl (5:50 mM) buffer, pH = 7.2 at 25 °C. Arrows are indicating the decrease/increase in intensity with increasing concentration of MESNA/Complexes.

Fig. 4.13. The decrease in viscosity (η) of CT DNA (100 μM) with successive addition of MESNA and complexes **1**-**5** (0 to 100 μM).

Fig. 4.14. The cleavage pattern of pBR322 plasmid DNA (50 ng) by MESNA (A); complex **1** (B); complex **2** (C); complex **3** (D); complex **4** (E) and complex **5** (F); after incubation for 1h at 37 °C, at different concentration of MESNA/Complexes, Control: DNA; Lane I: [DNA + (25 μM complex/MESNA)]; Lane II: [DNA+(50 μM complex/MESNA)]; Lane III: [DNA+(100 μM complex/MESNA)]; Lane IV: [DNA+(0.2 M NaN_3)+(100 μM complex/MESNA)]; Lane V: [DNA+(100 μM complex/MESNA)+(0.2 M H_2O_2)]; Lane VI: [0.2 M DMSO)+(100 μM complex/MESNA)]; Lane VII: [(0.2 M Ascorbic acid)+(100 μM complex/MESNA)].

Fig. 4.15. AO/EB staining of HCT-15 cell lines (A) control, (B) vehicle (DMSO) treated cells, (C) cells treated with IC_{50} value of complex **4** and (D) cells treated with IC_{50} value of complex **5**. Solid white arrows indicate the early apoptotic, white outlined arrows indicated the late apoptotic and solid red arrows indicated the necrotic cells.

Fig. 4.16. AO/EB staining of DU145 cell lines (A) control, (B) vehicle (DMSO) treated cells, (C) cells treated with IC_{50} value of complex **4** and (D) cells treated with IC_{50} value of complex **5**. Solid white arrows indicate the early apoptotic, white outlined arrows indicated the late apoptotic and solid red arrows indicated the necrotic cells.

Fig. 4.17. AO/EB staining of HeLa cell lines (A) control, (B) vehicle (DMSO) treated cells, (C) cells treated with IC_{50} value of complex **4** and (D) cells treated with IC_{50} value of complex **5**. Solid white arrows indicate the early apoptotic, white outlined arrows indicated the late apoptotic and solid red arrows indicated the necrotic cells.

Fig. 6.12. Emission spectra of IBF (66.7 μM) (A) and complexes (66.7 μM); **1** (B), **2** (C), **5** (D) in the absence and presence of CT DNA (2–20 μM) in Tris-HCl/NaCl (5:50 mM) buffer, pH = 7.2 at 25 °C. Arrows indicate the increase/decrease in emission intensity with increasing concentration of DNA.

Fig. 6.13. Fluorescence quenching titration spectra of EB–CT DNA ([DNA]/[EB] = 4) with successive addition of (2 – 20 μM) IBF(A), **1** (B); **2** (C), **5** (D), in Tris-HCl/NaCl (5:50 mM) buffer, pH = 7.2 at 25 °C [Excitation λ_{max} at 515 nm]. Inset is showing linear Stern-Volmer plots and arrow indicates a decrease in intensity with increasing concentration of quenchers.

Fig. 6.14. Stern-Volmer plots obtained from fluorescence quenching of IBF (66.7 μM) (A) and complexes (66.7 μM); **1** (B); **2** (C); **5** (D) by KI (0–72 mM), in the presence and absence of CT DNA (20 μM) in Tris-HCl/NaCl (5:50 mM) buffer, pH = 7.2 at 25 °C.

Fig. 6.15. Change in viscosity (η) of CT DNA (100 μM) with successive addition of MESNA and complexes **1-5** (0 to 100 μM), in Tris-HCl/NaCl (5:50 mM) buffer, pH = 7.2 at 25 °C.

Fig. 6.16. The cleavage pattern of pBR322 plasmid DNA (100 ng) by IBF (A); complex **1** (B); complex **2** (C); complex **5** (D), after incubation for 5 h at 37 °C, at different concentration of IBF/Complexes, in Tris-HCl/NaCl (5:50 mM), buffer, pH = 7.2 at 25 °C. Lane I: Control (DNA): Lane II: [DNA + (20 μM complex/IBF)]; Lane III: [DNA + (40 μM complex/IBF)]; Lane IV: [DNA + (60 μM complex/IBF)]; Lane V: [DNA + (80 μM complex/IBF)]; Lane VI: [DNA + (0.2 M H_2O_2) + (60 μM complex/IBF)]; Lane VII: [DNA + (60 μM complex/IBF)+(2 mM NaN_3)]; Lane VIII: [DNA+ (60 μM complex/IBF)] + (2 μL DMSO)].

Fig. 6.17. AO/EB staining of HCT-15 cell lines (A) control, (B) vehicle (DMSO) treated cells and (C) cells treated with IC_{50} value of complex **4**.

Fig. 6.18. AO/EB staining of Caco-2 cell lines (A) control, (B) vehicle (DMSO) treated cells, (C) cells treated with IC_{50} value of complex **2**.

Fig. 6.19. AO/EB staining of DU145 cell lines (A) control, (B) vehicle (DMSO) treated cells, (C) cells treated with IC_{50} value IBF and (D) cells treated with IC_{50} value of complex **4**. Solid white arrows indicate the early apoptotic, white outlined arrows indicated the late apoptotic and solid red arrows indicated the necrotic cells.

Fig. 6.20. Fragmentation pattern of DNA extracted from cell lines on treatment with complex 5, through agarose gel electrophoresis: (A) lane I: control (DNA extracted from DU145), lane II: DNA extracted from DU145 treated with complex **4**; lane III: DNA marker (50 base pairs); lane IV: DNA extracted from HCT-15 treated with complex **4** and lane V: control (DNA extracted from HCT-15. (B) lane 1: DNA marker (50 base pairs); lane II vehicle treated control (HeLa DNA); lane III: DNA extracted from HeLa treated with complex **4**.

Fig. 7.1. FTIR spectra of WR, sodium salt of WR (Wr Na) and complexes **1** and **2**.

LIST OF SCHEMES

LIST OF TABLES

LIST OF PUBLICATIONS

In the referred Journals

1. "Speciation and Multinuclear NMR Spectroscopic Studies of Di- and Trimethyltin(IV) Moieties with MESNA in Aqueous Medium"
   Ranjana Kumari, Mala Nath*
   J. Solution Chem. 2017, *46*, 1418–1433.

2. "Tri- and Diorganotin(IV) Derivatives of Non-Steroidal Anti-Inflammatory Drug Sulindac: Characterization, Electronic Structures (DFT), DNA Binding and Plasmid Cleavage Studies"
   Ranjana Kumari, Mala Nath*
   Appl. Organomet. Chem. 2017, e3661.

3. "Synthesis, Characterization and Binding Studies of Novel Diorganotin(IV) Complexes of Sodium 2−Mercaptoethanesulfonate"
   Ranjana Kumari, Mala Nath*
   Appl. Organomet. Chem. 2018, e4365.

TABLE OF CONTENTS

DEDICATED

TO MY

PARENTS, SISTER

&

BELOVED HUSBAND

CHAPTER - 1

Introduction

1.1. GENERAL INTRODUCTION

Metals play a significant role in various biological processes by affecting the structural and functional machinery of enzymes, biochemical reactions, and skeleton of various macromolecules such as vitamin B12, haemoglobin, myoglobin etc. [1-2]. Some metals have been assigned with structural, enzymatic and reactive roles, for example, iron (Fe) and manganese (Mn) act as enzyme, zinc (Zn) and calcium (Ca) provide structural integrity and flexibility to many proteins, iron (Fe) acts as oxygen transporter as a component of haemoglobin, potassium (K) and sodium (Na) function as carriers of charge in neurons and manganese (Mn) and magnesium (Mg) play an important role in the hydrolysis and group-transfer reactions. These diverse roles of metals in biochemical reactions arise vast opportunities for biological modulation. Despite being essential for all forms of life, most of the metals are toxic in excess. Metals and metal compounds have been used in therapeutics since 16th century [1, 3, 4], some therapeutically important metal-containing compounds include, platinum (anticancer), gold (antiarthritic), bismuth (antiulcer), silver (antimicrobial), vanadium (antidiabetic), iron (antimalarial) and antimony (antiprotozoal) [5]. The interactions and bonding between positively charged metal ions with electron rich biological molecules like proteins and DNA ignite an interest in the development of various means to use the metal and metal-containing compounds to modulate the biological systems. Presently, organometallic compounds with classical ligands are much more known for their catalytic, biosensing and biomimetic activities rather than their implication in medicines [6-8]. However, the attention has been steadily grown in applications of organometallic compounds in the medicinal field, over the past few decades. The discovery of antitumor properties of *cis*-platin by Rosenberg in 1965 led the foundation of interest in the metal complexes mainly in the chemistry of transition metals and main group metals. Severe drawbacks like, the development of tumor resistance and side effects of *cis*-platin fueled a new search for other organometallic compounds with better selectivity and fewer side effects. Organometallic compounds served as potential antitumour, antimicrobial and antimalarial agents; few of them have lately revealed the metal-specific modes of action through clinical trials [9]. A variety of medicinal and biological applications of organometallics due to their structural diversity and chemical tunability have emerged as a new field of research named bioorganometallic chemistry, in 1985 [10]. Organometallic therapeuticals, enzymes, proteins and peptides, molecular recognition in aqueous phases,

bioanalysis, pharmaceutical sensors, and toxicology and environment are included in present domains of bioorganometallic chemistry [11-13]. In principle, the organometallics with proper design of organic moiety can be tailored so as to deliver a metal ion to any part of the body. Few interesting features of organometallic compounds which make them fit to use in biological system compared to organic compounds are: (1) A variety of coordination numbers of metal in metal complexes, provide them high structural diversity. For example, an octahedral center with different substituents can form a variety of stereoisomers [14] which provides more flexibility to the complex and also aid to orient the substituents/ligands into the space so as they can better interact with the receptor pockets. Meggers et al. [15, 16] studied the ruthenium complexes as kinase inhibitors which explained the role of high structural diversity. (2) The prediction of ligand exchange reactions in the metal complexes makes them important candidates for combinatorial synthetic strategies and high biological activities [11]. (3) The characteristic properties of metals *viz.* catalytic properties, Lewis acidities, redox activities, ability to access radical, radioactivity, magnetic and spectroscopic properties, allow the tailored functions in metal complexes [17]. All the features described above are very important to design the new pharmacophores, which could not be acquired by mere organic synthesis.

1.1.1. General Overview of Organotin Chemistry

Löwig in 1852, first studied the organotin compounds, he prepared diethyltin by the reaction of ethyl iodide with a sodium-tin alloy. In the following year tetraethyltin was synthesized by Frankland, since then a significant number of alkyl and aryl organotin compounds have been synthesized [18]. Organotin compounds comprise of at least one Sn–C bond, where the carbon atom remains the part of an organic substituent. Organotin compounds are known to exist in two oxidation states, *i.e* +II and +IV. However, the organotin chemistry is essentially restricted to the +IV oxidation state because of the lesser stability of organotin(II) compounds, which tend to polymerize rapidly [19]. The organotin(II) compounds are known to exist either with bulky organic ligands [20, 21] or with the cyclopentadiene as organic substituent [22]. Most of the organotin(II) compounds contain multiple Sn–Sn bonds similar to that of organotin(IV) compounds. The inability of tin to use its d orbitals in chemical bonding is demonstrated by the high basicity (greater than any organic amine) of $N(SnMe_3)_3$ [23]. On the basis of the number of organic moieties present in the organotin compounds, they are classified as monoorganotin ($RSnX_3$), diorganotin (R_2SnX_2), triorganotin (R_3SnX) and tetraorganotins (R_4Sn), where R is

any alkyl/aryl group and X is an anionic species *viz.* halide, oxide, hydroxide and carboxylate etc. The Sn–C bond in organotin(IV) compounds are quite stable towards water, atmospheric O_2, and heat at temperatures up to 200 °C [24]. However, the latter can be cleaved by the action of strong acids, UV radiation, and electrophilic agents. The physical and chemical properties of organotins, were strongly influenced by both the number and length of the alkyl/aryl chains. Tin(IV) compounds generally form tetrahedral (td), trigonal pyramidal (TBP) or octahedral (Oh) geometries depending on the coordination number of tin. The R_3SnX species form trigonal bipyramidal (five-coordinated) structures, while the R_2SnX_2 complexes quite often form octahedral structures [23]. The coordination of organotin(IV) moieties to different ligands with specific donor atoms (S, N, O) can form a highly coordinated species due to the participation of the d orbitals, which can be rehybridized and form a hypercoordinated complex [25]. Moreover, the solubility of organotin compounds depends on the number/length of the organic moieties as well as the nature of the X group present. The factors which are primarily taken into consideration while determining the biological activity of the organotin(IV) compounds, ($R_nSnX_{4-n}(L)_x$) are: the nature of the organic group (R), halide or pseudohalide (X), and the donor ligand (L) attached to tin which can be altered in order to regulate the activity, to impart the specific features to achieve the action on desirable targeting site and minimize its side effects [26–28]. A number of applications of the organotin compounds are described in brief and main emphasis is given to their biological activities which are explained in detail.

1.1.2. Commercial Applications of Organotin Complexes

Organotin compounds found widespread applications in industrial, agricultural, synthetic and biological fields. Ross [29, 30] described the three major areas where organotin compounds were utilized commercially; it includes as (i) heat stabilizers, (ii) catalytic agents and (iii) biocidal compounds. The use of organotin compounds as polyvinyl chloride (PVC) stabilizers has increased extensively since its first use in 1940 [31]. Since then the organotin compounds become very popular because of their great efficiency (a small amount gives a high degree of clarity when added to transparent PVC), and having a low mammalian toxicity compared to other stabilizers. At the beginning, organotins were widely used as thermal stabilizers for PVCs and as transformer oil stabilizer, but later as the chemistry of organotin compounds was explored their applications were extended to the fields of catalysis and biological activities.

Organotin compounds have been used for the polymerization of polyurethanes, silicones and esterifications in the field of catalysis [30, 32]. The vulnerable Sn–C bonds (longer covalent bond, high polarizability and less thermodynamic stability) in organotin compounds make them good reagent and catalyst for multistep synthesis and selective reactions as they can deliver the attached groups to another reagent through radical or by polar mechanism. Organotin compounds have been used as homogeneous catalysts in polymer industry for diverse reactions such as polymerization, C–C bond formation, esterfication, ester hydrolysis, addition reactions, reduction reactions, dehydrogenation reactions, cross-coupling reactions, transmetallation reactions, stereo selective synthesis of alcohol and ketone derivatives, synthesis of enantiomerically pure α-amino acid derivatives, and catalysis of Reformatsky type reactions [33].

In 1950, Professor van der Kerk [34] and his team made significant contributions towards describing the biocidal properties of trialkyltin and triaryltin derivatives. The biocidal uses of organotin compounds as acaricide, fungicide and in agriculture, as preservatives of wood and for the protection of textiles, cordage fibers, paper, leather and electrical equipment etc. revealed their high toxicity towards living cells [35]. Fig 1.1 illustrates the role of different organotins in different fields. It is worth to note that the diorganotin compounds have been mainly used as heat stabilizers and triorganotin compounds were used for biocidal purpose [30].

1.1.3. Biological Applications of Organotin Complexes

Since 1929, a significant and fruitful research has been done on the biological or pharmaceutical role of organotin compounds and a number of publications have come up describing these compounds as an apoptotic inducer, antiviral, anticancer, antibacterial, antifungal, antineoplastic and anti-tuberculosis agents [23, 36, 37]. Nath et al. have been continuously involved in the design of novel organotin(IV) complexes with biologically important molecules such as amino acids, dipeptides, ascorbic acid, derivatives of fatty acids and constituents of DNA and RNA, and investigation of their biological activities such as anti fungal, antimicrobial, anti-inflammatory, cardiovascular and antitumour activities as well as their underlying mode of action [38-46]. Few examples from the last five years literature are

being discussed with respect to pharmacological action of organotin complexes by describing their antimicrobial (antibacterial, antifungal and antiviral) and antitumour activities.

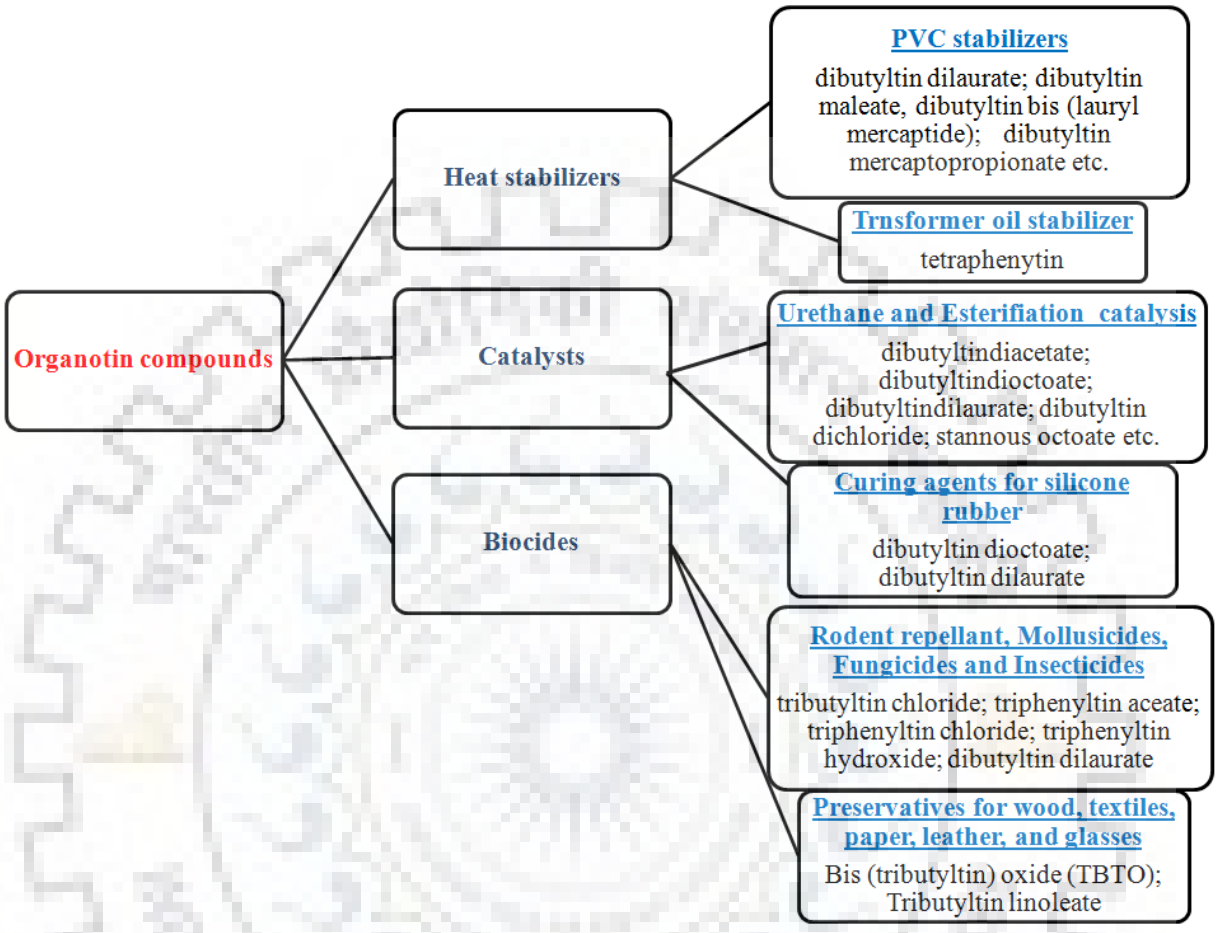

Fig 1.1. The role of different organotin compounds in various fields [30].

1.1.4. History of Organotin(IV) Compounds as Antitumor Agents

The cancer is one of the major causes of deaths worldwide; it takes more lives than AIDS, malaria and tuberculosis combined. According to International Agency for Research on Cancer 2017, the global cancer burden is increasing at an alarming pace, in 2030 alone a 21.6 million new cases of cancer are expecting to occur and 13.0 million deaths due to cancer are documented [47]. In India alone have over 17.3 lakh new cases of cancer and approximately 8.8 lakh deaths due to the cancer are estimated. Indian Council of Medical Research (ICMR) reported in 2016 the total number of new cancer cases is expected to be around 14.5 lakh which are likely to increase up to 17.3 lakh in 2020 [48]. The organometallic pioneered in the chemotherapeutic regime was *cis*-platin [49], which gains a lot of success for treating solid

malignancies [50] since its approval as chemotherapeutic drug in 1979 [51]. The cytotoxic effects of *cis*-platin arise due to its covalent bonding with DNA which forms cross links between the base pairs causing appreciable distortion of the helical structure to inhibit the replication of DNA and transcription (Fig. 1.2) [52]. The Pt^{2+} unit binds covalently to DNA, particularly at N_7 position of either of pyrimidine base *i.e.* guanine (G) or adenine (A) and form interstrand cross-links (Fig. 1.2) which opens up the cellular pathway (transcription inhibition, cell-cycle arrest, inhibit DNA repair) for apoptosis [53]. Despite, the clinical and commercial success of *cis*-platin, downsides were also identified with a number of side effects such as neurotoxicity, nephrotoxicity, ototoxicity, myelotoxicity, hemolytic anemia and the emergence of *cis*-platin resistance. Hence, the second generation platinum analogues *i.e.* carboplatin and oxaliplatin

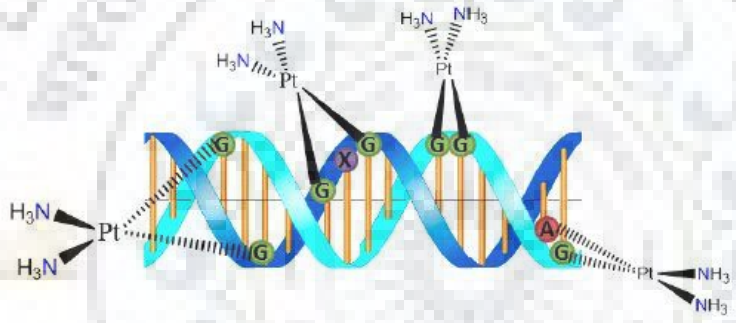

Fig. 1.2. DNA adduct formation with *cis*-platin moiety [52].

have entered in the regime of chemotherapeutics with broad antitumor spectrum and highly effective in testicular, ovarian, colorectal, cervix, lung cancers, with *cis*-platin combination chemotherapy or with other antitumour drugs [51]. Though the *cis*-platin and its analogues were used worldwide efficiently, but the Pt-resistance and severe side-effects stimulated researchers to look for unconventional chemotherapeutic alternatives with broad antitumor spectrum and to apprehend their underlying mode of action at cellular and molecular levels. In addition to the organometallic derivatives of Pt, other organometallic compounds derived from Sn, Au and Ru have emerged as potent antitumor agents due to their apoptotic inducing character, minimum toxicity and negative platinum-induced resistance [54, 55]. Crowe *et al.* [56] in (1980) and Saxena *et al.*[57] in 1989 synthesized and tested a number of organotin compounds for their bioactivity *in vitro* against P-388 lymphocytic leukaemia and different panels of human cancer cell lines. The antitumor studies of organotin(IV) compounds accelerated with a good pace and now, a number of researchers [58-60] have been indulged in

the synthesis and testing of these compounds against different cancer cell lines. Brown reported [58] triphenyltin acetate as anticancer agent for the first time and certain triphenyltin benzoates were found to exhibit exceptionally high *in vitro* antitumor activity [61] against mammary cancer (MCF-7) and colon adenocarcinoma (WiDr) cell lines afterwards. Few triphenyltin carboxylates have also unveil quite less values of ID_{50} compared to the commercially available anticancer drugs [62]. Few examples of potent organotin(IV) complexes from the literature have been cited in literature review.

1.1.5. Possible Mode of Action of Organotin Complexes

Commercially available antitumor drugs exert their action by targeting four potential sites *i.e.* nucleic acids, specific enzymes, microtubules and hormone/growth factor receptors. It has been reported that organotin(IV) compounds can induce cell death through apoptosis [63], but actual mechanism of apoptosis is not clear. Few researchers reported that organotin(IV) compounds interact with cell membrane, increasing their permeability, which enhances the process of ion exchange and ultimately leads to the inhibition of oxidative and photochemical phosphorylation. Nishikimi et al. [64] reported two major pathways to describe the apoptotic cell death; one is induced through a cytokine mediator and the other is regulated by mitochondrion dependent mechanism. Tributyltin(IV) moiety selectively interacts with thiol residues of the adenine so as to open up the permeability transition pore, thus decreasing the potential of mitochondrial membrane, resulting a release of cytochrome c from mitochondria [38]. Few literature reports revealed that the organotin(IV) complexes trigger the peroxide induced oxidation of lipids in cells which accumulate the hydroperoxides and leads to a decay of cell membranes, resulting apoptosis [65-66]. Organotin(IV) compounds exhibit redox property due to which they react with phosphorus containing biomolecules, (phospholipids, ATP, and nucleic acids) which leads to inhibition of the synthesis of phospholipids and their transport into the cell [65-67]. Organotin(IV) heterocyclic thioamides have been found to exhibit a lipoxygenase inhibitory activity [67]. Tributyltins increase the concentration of Ca^{2+} by activating L-type voltage-dependent Ca^{2+} channel (VDCC)s and induce programmed cell death [64]. Furthermore, the ability of tin atom to interact with free sulphydryl groups of tubulin proteins [68] leads to the distortion of protein structure and disrupt the normal processes which inhibit their dynamic behavior. The interaction of reagents like methyl-, phenyl- and tributyltin chlorides and diorganotin dichlorides with sulphydryl group which is distributed

across the both ends of microtubules, prevent its polymerization, thus interfere with the mitotic activities of cell cycle and leads to apoptosis [69]. The di- and tributyltin species selectively aggregate nearby nucleus, Golgi bodies and endoplasmic reticulum and destroy the structure of the latter and former which obstruct the ceramide metabolism and inositol triphosphate (IP3) induced intracellular Ca^{2+} mobilization and ultimately retard the membrane mediated signal transactions which are required for DNA synthesis [67].

In order to accommodate the analogy in mechanism of platinum based drugs, few researchers considered that organotin compounds may target DNA. But unlike *cis*-platin, dimethyltin(IV) dichloride revealed no binding affinity towards nitrogen bases of DNA [70]. However, many researchers demonstrated the occurrence of non-covalent interaction of organotin compounds either with sugar-phosphate backbone or insertion into the major or minor groove of DNA which have been mentioned in detail in next section.

1.1.6. Interaction of Organotin Complexes with DNA

Most antitumor agents are DNA–targeted, which exert their action *via* covalent or non-covalent binding with the structural entities of DNA. Non-covalent type of DNA interactions include intercalation, groove binding and electrostatic binding with DNA backbone and nucleobases [71]. Interaction of DNA with drug molecules can inflect the growth, division and gene expression of the cell by modifying the transcription and replication patterns. When a drug molecule interacts through covalent binding with DNA, it forms an irreversible DNA-drug adduct, which may inhibit the major metabolic processes related to DNA and leads to cell death. The covalent binders effectively bind to DNA which can distort the DNA backbone and can alter the basic functional machinery of the cell. Some metal complexes with aromatic side arms can bind to DNA either through metal coordination or through aromatic ligand intercalation [72]. In case of organtin(IV) complexes the interaction through covalent binding is very rare. The non-covalent DNA binder (groove binders and intercalators) are supposed to produce their effects by altering the DNA conformation and causing structure related perturbations which can interfere with the DNA-protein interactions and affect the very basic functions of the cell. This kind of binding is considered as reversible in nature and is preferential over irreversible covalent binding mode when the drug metabolism and toxic side effects are taken into account. Non-covalent DNA binders can promote conformational and

torsional changes in DNA and sometimes lead to nicks/breaks in DNA strands. These processes can alter the protein-DNA interactions and concomitantly affect the gene expression [73]. Further, this non-covalent drug–DNA binding is of three types: intercalation, groove binding and electrostatic or external binding [74].

1.1.6.1. Intercalative mode of binding: Intercalating agents stack between the adjacent base pairs of DNA without forming covalent bonds as well as without breaking up the H-bonds. They can stabilize the DNA helix through van der Waal's forces, hydrogen bonding and hydrophobic forces [75]. Adduct formed by DNA with interacting agent is less sensitive towards the ionic strength as the latter is stabilized by sufficient π-π electron overlap. To accommodate an intercalating agent between the DNA helix, the unwinding of base pairs must occur which can stabilize, lengthen and stiffen the helix structure [76]. The structure of the intercalating agent can decide the extent of unwinding, e.g. the intercalated proflavine unwind the helix by about 17° and ethidium cation to about 26°. The structural alteration may result in non-recognition of DNA-associated proteins such as polymerases, topoisomerases, DNA repair systems and transcription factors, which leads to inhibition of the transcription and replication processes [77]. Hindrance caused by ancillary ligands prevents the intercalation of less extended aromatic structures, so only partial intercalation can envisage in those cases. Intercalation is further of two types: classical intercalation and threading intercalation [78, 79]. When entire molecule is inserted between GpG base pairs which form the top and bottom layer of the intercalation site, the kind of intercalation is known as classical intercalation. Often, the threading intercalators consists of two side chains on either face of aromatic system where one of the side chains must slide from the site of intercalation so as to interact with of major and minor grooves to make the DNA-complexes adduct more stable. [80]. From the last two decades a significant number of organotin complexes with variety of ligand having O, N and S as potential donor atoms have been synthesized and found to be interacted with DNA through intercalative and partial intercalative modes. Organotin(IV) complexes derived from hydrazone Schiff bases reported by Hong et al. and Niu et al. [81, 82], organotin(IV) complexes of carboxylic acid derivatives by Sirajuddin et al. [83] and diorganotin(IV) mandelates synthesized by Nath et al. [84] are some recent examples of organotin(IV) derivatives acting as potential intercalators of DNA and altering the conformation of DNA which results in further biological action.

1.1.6.2. Groove-Binding: Groove binding of small molecules to major and the minor grooves of DNA occurs through hydrogen bonding and van der Waal's interaction. Minor groove binders generally possess few aromatic rings, which are connected through bonds having torsional freedom. Groove-binders induce very little modifications in the structure of the DNA helix as in case of organotin(IV) complexes of Schiff base, N'-[(1E)-(2-hydroxy-3-methoxyphenyl)methylidene]pyridine-3-carbohydrazone synthesized by Hong et al.[85].

1.1.6.3. Electrostatic or External Binding: Some of the molecules can show edge stacking interactions with the DNA phosphate backbone. Arjmand et al. [86] studied the electrostatic mode of DNA binding of organotin(IV) complexes derived from chromone Schiff base. Bulky or associated aggregates of ligand may interact with the phospodiester backbone of DNA in order to overcome the repulsive forces between the ligands [80].

1.1.7. Factors Influence the Biological Activities of Organotin(IV) Complexes

Different factors which affect the biological properties of organotin complexes are described thoroughly in this section:

1.1.7.1. Bond strength of tin-ligand: The cleavage of metal-ligand bond is the primary step to produce the biologically active species in most of the complexes, thus complexes with stronger Sn–O, Sn–N, and Sn–S bonds cannot dissociate easily to produce the corresponding active species *viz.* $[R_2Sn(IV)]^{2+}$ /$[R_3Sn(IV)]^{+}$ [87], thus, are less active than those with comparatively weaker and longer Sn–O/N/S bonds. A number of organotin(IV) compounds with N donor were tested for antitumor activity and found that the complexes with average Sn–N bond length > 2.39 Å are active and those with < 2.39 Å are inactive [88, 89].

1.1.7.2. Geometry of the complex: The binding capacity of organotin(IV) complexes towards DNA is highly dependable on the nature and the number of groups attached to tin atom. In general the metal complexes having td geometry are found more active than the corresponding complexes with TBP and Oh geometries [90]. The number of coordination positions available around tin is directly related to the activity of the complexes, irrespective to their nuclearity. However, high cytotoxic activity of many organotin(IV) compounds despite the unavailability of coordination position can be explained on the basis of their strong tendency as oxidation promoters or enzyme inhibitors not through DNA binding [91, 92].

1.1.7.3. Organic moiety attached to tin: Variation in organic group attached to the tin metal produce a significant difference. Parameters *viz.* size, hydrophobicity, availability of π-electrons, steric hindrance and the possibility of unrestricted H–bonding, can affect the intracellular intake of the organotins. Hansch and Verma [93] proposed that the cytotoxicity of organotin(IV) compounds is proportionally related to the hydrophobicity of the substituents attached to the tin, to a certain limit; beyond which it reverses the effect. However, the bulky organic moieties augment the dissociation of the complex to form active ionic species, which increase the transport of the active species into the cells and exert their cytotoxic effect [94, 95]. In some cases where organotin(IV) compounds containing phenyl groups have been found more active than with other alkyl substituents due to facile bonding of phenyl groups with biomolecules which is facilitated *via* π-π interactions. The observed order *i.e.* *n*-Bu > Ph and Et > Me can be described on the basis of increasing lipophilic character of the alkyl group with increase in chain length [36].

1.1.7.4. Synergistic effect of metals: Bimetallic complexes having tin along with another metal, exhibit high biological activity. Arjmand et al. [96] depicted the DNA interaction of Zn-Sn and Cu-Sn bimetallic complexes, where the tin species bind to DNA preferably through the phosphate backbone, while the zinc ions stimulate the cleavage of the phosphodiester bond. Thus, a combined action of both metals leads to higher activity of the bimetallic complex. Similarly, the polymeric diorganotin(IV) hydroxamato complexes, containing butyl moiety are the most active compounds, and the binuclear adduct is more active than the corresponding mono nuclear complexes [36].

1.1.7.5. Role of ligand: Ligands attached to tin metal plays an indispensable role in transportation and proper orientation of the molecule to the target as it checks the unnecessary reaction of metal species with various biomolecules underway. However, emphasis has given to the fact that the release of active species must be efficient, though in a controlled manner [97].

1.1.7.6. Electronic effect and basicity of the subtituents: Basu et al. [36] observed a significant difference in the activities of the chloro diorganotin(IV) complexes and their counterparts without chloro substituents and the complexes with chloro group were found more active. Electronic effect of the substituents on the ligand 4-X-benzohydroxamic acid can be explained by decrease in its activity as the electron withdrawing character of X decreases, *i.e.* Cl > OCH_3. However, a reverse relation between basicity of donor atom and activity the ligand

has been observed. In order to improve the activity, the basicity of the ligand must to be reduced by introducing some electron-withdrawing substituents *i.e* $-CN^{-}$, $-CF_3^{-}$, $-F^{-}$ etc. [97].

1.1.8. Solution/Speciation Studies of Organotin Compounds

In order to understand the distribution of the species of a particular compound in a system under study, it is must to account the data related to various equilibria established and stability constant calculated for the particular species involved. The stability constants of several organotin species formed by the hydrolysis with wide range of ionic strength were reported in the literature [41, 84, 98–105]. Inside the living systems organotins can interact with proteins, nucleic acids, carbohydrates and lipids biomolecules through heteroatoms like N, P, O, and S, thus, the discussion of their equilibria and formation of the different species of biologically active ligands with organotin is of considerable importance. The speciation study of organotin compounds have an absolute impact in the field of bioinorganic chemistry, in order to study the properties related to the chemical transformation of the species as it enters in the biological system. Evaluation of different chemical species throughout the metabolic pathway and within the body fluids and tissues can provide important information about the biological mechanisms regarding cellular uptake, transport, storage and excretion of the species. Since, various drugs are administered in solution form hence, the speciation analysis of these compounds in aqueous medium must be studied. Further, the contamination of natural resources and industrial sites with toxic metals *i.e.* tin, arsenic and lead etc. requires cleanup strategies for which the knowledge of the speciation analysis is must.

1.2. LITERATURE REVIEW

1.2.1. Organotin Complexes as Antimicrobial Agents

Few examples in reference to pharmacological action of organotin complexes by describing their antimicrobial (antibacterial, antifungal and antiviral) activities from the last five years have been discussed in this section.

Organotin(IV) derivatives of sodium 3-(benzo-[1,3-]dioxol-4-yl)propanoate have been tested for *in vitro* antibacterial and antifungal activities against six bacterial strains *(E. coli, B.*

subtilis, S. flexenari, P. aeruginosa, S. aureus, and S. typhi) and against fungal starins (*Trichophyton longifusus, Candida albicans, Aspergillus Flavus, Microsporum Canis, Fusarium Solani,* and *Candida glabrata*) [106]. All the compounds exhibited significant activity against bacterial strains however triorganotin(IV) derivatives were found more effective antifungal agents than the diorganotin(IV) compounds. Water soluble penta-coordinated diorganotin complexes of hydrazones, 3-methoxysalicylaldehyde Girard-T hydrazinim [R_2Sn((3-OMeSalGT)Cl (R = Ph, Me, Bu)] and 4-hydroxysalicylaldehyde Girard-T hydrazinim chloride [R_2Sn((3-OHSalGT)Cl (R = Ph, Me)] with square pyramidal geometry have been evaluated for antibacterial activity towards Gram-positive bacteria (*B. subtilis and S. aureus*) and Gram-negative bacteria (*E. coli and P. aeruginosa*) [107]. The complexes exhibited enhanced activity against all the bacterial strains compared to ligand, which may due to the delocalization of electron over the chelate ring after complexation hence increasing the lipophilicity and facilitated the permeation of complex through the lipid layer. Beside this the *Pseudomonas* bacteria which is resistant to many standard drugs was significantly inhibited by the complexes.

Diorganotin(IV) acetates, nicotinates and diorganotin(IV) dichloride adducts with ligands, 1,10-phenanthroline (Phen), 1,10-phenanthroline-5,6-dione (dione) and dipyridophenazine (dppz) were tested against *Escherichia coli*, *Staphylococcus aureus* and *Pseudomonas aeruginosa*. The dibutyltin(IV) derivatives exhibited the broadest range of activity compared to the dimethyl or diphenyltin(IV) derivatives. Similarly, a number of Schiff base complexes of 3-(2-hydroxyallylimino)indolin-2-one showed a promising activity against Gram-positive and Gram-negative bacteria *viz. Bacillus cereus, E. coli, Klebsiella species* and *Staphylococcus species* [108]. Di- and tri-organotin(IV) complexes of 4-((3,5-dimethylphenylimino)methyl)-2-methoxyphenol comprises good antibacterial and antifungal activity [109]. Organotin(IV) carboxylates of 3,5-dimethylbenzoate, were screened for anti-HCV (hepatitis C virus) potency by the Gaussia luciferase assay using infected Huh 7.5 cells (human hepatocellular cell) [110]. Molecular structures of the complexes are given in Fig.1.3. Structure-activity relationship studies identified the dibutyltin(IV) derivatives with skew trapezoidal bipyramidal geometry as a potent HCV inhibitor, with IC_{50} values equal to 0.69 nM. The UV–visible titration study evidenced the interaction of these complexes with viral DNA is due to their intercalation between the DNA strands.

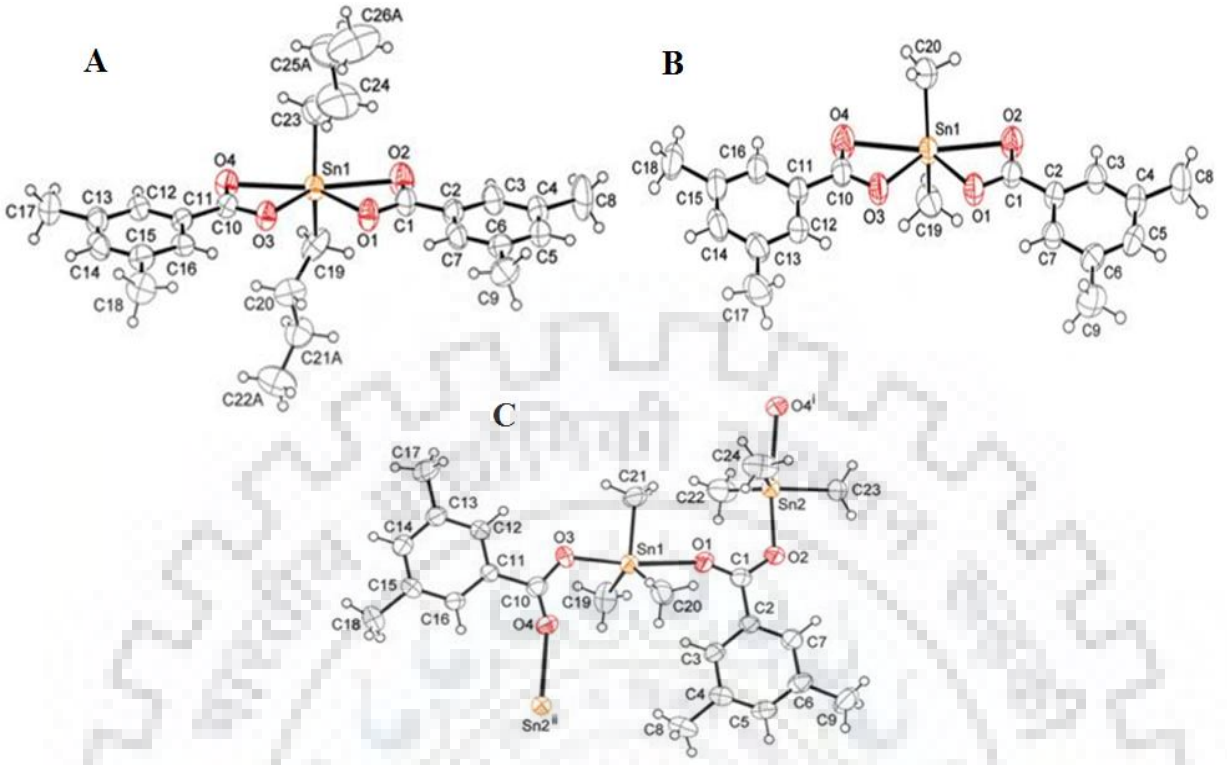

Fig. 1.3. ORTEP structures of (A) dibutyltin(IV), (B) dimethyltin(IV) and (C) trimethyltin(IV) complexes of 3,5-dimethylbenzoate, with displacement ellipsoids (50% probability level) [110].

The complex (tributylstannic [3-(2-fluorophenylamido)propionate] was found to exhibit substantial anti-HCV activity and claimed to be used as a potential anti-HCV agent in future [111]. Antimicrobial activities of diorganotin(IV) complexes of 3-trifluoromethyl-pyridine-2-thione and 5-trifluoromethyl-pyridine-2-thione were evaluated for antimicrobial activity against *S. aureus, A. baumanni, A. fumigates, B. subtilis, E. coli* and *P. aeruginosa* and were found quite active [112]. The position of the CF_3 groups seemed to influence the activity and 5-trifluoromethylpyridine-2-thionate was found more effective. The organotin(IV) complexes with 2-hydroxynaphthaldehyde-*N*(4)-ethylthiosemicarbazone (H_2DNET), of the type MeSnCl(DNET), BuSnCl(DNET), PhSnCl(DNET), and [Ph_2Sn(DNET] were found very active against microbial strains *Staphylococcus aureus, E. coli, Enterobacter aerogenes*, and *Salmonella typhi* [113]. Organotin(IV) complexes with amino ether Schiff base and dehydroacetic acid were found to exhibit minimum inhibitory concentration (MIC) values ranging 0.003–0.066 μM against Gram-positive bacteria (*Staphylococcus epidermidis* and *Staphylococcus hominis)* and Gram-negative-bacteria (*Pseudomonas aeruginosa* and *Klebsiella*

pneumoniae). Schiff base complexes of organotin have been found to possess significant activity against different bacterial strains, due to the presence of nitrogen and oxygen donor groups which might inhibit enzyme activity. Moreover, the high activity of the complexes can also be explained on the basis of chelation theory, according to which the potency of the Schiff base enhanced on coordination with tin atom [114]. Further, the bulkiness of phenyl derivatives makes them most active with highest zone of inhibition (ZOI) and lowest MIC, as phenyl group increases the lipophilicity as well as the polarity of M–C bond, which makes them highly active with the order Ph > Bu > Et ≥ Me [115]. In addition, the π–π interactions in phenyl group also play a key role in improving the bioactivity [116]. Plausible structures of diorganotin(IV) complexes of dehydroacetic acid are given in Fig. 1.4.

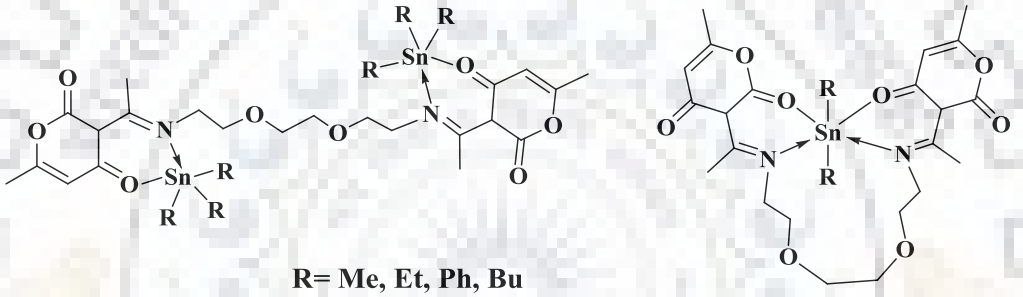

Fig. 1.4. Chemical structures of diorganotin(IV) complexes of dehydroacetic acid [116].

Dibutytin(IV) derivatives of (2-hydroxyphenyl)(pyrrolidin-1-yl)methanone thiosemicarbazone, (2-hydroxyphenyl)(pyrrolidin-1-yl)methanone phenylthiosemicarbazone, and (2-hydroxyphenyl)(pyrrolidin-1-yl)methanone semicarbazone have found the most active against few bacterial and fungal strains *viz. Klebsiella sp., Bacillus cereus, Staphylococcus sp., Escherichia coli, Rhizopus, Aspergillus, Alternaria, and Penicillium*. Further, activity increases on metallation which was explained by the metal ion absorption by the cell walls of microorganisms, which disturbs the respiration machinery of the cells and ultimately affect the synthesis of proteins essential for the cell growth [117]. The lipid membrane only allows the passage of lipophilic material. The chelate formation with metal ions reduces the polarity due to the overlapping of metal and ligand orbitals as well as mobilization of the positive charge between donor group and metal ion [118]. Trigonal bipyramidal (TPB), triphenyltin complexes of bisphosphoramidates $Ph_2P(O)XP(O)Ph_2$ (X = diamine) (Fig. 1.5), where adducts exhibited a marked activity against Gram-positive bacterium *B. Cereus* (IC_{50}=0.78 mg/mL [119].

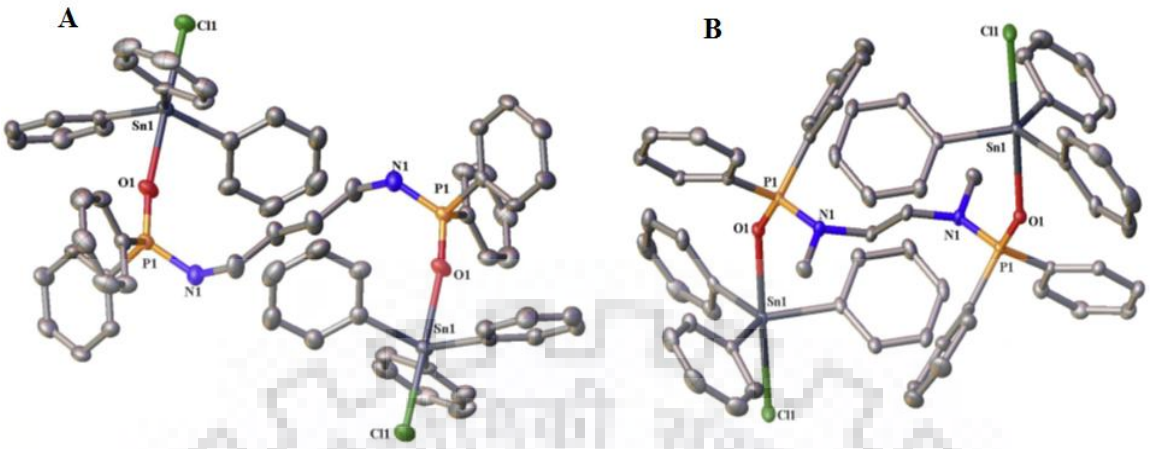

Fig. 1.5. Molecular structure of triphenyltin complexes of bisphosphoramidates $Ph_2P(O)XP(O)Ph_2$ with (A) X = $HN(CH_2)_2NH$ and (B) H_3C-$N(CH_2)_4N$-CH_3 [119].

Organotin(IV) complexes with ligand (2-(4-methoxy-2-nitrophenylcarbamoyl)benzoic acid) showed activity against the promastigote forms of leishmania major, which is comparable to commercial drug amphotericin B. The higher activity of the complex was due to interference of the complex molecule with mitochondrial function of parasite. In addition, the *in vitro* studies of these complexes also displyed higher antibacterial activity compared to 3rd generation antibiotics *i.e.* Tetracycline, Penicillin G, Ampicillin and Amoxicillin against *Klebsiella pneumonia, Streptococcus pyogenes, Staphlococcus epidermidis, Staphlococcus aureus, Serratia marcesscens, Pseudomonas aeruginosa, Escherichia coli* [83].

Most organotin(IV) complexes of bioactive fatty acids *viz.* undecylenic, caprylic and ricinoleic acids showed remarkable antibacterial action with small MIC values (some of which were close to 1.0 μg/mL), against *Staphylococcus aureus* strains, which is resistant to norfloxacin, erythromycin and tetracycline. At the same time a substantial cytotoxicity was associated with the use of organotin(IV) complexes as antibiotic adjuvants, which overcome this resistance and increase the potency of tetracycline against IS-58 strain by about 128-fold. The results reinforce the use of organotin(IV) complexes in association with antibiotics so as to inhibit the bacterial efflux pumps putatively and can act as effective adjuvant antibiotic candidates [120]. The cytotoxicity and the antibacterial activity of triphenyltin hydroxide, TPTH (a widely used pesticide) on mammalian cells were analyzed using HeLa cells, and *B. subtilis, E. coli* cells, respectively. The growth of HeLa cells was inhibited strongly (IC_{50} = 0.25 mM). An induced mitotic arrest occurs due to a strong depolymerization of interphase

microtubules and spindle abnormality. Molecular docking studies and *in vitro* experiments revealed that TPTH may possess overlapping binding sites with colchicine on tubulin with a distance of about 11 Å between them. Furthermore, the docking study of TPTH with DNA revealed that it can bind to minor groove of DNA at the A-T rich region. The studies corroborated that the TPTH causes toxicity in mammalian cells through DNA interactions and mitotic arrest. However, the antibacterial activity was perhaps through interactions of TPTH with DNA and not through FtsZ (prokaryotic homolog of tubulin) [121]. A diagrammatic representation of mode of action of TPTH is presented in Fig .1.6.

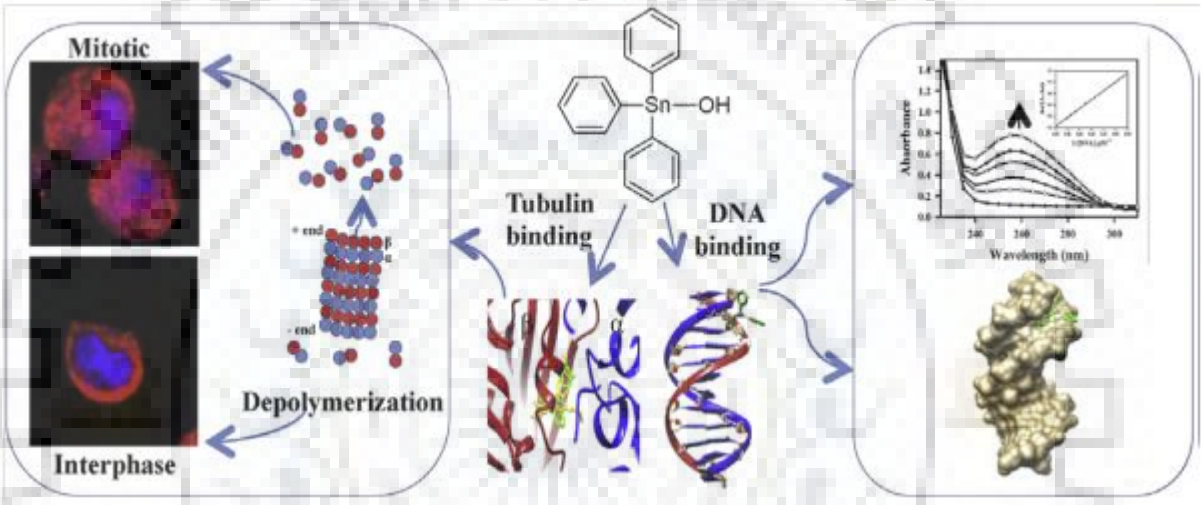

Fig. 1.6. General mode of action of triphenyltin(IV) hydroxide through interaction with microtubule and interaction with minor groove of DNA. Copyright Rathinasamy 2017 [121].

The *in vitro* test of organotin(IV) complexes *viz.* $(Ph_4P)_2[Sn(CH_3)_2(RSO_2N]CS_2)_2]$ (Ph_4P = tetraphenylphosphonium cation and R = CH_3, CH_3CH_2, C_6H_5, FC_6H_4) have been evaluated for antifungal activities against *Rhizoctonia solani* and *Botrytis cinerea*, which showed its remarkable activities, comparable to that of fungicides *viz.* manzate, dithiocarbamates ziram, bis(dimetilditiocarbamato)zinc and mancozeb (manganese/zinc ethylene bisdithiocarbamate), which are being used since 1960 and able to control a large number of plant diseases [122].

1.2.2. Organotin Complexes as Antitumour Agents

Few important examples of organotin complexes from recent past have been taken in order to

discuss the antitumour properties of organotin(IV) complexes.

Tabassum et al. [123] synthesized the $SnCl_4.H_2O$ and dimethyltin(IV) derivatives of N-glycoside (Fig. 1.7 A) (condensation product of D-glucosamine with ethylenediamine) with molecular formula $C_{15}H_{24}N_3O_6SnCl_3$ and $C_{17}H_{28}N_3O_5SnCl$, respectively, which were found to exhibit a high anticancer activity (*in vivo* and *in vitro*). These activities could be attributed to the fact that glucoconjugation enhanced the cancer targeting and selectivity. The chemotherapeutic potential of these complexes has been studied by analyzing their DNA interaction studies, which demonstrated a greater binding affinity and DNA photocleavage activity of dimethyltin(IV) derivatives. *In vitro* anticancer activity test revealed a significant cytotoxicity, (GI_{50} < 10 μg/mL) for $C_{17}H_{28}N_3O_5SnCl$ against DWD (human oral carcinoma) cell line. Furthermore, triphenyltin(IV) complex of 1-{(2-hydroxyethyl)amino}-2-amino-1,2-dideoxy-D-glucose (GATPT), a sugar based apoptosis inducer has been designed, which can modulate the hydro/lipophilicity of the complex and influence the delivery of the complex to the site of action [124] (Fig. 1.7 B). Various mechanistic studies at molecular level proved that GATPT induce apoptosis through a p53 dependent pathway involving cytochrome c and protein of Bcl-2 family. Further, it activates the caspase-3, which can inhibit the formation of tumor without affecting the other physiological function of the organism. GATPT is also having tumor suppressing properties with no toxicity suggested by *in vivo* antitumor studies in mice models. Furthermore, the structural features of GATPT help to explain its effectiveness on the grounds of: (i) the triphenyltin(IV) is a membrane active compounds, which acts as an ionophore to alters the permeability of mitochondrial membrane and change the activity of membrane enzymes, (ii) the N-glycoside being a lipophilic fragment, snatched by hydrophobic moieties of DNA and serves as a delivery vehicle to direct the tin metal to the internal parts of DNA [124].

Another recent example of carbohydrate-based (water-soluble) dimethyltin(IV) complexes with ethanolamine indicated the inhibition of the catalytic activity of human Topoisomerase I with very low concentration (IC_{50} in the range of 20-30 μM) compared to the standard drugs [125]. Zhang et al. [50] tested the dimethyltin(IV) complexes of D-fructose and D-maltose (Fig. 1.7 C), against Huh7 (human hepatoma) cancer cell lines and demonstrated a sufficient activity compared to standard drugs. Specific regulatory gene expression (MMP-2

and TGF-b) reveals that complexes can act as potent antiproliferative drug by inducing the morphological changes associated with apoptosis.

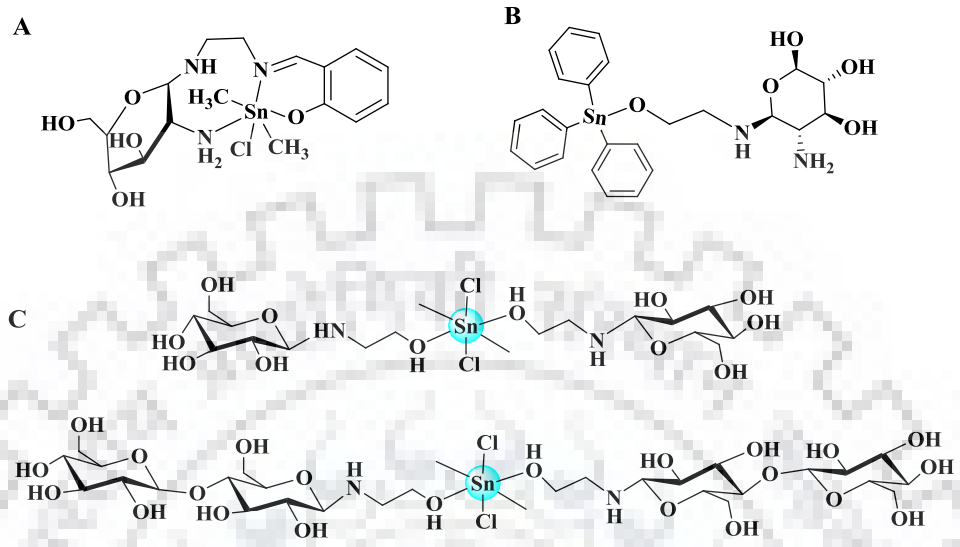

Fig. 1.7. Structure of (A) dimethyltin(IV) derivatives of N-glycoside, (B) 1-{(2 hydroxyethyl)amino}-2-amino-1,2-dideoxy glucose triphenyltin(IV) (GATPT) and (C) dimethyltin(IV) complexes derived from D-fructose and D-maltose [50, 123].

A number of organotin(IV) carboxylates represent the major class of organotin complexes which have been studied for their antitumour activity. Many of such complexes were tested against different cell lines and were found more active than the standard drugs, indicating potential of these complexes to be used as medicine in future. Selectivity of different organotin(IV) carboxylates for different cell lines can be attributed to their structural diversity and different substituents on the ligand of these complexes. It is believed that the organotin complexes with Sn–O covalent bond are more active than that of coordinate bonds. From the literature review it has been found that the butyltin(IV) carboxylates exhibited higher anticancer activity than the complexes with methyl, ethyl or octyl carbon chains [126-128]. Furthermore, the polynuclear organotin(IV) carboxylates results in lower activity which may be because of less access to the target due to the steric hindrance and a high coordination number around the tin atom [129]. In order to use the organotin complexes as potential anticancer drugs in future the research should be focused on the determination of the exact mechanism of action and further *in vivo* experimentation of the organotin(IV) carboxylates. Several organooxotin clusters have been synthesized and modified clinically by using spacers or tailed groups, such

as carboxylic acids, phosphonic acid, and arsonates [130]. Hence they evolved as a new class of pharmaceutical drug motifs due to their tremendous structural diversity and biological applications [130]. Tetranuclearstannoxane cluster (Sn(IV)-oxo-{di-o-vanillin}dimethyl dichloride) has been tested for *in vitro* cytotoxicity and revealed exceptionally high anticancer activity towards pancreatic cell lines even better than Adriamycin. Its docked model revealed that it binds with G-C rich region and hydrophobic pockets of minor groove of DNA (Fig. 1.8) [129].

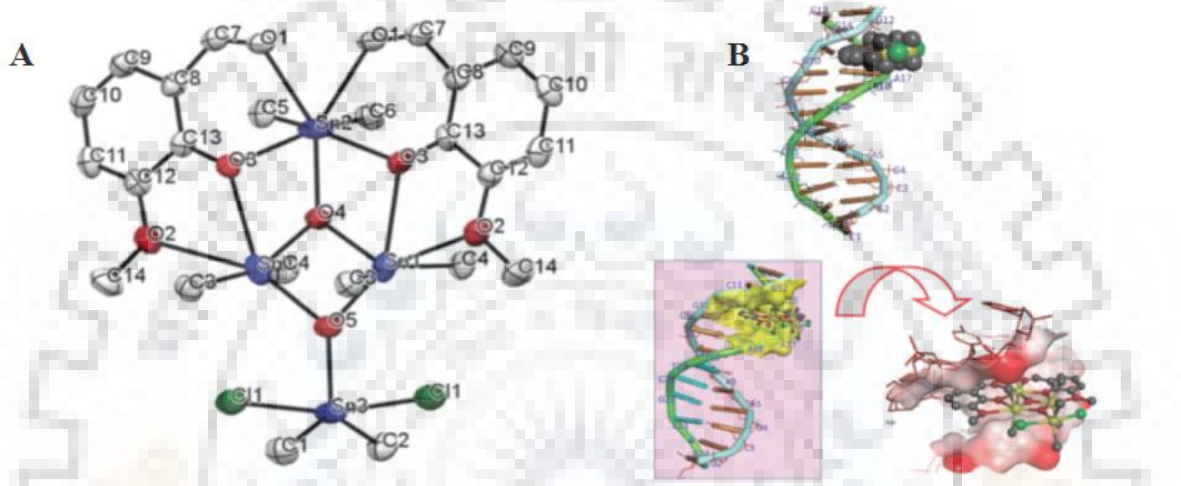

Fig. 1.8. Molecular structure of tetranuclearstannoxane cluster (Sn(IV)-oxo-{di-o-vanillin}- dimethyl dichloride) (A), docked model of tetranuclearstannoxane cluster into the G–C region of the minor groove of DNA (PDB ID: 1BNA) (B); Hydrogen atoms are omitted for clarity) [129].

Basu et al. [131] synthesized a series of dibutyltin(IV) compounds of 2-{(E)-4-hydroxy-3-[(E)-4-(aryl)iminomethyl]phenyldiazenyl}benzoic acids (L^nHH'; n = 1-2) having general formula $\{[Bu_2Sn(L_nH)]_2O\}_2$. These complexes were found to exhibit *in vitro* cytotoxicity against HCT116 (colon carcinoma) and A375 (melanoma) cell lines. The structural frame-work with central tetrametallic core (Fig.1.9) may be responsible for the higher activities of these complexes where the synergistic effect of *n*-butyl groups bonded to the tin may attributed towards the cytotoxicity. Organotin complexes with *o*-hydroxy benzoic acid or *p*-hydroxy benzoic acids were found to exhibit *in vitro* and *in vivo* cytotoxicity against the human cells lines *viz*. MCF-7 (breast cancer), HeLa (cervix cancer) and U2-OS (osteosarcomas) cell lines with IC_{50} value ranging 108–724 nM, 21–295 nM and 97–820 nM, respectively, which is even greater than *cis*-platin [132].

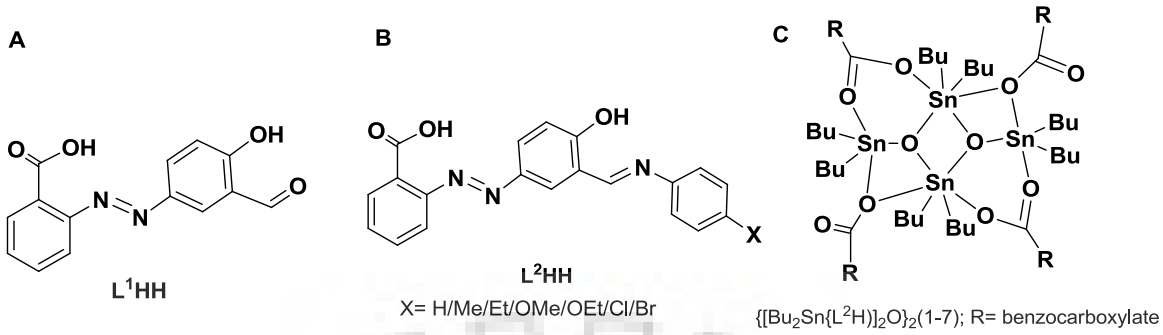

Fig. 1.9. Structure of (A) L^1HH', (B) L^2HH' and (C) structure of dibutytin(IV) complexes [131].

Tributyl and triphenyltin(IV) carboxylate complexes with coumarin moiety were found to exhibit a good biocompatibility and deep tissue penetration (over femto second laser with wavelength of 840 nm). These complexes could be accumulated in the cytoplasm and induce apoptotic cell death *via* mitochondrial dysfunction and ROS elevation pathway and showed a higher cytotoxicity than *cis*-platin [133]. Prokop et al. [134] synthesized dibutyltin(IV) derivatives of maleimide, maleic acid and citraconimide (Fig. 1.10), which have been found to act as moderate thioredoxin reductase (TrxR) inhibitors and triggered strong cytotoxicity in MCF-7 (breast cancer) and HT-29 (colon carcinoma) cells. These complexes were also found highly active in vincristine and daunorubicin resistant cells thus, can be used as a lead compounds to overcome the resistance towards antitumour drugs.

Dibutyltin(IV) and diphenyltin(IV) carboxylates based on an amide carboxylic acid 2-(1,3-dioxo-1*H*-benzo[de]isoquinolin-2(3*H*)-yl)acetic acid have revealed more cytotoxicity than *cis*-platin *in vitro* against HepG2 (hepatic cancer) and MCF-7 (breast cancer) cell lines [135]. Rojas-Oviedoa et al. [136] reported tributyltin derivatives of 4-oxo-4-(arylamino)butanoic acids and N-substituted succinamic acid which were found highly cytotoxic against three cervical cancer cell lines *viz.* HeLa, Ca Ski and ViBo. One of the compounds, (tributylstannyl 4-oxo-4-[(3-trifluoromethyl-4-nitrophen-1-yl)amino]butanoate), exhibited excellent cytotoxicity with IC_{50} value of 0.43 μM, against the HeLa cell line. Further, the organotin polymers are also be the focus of research due to their wide range of regression against different cancer cell lines associated with ovarian, colon, lung, prostate and pancreatic cell lines [80]. Milaeva et al. [137]

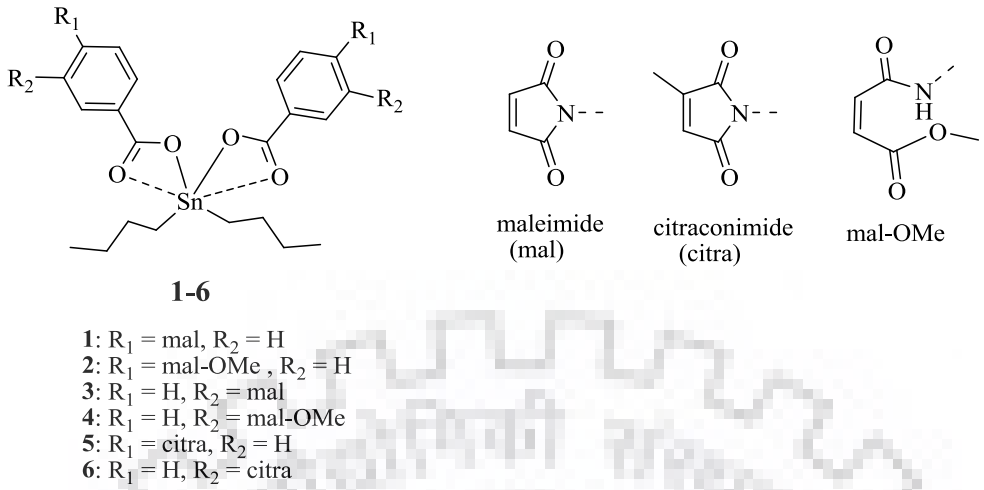

Fig. 1.10. Chemical structures of dibutyltin(IV) derivatives of different carboxylic acids [134].

synthesized organotin complexes with Sn–S bonds of formulae $R_2Sn(SR')_2$ and R_3SnSR' and $Sn(SR')_4$ (R= Me, Et, Bu, Ph) (R' = 3,5-di-tert-butyl-4-hydroxyphenyl), which were effectively interacted with the tubulin (cholchicine bind site), and acted as promising antimitotic agents. The *in vitro* cytotoxicity results against MCF-7 and HeLa and normal human fetal lung fibroblast cells (MRC-5) revealed their high cytotoxicity towards cancer cell lines and low cytotoxicity towards normal cells. Triphenyltin complex due to its lipophilic character demonstrated the highest activity against both cell lines *i.e.* 250 nM for MCF-7 and 160 nM for HeLa. Furthermore, triorganotin(IV) complexes revealed a higher cytotoxicity due to the same reason [137]. Hong et al. [138] reported diorganotin(IV) complexes from salicylaldehyde nicotinoyl hydrazone (Fig. 1.11), which revealed high activity against three drug-resistant human tumor cells lines, A549 (lung cancer), HeLa and MCF-7. Moreover, both the complexes proved to be strongly interacted with BSA (Bovine serum albumin). It was also found that organotin complexes can be transported in protein through binding with tyrosine residue. Liu et al. [81] synthesized organotin(IV) complexes Me_2SnL^1, Ph_2SnL^1, Me_2SnL^2 and Ph_2SnL^2 (H_2L^1 = 5-chlorosalicylaldehyde isonicotinoyl hydrazone and H_2L^2 = 2-hydroxy-4-methoxy-benzaldehyde isonicotinoyl hydrazone). All the complexes exhibited significant cytotoxicity against A549 and HeLa cancer cell lines and mononuclear complex with distorted TBP geometry was found to exhibit maximum cytotoxicity against HeLa cells. These complexes showed an intercalative mode of binding with CT DNA.

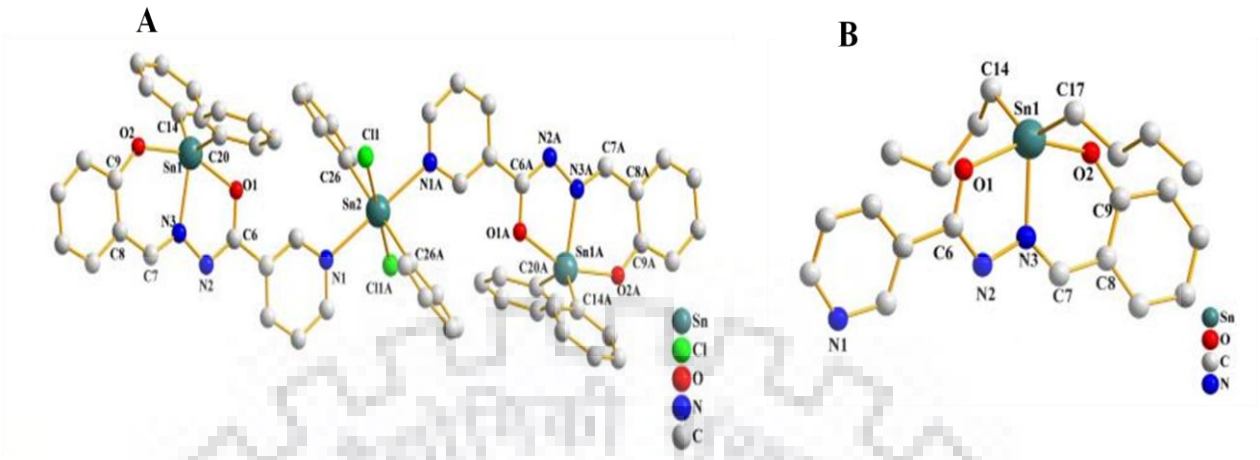

Fig. 1.11. Molecular structure of diphenyltin(IV) complexes of salicylaldehyde nicotinoyl hydrazone, showing a trimers with six coordinating geometry at central tin and distorted TBP geometry at the other tin atoms (A) and dibutyltin(IV) derivative of the same ligand adopted distorted TBP geometry at the tin atom (B) [138].

Salam et al. [139] synthesized the complexes of organotin(IV) chloride(s) with a tridentate ligand, 2-hydroxy-5-methoxybenzaldehyde-N(4)-methylthiosemicarbazone (H_2dmmt) *viz.* [MeSnCl(dmmt)], [BuSnCl(dmmt)], [PhSnCl(dmmt)] and [Ph_2Sn(dmmt)], which have been tested for *in vitro* cytotoxicity against HCT116 (human colorectal cancer) cell lines. The results indicated that the cytotoxicity of the complexes distinctively depend on the nature of organic group attached to the tin metal which follows the order Ph_2 > Ph > Me > Bu.

Yang et al. synthesized [140] di- and trialkyltin(IV) compounds with N-[(1E)-(2-hydroxy-3-methoxyphenyl)methylidene]pyridine-4-carbohydrazone. Al1 the complexes were momomeric with distorted TBP geometries unlike the trimethyltin(IV) complex in which six molecules were linked by the weak Sn–N interaction resulted in an interesting 72-membered crown-like macrocycle, presented in Fig. 1.12. The DNA binding studies of these complexes revealed a groove binding and partial intercalative mode of binding with DNA. The *in vitro* cytotoxic activities against human cancer cell lines, HL-60 (promyelocytic leukemia), A549 (lung cancer), and colon cancer cell lines *viz.* HT-29, HCT-116 and Caco-2, revealed that dibutyltin(IV) and diphenyltin(IV) complexes having remarkable regression against the tested cell lines which can make them promising antitumor candidates in *cis*-platin resistant cell lines.

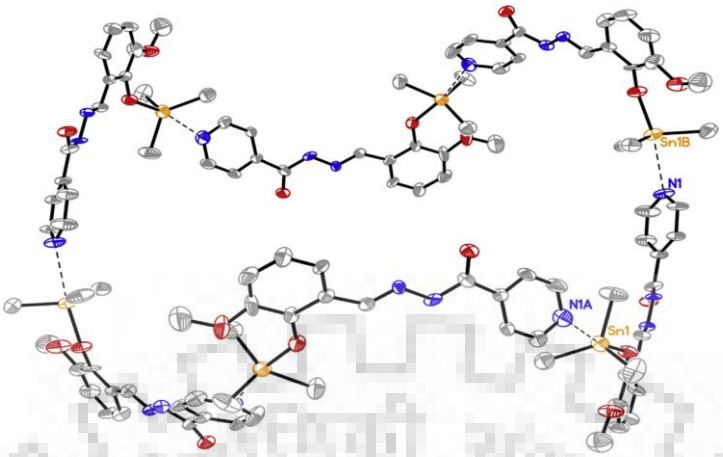

Fig. 1.12. The supramolecular structure of dibutyltin(IV) complex of N-[(1E)-(2-hydroxy-3-methoxyphenyl)methylidene]pyridine-4-carbohydrazone formed by intermolecular weak Sn–N interactions [140].

The literature review revealed that the organotin(IV) complexes could be the best substitute for platinum based drugs and can be seen as potential future chemotherapeutics in the field of cancer chemotherapy, with minimum side effects, no drug resistance and broad spectrum of activity.

1.2.3. Solution/Speciation Studies of Organotin Compounds

Speciation analysis of the organotin(IV) complexes with different biomolecules in aqueous medium have been discussed in this section in order to understand their distribution in the body fluids and tissues.

The chemistry of coordination of $Me_2Sn(IV)^{2+}$ to an antihypertensive drug, captopril {N-[(S)-3-mercapto-2-methylpropionyl]-$_L$-proline, was studied by Nagy et al. [141], in aqueous solution through potentiometric titration and Mössbauer spectroscopy in the pH range 2–11 (I = 0.1 M, $NaClO_4$, 298 K). The studies indicated the presence of only monomeric species with 1:1 metal-to-ligand ratio (ML) in the solution at acidic and physiological pH, where, complex adopted TBP geometry with axial position occupied by –COO and H_2O molecule and equatorial position with $–S^-$. With increasing pH (in weakly basic pH range) the complexes MLH and ML_2 were formed, in which the –COO group might have been displaced from the coordination sphere by an OH and an S (of other ligand).

The interaction of $Me_2Sn(IV)^{2+}$ and $Me_3Sn(IV)^{+}$ with dipeptides *viz.* tyrosylalanine, glycyltyrosine and glycylisoleucine, in aqueous solution (I = 0.1M KNO_3, 298 K) have been studied potentiometrically and structures of species formed were estimated through Mössbauer spectroscopy. The studies revealed that the dipeptides coordinated through COO^-, N^- and NH_2 with organotin species and form TBP geometry around tin atom, which is dominant species at the physiological pH range. In the range of basic pH the hydroxo species, *viz.* ($Me_3Sn(OH)$ and $Me_2Sn(OH)_2$ were formed in significant amount [142]. The potentiometric study included the interaction between dimethyltin(IV)/diethyltin(IV) cations and amino acids at *I* = 0.1 M, $NaNO_3$, 298 K was reported by Shoukry et al. [143], which revealed the involvement of the $–NH_2$ group of the amino acid in the complexation with $(CH_3)_2Sn(IV)^{2+}$. Further the dimethyltin(IV) complexes were found more stable than diethyltin(IV) complexes which may be due to the steric crowding experienced by incoming ligand in the latter.

Jancsó et al. studied the coordination of DNA constituents (5'-GMP, 5'-ATP, 5'-d(CGCGCG)$_2$, D-ribose and 2-deoxy-D-ribose) with dimethyltin(IV) in aqueous medium, potentiometrically. The studies revealed the coordination of the phosphate group with organotin(IV) species occur in acidic medium and with hydroxy groups of the sugars of two nucleotides occur at basic pH, whereas the nitrogen bases of 5'-ATP and 5'-GMP could not be coordinated to dimethyltin(IV). According to the formation constant/stability constant calculation it has been revealed that triphosphates can coordinate more strongly than monophosphate with the metal. ^1H and ^{31}P NMR (1-D, 2-D) demonstrated that in the pH range 4.5–7 the phosphate groups of the DNA binds strongly with dimethyltin(IV), whereas the sugar and bases do not coordinate at this pH [144].

1.2.4. Organotin(IV) Complexes with Clinically used Drugs

The use of organometallic compounds as chemotherapeutics remained a fascinating concept because of the large possibility of the modification in their physical and chemical properties. The properties such as solubility, oxidation state, ligand exchange rate, balance between lipophilicity and hyhrophilicity can be modified, so as to increase the potency and decrease the side effects. The coordination of biologically and pharmacologically active molecules with metals could be the best way to design the new therapeutics with reduced toxicity, enhanced potency, lowering in therapeutic dose and avoiding drug resistance. Many researchers adopted

this idea and synthesized the complexes of organotin(IV) compounds with commercially available drugs in order to achieve the desired features. In this way the metal can stabilize the drug which in turn may help the metal complex in transportation in order to reach their potential target and avoid needless side reactions [145–147]. In the view of this a number of organotin(IV) complexes with commercially available drugs have been synthesized and many of them exhibited improved biological activities. Danish et al. [145] have found that the organotin(IV) complexes of antibiotic cefixime increase the efficacy of drug manyfold. Other complexes of organotin(IV) moieties with antibiotics such as penicillin-G, tetracyclines [23], cephalexin [148], amoxicillin, ampicillin, methacillin [149, 150] chloramphenicol and cycloserine [150] have been reported and few of them were exhibited good amount of cytotoxicity against *Ciona intestinalis, Ascidia malaca* and specrmatocyte chromosome of *Brachidontes pharaonis.* A number of complexes with non steroidal anti-inflammatory drugs (NSAIDs), such as tolfenamic acid [151], diclofenac [152], mefenamic acid [153], flufenamic acid [154], esters of anthranilic acid [155], and oxicam family NSAIDs; Piroxicam, Tenoxicam and Lornoxicam [156, 157] have been reported in the literature. Few crystal structures of complexes are shown in Fig. 1.13. The complexes of meclofenamic acid (Hmeclo) and its metal complexes, $[Me_2(Meclo)SnOSn(Meclo)Me_2]_2$ and $Ph_3Sn(Meclo)$ were screened against *Mycobacterium tuberculosis* H37Rv, among which $Ph_3Sn(Meclo)$ exhibited remarkable (92–100%) inhibitory activity with MIC values in the range of 3.13–0.78 μg/mL. Generally, compounds with MIC ≤ 1 μg/mL are considered as a novel class of compounds with an excellent lead [158]. The triphenyl esters of NSAIDs were screened against Vero cells, the $Sn(Ph)_3$ derivative of dmpa: [dmpa = [2-(2,3-dimethylphenylamino)benzoic acid] was found to exhibit significantly high cytotoxicity with IC_{50} = 1.89 μg/mL. Further, the triphenyl esters of anthranilic acids (menamic acid, tofenamic acid, flufenamic acid and diclofenac) were exhibited an appreciable anti-tuberculosis activity. Flufenamic acid (flu) and its organotin complexes were tested *in vitro* for anti-proliferative activity against A549 cancer cell line where its dibutyltin(IV) derivatives *i.e.* $[Bu_2(flu)SnOSn(flu)Bu_2]_2$ and $[Bu_2Sn(flu)_2]$ exhibited significant regression against tested cell line with ID_{50} value 0.24 ± 0.1 and 0.35 ± 0.1 μg/mL, respectively, which is lower than the international activity criterion for synthetic agents [157]. The NSAIDs from the class of fenamates, along with their $Ph_3Sn(IV)$ complexes *viz.* $Sn(Ph)_3$ (dmpa): [dmpa = [2-(2,3-dimethylphenylamino)benzoic acid] and $Ph_3Sn(mef)$: [mef = mefnamic acid] have been screened against A-549, L-929 (mouse fibroblast) , T-24 (bladder

cancer cell line) and MCF-7, which were exhibited a significant cytotoxicity against tested cell lines with IC_{50} values in the range from 0.2–60, 0.4–7, 0.3–5 and 0.2–27 μM against A-549, L-929, T-24 and MCF-7 cell lines, respectively. The activity of the molecules were seemed to be influenced by the structural as well as electronic factors of the complexes [151].

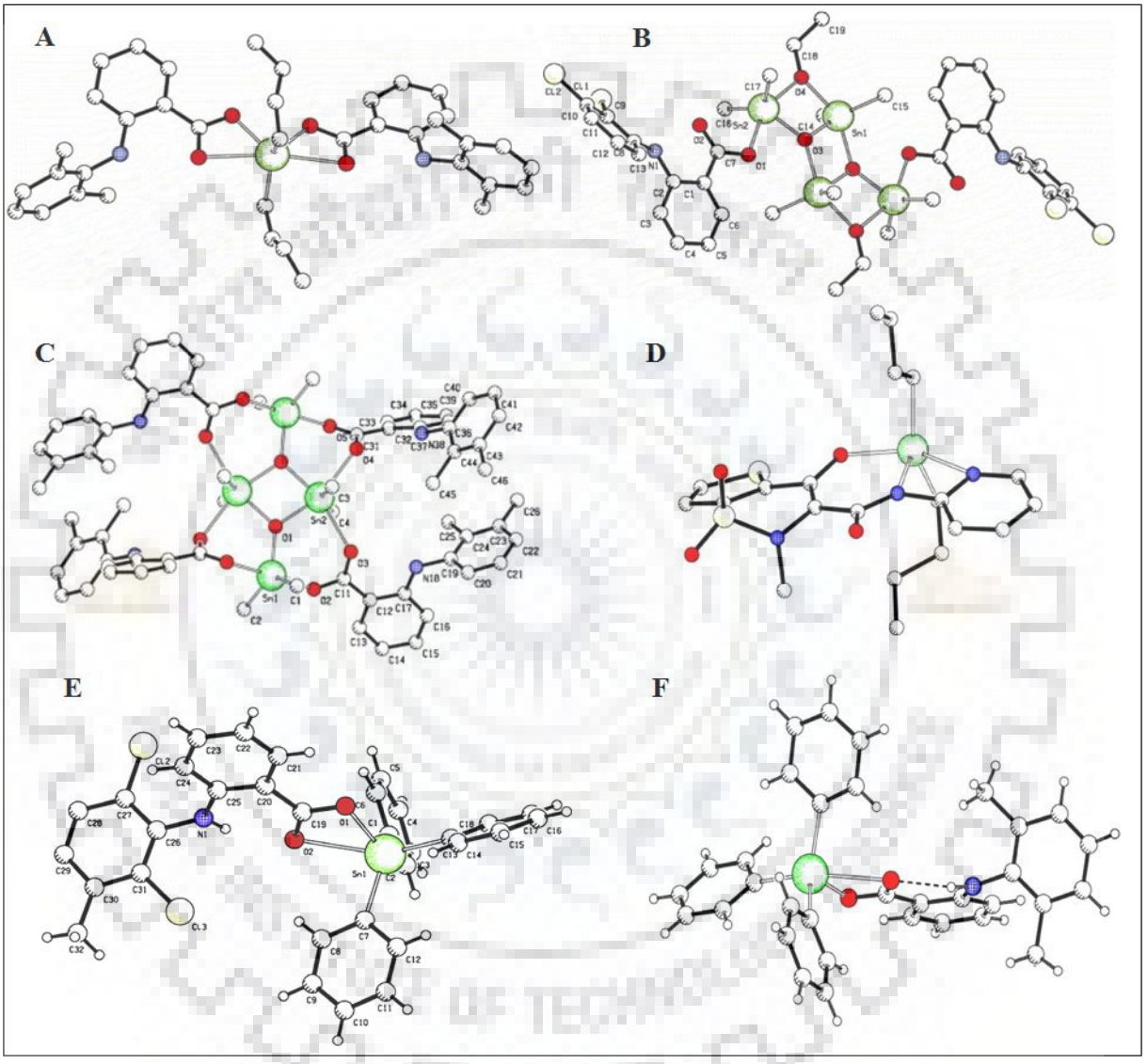

Fig. 1.13. Perspective view of (A) Bu_2Sn derivative of 2-(2,6-dimethylanilino)benzoic acid, (B) $[(Me_2Sn)_4(DCAB)_2)O_2(OC_2H_5)$, [HDCAB = 2-(2,3-dichloroanilino)benzoic acid, (C) $[Me_2Sn(mef)O(mef)SnMe_2]_2$, [Hmef = mefenamic acid], (D) $Bu_2Sn(tenox)]_n$, [tenox = tenoxicam], (E) $Ph_3Sn(meclo)$, [Hmeclo = meclofenamic acid] and (F) $Ph_3Sn(DMAB)$, [HDMAB = 2-(2,6-dimethylanilino)benzoic acid] [153].

The organotin complexes of the NSAID, indomethacin (Indo) with TBP geometry around the tin atom *viz.* $[Me_2(Indo)SnOSn(Indo)Me_2]_2$ and $[Bu_2(Indo)SnOSn(Indo)Bu_2]_2$ [159] and naproxen *viz.* $[Bu_2Sn(naproxen)_2]$ [160] have been synthesized and $Bu_2Sn(IV)$ complexes of naproxen were reported to exhibit sufficient antitumour activity against rat leiomyosarcoma cells (LMS) and human osteosarcoma (U2OS) [160]. Varshney et al. [161] synthesized the highly active Schiff bases of sulpha drugs against Gram-positive and Gram-negative bacteria *viz. Penicillium crysogenum, Aspergillus niger* and *Fusarium oxysporum*. Their tin complexes were found to exhibit more activity than ligands indicating an increase in the activity on metallation. Di- and triorganotin(IV) complexes of aspirin, paracetamol and metronidazol have been screened for antifungal activity on *Candida albicans* and for antibacterial activity against six strains of bacteria. The Bu_2Sn derivative of aspirin exhibited the activity against all the strains and Bu_3Sn(paracetamol) and Bu_3Sn(metronidazol) displyed the maximum zone of inhibition for bacterial strains. Bu_3Sn(metronidazol) with Oh geometry displayed the maximum antifungal activity among all the synthesized complexes [162].

A series of mono-, di- and triorganotin drivatives of the different NSAIDs *viz.* mefenamic acid, ibuprofen, anthranilic acid, flurbioprofen and ketoprofen with td geometry in solution state were tested against different fungal and bacterial strains, triorganotin(IV) derivatives were found to exhibit more activity against fungi. Diorganotin(IV) derivatives of flurbioprofen exhibited high activity against *Trichophyton longifusum*. All the monoorganotin derivatives were inactive against bacterial strains and di- and triorganotin complexes exhibited remarkable antibacterial activity against all the tested strains [163, 164].

These studies define a relationship between the activity of the organotin(IV) derivatives with the corresponding nature and structure of ligands and the nature of heteroatom (O, N and S) bonded to organotin(IV) moiety. Such a structural specificity instigates us to design new organotin complexes of commercially available drugs with potential chemotherapeutic value.

1.3. FORMULATION OF PROBLEM

The literature reviewed so far is helpful in understanding the importance of a huge number of organotin complexes, but the mode of action of these complexes inside the biological system is still a matter of debate. The inferences came out from the literature survey are listed herein:

1. As the organotin(IV) complexes with wide variety of structure and functions are being synthesized progressively in recent years, the studies which include the measurement and the characterization of different organotin species in the environment and inside the living system in order to understand their reactivity, toxicity and bioavailability, are of much interest. The biological behaviour of organotins in environment and biological system is totally species dependant hence, their speciation in aqueous medium and at physiological pH must be studied. Though, substantial work on speciation studies of organotin(IV) derivatives is already available in literature but the studies including drug molecules are sparsely known.
2. A huge number of organotin complexes with biologically important ligand molecules such as amino acids, carbohydrates, DNA constituents etc. have been reported and studies regarding their possible mode of action and DNA binding were available in the literature, but the similar studies of organotin(IV) complexes with commercially available drug molecules are very less. Complexation of organotin with non steroidal anti-inflammatory drugs (NSAIDs) and other easily available drugs either leads to an increase in the potency of drug molecules or acting as a bioactive entity with different functions altogether. The standard drugs would acts as effectual carrier of active organotin species at the site of action and when release from the complexes does not produce any side effect as they are already tested and well known about their action. In this way the drugs can produce their own action along with that of organotin species due to synergistic effect.
3. Designing new metallotherapeuticals with target specific action are demanding in present days. In order to explore the biological activities especially cytoyoxicity of the organotin-drug complexes and their course of interaction with DNA in relation to the structural features of the complexes have to be studied which is considerably rare in the literature.
4. Different mechanistic approaches of organotin(IV) complexes have been estimated with a variety of techniques, but the actual mode of action of organotins(IV) and their derivatives still remains a matter of discussion which should be explored further with related *in vitro* and *in vivo* studies.

1.4. WORK ORGANISATION

The organization of the present work is done in order to achieve the desired objectives and detailed studies are described in consecutive chapters.

1. The speciation study of di- and trimethytin(IV) moieties with a prodrug 2-mercaptoethane sulfonate (MESNA) in aqueous medium has been described in order to understand their interaction with each other to form different complex/hydrolyzed species and their bioavailability at physiological pH. The characterization of different species formed has been done by multinuclear (^{1}H, ^{13}C, ^{119}Sn NMR) NMR spectroscopy.
2. Further, to explore the chemistry of organotin(IV) moieties with MESNA in solid and solution state, organotin(IV) complexes with MESNA have been synthesized and their structural features were explored through elemental studies, FTIR, NMR (^{1}H, ^{13}C, ^{119}Sn) and mass spectroscopic studies. Their potential pertaining to the field of pharmaceutics has been studied *via* their DNA binding abilities through different photophysical studies.
3. Similar studies of organotin(IV) complexes of NSAIDs (Sulindac and Aspirin) and an anticoagulant drug (Warfain) have been carried out, to have an insight into their DNA binding potential pertaining to their structure activity relationship.
4. The cytotoxic potential of the designed complexes has been evaluated through MTT assay, against various cancer cell lines (DU145 (prostate adenocarcinom), MCF-7 (mammary cancer), HeLa (cervix cancer), LNCaP (androgen-sensitive human prostate adenocarcinoma) and HCT-15 (colon adenocarcinoma), of human origin.
5. An effort has been put to investigate the cause of cell death through acridine orange (AO)/ethidium bromide (EB) staining of cancer cells and DNA fragmentation assay with the complexes exhibited good cytotoxicity.

CHAPTER - 2

Material and Methods

2.1. MATERIALS

2.1.1. Solvents

For synthesis work specially dried absolute methanol (Rankem chemicals and S.D. Fine Chemicals limited) and benzene (Qualigens)/(ACS, AR) were used. For washing and recrystallization purpose solvents such as chloroform (Rankem, LR), acetone (Rankem, LR), ethanol (AR), *n*-hexane (S.D Fine), petroleum ether (b.p. 40–60 °C) (Qualigenes, LR), toluene (Merck) and acetonitrile (Sigma-Aldrich > 99.9 %) were used as received. DMSO (Rankem LR) was used for biological studies and HPLC grade acetonitrile (Sigma-Aldrich > 99.9 %) was used for recording ESI MS mass spectra.

2.1.2. Chemicals Used for Synthesis

Drugs: MESNA (Sigma Aldrich (99.9%)), Warfarin (Sigma Aldrich (98%)), Sulindac drug (Sigma Aldrich (98%)), Aspirin (Alfa Aesar (97%)), 1,10-phrnanthroline monohydrate (Himedia) and organotin compounds: dimethyltin(IV) dichloride (Sigma Aldrich (97%)), trimethyltin(IV) chloride (Sigma Aldrich (97%)), dibutyltin(IV) oxide (Merck), tributyltin(IV) chloride (Merck (96%)), diphenyltin(IV) dichloride (Sigma Aldrich (96%)), triphenyltin(IV) chloride (Merck (99%)) and dioctyltin(IV) oxide (Merck) were used for synthesis without further purification.

2.1.3. Chemicals Used for Biological Studies and Other Chemicals

3-(4,5-Dimethylthiazol-2-yl)-2,5-diphenyltetrazolium bromide (MTT) (Hi-media), phosphate buffer saline (PBS) (Himedia), Agarose (Himedia), isoamyl alcohol (Merck), RNAase 50X TAE buffer (Himedia), tris(hydroxymethyl) aminomethane (Genei), supercoiled pBR322 plasmid DNA (Genei), sodium salt of calf thymus DNA (CT DNA) (Himedia)/(Sigma Aldrich), NaCl (Merck), EDTA disodium salt (Thomas baker (99%)), glycerol (Merck (98%), bromophenol blue (Himedia (pH range 3.0–4.6)), boric acid (Glaxo laboratories (India)), ethidium bromide (Himedia (95%)), oxalic acid (Merck), NaOH (Thomas Baker, LR) sodium metal (Merck, LR), triethylamine (Rankem, AR) and KNO_3 (Merck) were used as received. Dry N_2 (Sigma Aldich) was used for thermal syntheses to maintain an inert atmosphere for optimum reaction conditions. The stock solution of CT DNA has been prepared in Tris–HCl/NaCl buffer (pH 7.2, 5:50 mM), which gave a UV absorbance band at 260 nm and purity of CT DNA was ascertained by using the ratio of absorbance at wavelength 260 nm to 280 nm, which was 1.86:1, indicated that the DNA was free from proteins. The concentration of CT DNA was analyzed by using absorbance obtained at 260 nm and an extinction coefficient of 6600 $dm^3\,mol^{-1}\,cm^{-1}$ [165].

2.2. INSTRUMENTATION AND METHODS

This section gives the details of instrumentation techniques and methods employed for characterization of the synthesized complexes and their interaction with DNA and other studies.

The melting points (m.p.) of the all synthesized complexes were determined with an OptiMelt, Automated melting point system (SRS) and were uncorrected.

2.2.1. Potentiometric Measurements and Calculation of Stability Constant

Orion 960 plus autotitroprocessor (equipped with a glass Orion Ross flow electrode) was used to carry out all the potentiometric measurements in aqueous media at 298.15 ± 0.1 K. Protonation constant of ligand and the formation constants of the complex species formed under given experimental conditions, were calculated with the help of a computer program, SCOGS by evaluating the pH-metric experimental data along with tentative values of the constants, ionic product of water (298.15 ± 0.1 K) and ionic strength (0.1 M KNO_3), which were given as inputs. The data obtained from the SCOGS program was used to draw the speciation curves (in Origin Pro 8.0 software) which can be used to elucidate various equilibria involved in complex formation. Further details of experimentation are described in Chapter 3.

2.2.2. Microwave Assisted Syntheses

Microwave assisted syntheses were carried out in an open glass vessel microwave oven (Magicook 20S (Galaxy) Whirlpool) with a rotating tray and having maximum microwave energy output of 800 W. The syntheses of organotin complexes were carried out by repeated irradiation of the finely ground homogeneous paste of precursors at different energy radiations in a small beaker or in Petri dish.

2.2.3. Density Functional Theory (DFT) Calculations

Geometry optimization and frequency calculation of synthesized complex molecules were accomplished with a Gaussian-09 and Gaussian-16 program package [166] provided by computer lab, Department of Chemistry, IIT Roorkee and frontier molecular orbitals were generated by using Gauss View 5.0 program. Computations were carried out with the B3LYP function and LANL2DZ basis set [167] was used to describe all the atoms including tin metal. The results of

calculations and Frontier molecular orbitals (HOMO-LUMO) generation were achieved by using Gauss View 5.0.

2.2.4. Elemental Analysis

Elemental analysis (carbon, hydrogen and sulfur) of all the complexes was carried out with a Vario MICRO V3.1.1 CHNS elemental analyzer at the Department of Chemistry, IIT Roorkee, India. Analysis of tin (Sn) content in all synthesized complexes was done gravimetrically by SnO_2 as previously reported [168]. The specific amount of sample (0.10 g) was treated with few drops of conc. H_2SO_4 acid in silica crucible followed by a mixture of conc. HNO_3 and conc. H_2SO_4 (3:2, v/v), which was then heated to evaporate the acid present and then ignited to form SnO_2, which was weighed.

2.2.5. Spectroscopic/Spectrophotometric Studies

2.2.5.1. Fourier Transform Infrared (FTIR) spectroscopy

Fourier Transform Infrared (FTIR) spectroscopy of the compounds were performed with a Thermo Nicolet (6700) FTIR spectrophotometer within a range 400–4000 cm^{-1} using KBr discs in the Department of Chemistry, IIT Roorkee.

2.2.5.2. Nuclear Magnetic Resonance (NMR) Studies

The ^{1}H NMR and ^{13}C NMR spectra were recorded with a JEOL Delta ECX, 400 MHz NMR spectrometer using TMS as an internal reference in solvent DMSO-d_6 and $CDCl_3$ at 25 °C in the Department of Chemistry IIT Roorkee, whereas ^{119}Sn NMR spectra were recorded with Bruker AVANCE (500.13 MHz) spectrometer using tetraphenyltin(IV) as an external reference in Institute Instrumentation Centre (IIC) at IIT Roorkee. ^{1}H, ^{13}C and ^{119}Sn NMR for characterization of species formed in potentiometric studies were recorded in H_2O–D_2O (9:1) solvent mixture at 298K. The water resonance was suppressed during the recycling delay for ^{1}H NMR. JEOL-Delta software package (version 5.0.4) was used for the purpose of NMR pulse sequences and data processing.

2.2.5.3. Electrospray Ionization (ESI) Mass Spectrometry

Electrospray ionization (ESI) mass spectra were recorded with a micrOTOF–Q II 10328, mass

spectrometer in Department of Chemistry, IIT Roorkee.

2.2.5.4. Electronic Absorption Spectrophotometric Studies

Electronic absorption spectra were recorded with a Shimadzu UV-1800, UV–visible spectrophotometer in a quartz cell (1 mL) having 1 cm path length, at Department of Chemistry, IIT Roorkee. Further details of methods employed and concentrations used for different compounds are mentioned in their respective Chapters.

2.2.5.5. Fluorescence Spectrophotometric Studies

The emission spectra were recorded with a HORIBA Scientific Fluoromax-4 Spectrophotometer, equipped with a xenon lamp, in a quartz cell of 1 cm path length, at Department of Chemistry, IIT Roorkee. Absorption and excitation slit widths were set as per requirement of the experiment. Further details of methods employed and concentrations used for studies are mentioned in the respective chapters.

2.2.6. Circular Dichroism (CD) Studies

The circular dichroism (CD) studies were carried out, using a Chirascan Spectropolarimeter (Applied Photophysics) equipped with xenon lamp source, the CD spectra were recorded at 25 °C in the range 200–400 nm with a quartz cuvette (400 μL) of 0.1 cm path length and the final spectra were obtained as an average of two repeats. Throughout the experiment the instrument was continuously purged with pure nitrogen gas with the help of nitrogen generator.

2.2.7. Viscosity Measurements

Viscosity measurements were carried out on an Anton Paar Rheometer (Anton Paar strasse 20804 Graz Austria) which was kept at 25 °C by a chiller unit and the pH of the solution was kept constant at 7.2 by diluting all the samples in Tris–HCl/NaCl buffer (pH = 7.2). A steel cone with 60 mm diameter and an angle of 2° was used for viscosity measurement.

2.2.8. Gel Electrophoresis Studies

The plasmid DNA cleavage experiments were carried out with a Genei submarine electrophoresis unit which can maintain a potential of 50–250 V and gels were visualized and photographed using

the Gel Documentation System (Bio-Rad, USA) at Department of Nanotechnology, IIT Roorkee.

2.2.9. Single Crystal X-Ray Diffraction Studies

The collection of single crystal diffraction data was carried out by using Bruker Kappa Apex-II diffractometer provided with a graphite monochromated Mo Kα radiation (λ= 0.71073 Å) source at room temperature at IIC, IIT Roorkee. A suitable sized crystal with dimentions 0.25 x 0.20 x 0.17 mm was mounted on glass fibre and used for acquisition of diffraction data. The crystal structure was solved by processing the diffraction data through Direct method with SIR-92 programme [169]. All the non hydrogen atoms were refined anisotropically, with a full matrix least-squares technique (based on F^2) using SHELXL-2014/6 programme [170]. The Mercury 3.8 software was used to generate the descriptive ORTEP and cell packing diagram.

2.3. BIOLOGICAL STUDIES

2.3.1. Antitumor Screening/Cytotoxicity Studies (MTT Assay)

Newly synthesized organotin(IV) complexes of different drugs were evaluated for cytotoxicity and cell viability *in vitro* against some cancer cell lines of human origin *viz.* HCT-15 (colon adenocarcinoma), HeLa (cervical cancer), DU145 (prostate cancer) cell lines, MCF-7 (breast cancer), LNCaP (androgen-sensitive prostate adenocarcinoma), Caco-2 (colorectal adenocarcinoma) along with human embryonic kidney cell line (used as a standard), which were purchased from National Center for Cell Science (NCCS) Pune, India. Analysis of cell viability was done through a calorimetric method based on MTT (3-[4,5-dimethylthiazole-2-yl]-2,5-diphenyltetrazolium bromide) [171], which on reduction yields MTT-formazan (purple in colour) crystals in living cells. DMSO/ethanol (depends on solubility) is used to prepare the stock solutions of complexes. On the first day of experiment, 5×10^3 (approximately) cells per well in 200 μL of culture medium were seeded into 96-well flat bottom microtitre culture plates (Corning, New York, USA) preincubated for 48 h at 37 °C in 8.5% CO_2 and cells were allowed to adhere. On next day dilutions of the test/reference compounds (organotin complexes) ranging from 0−200 mM were prepared in DMSO/ethnanol. On third day, a negative control (with same concentration of DMSO as used for preparing dilutions) and 50 μL of each dilution (test and reference) were added in triplicate to three consecutive wells and cell cultures were then incubated at 37 °C with 5% CO_2 for 24 h. On day 4, cultures were assayed by adding 10 μL (5 mg/mL) MTT and again incubated

for 4 h at 37 °C. After that the MTT containing media was aspirated and 200 µL DMSO and 25 µL sorensen glycine buffer (0.1 M of glycine and 0.1 M of NaCl, at pH 10.5) were added to lyse the cells and solubilise purple formazon. The absorbance values of the cell lysates were measured on a Dynatech MR 5000 microplate reader at 584 nm. The vehicle/negative control was added to acertain the non-cytotoxic nature of the solvent (DMSO/methanol) used for dilution preparation. *Cis*-platin and 5-fluorouracil (standard anticancer drugs) were used as standards.

The % inhibition was calculated as given below:

$$\% \text{ Inhibition} = \frac{\text{Mean OD of negative control} - \text{Mean OD of treated cells}}{\text{Mean OD of negative control}} \times 100$$

2.3.2. Acridine Orange (AO)/Ethidium Bromide (EB) Staining of Cells

Acridine orange/ethidium bromide staining of cancer cells were performed to ascertain the cause (apoptosis or necrosis) of cell death by analyzing the plasma-membrane permeability, nuclear morphology as well as the chromatin condensation. The assay was performed as described by Takahashi et al. [172] in which cells were stained with acridine orange (AO)/(100 µg/mL) /ethidium bromide (EB) (100 µg/mL of EB) dye mixture. The 6-well plate was seeded with 0.5×10^6 cells and incubated for 24 h by adding the test compounds at their respective IC_{50} values and *cis*-platin as positive control. The resultant mixture was washed with PBS and then the buffer-dye solution (500 µL of AO/EB dye mixture dissolved in PBS) was added to the plate and the cells were analysed under a fluorescent microscope (Ziess, Axiovert 25, Germany).

2.3.3. DNA Fragmentation Assay

The process of apoptosis leads to the DNA degradation at interlinked nucleosomal units, resulted into a step like structure comprises equal bands of DNA when subjected to gel electrophoresis [173, 174]. The cancer cells (3×10^6) were centrifuged after the treatment with inhibitory concentration (IC_{50} value) of the test compounds. The pellet of apoptotic and intact cell obtained after centrifugation were washed with PBS (phosphate buffer saline) and lysed with a 400 µL hypotonic lysis buffer (10 mM tris (pH, 7.4) + 10 mM EDTA + 0.2% triton X-100) for 15 min at ambient temperature. The cell containing buffer again centrifuged (13000 rpm) for 15 min from which 350 µL of supernatant was again lysed with 106 µL of digestion buffer (40 mM EDTA + 10 mM tris-HCl (pH, 8) + 1% SDS 150 mM NaCl + 0.2 mg/mL proteinase K) at 37 °C for 4 h. DNA

was extricate with chloform/phenol/isoamyl alcohol (25:25:1, v/v/v). The pellet thus obtained was washed with ethanol and again suspended for the digestion of RNA with RNAase (50 µg/mL) in digestion buffer (15 µL, 10 mM tris + 1mM EDTA (pH, 8.5)) at 37 ℃ for 1 h.

The DNA samples obtained were mixed with the loading dye, which were loaded onto the wells of agarose gel (0.8 % in TAE buffer) stained with ethidium bromide (2 µL from 10 mg/mL stock). The submerged electrophoresis was performed in running buffer (0.5X TAE) at 80 V for 1-2 h, which fractionates the DNA fragments. The gel was then photographed under a UV illuminator of gel documentation system.

CHAPTER - 3

Speciation and Multinuclear NMR Spectroscopic Studies of Di- and Trimethyltin(IV) Moieties with MESNA in Aqueous Medium

3.1. INTRODUCTION

A tremendous research has been done in the field of non-platinum chemotherapeutics in order to get a substitute for platinum based drugs because of their narrow spectrum of activity, a number of undesirable side effects, inherent intrinsic resistance and high cost [175]. Among other noteworthy non-platinum chemotherapeutic metallopharmaceuticals possibilities, organotin compounds have emerged as potential future pharmaceuticals as antitumor agents in the last 25 years [58, 104, 176-178]. The antitumor activity of the diorganotin compounds, R_2SnX_2 (X = halogen, O, S or N) is due to the of formation of $R_nSn^{(4-n)+}$ (n = 1 or 2) moiety which is believed to be an active species [179]. The nature of the coordinated ligand (X) and the ease of dissociation of Sn–X bond impart an important role in the transportation of these active species to the site of action [180] where it may bind with DNA or certain proteins. From the literature review [36, 97, 181] the importance of organotin compounds with S-containing ligands could not be denied due to their implication in cancer prophylaxis and can further be used for modeling of organotin binding to sulphur containing macromolecules.

Being a non-toxic drug, sodium 2-mercaptoethane sulfonate (MESNA) is known for its uroprotective effect in cancer chemotherapy, to reduce nephrotoxicity related to carboplatin [182] and *cis*-platin [183]. The interaction between MESNA and platinum metal complexes has been extensively studied under biological conditions [184], in addition to this MESNA also possesses strong mucolytic properties, alone or in combination with anti-inflammatory drugs [185]. Furthermore, complexes of rhenium and technetium-99m with MESNA have also been studied for radiopharmaceutical purposes [186]. Despite obvious biological activities of MESNA, very limited work has been done in the area of interaction of MESNA with metal ions in solid state and solution phase. The studies of interactions of organotin compounds with different ligands in various composition of natural water having varying ionic concentration pertaining to their environmental and biological interest, have been thoroughly studied by various research groups [41, 99, 141, 187–192]. Their solution equilibrium studies provide important information on the biospeciation of active organotin species and thus on their bioavailability. The wide success of organotin compounds in the area of chemotherapeutics and above mentioned interesting properties of MESNA toward biological systems attracted our attention to explore the organotin–MESNA system in aqueous medium to get an insight into the formation of possible species and their

structures. The present Chapter describes the equilibrium behavior and speciation model for the di- and trimethyltin(IV) and MESNA systems in aqueous solution, with 0.1 M KNO_3 over a wide range of pH. Scheme 3.1. represents the deprotonation of MESNA.

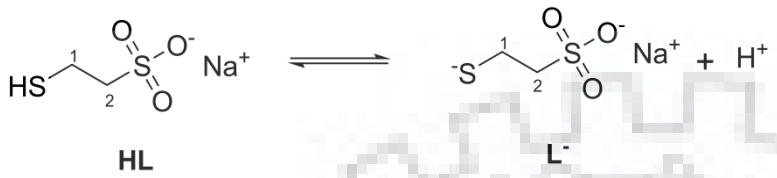

Scheme 3.1. Deprotonation of thiol group of MESNA.

3.2. EXPERIMENTAL SECTION

3.2.1. Safety Considerations

Di- and trimethyltin are toxic to aquatic life (Regulation (EC) No 1272/2008 [EU-GHS/CLP]), and corrosive in nature according to EU Directives 67/548/EEC or 1999/45/EC [41, 190]. They also cause hepatotoxicity and neurotoxicity, severe skin burns, eye damage and respiratory irritation. Trimethyltin chloride is more fatal and causes neuronal necrosis. So, all possible precautions have been taken to avoid direct contact to both di- and trimethyltin compounds. Proper clothing and necessary accessories like mask, safety glasses for eyes and gloves have been used during material handling. All tin containing waste materials have been disposed of in accordance with their material safety data sheet provided along with the chemicals.

3.2.2. Potentiometric Measurements

Orion 960 plus autotitroprocessor (equipped with a glass Orion Ross flow electrode) was used to carry out all the potentiometric measurements in aqueous media at 298.15 ± 0.1 K. Before each titration, the electrode was calibrated with standard buffer solutions of pH 4.0 ± 0.05, 7.0 ± 0.05 and 9.2 ± 0.05. The ionic strength of all the solutions was adjusted to 0.1 M by using aqueous KNO_3 solution. To exclude the atmospheric CO_2 and O_2 from the solutions being titrated, a purified nitrogen gas was bubbled with continuous stirring. Different sets of solution (50 mL) were prepared and titrated potentiometrically with standard NaOH solution (0.1 M) (carbonate free) up to pH 10.5–11.05 (40–60 data points) in aqueous media, are mentioned below:

a) 2.0×10^{-3} M (HL) and 0.1 M KNO_3

b) 2.0×10^{-3} M Me_3SnCl/Me_2SnCl_2 and 0.1 M KNO_3

c) Me_2SnCl_2/ Me_3SnCl to (HL) ratio in mixture was varied from 1:1 to 1:2

(2.0×10^{-3} M Me_3SnCl/Me_2SnCl_2 2.0×10^{-3} M (HL) and 0.1 M KNO_3 for 1:1 and 2.0×10^{-3} M Me_3SnCl/Me_2SnCl_2 4.0×10^{-3} M (HL) and 0.1 M KNO_3 for 1:2 solution mixture).

No precipitation was observed under the studied concentration range of ligands in the presence of Me_2Sn^{2+}/Me_3Sn^{+}. The pH-metric data obtained from titrating solution mixtures (**a**), (**b**) and (**c**) were utilized in the calculation of protonation constant of (HL), the hydrolysis constants of Me_2Sn^{2+}/Me_3Sn^{+} and the formation constants of the various complex species formed in Me_3SnCl/Me_2SnCl_2–(HL) systems, respectively. In order to check the reproducibility of the results each set of solutions mentioned above was titrated twice.

The species formed in the studied systems were characterized by the general equilibrium process 3.1, whereas Eq. 3.1a gives the formation constants for these generalized species:

$$pM + qL + rH \rightleftharpoons M_pL_qH_r \qquad (3.1)$$

$$\beta pqr = [M_pL_qH_r] / [M]^p[L]^q[H]^r \qquad (3.1a)$$

Equilibrium 3.2a/3.2b, describe the hydroxo species formation and their formation constants are given by Eq. 3.2c.

$$pM + qL \rightleftharpoons M_pL_qH_{-r} + rH \qquad (3.2a)$$

$$pM + qL + rOH \rightleftharpoons M_pL_q(OH)_r \qquad (3.2b)$$

$$\beta_{M_pL_qH_{-r}} = \frac{[M_pL_qH_{-r}][H]^r}{[M]^p[L]^q} = \frac{[M_pL_q(OH)_r](K_W)^r}{[M]^p[L]^q[OH]^r} = \beta_{M_pL_q(OH)_r}(K_W)^r \qquad (3.2c)$$

Where, M = $[Me_2Sn]^{2+}/[Me_3Sn]^{+}$, L = non-protonated ligand/deprotonated ligand and H = proton, and *p* and *q* are positive integers or zero; *r* is positive for a protonated species and negative for hydroxo species. Charges are omitted to avoid the complexity of equation, which can be calculated easily, as fully protonated neutral ligand under study is abbreviated as HL *i.e.* undissociated sodium 2-mercaptoethane sulfonate, $HSCH_2\text{-}CH_2\text{-}SO_3Na$ (MESNA).

Protonation constant of ligand and the formation constants of the complex species formed under given experimental conditions, were calculated with the help of computer program, SCOGS [20–23] by evaluating the pH-metric experimental data along with tentative values of the constants, ionic product of water (298.15 ± 0.1 K) and ionic strength (0.1 M KNO_3), which were given as inputs [20–23]. The values refined through the several iterations, and corresponding to minimum standard deviation are accepted as final. The values of standard deviation for final set of log β values, for different systems *i.e.* Me_3SnCl-HL(1:1), Me_3SnCl-HL(1:2), Me_2SnCl_2-HL(1:1) and Me_2SnCl_2-HL(1:2) are 0.0713, 1.5734, 0.0755, 0.1345, respectively. The data obtained from the SCOGS program was used to draw the speciation curves (in Origin Pro 8.0 software) which can be used to elucidate various equilibria involved in complex formation.

3.2.3. NMR Measurements

^{1}H and ^{13}C NMR were recorded at operating frequency 399.78 and 100.52 MHz, respectively, on a Jeol Delta ECX (400 MHz) NMR spectrometer and ^{119}Sn NMR were recorded at 186.50 MHz on a Bruker Avance (500 MHz) NMR spectrometer using tetraphenyltin(IV) as an external reference in H_2O–D_2O (9:1) solvent mixture at 298K. JEOL-Delta software package (version 5.0.4) was used for the purpose of NMR pulse sequences and data processing. The experimental parameters for $^{1}H/^{13}C$ NMR were as follows: spectral width 30/250 ppm, number of data points 6554/52428, number of scans 64/4000, acquisition time 0.27 /1.04 s, relaxation delay 3s/2s, and 90° pulse width 6.5/10 μs. For ^{119}Sn NMR, spectral width is 540 ppm, number of data points 65536, number of scans for Me_3SnCl-HL/Me_2SnCl-HL system are 2000-4000/4000-8000 and acquisition time 0.33 s. The water resonance was suppressed during the recycling delay for ^{1}H NMR.

3.3. RESULTS AND DISCUSSION

3.3.1. Potentiometric Measurements

MESNA was assumed a monoprotic ligand which coordinated to Sn metal by dissociating a proton which is attached to S-atom of the thiol group. No protonation of the drug has been occurring during the course of titration in the studied pH range. Change in pH of different solution sets with increasing volume of NaOH is represented by Fig. 3.1. Table 3.1 presents the calculated values of protonation constant of MESNA, stability constant/formation constant of Me_2SnCl_2/Me_3SnCl–(HL) (1:1) and (1:2) systems and hydrolysis constants of various organotin hydroxo species. The

protonation constant of MESNA [193] and hydrolysis constants of organotin species are calculated in the present study which are in fair agreement with that of already reported in literature [188, 194, 195]. Speciation diagrams of Me_2SnCl_2–(HL) (1:1) and (1:2) systems are given in Fig. 3.2 (a) and (b) respectively and Fig. 3.3 (a) and (b) represent Me_3SnCl–(HL) (1:1) and (1:2) systems, respectively.

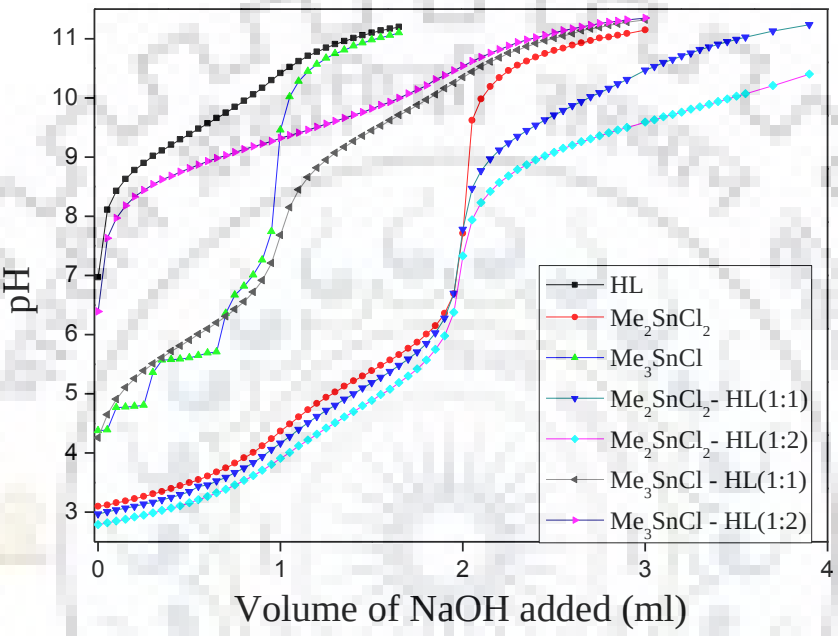

Fig. 3.1. Change in pH of different systems with increasing volume of NaOH.

3.3.1.1. Dimethyltin(IV)-(HL) System

The cation, Me_2Sn^{2+} was extensively hydrolyzed to form a series of mono- and polynuclear hydroxo species i.e. ($[Me_2Sn(OH)]^+$, $[Me_2Sn(OH)_2]$, $[Me_2Sn(OH)_3]^-$, $[(Me_2Sn)_2(OH)_2]^{2+}$ and $[(Me_2Sn)_2(OH)_3]^+$) [27], which is represented by the general equilibrium 3.3.

$$x Me_2Sn^{2+} + y H_2O \rightleftharpoons \{(Me_2Sn)_x(OH)_y\}^{(2x-y)+} + y\, H^+ \qquad (3.3)$$

(Where x = 1, y = 1, 2, 3; x = 2, y = 2, 3; x = 3, y = 4; x = 4, y = 6).

In present study, the hydrolysis of Me_2SnCl_2 has been investigated in the pH range 3.0 −11.0 at 298.15 ± 0.1K and I = 0.1 M KNO_3 and calculated $\log_{10} \beta$ values for hydrolysed species (Table 3.1) are in fair agreement with the values reported by Stefano et al. [194]. Occurrence of very high

Table 3.1. Protonation constant ($\log_{10} K$) of ligand (Mesna), formation constants ($\log_{10} \beta$) of the organotin(IV) complexes and hydrolysis constants of the dimethyltin(IV) and trimethyltin(IV) cations at 298.15 ± 0.1 K, I = 0.1 M KNO_3 ; $\beta_{pqr} = [M_pL_qH_r]/[M]^p[L]^q[H]^r$; Standard deviations given in parentheses.

Species			$\log_{10} K$/ $\log_{10} \beta$
(HL)			
p q r			$H^+ + (L)^- = HL$
011	$\log_{10} \beta$ (HL)		9.54 (0.2)[a], 9.08[b]
pK_1 (HL) = $\log_{10} \beta_{011}$			
$Me_2Sn(IV)$-(HL)(1:1) and (1:2)			
110	$\log_{10} \beta$	$[Me_2Sn(L)]^+$	9.62 (3)[a]
11–1	$\log_{10} \beta$	$[Me_2Sn(L)(OH)]$	4.53 (1)[a]
12–1	$\log_{10} \beta$	$[Me_2Sn(L)_2(OH)]^-$	8.20 (2)[a]
$Me_3Sn(IV)$-(HL) (1:1) and (1:2)			
110	$\log_{10} \beta$	$[Me_3Sn(L)]$	6.12 (2)[a]
11–1	$\log_{10} \beta$	$[Me_3Sn(L)(OH)]^-$	–3.57 (3)[a]
Hydrolysis Constants			
		$Me_2Sn(IV)^{2+}$	$Me_3Sn(IV)^+$
10 –1	β	$[Me_2Sn(OH)]^+$	–3.16 (3)[a] (–3.12)[c] β $[Me_3Sn(OH)]$ –6.12 (0.1)[a] (–6.26)[d,e]
10 –2	β	$[Me_2Sn(OH)_2]$	–8.60 (3)[a] (–8.43)[c] β $[Me_3Sn(OH)_2]^-$ –18.87 (0.1)[a] (–17.63)[d]
10 –3	β	$[Me_2Sn(OH)_3]^-$	–19.82 (4)[a] (19.45)[c]
20 –2	β	$[(Me_2Sn)_2(OH)_2]^{2+}$	–5.28 (2)[a] (–5.05)[c]
20 –3	β	$[(Me_2Sn)_2(OH)_3]^+$	–10.00 (5)[a] (–9.75)[c]

[a] This work; [b] Ref. [188];[c] Ref. [189];[d] Ref. [97]; [e] Ref. [41]

value of standard deviations during calculation by SCOGS program due to inclusion of polynuclear organotin-hydroxo species such as $(Me_2Sn)_2(OH)_4$, $[(Me_2Sn)_3(OH)_4]^{2+}$, $[(Me_2Sn)_4(OH)_5]^{3+}$ and $[(Me_2Sn)_4(OH)_6]^{2+}$, reported by Natsume *et al.* [179], leads to their rejection in present study. Formation of latter species is totally concentration dependent whereas present experimental concentration does not allow their formation. A number of species, *viz.*

$[Me_2Sn(L)]^+$, $[Me_2Sn(L)(OH)]$, $[Me_2Sn(L)_2(OH)]^-$, $[Me_2Sn(OH)]^+$, $[Me_2Sn(OH)_2]$, $[Me_2Sn(OH)_3]^-$ $[Me_2Sn\ (LH_{-1})]^+$, $[Me_2Sn(LH_{-1})(OH)]$, $[Me_2Sn(L)(OH)_2]^-$, $[Me_2Sn(L)_2]$ and $[SnMe_2(L)_2(OH)_2]^{2-}$ are considered for 1:1 and 1:2, Me_2Sn(IV):(HL) systems but introduction of last five species in species matrix resulted in a very high standard deviation, hence their formation is ruled out in present study. The hydrolysis products of Me_2SnCl_2 and complexes formed in the solution mixture were completely soluble at this concentration over the studied pH range, and there was no precipitation observed during titration with HL at given concentration of 1:1 and 1:2 (metal:ligand) systems.

A small amount of unreacted Me_2Sn^{2+} metal remained in mixture solution at initial pH which later consumed completely till pH ~ 5. Complex ion, $[Me_2Sn(L)]^+$ (43.3 % in 1:1 and 61.9 % in 1:2 system) with high value of formation constant ($\log_{10}\beta$ = 9.62 ± 0.2), exists at initial pH ~ 3.0, which was formed by the reaction of Me_2Sn^{2+} with one mole of HL according to Eq. (3.4a). Strong complexation tendency of deprotonated thiol group of MESNA towards Me_2Sn^{2+} suppresses its hydrolysis to a large extent. Disappearance of thiol proton resonance in ^{1}H NMR spectra of equilibrium mixture at all pHs provides an evidence for the coordination of the ligand *via* thiol group of ligand. With an increase in pH of solution mixture, extent of $[Me_2Sn(L)]^+$ species first increases and goes up to maximum (53.1 % in 1:1 and 75.6 % in 1:2 system) at pH ~ 3.75. Further addition of alkali leads to formation of a mixed ligand–hydroxo species $[Me_2Sn(L)(OH)]$ (Eq. 3.4b), which is predominating at pH ~ 7 (67.2 % in 1:1 and 89.9 % in 1:2 system), formed by the deprotonation of one of the H_2O molecules [179] coordinated to $[Me_2Sn(L)]^+$. Further replacement of water molecule by deprotonated ligand in latter species form $[Me_2Sn(L)_2(OH)]^-$ (Eq. 3.4c), with its highest percentage in basic medium, at pH~10.4 (29.4 % in 1:1 and 38.5 % in 1:2 system).

$$Me_2Sn^{2+} + HL \rightleftharpoons [Me_2Sn(L)]^+ + H^+ \quad (3.4a)$$

$$[Me_2Sn(L)]^+ + OH^- \rightleftharpoons [Me_2Sn(L)(OH)] \quad (3.4b)$$

$$[Me_2Sn(L)(OH)] + HL \rightleftharpoons [Me_2Sn(L)_2(OH)]^- + H^+ \quad (3.4c)$$

$$Me_2Sn^{2+} + OH^- \rightleftharpoons [Me_2Sn(OH)]^+ \quad (3.5a)$$

$$[Me_2Sn(OH)]^+ + OH^- \rightleftharpoons [Me_2Sn(OH)_2] \quad (3.5b)$$

$[Me_2Sn(L)(OH)] + OH^- \rightleftharpoons Me_2Sn(OH)_2 + (L)^-$ (3.5c)

$Me_2Sn(OH)_2 + OH^- \rightleftharpoons [Me_2Sn(OH)_3]^-$ (3.5d)

Apart from this, the hydroxy species of metals are also formed (shown by Eqs. 3.5a, 3.5b, 3.5c and 3.5d) in solution mixture and co-exist with complex species but, in lesser amount and at higher pH in comparison to that in hydrolysis of pure metal. However, the formation of $Me_2Sn(OH)_2$ which is predominating at pH 10.4 (49.3 % for 1:1 and 27.6 % for 1:2 systems), also takes place (Eq. 3.5c) slowly with the release of the $(L)^-$ (25.4 % for 1:1 and 41 % for 1:2 systems) from the complexes. The species distribution diagram for 1:1 and 1:2 systems are shown in Fig. 3.2 (A) and Fig. 3.2 (B), respectively. Above pH~9, further hydrolysis takes place, resulting $[Me_2Sn(OH)_3]^-$ (28.6 % for 1:1 and 27.6 % for 1:2 system at pH 10.4), according to Eq. 3.5d. Similar complex species have been formed in both 1:1 and 1:2 systems with only difference in their percentage/amount, which is higher for 1:2 system, and hydrolysed species (slightly lower for 1:2 system), which can be clearly represented by the species distribution curves as shown in Fig. 3.2 (A) and 3.2 (B), respectively. A higher percentage of complex species in case of 1:2 system as compared to 1:1 system, at same pH, probably due to the higher concentration of the ligand in 1:2 system. A competitive existence among complex species and metal hydroxides has been observed throughout the studied pH range.

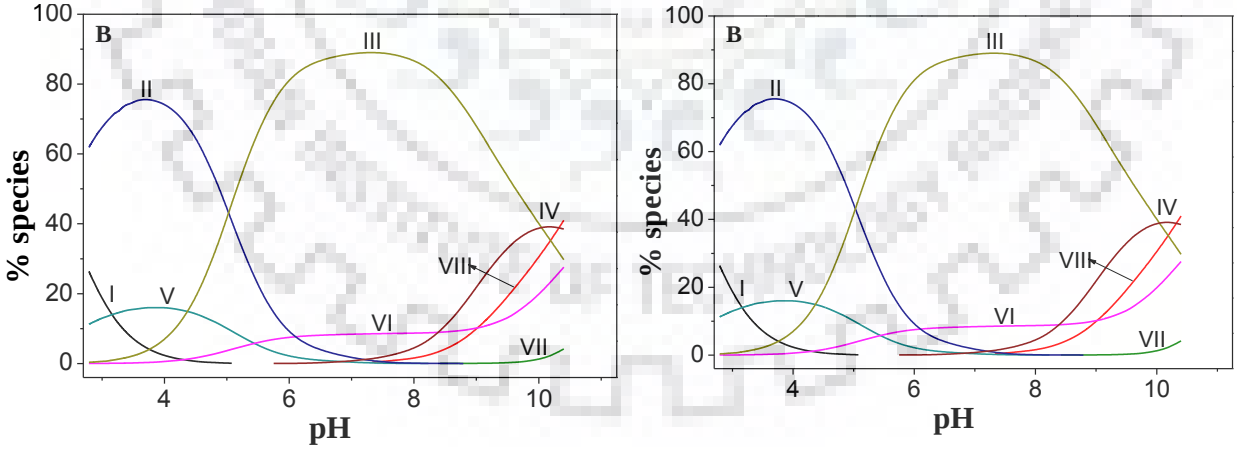

Fig. 3.2. Speciation diagram for $Me_2Sn(IV)$–(HL) (A) 1:1 and (B) 1:2 (metal:ligand) systems, where I $[Me_2Sn]^{2+}$; II $[Me_2SnL]^+$; III $[Me_2SnL(OH)]$; IV $[Me_2SnL_2(OH)]^-$; V $[Me_2Sn(OH)]^+$; VI $[Me_2Sn(OH)_2]$; VII $[Me_2Sn(OH)_3]^-$; VIII $[L]^-$.

3.3.1.2. Trimethyltin(IV)-(HL) System

Formation of binuclear species during hydrolysis of Me_3SnCl was found in fairly concentrated solution, which was evidenced by various reports available in literature [103, 180]. Whereas, only momonuclear species, $[Me_3Sn(OH)]$ and $[Me_3Sn(OH)_2]^-$ have been observed in the present model. Following equilibrium (3.6) represents hydrolysis of Me_3Sn^+(IV) system.

$$[Me_3Sn\,(H_2O)_2]^+ + H_2O \rightleftharpoons [Me_3Sn\,(H_2O)(OH)] + H_3O^+ \qquad (3.6)$$

The calculated $\log_{10}\beta_{10-1}$ value for hydrolysis products, $[Me_3Sn(OH)]$ and $[Me_3Sn(OH)_2]^-$ are in fair agreement with the previously reported values obtained in 0.1 M KNO_3, and are presented in Table 3.1. No polymeric species has been observed in the studied concentration range.

In case of 1:2 (Metal:Ligand) system, the initial pH of solution mixture is 6.18, which is high in comparison to the initial pH of 1:1 system (pH = 4.22). This may be due to the double amount of ligand ($HS\text{-}CH_2\text{-}CH_2\text{-}SO_3Na$) present in the solution. In Me_3Sn(IV)-(HL) system very high amount of unreacted metal was present at pH = 4.26, which was consumed slowly and completely reacted or hydrolysed till pH = 8.75 ± 0.07 in both the (1:1 and 1:2) systems. The complex species, $[Me_3Sn(L)]$ was formed (Eq. 3.6a), which is predominating at pH = 7.65 ± 0.03 (37% for 1:1 and 57.4% for 1:2 system). Further addition of alkali leads the conversion of $[Me_3Sn(L)]$ into a mixed ligand-hydroxo species, $[Me_3Sn(L)(OH)]^-$ according to Eq. (3.6b) as pH increases beyond 6.8 ± 0.41, and increases gradually as pH reaches at 11.0 (30.2% for 1:1 and 46.5% for 1:2 system), as shown in the species distribution curve (Fig. 3.3 (A) and Fig. 3.3 (B). In 1:2 system a very small amount (1.57%) of $[Me_3Sn(L)_2(OH)]^{2-}$ was also formed (Eq. 3.6c) unlike 1:1 system. Monohydroxide species, $[Me_3Sn(OH)]$ persists throughout the titration in the experimental pH range (4.26 to 11.0) whereas dihydroxy species, $[Me_3Sn(OH)_2]^-$ came into existence at pH ~ 10 and is present in an extremely low concentration, formed according to Eq. 3.7a and 3.7b, respectively. Along with all these species free ligand species is also present in both the systems.

$$(Me_3Sn)^+ + (HL) \rightleftharpoons [Me_3Sn(L)] + H^+ \qquad (3.6a)$$

$$[Me_3Sn(L)] + OH^- \rightleftharpoons [Me_3Sn(L)(OH)]^- \qquad (3.6b)$$

$$[Me_3Sn(L)(OH)]^- + HL \rightleftharpoons [Me_3Sn(L)_2(OH)]^{2-} + H^+ \qquad (3.6c)$$

$(Me_3Sn)^+ + OH^- \rightleftharpoons [Me_3Sn(OH)]$ (3.7a)

$[Me_3Sn(OH)] + OH^- \rightleftharpoons [Me_3Sn(OH)_2]^-$ (3.7b)

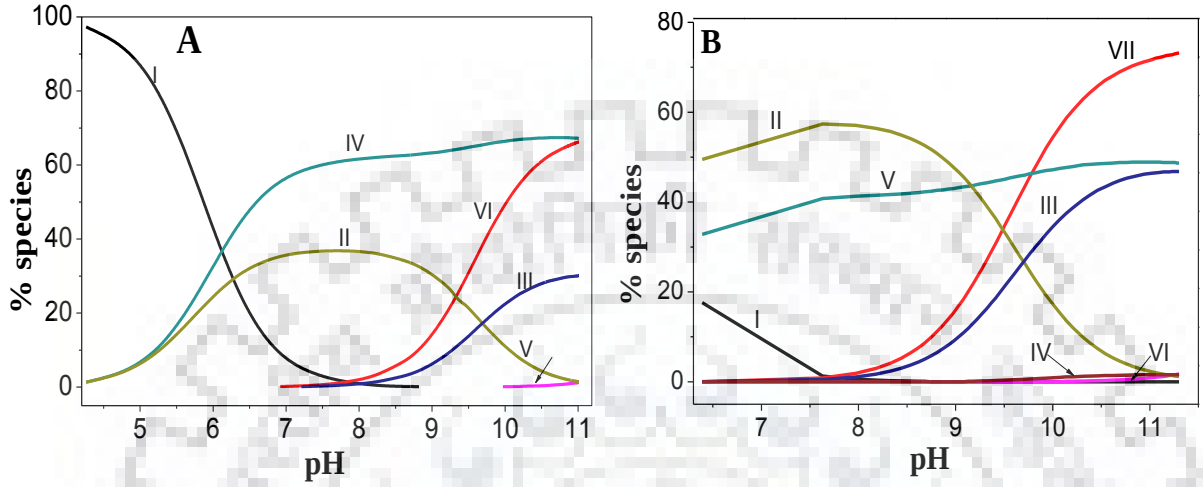

Fig. 3.3. Speciation diagram for (A) 1:1 and (B) 1:2, Me_3Sn(IV)-(HL) systems Where I $[Me_3Sn]^+$; II $[Me_3SnL]$; III $[Me_3SnL(OH)]^-$; IV $[Me_3Sn(OH)]$; V $[Me_3Sn(OH)_2]^-$; VI $[L]^-$; VII $[Me_3Sn(OH)_3]$.

3.3.2. Multinuclear NMR Studies

The multinuclear (^1H, ^{13}C and ^{119}Sn) NMR spectra of mixture solutions recorded at different pH proved to be an important tool to support the existence of different species in the given experimental conditions and to propose their possible geometry. In order to obtain high quality spectra within a normal detection time interval, the ^1H NMR was recorded with concentration, [M] = 1.0×10^{-2} M and [HL] = $(1.0–2.0) \times 10^{-2}$ M, ^{13}C NMR experiments were performed by increasing the concentration to two fold, [M] = 2.0×10^{-2} M and [HL] = $2.0–4.0 \times 10^{-2}$ M, which was further increased two fold to record the ^{119}Sn NMR. Concentrations were optimized to avoid the precipitation during the NMR experiments, despite this, turbidity was appeared in Me_2Sn(IV)–HL (1:2) system after pH 7.4, during the time required to record ^{119}Sn NMR spectra. The values of chemical shifts (ppm), two bond heteronuclear couplings constant $^2J(^1H–^{119}Sn)$ obtained from ^1H NMR data, along with the values of ∠C–Sn–C which are calculated by using the Lockhart and Manders equations [196] are presented in Table 3.2. ^{13}C and ^{119}Sn NMR data are given in Table 3.3 and Table 3.4, respectively. Some representative ^1H NMR, ^{13}C NMR spectra are presented in Fig 3.4 to Fig. 3.6. ^1H, ^{13}C and ^{119}Sn NMR data are provided in Table 3.5 and

Table 3.6. The chemical shifts and coupling constants $^{2}J(^{1}H–^{119}Sn)$ values obtained from ^{1}H and ^{13}C NMR data as well as expected geometries of hydroxo species were compared with the already reported values given by Surdy et al. [197]. ^{119}Sn NMR resonances of the different hydrolyzed species of di- and trimethyltin cations were also compared with values which are already reported [98]. ^{119}Sn NMR spectra for Me_2Sn–(HL) (1:1) and (1:2) systems are presented in Fig 3.7.

3.3.2.1. NMR measurements of Dimethyltin(IV)-(HL) System

Despite the existence of more than one species in the solution mixture only one sharp resonance of methyl proton was obtained this is due to the fact that the species formed at a particular pH are in fast mutual exchange relative to the NMR timescale. Line widths of methyl proton are found in the range 3.85–22.18 Hz. The resonances for the different species and the free ligand can be observed from the ^{1}H NMR spectra. With the increase in the pH of the solution, ^{1}H NMR spectra of both 1:1 and 1:2 $Me_2Sn(IV)$–(HL) systems revealed a shift in methyl (bound to Sn) proton, towards higher fields and a decrease in values of $^{2}J(^{1}H–^{119}Sn)$ coupling constants. A similar trend has already been reported in Me_2Sn–captopril/dipeptide/heterocyclicthiones systems [99, 141, 197]. Two sets of chemical shift values corresponding to ligand were obtained from ^{13}C NMR, which clearly indicated the presence of more than one species but the coupling constant due to broadening of CH_3–Sn signal, could not be determined. Information regarding possible coordination number around Sn metal was obtained from calculated values of ∠C–Sn–C, which was further confirmed from ^{119}Sn NMR spectra recorded at different pHs. Chemical shift value (δ) in the range 200 to –60 ppm, –90 to –190 ppm and –210 to –400 ppm corresponds to four, five and six coordination number around Sn centre [198]. In $Me_2Sn(IV)$–(HL) system at pH 4.5 ± 0.2, the calculated average ∠C–Sn–C (°) is 132±1, which could not clearly indicate the presence of octahedral (Oh) or trigonal bipyramidal (TBP) geometry with axial/equatorial methyl groups. This intermediate value is probably due to, either simultaneous existence of both distorted Oh and TBP geometries in fast mutual exchange, or the presence of a highly distorted Oh structures, as found in case of the hydrolysis of $Me_2Sn(IV)^{2+}$ [199] and $Me_2Sn(IV)^{2+}$ captopril/dipeptide systems [141, 197].

In $Me_2Sn(IV)$–(HL) (1:1) system, at pH ~ 4.5 predominant species are $[Me_2Sn(L)]^{+}$ and $[Me_2Sn(OH)]^{+}$ having methyl (bound to Sn) protons resonance at δ = 0.77 ppm, further downfield shift in methylene protons resonance of ligand indicate the formation of $[Me_2Sn(L)]^{+}$/ $[Me_2Sn(OH)]^{+}$ species. Corresponding ^{13}C NMR chemical shifts of these species are observed at δ

= 5.06 ppm. Observed ^{2}J ($^{1}H–^{119}Sn$) and calculated value of ∠C–Sn–C for $[Me_2Sn(L)]^{+}$ complex species are 84 Hz and 136°, respectively, which indicate highly distorted Oh geometry of complex species with methyl groups at *cis* position which might be in equilibrium with its *trans* counterpart (Scheme 3.2 b1/b2), which is also supported by the occurrence of splitted ^{1}H NMR signal of methyl at low temperature (5 °C/15 °C) (Fig. 3.8). ^{119}Sn NMR chemical shift values at 331.45±2.54 ppm indicated the presence of two species, with Oh geometry. At pH ~ 7, $[Me_2Sn(L)(OH)]$ is predominating species along with $[Me_2Sn(OH)_2]$, with methyl ^{1}H and ^{13}C resonances at –0.68±0.03 ppm and 3.66 ppm, respectively. Both the species co-existed in relatively slow equilibrium which could be explained by very high value of line width (22.18) of methyl proton. $^{2}J(^{1}H–^{119}Sn)$ could not be calculated for these species due to line broadening. ^{119}Sn NMR chemical shift value at δ = –173.84 ppm and 36.84 ppm revealed the existence of species with TBP geometries and tetrahedral (td) geometries of $[Me_2Sn(L)(OH)]$ and $[Me_2Sn(OH)_2]$, respectively (Scheme 3.2(c), (e)). Furthermore, the existence of another species, $[Me_2Sn(L)_2(OH)]^{-}$ and $[Me_2Sn(L)(OH)]$ at pH ~ 9.5 with TBP geometry was revealed by methyl proton resonance at 0.64 ppm, ^{13}C NMR at 0.86 ppm and calculated ∠C–Sn–C = 123°, which was further confirmed by ^{119}Sn NMR chemical shift value at δ = –173.73 ppm. Around pH ~ 11.0 the species exhibits a ^{1}H NMR shift at δ = 0.63 ppm with $^{2}J(^{1}H–^{119}Sn)$ = 74 Hz, ∠C–Sn–C = 124° and ^{119}Sn chemical shift value at δ = –147.70 ppm, suggesting a distorted TBP geometry of $[Me_2Sn(L)_2(OH)]^{-}$ (Scheme 3.2(d). The resonance at δ = 91.76 ppm in ^{119}Sn NMR may be attributed to $[Me_2Sn(OH)_2]$ (Scheme 3.2(e)). As already explained, for $Me_2Sn(IV)$–HL (1:1) and (1:2) systems similar species have been existed in the given experimental conditions with only difference in their percentage amount, which was clearly indicated by ^{1}H, ^{13}C and ^{119}Sn NMR data and percentage of species at given pH as given in Tables 3.2, 3.3 and 3.4, respectively.

3.3.2.2. NMR measurements of Trimethyltin(IV)-(HL) System

In aqueous solution $(CH_3)_3Sn(IV)$ cation may exhibit a TBP geometry [200], with three methyl groups in equatorial positions and two water molecules in axial positions (Scheme 3.3(a)). Formation of complexes takes place when water molecule was displaced by ligand molecule. However, as a result of the fast equilibrium between different methyl positions relative to the NMR time scale, an average value of $^{2}J(^{1}H–^{119}Sn)$ was obtained. Presence of multiple methyl proton (bound to tin) resonances of varying intensities in the ^{1}H NMR spectra at different pHs (Table 3.2)

for $Me_3Sn(IV)$–HL system indicates the presence of more than one species in the solution. In both, (1:1) and (1:2) systems similar complex species were formed, which were revealed by ^{1}H, ^{13}C and ^{119}Sn NMR data as presented in Tables 3.2, 3.3 and 3.4, respectively.

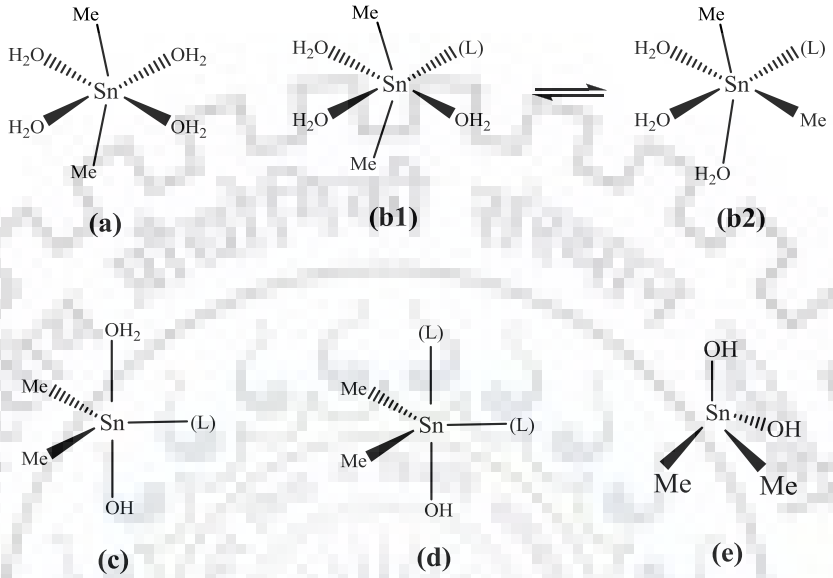

Scheme 3.2. Possible geometrical structures of dimethyltin(IV)-(HL) complex species: (a) $[Me_2Sn(H_2O)_4]^{2+}$, (b1/b2) isomers of $[Me_2Sn(L)]^{+}$ (c) $[Me_2Sn(L)(OH)]$, (d) $[Me_2Sn(L)_2(OH)_2]$ and (e) $[Me_2Sn(OH)_2]$ (Charges on the species are omitted for the sake of simplicity).

On the basis of observed value of $^{2}J(^{1}H–^{119}Sn)$ = 70 Hz and calculated ∠C–Sn–C = 120°, a TBP geometry was assigned to the predominating species, $[Me_3Sn(H_2O)_2]^{+}$, at pH ~ 4.22 (1:1 system) having chemical shift value of ^{1}H and ^{13}C NMR (methyl group bound to Sn) observed at δ = 0.43 ppm and δ = –1.74 ppm, respectively. ^{119}Sn NMR resonances observed at δ = 39.55 ppm and 18.62 ppm, further support the proposed geometry of the species [98]. Another peak of very low intensity in ^{1}H NMR at δ = 0.43 ppm corresponds to $[Me_3Sn(L)]^{+}$, owing to its very low percentage, the expected ^{13}C and ^{119}Sn resonances could not be observed for this species. In the pH range 6.3–7.9, the ^{1}H chemical shift value, $^{2}J(^{1}H–^{119}Sn)$ and ∠C–Sn–C of major species, $[Me_3Sn(OH)]$ were observed at 0.39±0.04 ppm, 63±6 Hz and 113°, respectively. Whereas in the same pH range $[Me_3Sn(L)]$ also exists having $^{2}J(^{1}H–^{119}Sn)$ = 72±5 and ∠C–Sn–C = 122±5°. On the bases of coupling constants and calculated ∠C–Sn–C angles, both the species are proposed to exhibit distorted TBP geometry in which *cis* and *trans* methyl groups are possibly in fast mutual exchange (Scheme 3.3 (b1)/(b2)/(b3)). This fact is further supported by recording the ^{1}H NMR at

variable temperature. At low temperature (5 °C/15 °C) the signal for methyl protons was found to be splitted, which might happen due to a difference in their magnetic environment *i.e.* presence of *cis* and *trans* isomers but the corresponding satellites have not been resolved. However, at room temperature and higher temperature (40 °C/50 °C) *cis* and *trans* methyl gave a single peak. We could not record ^{1}H NMR at further lower temperatures because of the freezing of water/D_2O in the system. A significant decrease in the ^{13}C NMR chemical shift, from –1.74 to –4.39 ppm also explained the existence of $[Me_3Sn(L)]/[Me_3Sn(OH)]$ in $Me_3Sn(IV)$–(HL) system. ^{119}Sn NMR resonances at δ = 71.42 and –132.88 ppm provide evidence for the distorted td/distorted TBP geometries [98] of $[Me_3Sn(OH)]$ and $[Me_3SnL]$ species, respectively. Furthermore, the observed values of $^{2}J(^{1}H–^{119}Sn)$ coupling constants, calculated ∠C–Sn–C and ^{119}Sn NMR observed at all pHs (Tables 3.2, 3.3 and 3.4) suggested the presence of 4- or 5-coordinated $[Me_3SnL]/[Me_3SnL(OH)]^-/[Me_3SnOH]/Me_3Sn(OH)_2$ complex species, having a distorted tetrahedral/distorted trigonal bipyramidal geometry (Scheme 3.3 (b–d)).

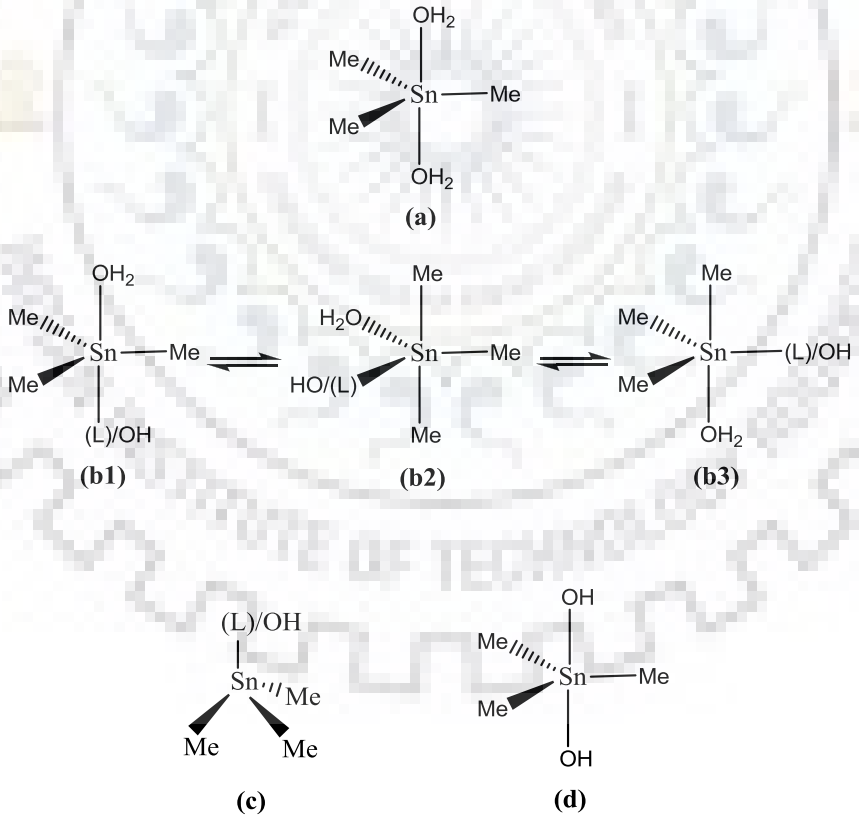

Scheme 3.3. Possible geometrical structures of trimethyltin(IV)-(HL) complex species: (a) $[Me_3Sn(H_2O)_2]^+$, (b1/b2/b3) isomers of $[Me_3Sn(L)]/[Me_3Sn(OH)]$, and (c) $[Me_3Sn(L)(OH)]^-$ and (d) $[Me_3Sn(OH)_2]^-$ (Charges on the species are omitted for the sake of simplicity).

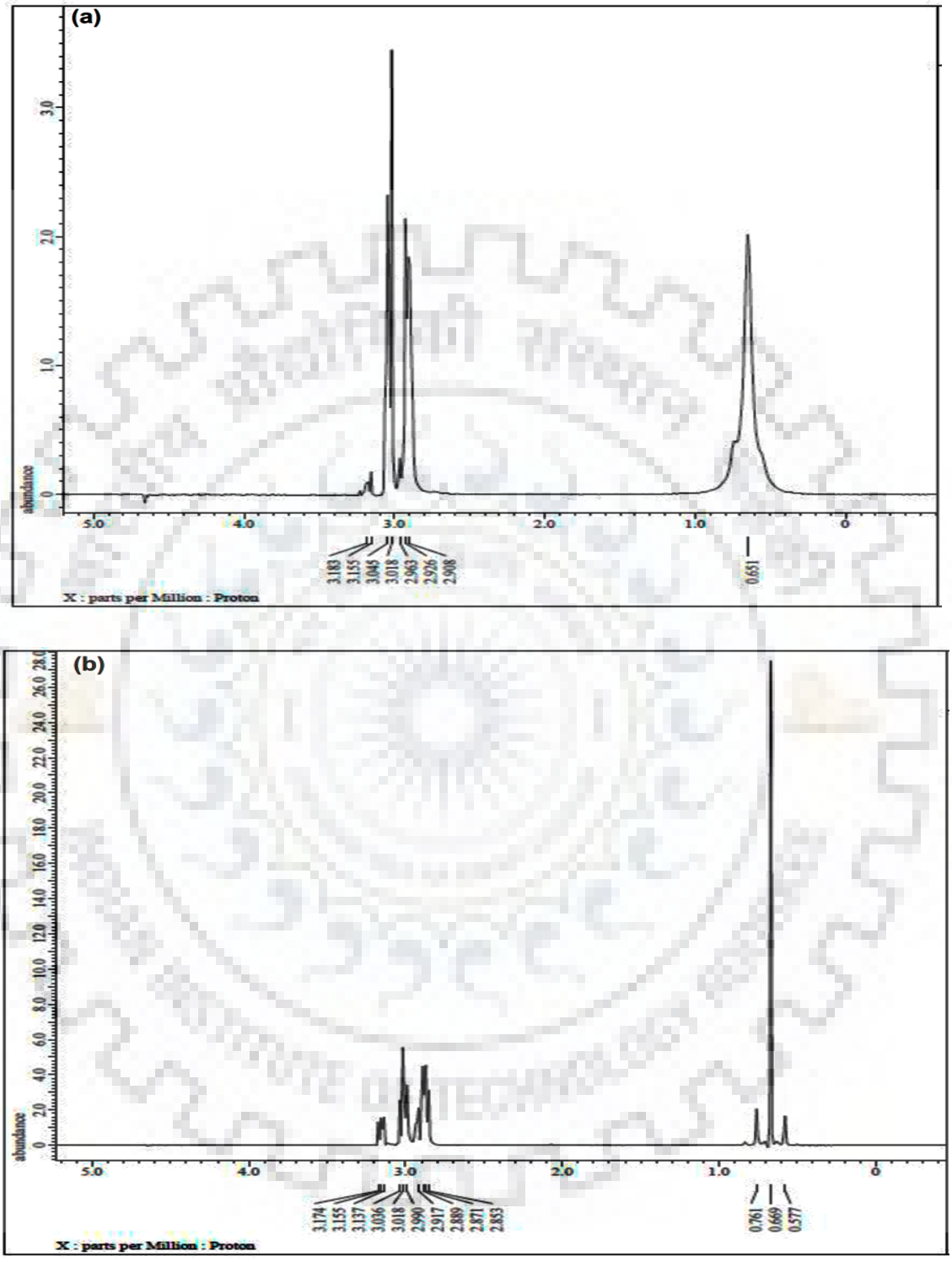

Fig. 3.4. ^{1}H NMR spectra for Me_2Sn–(HL) (a) (1:1) system at pH 7.01 (b) (1:2) system at pH 10.1; Solvent H_2O:D_2O (9:1) mixture.

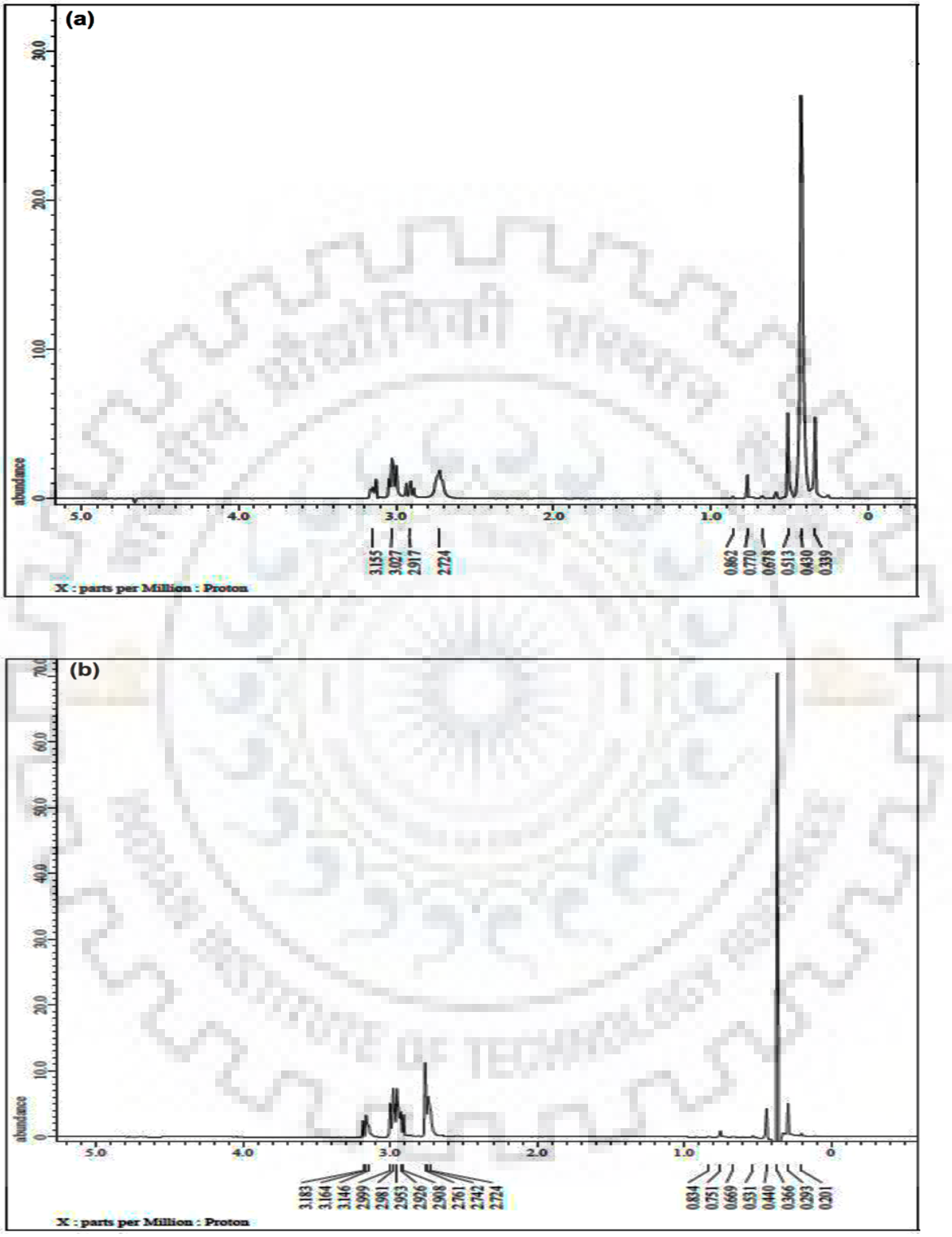

Fig. 3.5. ^{1}H NMR spectra for Me_3Sn–(HL) (a) (1:1) system at pH 4.22 (b) (1:2) system at pH 7.90; Solvent H_2O:D_2O (9:1) mixture.

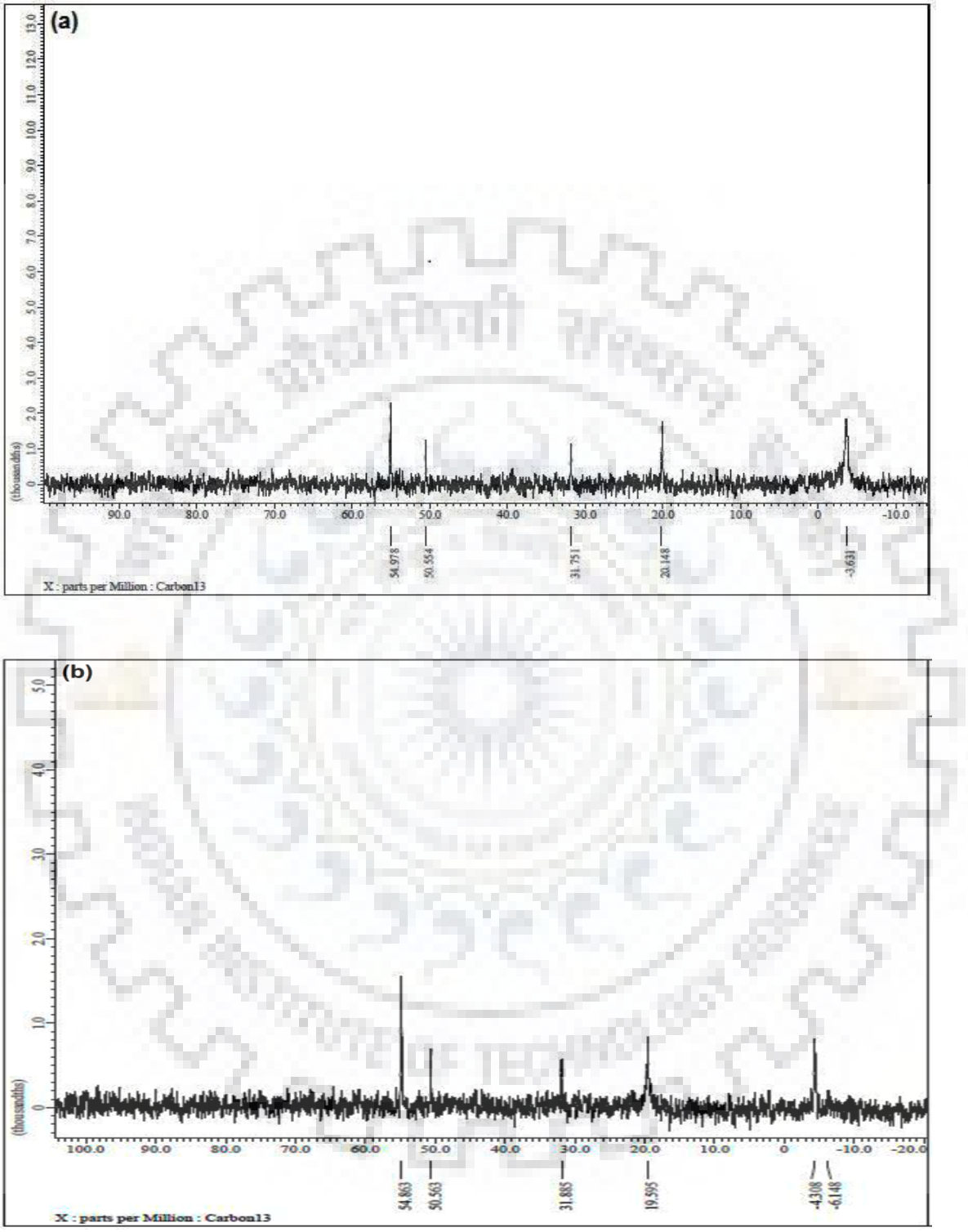

Fig. 3.6. ^{13}C NMR spectra for Me_3Sn–(HL) (a) (1:1) system at pH 7.48 (b) (1:2) system at pH 6.30. Solvent H_2O:D_2O (9:1) mixture.

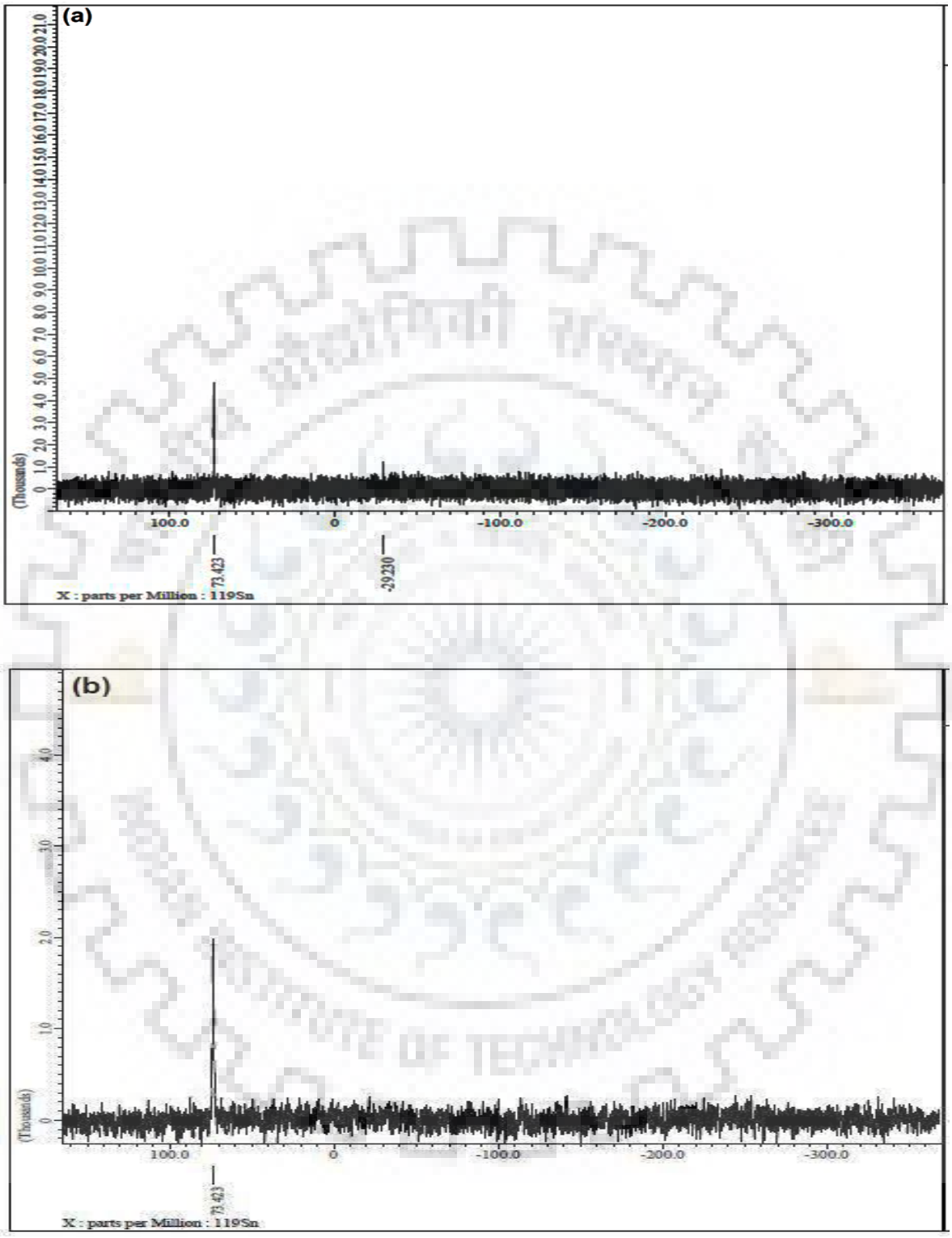

Fig. 3.7. ^{119}Sn NMR spectra for Me_2Sn–(HL) (a) (1:1) system at pH 9.85 (b) (1:2) system at pH 6.13. Solvent H_2O:D_2O (9:1) mixture.

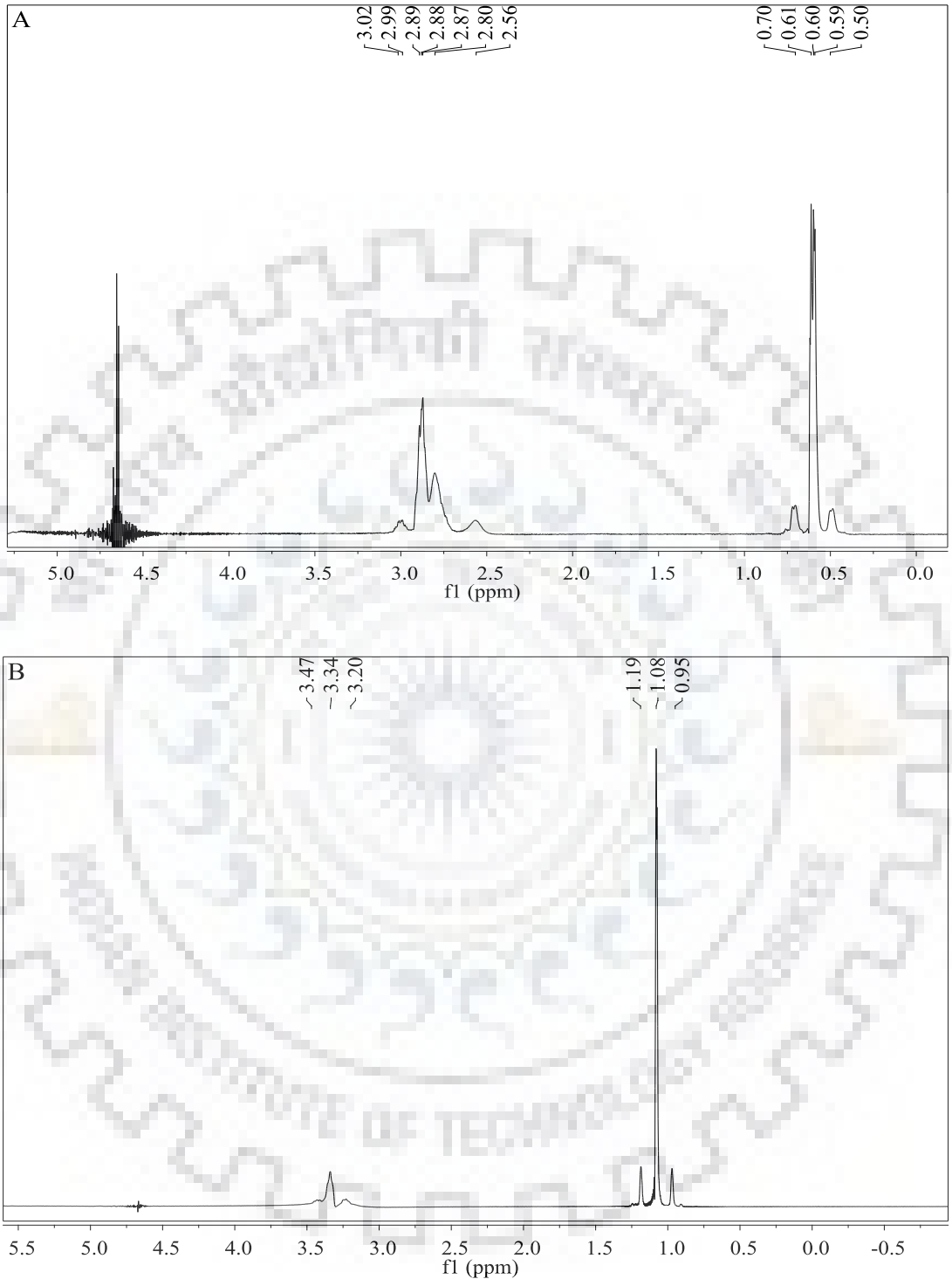

Fig. 3.8. ^{1}H NMR spectra of $Me_2Sn(IV)$–(HL) (1:1) system recorded at different temperature (pH ~ 5), (A) at 5 °C ; (B) at 50 °C; in solvent: H_2O:D_2O (9:1).

Table 3.2. ^{1}H NMR spectroscopic data of di- and trimethyltin(IV) –(HL) mixtures at different pHs in solvent: H_2O:D_2O (9:1).

pH	Species(%)[a]	CH_3[b] [^2J(^{1}H-^{119}Sn)]	Line width (Hz)[c]	∠C–Sn–C[d]	H1	H2	H3
	MESNA (HL)	–	–	–	2.73(t) Sp. 2.91 (d)	3.04 (t) 3.16 (t)	2.07
	$[Me_2Sn(H_2O)_4]^{2+}$	0.82 [103]	6.70	168	–	–	–
For Me_2Sn(IV)–(HL) mixture 1:1 system							
4.51	$[Me_2Sn(L)]^+$ (47.3), $[Me_2Sn(OH)]^+$ (34.6), $[Me_2Sn(L)(OH)]$ (12.4), $[Me_2Sn(OH)_2]$ (4.07), $[Me_2Sn(H_2O)_4]^{2+}$ (1.55).	0.77 (s) [84]	3.64	136	2.95 (br)	3.05 (t)	–
7.01	$[Me_2Sn(L)(OH)]$ (65.5), $[Me_2Sn(OH)_2]$ (31.3), $[Me_2Sn(L)_2(OH)]^-$ (0.27), $[Me_2Sn(OH)]^+$ (0.14), $[Me_2Sn(L)]^+$ (0.13).	0.65 (s) [nd]	22.18	–	2.92 (t) 2.96 (s)	3.03 (t) 3.17(d)	–
9.50	$[Me_2Sn(OH)_2]$ (43.4), $[Me_2Sn(L)(OH)]$ (30.3), $[Me_2Sn(L)_2(OH)]^-$ (25.4), $[Me_2Sn(OH)_3]^-$ (0.91).	0.64 (s) [73]	5.64	123	2.89 (t) 2.95 (s)	3.03 (t) 3.12 (br)	–
11.01	$[Me_2Sn(OH)_2]$ (44.3), $[Me_2Sn(OH)_3]^-$ (28.6), $[Me_2Sn(L)_2(OH)]^-$ (22.0), $[Me_2Sn(L)(OH)]$ (5.12).	0.63 (s) [74]	3.85	124	2.74 (t) 2.95 (s)	3.02 (t) 3.12 (br)	–

Contd…

For $Me_2Sn(IV)$–(HL) mixture 1:2 system							
4.53	$[Me_2Sn(L)]^+$ (74.4), $[Me_2Sn(OH)]^+$ (15.6), $[Me_2Sn(H_2O)_4]^{2+}$ (6.52), $[Me_2Sn(L)(OH)]$ (2.01), $[Me_2Sn(OH)_2]$ (0.16).	0.81(s) [80]	6.15	131	2.76 (br) 2.94 (t)	3.05 (t) 3.16 (t)	–
7.40	$[Me_2Sn(L)(OH)]$ (89.9), $[Me_2Sn(OH)_2]$ (8.52), $[Me_2Sn(L)_2(OH)]^-$ (0.97), $[Me_2Sn(L)]^+$ (0.45), $[Me_2Sn(OH)]^+$ (0.11).	0.71 (s) [73]	6.60	123	2.88 (t)	3.03 (t) 3.17 (t)	–
10.1	$[Me_2Sn(L)(OH)]$ (39.3), $[Me_2Sn(L)_2(OH)]^-$ (39.0), $[Me_2Sn(OH)_2]$ (20.3), $[Me_2Sn(OH)_3]^-$ (1.31).	0.67 (s) [74]	5..04	124	2.87 (t) 2.92 (t)	3.02 (t) 3.16 (t)	–
For $Me_3Sn(IV)$–(HL) mixture 1:1 system							
	$[Me_3Sn(H_2O)_2]^+$	0.40 [66]	6.90	116	–	–	–
4.22	$[Me_3Sn(H_2O)_2]^+$ (97.3), $[Me_3Sn(OH)]$ (1.34), $[Me_3Sn(L)]$ (1.33).	0.43 (s) [70] 0.77 (s) [74]	6.72 3.57	120 124	2.72 (t) 2.92 (t)	3.03 (t) 3.16 (t)	–
7.41	$[Me_3Sn(OH)]$ (58.70), $[Me_3Sn(L)]$ (36.4), $[Me_3Sn(H_2O)_2]^+$ (4.77), $[Me_3Sn(L)(OH)^-]$ (0.12).	0.39 (s) [62] 0.70 (s) [77]	5.10 16.40	113 127	2.74 (t) 2.94 (t)	3.14 (t) 3.16 (br)	–
9.64	$[Me_3Sn(OH)]$ (65.2), $[Me_3Sn(L)]$ (18.8), $[Me_3Sn(L)(OH)]^-$ (16.0).	0.31(s) [62] 0.19 (s) [n.d.] 0.66(s) [73]	3.81 4.58	113 123	2.73 (br) 2.90(t)	2.94 (t) 3.15 (t)	–

Contd…

11.17	$[Me_3Sn(OH)]$ (67.2), $[Me_3Sn(L)(OH)^-]$ (30.2), $[Me_3Sn(OH)_2]^-$ (1.34), $Me_3Sn(L)]$ (1.32).	0.31(s) [62] 0.65(s) [77]	3.55 6.13	113 127	2.73 (t) 2.91 (br)	2.95 (t) 3.16 (t)	–
For Me_3Sn(IV)–(HL) mixture 1:2 system							
6.30	$[Me_3Sn(L)]$ (49.5), $[Me_3Sn(OH)]$ (32.8), $[Me_3Sn(H_2O)_2]^+$ (17.6), $[Me_3Sn(L)(OH)]^-$ (0.02).	0.43 (s) [70] 0.81 (s) [84]	4.04 4.33	127 136	2.72 (t) 2.92 (t)	3.04 (t) 3.16 (t)	–
7.90	$[Me_3Sn(L)]$ (57.4), $[Me_3Sn(OH)]$ (40.8), $[Me_3Sn(H_2O)_2]^+$ (1.26), $[Me_3Sn(L)(OH)^-]$ (0.49),	0.37 (s) [59] 0.75 (s) [66]	3.62 5.61	112 116	2.73 (t) 2.92 (t)	2.98 (t) 3.16 (t)	–
9.75	$[Me_3Sn(OH)]$ (46.3), $[Me_3Sn(L)(OH)]^-$ (28.4), $[Me_3Sn(L)]$ (24.7), $[Me_3Sn(L)_2(OH)^{2-}]$ (0.62).	0.38 (s) [62] 0.75 (s) [66]	3.72 3.56	113 116	2.75 (t) 2.92 (t)	2.99 (t) 3.17 (t)	–
11.00	$[Me_3Sn(OH)]$ (67.2), $[Me_3Sn(L)(OH)]^-$ (30.2), $[Me_3Sn(OH)_2]^-$ (1.34), $Me_3Sn(L)]$ (1.32).	0.35 (s) [62] 0.72 (s) [66]	3.51 3.65	113 116	2.71 (t) 2.91 (br)	2.94 (t) 3.16 (t)	–

br: broad; s: singlet; t: triplet

[a] Percentage of species from speciation diagram

[b] Values in square bracket [ ] are $^2J(^{119}Sn–^1H)$ in Hz; [n.d.] not determined because the satellite peaks are not resolved

[c] Line width = the half line-width of the methyl protons

[d] Calculated using the equation, θ ($\angle$C–Sn–C) = $0.0161|^2J(^1H–^{119}Sn)|^2 – 1.32|^2J(^1H–^{119}Sn)| + 133.4$, Ref. [196]

Table 3.3. ^{13}C NMR spectroscopic data of di- and trimethyltin(IV) – (HL-1) mixtures at different pHs in solvent: H_2O:D_2O (9:1).

pH	Species(%)[b]	CH_3	C1	C2
	$Me_2Sn(H_2O)_4]^{2+}$	9.60	–	–
	MESNA (HL)	–	18.62	54.43
	For Me_2Sn(IV)–(HL) mixture 1:1 system			
4.50	$[Me_2Sn(L)]^+$ (47.3), $[Me_2Sn(OH)]^+$ (34.6), $[Me_2Sn(L)(OH)]$ (12.4), $[Me_2Sn(OH)_2]$ (4.07), $[Me_2Sn(H_2O)_4]^{2+}$ (1.55).	5.06	20.93 31.86	54.48 50.52
7.01	$[Me_2Sn(L)(OH)]$ (65.5), $[Me_2Sn(OH)_2]$ (31.3), $[Me_2Sn(L)_2(OH)]^-$ (0.27), $[Me_2Sn(OH)]^+$ (0.14), $[Me_2Sn(L)]^+$ (0.13).	3.66	20.94 29.51	54.54 50.76
11.01	$[Me_2Sn(OH)_2]$ (43.4), $[Me_2Sn(L)(OH)]$ (30.3), $[Me_2Sn(L)_2(OH)]^-$ (25.4), $[Me_2Sn(OH)_3]^-$ (0.91).	0.59	20.57 31.71	50.30 54.91
	For Me_2Sn(IV)–(HL) mixture 1:2 system			
3.50	$[Me_2Sn(L)]^+$ (74.4), $[Me_2Sn(OH)]^+$ (15.6), $[Me_2Sn(H_2O)_4]^{2+}$ (6.52), $[Me_2Sn(L)(OH)]$ (2.01), $[Me_2Sn(OH)_2]$ (0.16).	4.82	20.95 31.46	50.63 54.67
7.50	$[Me_2Sn(L)(OH)]$ (89.9), $[Me_2Sn(OH)_2]$ (8.52), $[Me_2Sn(L)_2(OH)]^-$ (0.97), $[Me_2Sn(L)]^+$ (0.45), $[Me_2Sn(OH)]^+$ (0.11).	1.71	20.71 31.67	50.41 54.80

Contd…

			20.58	
10.07	$[Me_2Sn(L)(OH)]$ (39.3), $[Me_2Sn(L)_2(OH)]^-$ (39.0), $[Me_2Sn(OH)_2]$ (20.3), $[Me_2Sn(OH)_3]^-$ (1.31)	0.86	31.73	50.52 54.80

For $Me_3Sn(IV)$–(HL) mixture 1:1 system

	$[Me_3Sn(H_2O)_2]^+$	–1.68	–	–
4.22	$[Me_3Sn(H_2O)_2]^+$ (97.3), $[Me_3Sn(OH)]$ (1.34), $[Me_3Sn(L)]$ (1.33).	–1.74	18.62 27.57 31.76	50.60 54.41
7.48	$[Me_3Sn(OH)]$ (58.70), $[Me_3Sn(L)]$ (36.4), $[Me_3Sn(H_2O)_2]^+$ (4.77), $[Me_3Sn(L)(OH)]^-$ (0.12).	–3.63	20.15 31.75	50.55 54.98
9.64	$[Me_3Sn(OH)]$ (65.2), $[Me_3Sn(L)]$ (18.8), $[Me_3Sn(L)(OH)]^-$ (16.0).	–3.57	20.07 31.88	50.54 55.06
11.17	$[Me_3Sn(OH)]$ (67.2), $[Me_3Sn(L)(OH)^-]$ (30.2), $[Me_3Sn(OH)_2]^-$ (1.34), $Me_3Sn(L)]$ (1.32).	–3.34	19.89 31.88	50.33 55.14

For $Me_3Sn(IV)$–(HL) mixture 1:2 system

6.30	$[Me_3Sn(L)]$ (49.5), $[Me_3Sn(OH)]$ (32.8), $[Me_3Sn(H_2O)_2]^+$ (17.6), $[Me_3Sn(L)(OH)^-]$ (0.02).	–4.31	19.59 31.88	50.56 54.86
7.90	$[Me_3Sn(L)]$ (57.4), $[Me_3Sn(OH)]$ (40.8), $[Me_3Sn(H_2O)_2]^+$ (1.26), $[Me_3Sn(L)(OH)]^-$ (0.49).	–4.39	19.60 31.81	50.53 54.88
9.70	$[Me_3Sn(OH)]$ (46.3), $[Me_3Sn(L)(OH)^-]$ (28.4), $[Me_3Sn(L)]$ (24.7), $[Me_3Sn(L)_2(OH)]^{2-}$ (0.62).	–4.34	19.67 31.86	50.54 55.07
11.00	$[Me_3Sn(OH)]$ (67.2), $[Me_3Sn(L)(OH)]^-$ (30.2), $[Me_3Sn(OH)_2]^-$ (1.34), $Me_3Sn(L)]$ (1.32).	–4.01	19.68 31.84	50.36 55.63

Table 3.4. ^{119}Sn NMR spectral data of di- and trimethytin(IV)–(HL) solution mixtures at different pHs (Solvent: H_2O:D_2O (9:1)).

pH	^{119}Sn δ/ppm	Number of Scans
For $Me_2Sn(IV)$ + (HL-1) mixture 1:1 system		
2.97	–328.91, –40.22	3800
7.43	36.84, –173.73	8000
11.03	91.76, –147.70	8000
For $Me_2Sn(IV)$ + (HL-1) mixture 1:2 system		
2.82	–333.99, –43.16	4000
7.40	–72.32	8000
For $Me_3Sn(IV)$ + (HL-1) mixture 1:1 system		
4.50	39.53, 18.60	3600
7.11	74.21	2000
9.85	73.42, –29.23	3600
11.14	73.42, –124.91	3600
For $Me_3Sn(IV)$ + (HL-1) mixture 1: 2 system		
6.13	73.42	2400
7.30	71.42, –132.88	2400
11.00	72.42	3400

Table 3.5. ^{1}H NMR data of $Me_2Sn(IV)$–(HL) (1:1) system recorded at different temperature (pH ~ 5) in solvent: H_2O:D_2O (9:1).

Temperature	H1	H2	Me_3Sn	∠ Me-Sn-Me
5°	2.80 (br) 2.56 (br)	2.87-2.89 (br) 2.99-3.02 (br)	0.61, 0.60, 0.59 (sp)	130.84°
15°	2.64-2.70 (br)	2.92-3.02 (m) 3.08-3.13 (br)	0.71, 0.73 (sp)	136.12°
25°	2.95-2.98 (br)	3.07-3.10 (t) 3.17-3.21 (m)	0.82 (s)	136.12°
40°	3.11-3.16 (br)	3.23-3.24 (m) 3.31-3.36 (br)	0.98 (s)	141.92°
50°	3.19-3.25 (br)	3.41-3.47 (br))	1.08 (s)	155.06°

Table 3.6. ^{1}H NMR data of $Me_3Sn(IV)$–(HL) (1:1) system recorded at different temperature (pH ~ 8) in solvent: H_2O:D_2O (9:1).

Temperature	H1	H2	Me_3Sn	∠ Me-Sn-Me
5°	2.55-2.62 (br)	2.75-2.84 (br) 2.97-3.05 (br)	0.22, 0.16 (sp) 0.54 (s)	–
15°	2.64-2.73 (br)	2.86-2.95 (br) 3.06-3.16 (br)	0.31, 0.27 (sp) 0.64 (s)	–
25°	2.76-2.80 (m)	2.79-2.99 (m) 3.18-3.22 (m)	0.36 (s) 0.72 (s)	114.86°
40°	2.93-2.97 (m)	3.16-3.18 (m) 3.34-3.37 (m)	0.53 (s) 0.87 (s)	114.86°
50°	3.00-3.06 (m	3.22-3.28 (m) 3.43-3.46 (m)	0.62 (s) 0.96 (s)	114.86°

br: broad; s: singlet; t: triplet

CHAPTER - 4

Synthesis, Characterization, DNA Binding, DNA Cleavage and Cytotoxicity Studies of Novel Diorganotin(IV) Complexes of Sodium 2-mercaptoethane sulfonate

4.1. INTRODUCTION

Despite the remarkable effectiveness of *cis*-platin in cancer treatment, it has been suffered by a number of serious side effects and the emergence of drug resistance, which prompted various research groups to develop innovative non-platinum chemotherapeutics with better potency and lesser side effects. Considering this fact a number of organometallic compounds have been tested for their anticancer effects, in order to optimize their efficacy and reduce the undesirable side effects [19, 97, 201, 202]. During the last few decades organotin compounds occupy an important place in cancer chemotherapy reports [203, 204]. A number of organotin(IV) complexes with S-donor lignads *viz.* thioamides (5-chloro-2-mercaptobenzothiazole, 2-mercaptonicotinic acid, 2-mercaptobenzoxazole and 2-mercaptopyrimidine) and 2,6-di-tert-butyl-4-mercaptophenol with tetrahedral/trigonal bipyramedal geometries were synthesized and few of them were found to exhibit excellent cytotoxicity with IC_{50} value as low as 5.5 nM [36, 137, 205, 206]. These results impelled us to synthesize the organotin(IV) complexes with S-donor ligand and investigate its possibility of binding with DNA and fragmentation of DNA, as these molecules interact *via* various non-covalent modes and alter the local structure of DNA, and concomitantly affect the process of gene-expression [104, 124, 207, 208].

MESNA (sodium 2-mercaptoethanesulfonate) is a low molecular mass drug, used as a chemoprotectant to prevent side effects caused by various anticancer drugs. It prevents hemorrhagic cystitis induced by cyclophosphamide and ifosfamide, ovarian damage and nephrotoxicity induced by *cis*-platin, plasma protein oxidation induced by doxorubicin and oxidative stress induced by ischemia reperfusion [209-213]. Furthermore, MESNA has a protective effect against ethanol-induced oxidative stress and inflammation called as gastric mucosal damage [214]. MESNA can form complexes with metal ions such as Pd(II), Pt(II), Ag(I), Cd(II) and Zn(II) with multiple anionic sulfonate sites. The platinum complex exhibited less cytotoxicity but impressive antiviral activity against HIV-1 and HIV-2, herpes simplex virus type 1 (HSV-1) and HSV-2, human cytomegalo virus, vesicular stomatitis virus (VSV), influenza A virus, respiratory syncytial virus (RSV), Sindbis virus, Junin virus and Tacaribe virus [215]. Few hydrated di- and triorganotin(IV) complexes of MESNA have been tested *in vivo* in P-388 leukaemic mice and the complexes with diphenyltin and dimethyltin moieties were found to be cytotoxic towards the cancer cells [216]. Though, the pharmaceutical importance of MESNA is well known but structure and study of its metal complexes are scarcely known in literature. This chapter describes the

synthesis and characterization of diorganotin(IV) complexes of MESNA and introspection of their DNA binding modes and DNA cleavage activity. In order to corelate the DNA intercation with cytotoxic profile of compounds, MTT assays were performed on HeLa (cervical cancer), DU145 (human prostate) and HCT-15 (human colon) cancer line and further, their mode of action was inquired through acridine orange (AO)/ethidium bromide (EB) and DNA fragmentation assays.

4.2. EXPERIMENTAL SECTION

4.2.1. Synthesis

4.2.1.1. Synthesis of Diorganotin(IV) Complexes of MESNA by Microwave Assisted Method

Microwave assisted syntheses were carried out in an open glass vessel microwave oven with maximum microwave energy output of 800 W. In order to synthesize complexes **2** and **3**, MESNA (1 mmol, 0.164 g) and dibutyltin oxide (0.5 mmol, 0.124 g) or dioctyltin oxide (0.5 mmol, 0.181 g) were finely ground together to obtain a homogeneous mixture. A paste of this mixture was made by adding few drops of methanol and irradiated for 1 min in a microwave oven at 560 Watt, in a Petri dish. The reaction mixture was then allowed to cool at ambient temperature and again irradiated for 1 min, this process was repeated for 4–5 times. A 250 mL beaker filled with water was placed in the microwave oven during the whole irradiation time which was refilled after every cycle of irradiation. The resulted product was scratched and washed with a mixture of methanol and petroleum ether (40–60 °C), (1:1 v/v), in order to get rid of remained reactants. Synthesis of complex **5** was carried out by irradiating complex **2** (0.4 mmol, 0.224 g) and 1,10-phenanthroline (0.4 mmol, 0.079 g) at 480 Watt, in microwave oven in a similar manner as mentioned above.

4.2.1.2. Synthesis of Diorganotin(IV) Complexes of MESNA by Thermal Method

To a solution of MESNA (1 mmol, 0.164 g in 15 mL methanol) was added 10 mL methanolic solution of dimethyltin(IV) dichloride (0.5 mmol, 0.110 g) or diphenyltin(IV) dichloride (0.5 mmol, 0.172 g). To the resulting solution 1 equivalent triethylamine (0.139 mL) was added and stirred vigorously for 8 h, under dry nitrogen and then refluxed for 1 h and excess solvent was vaporized under reduced pressure. The product obtained was purified by dissolving the excess reactants and $(C_2H_5)_3N.HCl$ formed during the reaction in chloroform and final product then obtained was dried under vacuum.

4.2.2. Details of DNA Binding Studies

All the experiments done to elucidate the mode and extent of MESNA/studied complexes towards DNA, were carried out by preparing an appropriate dilution of stock solution (in DMSO) of complexes in Tris–HCl/NaCl buffer (pH 7.2, 5:50 mM), so as the final dilution having not more than 1% DMSO. The complexes **3**, **4** and **5**, in tris buffer were slowly started precipitating when placed for more than 24 hours, because of the slow lysis of Sn-S bonds in aqueous solution as reported previously [217]. In order to avoid degradation and precipitation of the complexes, all the dilutions prepared were utilized within 24 hours while placing at 25 °C. CT DNA stock solution once prepared should not be used more than 3 days.

4.2.2.1. UV-Visible Spectrophotometric Titration

The UV–visible spectra of MESNA and complexes **1-5,** (1.0×10^{-3}, 2.5×10^{-4}, 1.5×10^{-4}, 1.6×10^{-4}, 5.6×10^{-5}, 4.2×10^{-5} M, respectively) were recorded in the absence and presence of CT DNA. Absorbance (A) of MESNA and complexes **1-5,** was obtained with successive addition of CT DNA ($4.6–5.6\times10^{-4}$ M) while keeping total volume constant. In order to eliminate the absorbance due to CT DNA the reference solution was maintained at equal concentration of CT DNA to that of working solution. The intrinsic binding constant (K_b) of the complex to CT DNA was determined by using Wolfe Shimmer equation [218] given below:

$$\frac{[\mathrm{DNA}]}{|\varepsilon_a - \varepsilon_f|} = \frac{[\mathrm{DNA}]}{|\varepsilon_a - \varepsilon_f|} + \frac{1}{|\varepsilon_b - \varepsilon_f|} \times \frac{1}{\mathrm{Kb}}$$

Where [DNA] is the concentration of CT DNA, ε_a is the apparent extinction coefficient, ε_f and ε_b corresponds to the extinction coefficient of the metal complexes in free and in fully bound form, respectively. In plots of [DNA]/($\varepsilon_a - \varepsilon_f$) vs [DNA], K_b was determined from the slope to intercept ratio.

4.2.2.2. Fluorescence Studies

All the fluorescence emission experiments were carried out by diluting stock solution of the studied complexes prepared in 1% DMSO with Tris–HCl/NaCl buffer (pH =7.2) at 25 °C. MESNA and complexes **1-4** were excited at 201 nm and complex **5** was excited at 226 nm. Emission spectra were recorded in the range 250 nm to 650 nm with a slit width 5 nm for both excitation and the emission. MESNA and complex **1** were not found to emit in this range and were

considered as fluorescence inactive. DNA binding experiment was carried out by recording the emission spectra of complexes **2-5** (100 μM) alone and with increasing concentrations (1.3 – 13×10^{-5} M) of CT DNA. In the fluorescence quenching assay of EB, the emission spectra of a pre-incubated solution of CT DNA (40 μM) and EB (7.5 μM) in the absence and presence of increasing concentration of MESNA and complexes **1-5** ($2 – 35\times10^{-5}$ M), were recorded. The EB–CT DNA complex ([DNA]/[EB] = 5.3) was excited at 515 nm and emission spectra were observed in the range 525–700 nm with a slit width of 2 nm. In another experiment potassium iodide (KI) quenching was studied in which emission spectra of complexes **2-5** (100 μM) were recorded in the absence and the presence of CT DNA (100 μM) with subsequent addition of KI (0–20 mM). Stern-Volmer quenching constants K_{sv} in both the quenching experiments were evaluated using the classical Stern-Volmer equation [219].

$$\frac{Io}{I} = 1 + Ksv.\,[Q]$$

Where I_o and I represented the emission intensities in the absence and presence of the quencher, respectively and [Q] is the quencher concentration. K_{sv} (linear Stern–Volmer constant) calculated from the value of slope in a plot of I_0/I versus [Q] (intercept value=1).

4.2.2.3. Circular Dichroic Studies and Viscosity Measurement Studies

Circular dichroic spectroscopic changes were studied by recording the spectra of CT DNA (100 μM) with and without adding MESNA/complexes (**1-5**) (8–25 μM). Changes in the negative and positive bands were observed closely in order to find the prevailing mode of binding of molecules with CT DNA. Further, mode of binding between CT DNA and MESNA/complexes (**1-5**) was elucidated through viscosity measurement experiments which, were performed by keeping the CT DNA concentration at 100 μM while varying complex concentrations (0 to 100 μM).

4.2.3. Gel Electrophoresis

DNA cleavage study was performed using supercoiled pBR322, E. coli plasmid DNA. The supercoiled DNA (50 ng) was treated with varying concentrations of MESNA and complexes **1–5** ($2.5 – 10\times10^{-5}$ M) in buffer solution (5:50 mM Tris–HCl/NaCl, pH 7.2) and were incubated for 1 h at 37 °C. Incubated samples were then treated with 2 μL loading buffer (30 mM EDTA, 0.05 % (w/v) glycerol, 36% (v/v) bromophenol blue) and were loaded onto agarose gel (0.8%) containing

EB (0.5 μg/mL). The agarose gel was run in 0.5X TBE buffer at 50 V/cm for 3.5 h. Bands formed by moving plasmid DNA were visualized and photographed. Details of chemicals, instrumentation and method used for various studies are described in Chapter 2.

4.2.4. DFT Study and Computational Details

The geometries of MESNA and complexes **1-5** were optimized by DFT calculations using the Gaussian 09 program. Computations were carried out with the B3LYP function and LANL2DZ basis set [220] was used to describe all the atoms including tin metal. The fundamental vibrational frequencies were calculated along with the geometry optimization, which were compared with the experimental values of FTIR of corresponding complexes in order to estimate the approximate geometry of complexes.

4.3. RESULTS AND DISCUSSION

4.3.1. Synthetic Aspects

The reaction between MESNA and diorganotin(IV) chlorides/oxides in 1:2 ratio led to the formation of diorganotin(IV)–MESNA complexes **1-4** as described in experimental section and represented as Scheme 4.1. The method (i) represents the reaction between diorganotin(IV) chlorides (dimethyltin dichloride/diphenyltin dichloride) and method (ii) represents the reaction of diorganotin(IV) oxides (dibutyltin oxide/dioctlyltin oxide) with MESNA. The method (iii) in Scheme 4.2 describes the synthesis of complex **5** in which complex **2** and 1,10-phenanthroline were taken in 1:1 ratio, and irradiated in the microwave oven. The method (i), represents the formation of complexes **1** and **4**, in which HCl formed with the progress of the reaction is reacted with added $(C_2H_5)_3N$ to form $(C_2H_5)_3N.HCl$, which was easily removed by recrystallization of the complexes with $CHCl_3$. The reaction, given by the method (ii) (synthesis of complexes **2** and **3**) was accomplished by irradiation in microwave oven where H_2O condensed during the reaction is vaporized and no tedious setup was required to remove the H_2O formed in the reaction, as the reaction proceeded. The complexes **1**, **2** and **4** are different from the similar complexes reported previously [216, 217], with respect to the absence of water of crystallization in the present complexes. This difference may be attributed to the different reaction methodologies adopted for the synthesis. Furthermore, the complex **5** was synthesized according to the method (iii) in a microwave oven as described in experimental section. All the complexes formed are soluble in

methanol, DMSO and acetonitrile and stable towards air and moisture. The melting point and analytical data of the synthesized complexes are summarized in Table 4.1., and their spectroscopic data are described in Table 4.2–4.4.

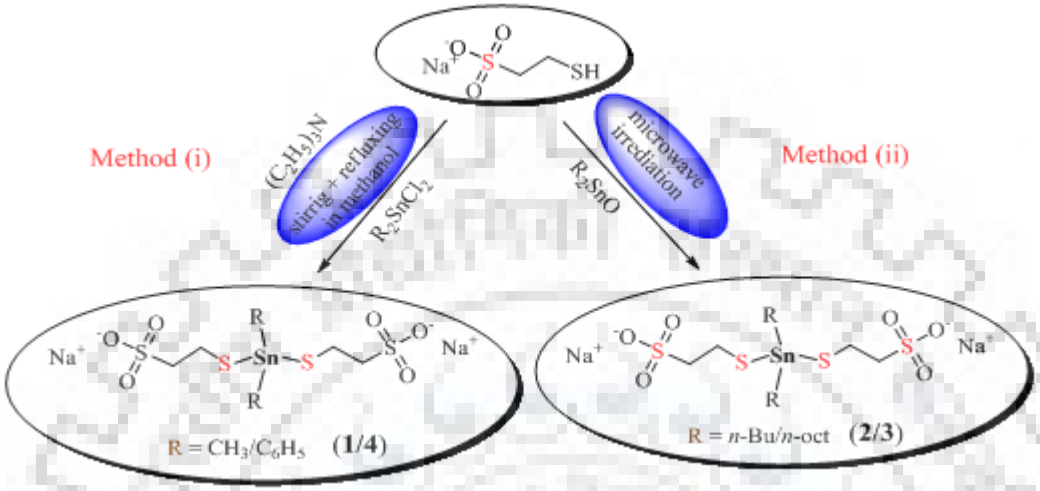

Scheme 4.1. Synthetic route opted for synthesis of complexes 1-4.

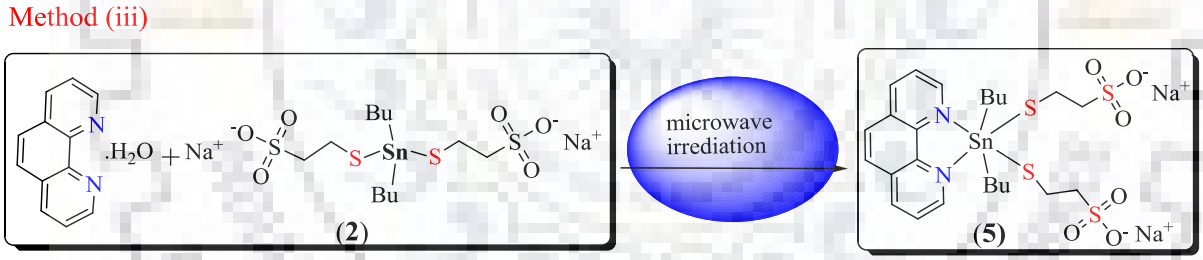

Scheme 4.2. Synthetic route opted for the synthesis of complex 5.

4.3.2. FTIR Spectroscopic Study

The IR spectroscopic data recorded for all the complexes are tabulated in Table 4.2. The representative spectra of MESNA and complexes **2** and **3** are given in Fig. 4.1. A medium intensity IR band at 2571 cm^{-1} attributed to S–H stretching frequency of MESNA [167] disappeared when latter was coordinated through sulphur atom of the thiol group with tin metal to form complexes **1-5**. A strong intensity bands at 1214 cm^{-1} and 1059 cm^{-1} which were assigned to SO_3 asymmetric and symmetric bands indicate a negligible shift in their frequency after complexation, reveals that there is no interaction between the oxygen of SO_3 and tin metal in complexes in the solid state. A

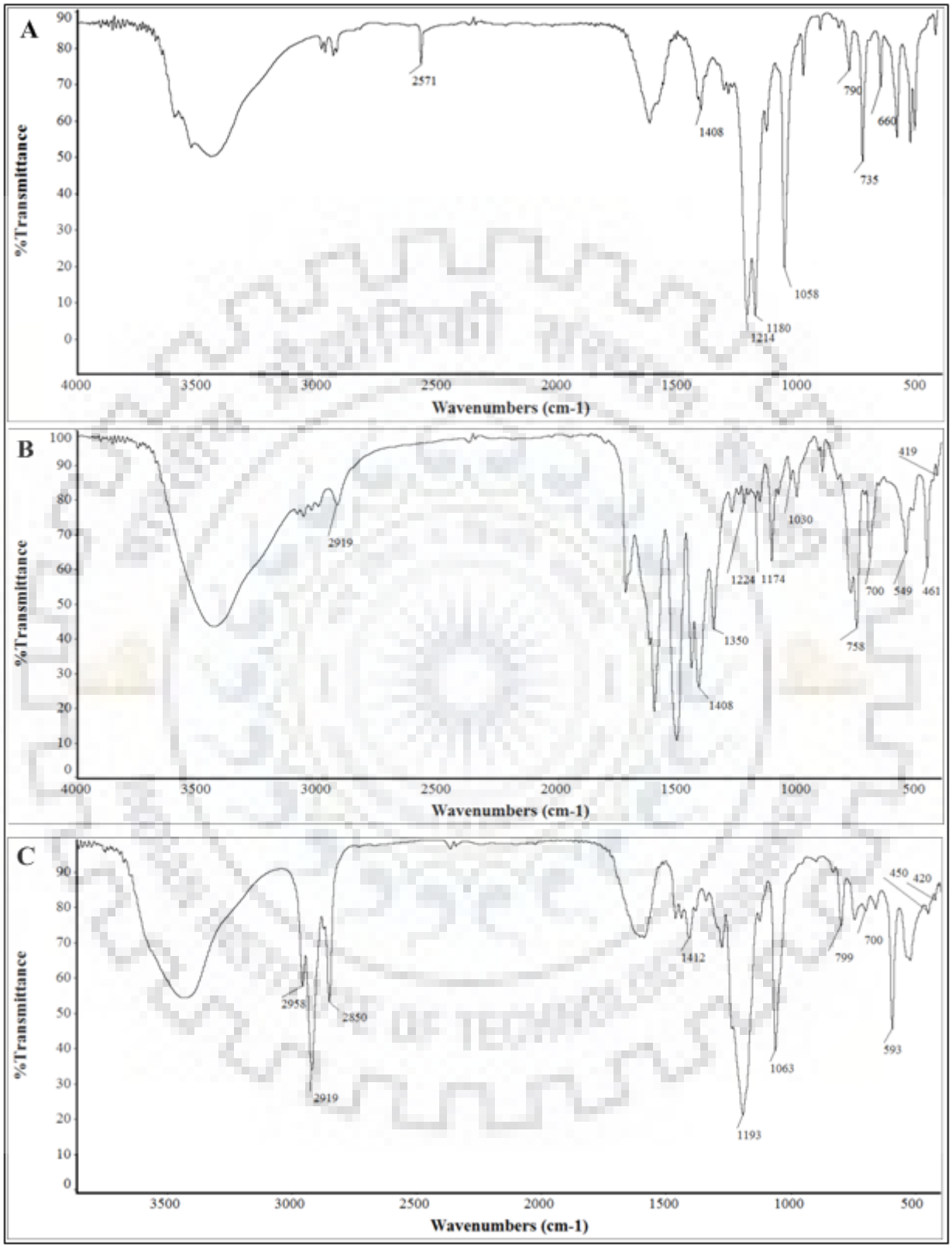

Fig 4.1. FTIR spectra of MESNA (A), complex 2 (B) and complex 3 (C).

strong intensity band at 786 cm^{-1} appeared in IR spectra of MESNA due to C–SO_3 stretching revealed a minimal shift after complexation. However, a significant shift in stretching frequency of C–SH band in MESNA from 658 and 733 cm^{-1} to 700–730 and 728–754 cm^{-1}, respectively, in the complexes is possibly due to the co-ordination of sulphur atom of the thiol group with tin metal. Furthermore, the presence of medium and small intensity bands in the region 450–478 cm^{-1} and 438-419 cm^{-1} in the complexes due to the presence of asymmetric and symmetric Sn–S vibrational frequency supported the formation of complexes. Vibrational stretching bands of Sn–C bond which appeared in the FTIR spectra of complexes in the region 549–593 cm^{-1} also reveal the complexation of MESNA with organotin moieties. In the complex **5** the characteristic bands at 1620 cm^{-1} and 1520 cm^{-1} are assigned to aryl C=N and C=C ring vibrations, respectively, of 1,10-phenanthroline [221]. A shift towards higher frequency in C=N stretching band can explain the complexation of 1,10-phenanthroline with tin metal through the nitrogen atoms.

4.3.3. Multinuclear (^{1}H, ^{13}C, and ^{119}Sn) NMR Spectroscopic Studies

The ^{1}H, ^{13}C and ^{119}Sn NMR spectroscopic data are presented in Table 4.3 and Table 4.4, respectively, and characteristic spectra of few complexes are given in Fig. 4.2 to Fig. 4.4. Signals and chemical shift values for all the protons present in the complexes are in accordance with their proposed structures. The ^{1}H NMR spectrum of MESNA in DMSO-d_6 does not show the resonance for thiol (-SH) proton thus ^{1}H NMR spectra of complexes do not yield any information regarding the deprotonation of the thiol group. In case of MESNA only one broad signal of two methylene protons is found in the range 2.63–2.69 ppm because of overlapping in their chemical shift values, however, the formation of complexes resolved the overlapped signals by causing an appreciable downfield shift to methylene protons. Whereas, the methylene protons attached directly to the sulphonate group are likely to experience much more deshielding effect. The ^{1}H NMR spectra of the complexes exhibited the proton signals of the corresponding organotin moieties flanked with satellites due to the tin metal. The satellite signals are clearly visible in NMR spectra of complexes **1**, **2**, **4** and **5**, their $^{2}J(^{1}H\text{-}^{119}Sn)$ coupling constant are 68, 66, 64 and 100 Hz, respectively. The ∠C–Sn–C is calculated by utilizing $^{2}J(^{1}H\text{-}^{119}Sn)$ value with the help of Lockhart and Mander's equations [222] which comes out to be 118°, 116°, 115° and 162° for complexes **1, 2, 4** and **5**, respectively, which indicate that the complexes **1, 2** and **4** either exhibiting highly distorted tetrahedral (td) or trigonal-bipyramidal (TBP) geometries and complex **5** exhibiting slightly

distorted octahedral (Oh) geometry. Due to the proximity of proton resonances of octyl moiety in complex **3** satellites could not be resolved.

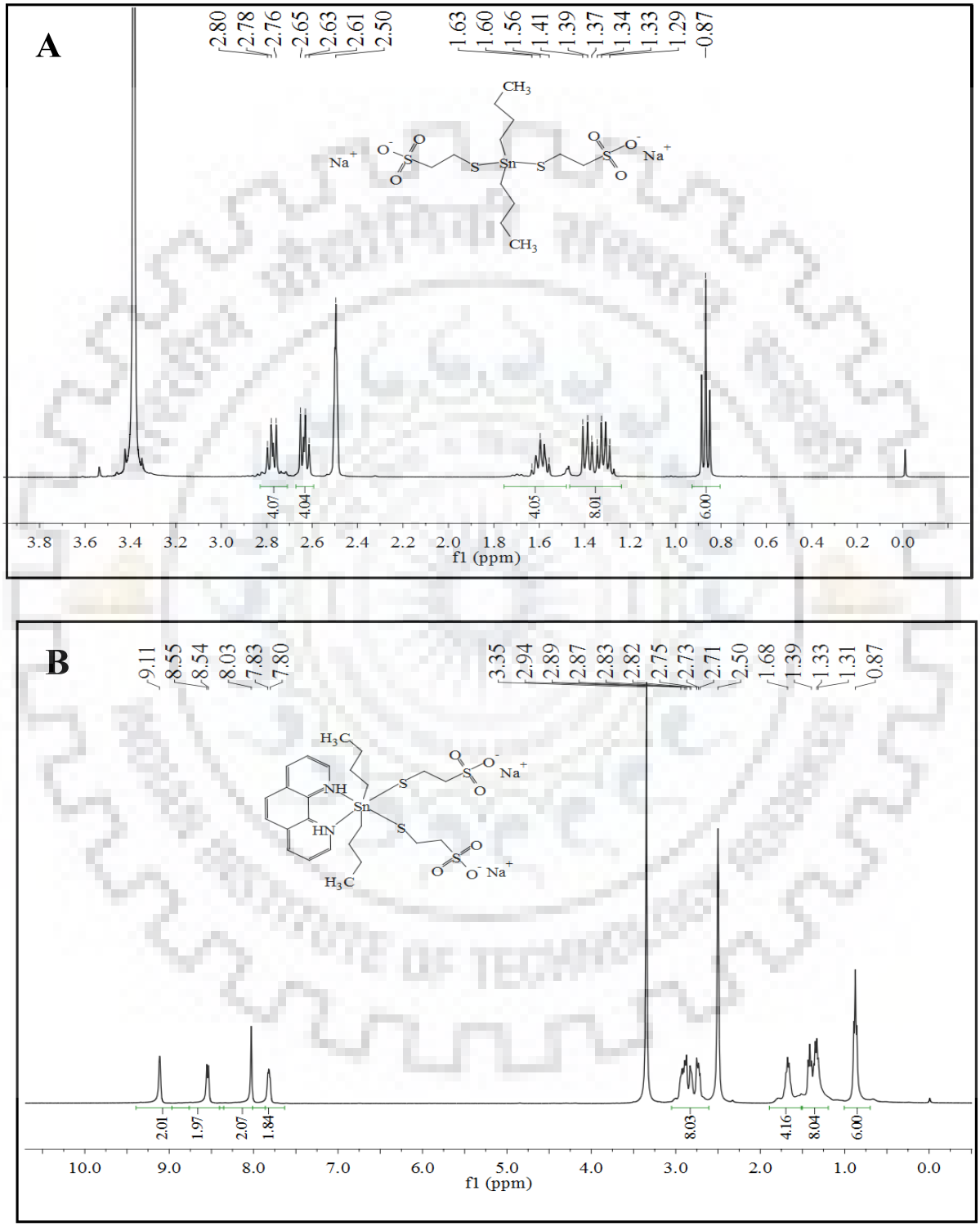

Fig. 4.2. ^{1}H NMR spectra of complex 2 (A) and complex 5 (B) in DMSO-*d*$_6$.

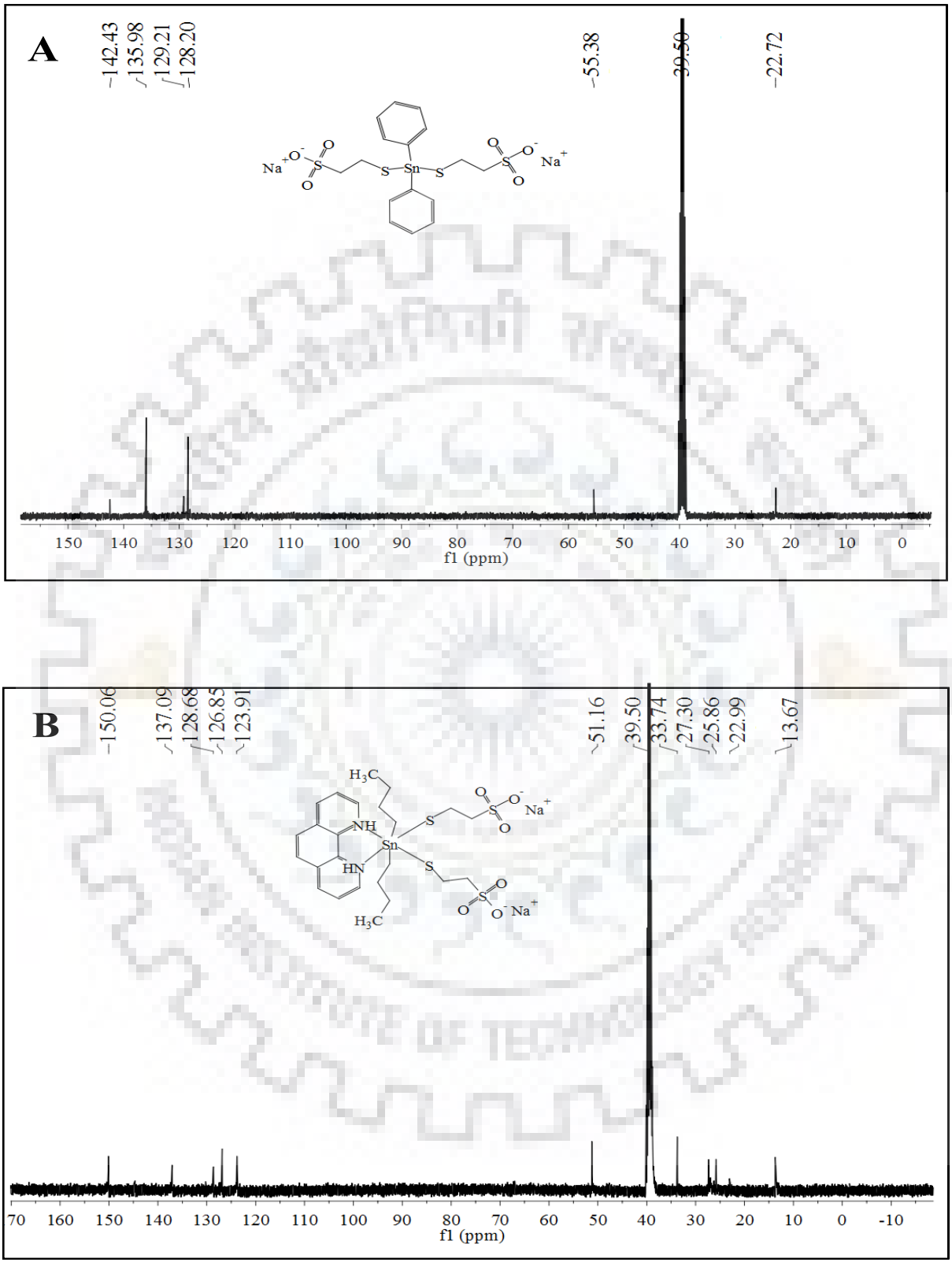

Fig. 4.3. ^{13}C NMR spectra of complex 4 (A) and complex 5 (B) in DMSO-d_6.

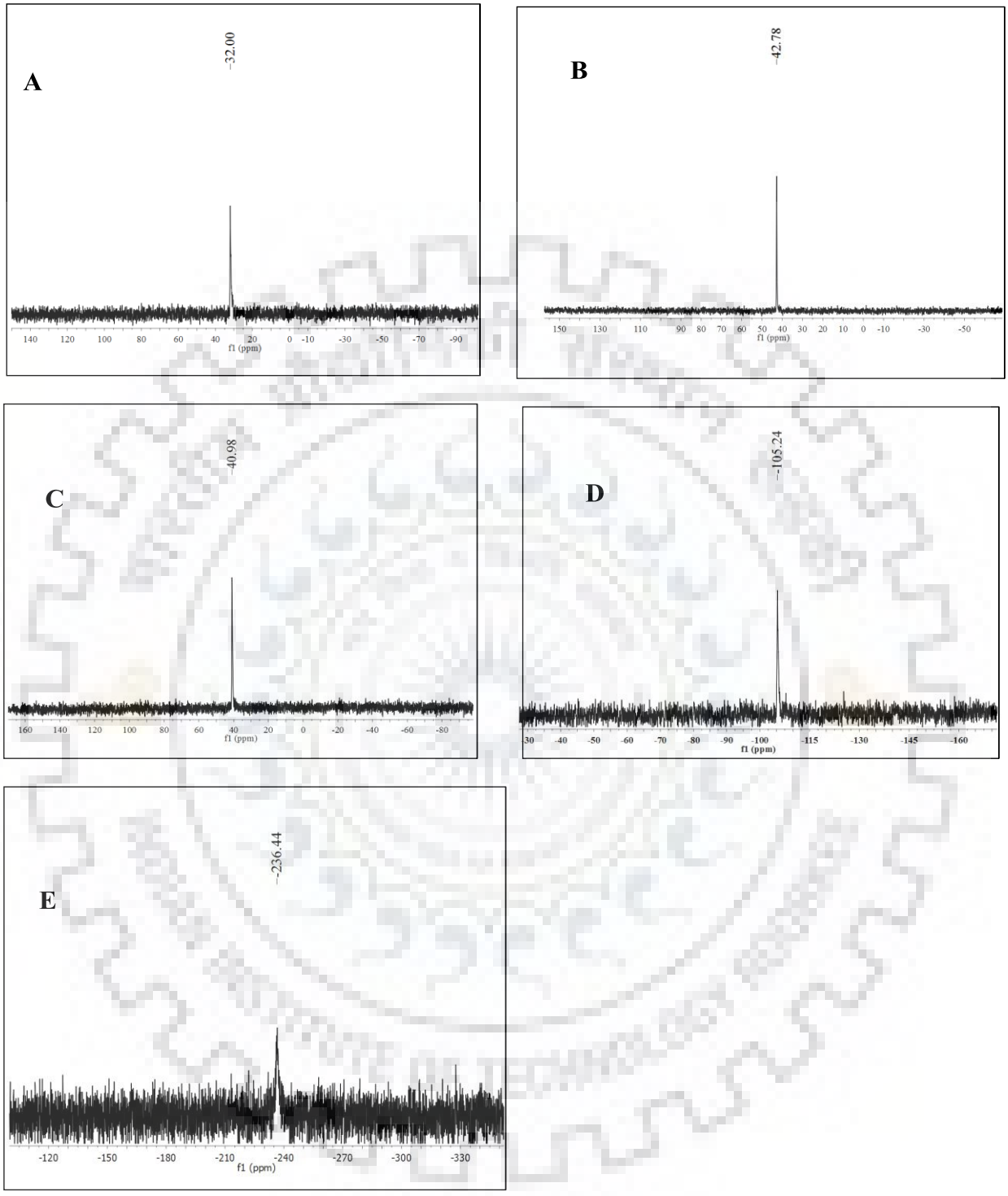

Fig. 4.4. ^{119}Sn NMR spectra of MESNA (A) and complexes: 1 (B), 2 (C), 3 (D), 4 (E) and 5 (F) in DMSO-*d*$_6$.

Table 4.1. Physical properties and analytical data of organotin(IV) complexes of MESNA.

Complex /Ligand	Complex (Empirical Formula)	Molecular weight	Colour & Physical state	Yield (%)	Decompos-ition temperature (°C)	Analysis (Calculated) (%)			Observed
						C	H	S, N[a]	Sn
MESNA	$C_2H_5NaO_3S_2$ (HL)	164.2	White solid	–	250	–	–	–	–
1	**[$Me_2Sn(MESNA)_2$]** ($C_6H_{14}Na_2O_6S_4Sn$)	475.1	White solid	78	290	15.19 (15.17)	2.99 (2.95)	27.31 (27.00)	24.66 (24.99)
2	**[$Bu_2Sn(MESNA)_2$]** ($C_{12}H_{26}Na_2O_6S_4Sn$)	559.9	White solid	92	190	25.56 (25.77)	4.58 (4.64)	22.80 (22.93)	20.68 (21.23)
3	**[$Oct_2Sn(MESNA)_2$]** ($C_{20}H_{42}Na_2O_6S_4Sn$)	672.1	White solid	86	150	35.12 (35.77)	6.11 (6.25)	18.89 (19.10)	17.08 (17.68)
4	**[$Ph_2Sn(MESNA)_2$]** ($C_{16}H_{18}Na_2O_6S_4Sn$)	599.3	White solid	82	238	32.28 (32.07)	3.29 (3.22)	21.80 (21.40)	18.98 (19.81)
5	[**$Bu_2SnL_2(MESNA)_2$. Phen**] ($C_{24}H_{34}N_2Na_2O_6S_4Sn$)	739.5	Light pink solid	76	Above 300	38.58 (38.94)	3.12 (3.22)	3.26 (3.79) 16.92[a] (17.31)	15.88 (16.09)

[a]for complex 5 only: Phen=1,10-phenanthroline; MESNA = Sodium 2-mercaptoethane-sulfonate

Table 4.2. FTIR spectroscopic data of ligand and organotin(IV) complexes (1-5) of MESNA.

Ligand/ Complex[a]	*ν*(S–H)	*ν*(SO_3)	*ν*(C–SO_3)	*ν*(C–S)	*ν*(C–C), *ν*(C=N)[b], *ν*(C=C)[b]	*ν*(Sn–S)	*ν*(Sn–C), *ν*(Sn–N)[b]
MESNA	2571 (m)	1181(s), 1214 (sp)	1058 (m)	658 (m)	2928 (m)	–	–
1	–	1192(s), 1212(s)	1049 (s)		2946 (s), 2926 (s)	478(m), 438(w)	583 (m)
2	–	1174 (w), 1224 (w)	1030 (s)	728 (m)	2958 (s), 2919 (m)	461 (m) 419 (m)	549(m)
3	–	1193(s), 1124 (m)	1062 (s)	700 (m)	2957 (s), 2921 (s), 2850 (s)	450 (m), 420 (m)	593 (m)
4	–	1183 (s), 1204 (s)	1059 (s)	698(m)	3016 (s), 2926 (m)	448 (m), 406 (m)	–
5	–	1194 (s), 1123 (m)	1051 (m)	730 (m),	2957 (s), 2921 (s), 1620 (s)[b], 1520 (s)[b]	441 (w)	589 (m), 460 (m)[b]

[a]complex number as given in Table 4.1, [b]for complex 5 only; MESNA = Sodium 2-mercaptoethane-sulfonate;

m = medium, s = strong; w = weak; sp = splitted

Table 4.3. ^{1}H, and ^{13}C NMR spectroscopic data of organotin(IV) complexes of MESNA in DMSO-d_6.

Ligand/ Complex[a]	^{1}H NMR δ (ppm) (399.78 MHz), DMSO-d_6
MESNA	2.63–2.69 (m, 4H, H–1,2)
1	2.64 (t, 4H, H-1); 2.79 (t, 4H, H-2); 0.69 (t, 6H, CH_3); $^{2}J(^{1}H–^{119}Sn)$ = 68 Hz, [θ = 118°][b]
2	2.63 (t, 4H, H-1); 2.78 (t, 4H, H-2); 0.87 (t, 6H, H-δ,); 1.29–1.34 (m, 4H, H-*β*); 1.37–1.41 (m, 4H, H-*γ*); 1.56–1.63 (m, 4H, H-*α*), $^{2}J(^{1}H–^{119}Sn)$ = 66 Hz, [θ = 116°][b]
3	2.64 (t, 4H, H-1); 2.78 (t, 4H, H-2); 0.85 (t, 6H, H-*i*); 1.21–1.25 (br, 20H, H-(*h*-*γ*)); 1.39 (t, 4H, H-*β*); 1.58–1.65 (m, 4H, H-*α*).
4	2.68 (t, 4H, H-1); 2.78 (t, 4H, H-2); 7.81 (d, H-*o*, 4H); 7.40 (d, H-*p*,*m*, 6H); $^{2}J(^{1}H–^{119}Sn)$ = 64 Hz, [θ = 115°][b]
5	2.63 (t, 4H, H-1); 2.88 (t, 4H, H-2); 9.11 (d, 2H, C-1'); 7.82 (t, 2H, C-2'); 8.55 (d, 2H, C-3'); 8.03 (s, 2H, C-5'); 0.87 (t, 6H, H-*δ*); 1.31–1.39 (br, 8H, H-*β* H-*γ*); 1.68 (m, 4H, H-*α*), $^{2}J(^{1}H–^{119}Sn)$ = 100 Hz, [θ = 162°][b]
^{13}C NMR δ (ppm) (100.53 MHz), DMSO-d_6	
MESNA	19.82 (C–1), 55.25 (C–2)
1	22.41 (C–1); 55.68 (C–2); 2.15 (C-α, Bu_2Sn)
2	20.81(C–1); 55.89 (C–2); 13.67 (C-*δ*); 26.11 (C-*γ*); 27.97 (C-*β*); 22.30 (C-*α*).
3	21.05 (C–1); 55.88 (C–2); 14.06 (C-*i*); 22.19 (C-*h*); 25.66 (C-*δ*–*g*); 31.37 (C-*γ*); 33.08 (C-*β*); 28.74 (C-*α*).
4	22.72, 33.78 (C-1); 55.38, 51.25 (C–2), 142.43 (C-*i*); 135.98 (C-*o*); 128.20; (C-*m*), 129.21 (C-*p*).
5	22.72, 33.78 (C-1); 51.25, 55.38 (C–2); 150.06 (C-1'); 123.91 (C-2'); 137.09 (C-3'); 128.53 (C-4'); 126.85 (C-5'); 146.25 (C-6'); 13.67 (C-*δ*); 25.86 (C-*γ*); 27.30 (C-*β*); 22.99 (C-*α*)

[a]complex number as given in Table 4.1; [b]detremined through (θ=[0.0161$^{2}J(^{119}Sn-^{1}H)]^{2}$–1.32[$^{2}J(^{119}Sn-^{1}H)$+133.4] [196]; MESNA =Sodium 2-mercaptoethane sulfonate; s: singlet; d: doublet; t: triplet; m: multiplet; br: broad;

α α β γ δ α β γ δ f g h i

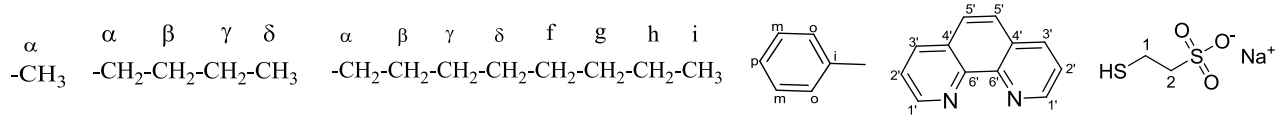

Table.4.4. ^{119}Sn NMR spectroscopic data of organotin(IV) complexes of ibuprofen in DMSO-d_6 (186.50 MHz).

Ligand/ Complex[a]	^{119}Sn NMR δ (ppm),
1	32.00
2	42.78
3	40.98
4	–105.24
5	–236.00

[a]complex number as given in Table 4.1.

In addition to the proton resonances obtained for complex **2**, the ^{1}H NMR spectrum of complex **5** having additional chemical shift values corresponding to 1,10-phenanthroline protons in the region 7.80–9.11 ppm. No resonance corresponding to H_2O in the spectrum of complex **5** was obtained which indicates loss of coordinated H_2O of phenanthroline monohydrate during the reaction. In the decoupled ^{13}C NMR spectra of the complexes **1-5** the resonances corresponding to the methylene carbon of MESNA and the organic moiety of tin were assigned by rigorous analysis of chemical shift. The signal of methylene carbon (bonded to thionyl group), at 19.82 ppm which is observed for free MESNA, is shifted to 21.76 ± 1.9 ppm in all the complexes showing a significant downfield shift due to complexation. However, a small shift in resonance frequency of the methylene carbon bonded to sulphonate group indicates a little effect on that carbon atom due to complexation.

Chemical shift values in ^{119}Sn NMR spectra play an important role in depicting the co-ordination number of the tin metal, thus in determining the geometry of the complexes. Complex **1-3** having chemical shift values at +32, +42 and +40 ppm, respectively, revealed four coordination number of tin atom [196] which is in consistence with the previously reported complexes where the Sn environment of dimethyl-, diphenyl- and dibutyltin complexes of MESNA was tetrahedral, as revealved with their ^{ll9}Sn Mössbauer spectroscopic study [216, 217]. Complex **4** having chemical shift value –105 ppm, which corresponds to four coordinated tin atom, because the replacement of aliphatic groups attached to tin, by phenyl groups induces upfield shifts in ^{119}Sn NMR chemical shift value [198]. ^{119}Sn chemical shift value of complex **5** is –236 ppm which indicates six coordination number of the tin atom in this complex having Oh geometry.

4.3.4. ESI MS Mass Spectrometry

The ESI–MS spectra for diorganotin(IV) complexes were recorded in the range m/z 200–1000, using acetonitrile solvent in positive-ion mode. All the complexes were characterized by molecular ion peaks corresponding to $[M+Na]^+$ *viz.* *m/z* = 498.8; *m/z* = 582.9; *m/z* = 694.4; *m/z* = 622.6; *m/z* = 763.4 for complexes **1-5**, respectively, which were used to determine the molecular weight of the complexes. The representative mass spectrum of complex **2** is given in Fig. 4.5.

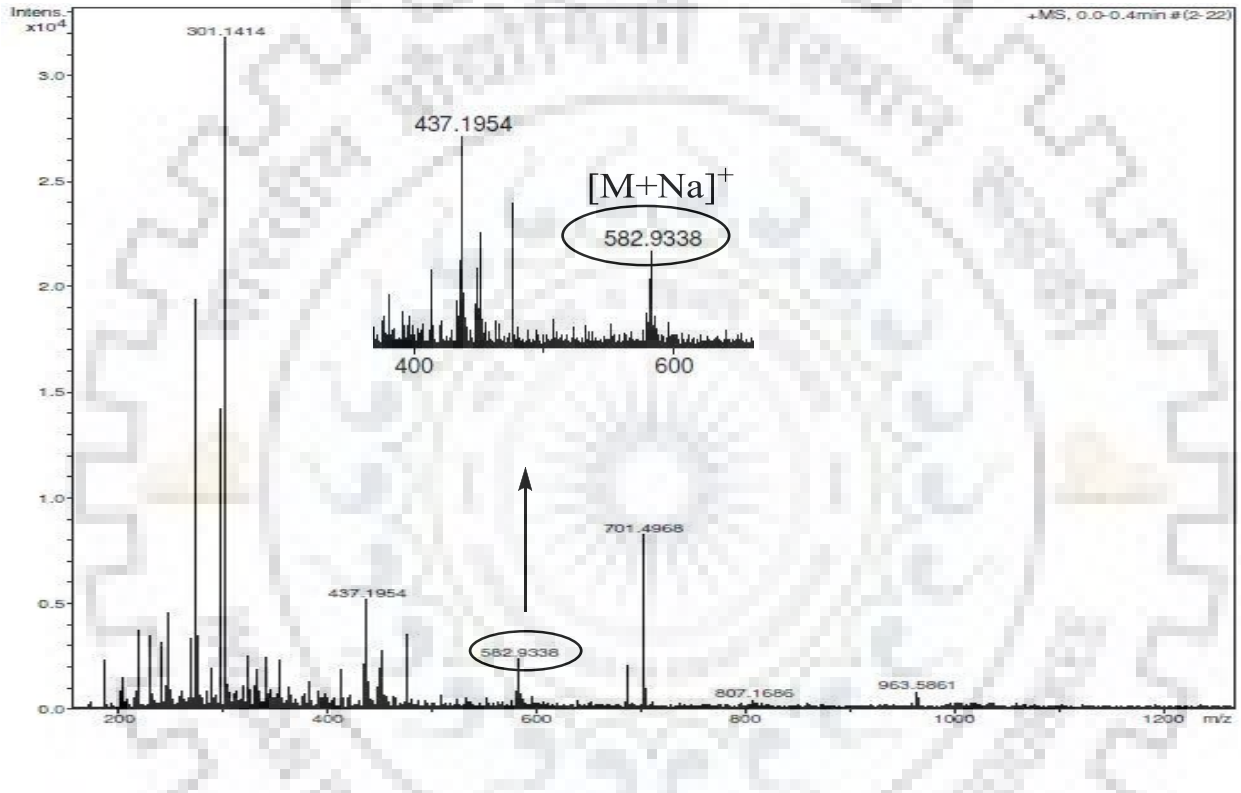

Fig. 4.5. ESI MS spectrum of complex 2 in methanol-acetonitrile mixture (1:3, v/v).

4.3.5. Geometry Optimization (DFT Calculations)

The complexes with proposed geometry were designed with the help of Chemcraft software and then subjected to full geometry optimization through Gaussian 09 software package [223] The Ligand (MESNA) and its organotin complexes were optimized with B3LYP function, and 6-31G (d,p) and LANL2DZ basis set for ligand and complexes, respectively. All the imaginary frequencies in the harmonic frequency calculation are zero which implies that the optimized geometries are very likely at global minima on the potential energy surface. Fig. 4.6. presents the optimized structure of MESNA and its complexes. Complexes **1-4** were optimized with distorted

tetrahedral geometries, and the ∠C–Sn–C obtained from ^{2}J values for complexes **1**, **2**, **4** and **5** are 118°, 116°, 115° and 162°, respectively, which are fairly close to the values, 115°, 116°, 112° and 164° obtained for these complexes from their optimized structures. Calculated ∠C–Sn–C and experimentally obtained IR frequencies of MESNA and complexes **1–5** were found in good agreement with those of calculated by DFT. The energy of MESNA and complexes **1–5** in the gaseous state, HOMO–LUMO energy gap and calculated ∠C–Sn−C are presented in Table 4.5. Frontier molecular orbitals (HOMO–LUMO) for all the synthesized complexes and MESNA generated by Gaussian 09 are provided in Fig.4.7. For all the complexes S atom which is attached to the tin moiety is the centre for HOMO, whereas LUMO is distributed over the tin atom, S of thiol and ethylene groups of MESNA.

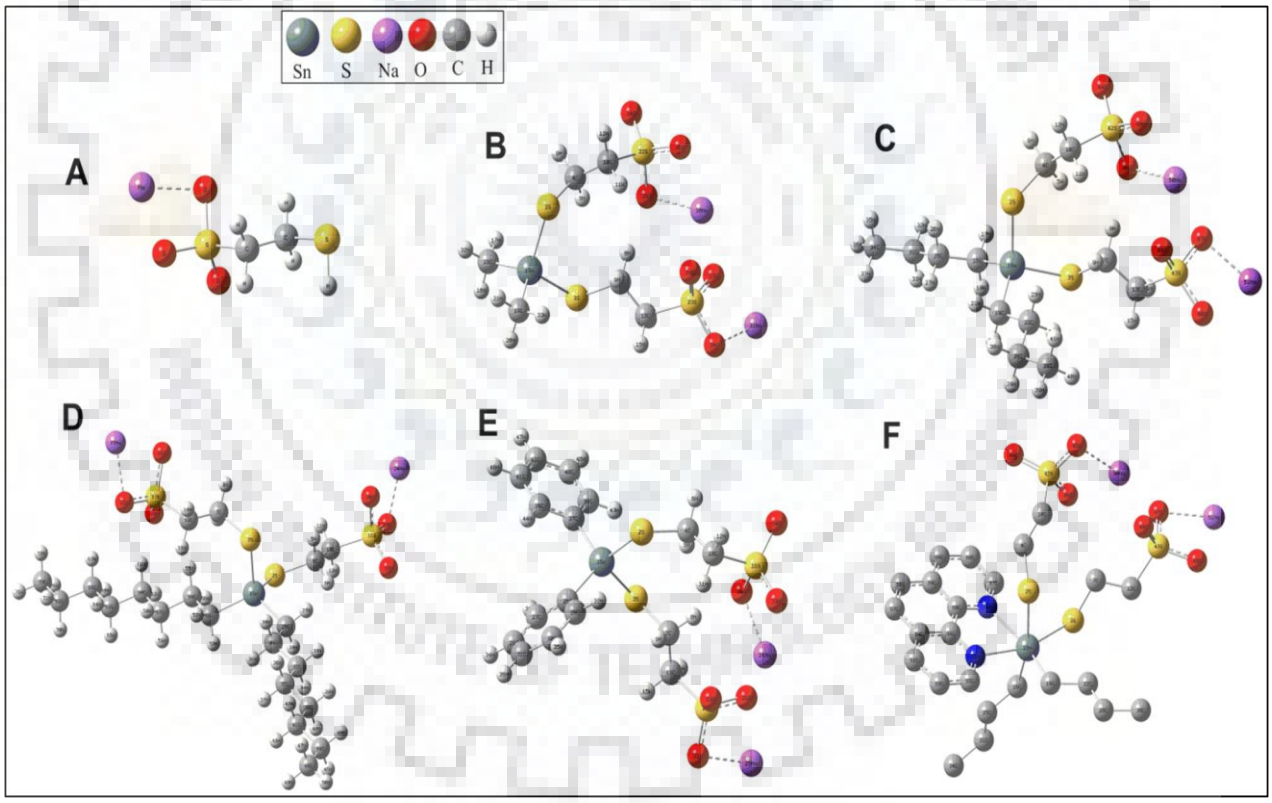

Fig. 4.6. Optimized geometries (ground state) for MESNA (A) at at B3LYP/6-31G level and complexes 1 (B); 2 (C); 3 (D); 4 (E); 5 (F); at B3LYP/LANL2DZ level.

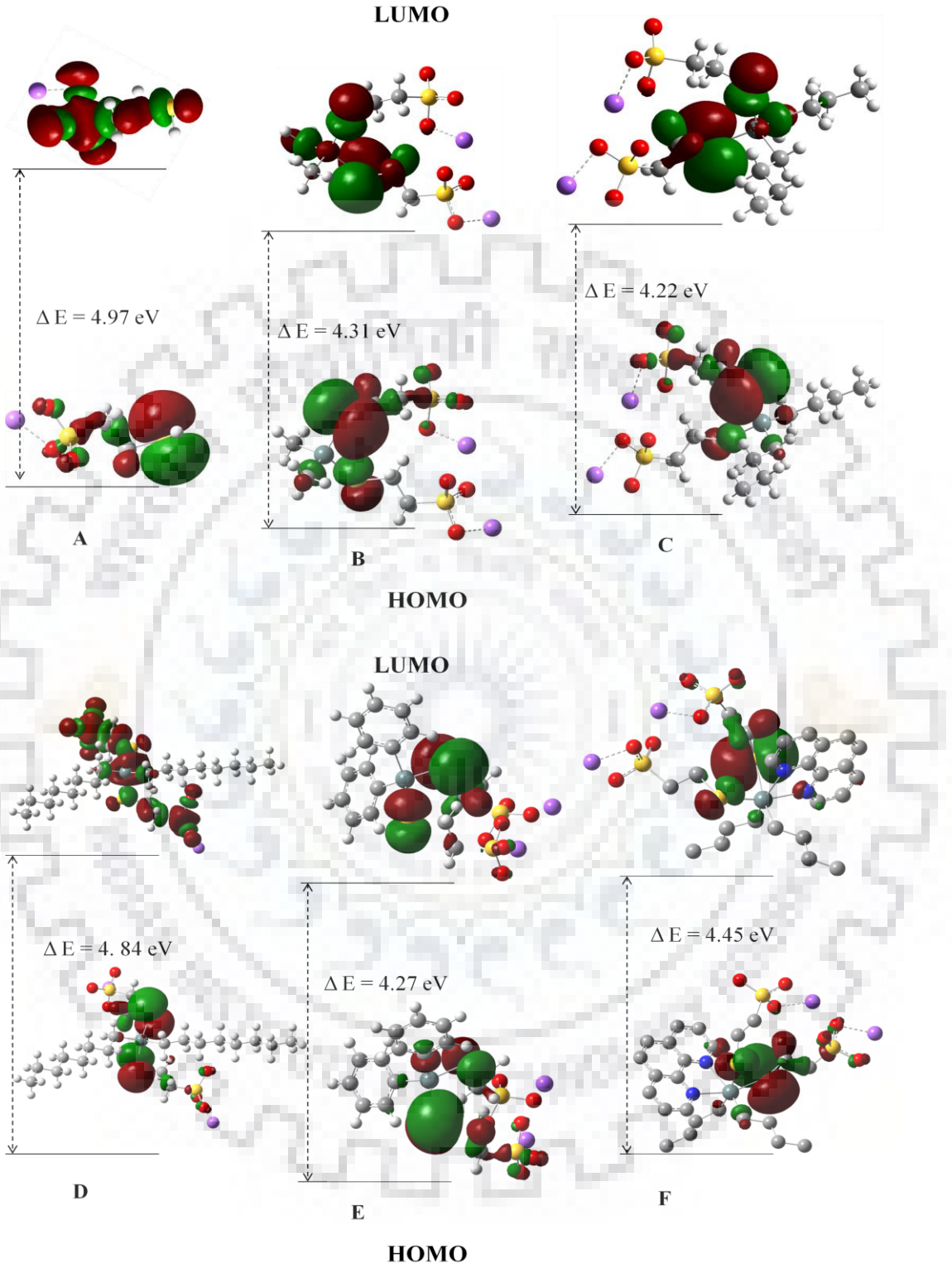

Fig. 4.7. Frontier molecular orbitals HOMO-LUMO of MESNA (A), complexes: 1 (B), 2 (C), 3 (D), 4 (E) and 5 (F) derived from DFT calculation using B3LYP/LANL2DZ level of theory.

Table 4.5. Summary of DFT calculations performed on diorganotin(IV) complexes 1-5 with B3LYP function, LANL2DZ basis set.

Ligand/ complex[a]	Energy of optimized geometry (a.u)	Angle C–Sn–C(°) (calculated from ^2J values)	Angle C–Sn–C (°) (calculated from DFT	$E_{(HOMO)}$, $E_{(LUMO)}$ (eV)	$E_{(HOMO)}$– $E_{(LUMO)}$ (eV)
MESNA	–1149.67	–	–	–6.7570 –1.7854	4.97
1	–1230.32	118	115	–6.4057 –2.0980	4.31
2	–1805.41	116	116	–6.2832 –2.0654	4.22
3	–1584.06	–	118	–6.1787 –1.3416	4.84
4	–2680.65	115	112	–6.3665 –2.0994	4.27
5	–2410.79	162	164	–5.2160 –2.7702	2.45

[a]complex number as given in Table 4.1.

4.3.6. DNA Binding Studies

4.3.6.1. UV-visible Spectrophotometric Titrations

The mode and extent of binding of MESNA and complexes **1-5** with CT DNA were scrutinized by recording UV-visible spectra of each molecule with successive addition of CT DNA. A band due to intra-ligand n–π^* transitions in the region of 200-250 nm was observed in case of MESNA and complexes **1-4**, whereas the complex **5** exhibited two bands in the region 200-300 nm due to n–π^* and π–π^* transitions. Successive addition of CT DNA in each complex solution leads to a hypochromism and significant red shift in each spectra (clearly seen in Fig. 4.8), which suggests stacking of compounds in between the base pairs of DNA resulted in intercalation and can be explained by the interaction between π^* orbital of intercalating ligands with π orbital of DNA base pairs [166, 224]. The coupling of partially filled π orbital decreases the probability of transitions and concomitantly resulting in hypochromism. Furthermore, the red shift is as a result of the decrease in the transition energy due to coupling. In order to compare the binding strength of the complexes with CT DNA, the intrinsic binding constants (K_b) were calculated from the ratio of the

slope to the intercept from the plots of [DNA]/($\varepsilon_a - \varepsilon_f$) vs [DNA]. The values of K_b for complexes **1-5** are 1.24×10^3, 4.22×10^3, 1.09×10^3, 2.25×10^3 and 3.44×10^3 M^{-1}, respectively, which is about 1.5 to 5 times higher than that of K_b (8.13×10^2 M^{-1}) evaluated for MESNA. Highest K_b among the studied complexes is for complex **2** *i.e.* dibutyltin complex of MESNA. The high K_b value of this complex is attributed to the hydrophobic interaction of butyl group with hydrophobic pockets of DNA which provides the additional stability to the DNA-ligand adduct [124]. In case of MESNA the negatively charged sulphonate group repels the phosphate group of DNA which prevents its proper stacking in the base pairs of DNA. The large size of octyl chain in complex **3** makes the intercalation difficult, however planar phenyl rings of complex **4** assists the intercalation and planar structure of 1,10-phenanthroline ligand in case of complex **5** facilitates the stacking within the CT DNA base pairs. However, the small K_b value for the complex **5** may be attributed to the partial insertion of phenanthroline moiety into the DNA base pairs [87]. As the observed K_b values for complexes **1-5** are quite low in comparison to that of a classical intercalator such as EB (3×10^6 M^{-1}) [225], and other known intercalators *viz.* isoxazocucumine (6.3×10^3 M^{-1}) and lumazine (1.74×10^4 M^{-1}) [226], which implies a partial intercalative mode of interaction of synthesized complexes with CT DNA.

4.3.6.2. Fluorescence Titration Studies

To further investigate the interaction of MESNA and complexes **1-5** with CT DNA, fluorescence titrations were performed. MESNA and complex **1** were found fluorescence inactive in the UV-visible range. Complexes **2-5** were found to exhibit weak emission spectra in the range 300-600 nm with maxima around 394 nm. Binding of complexes with CT DNA can be inferred by a change in fluorescence intensity of complexes with increasing concentration of CT DNA ($1.3–13\times10^{-5}$ M) while maintaining a constant concentration of complexes (100 μM) throughout the experiment. With subsequent addition of CT DNA in the solution of complexes **2-5**, the emission intensity increases gradually with appreciable red shift (Fig. 4.9), which is indicative of intercalation of these complexes with CT DNA. In the presence of DNA, the metal complex is bound in a hydrophobic environment which makes the complex molecules less accessible to the polar solvent molecules leads to increase in their fluorescence intensity [227, 228]. Hence, there may be a partial intercalative type of interaction of all the complexes with CT DNA. Table 4.6 presents the various parameters involved in fluorescence spectra.

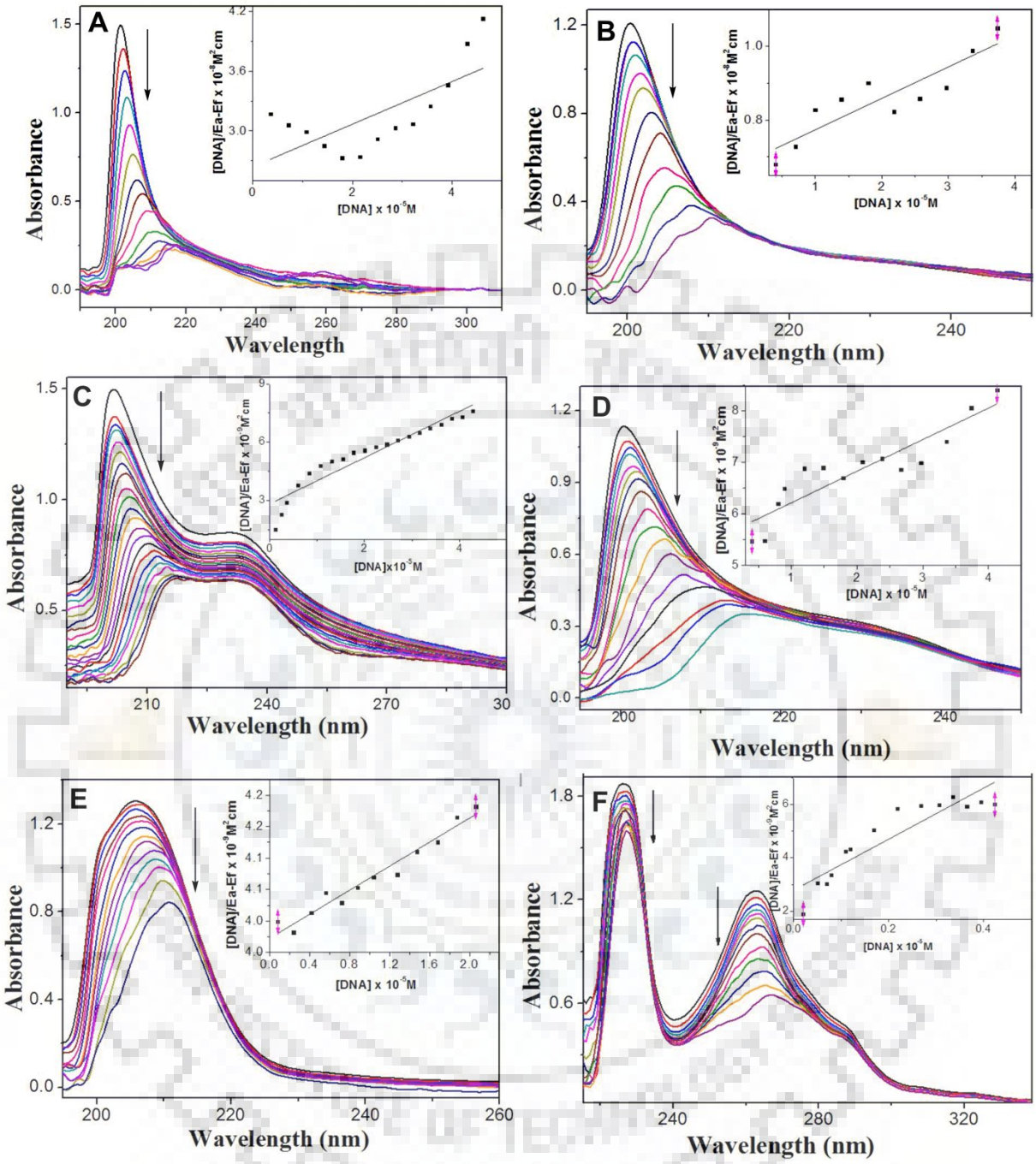

Fig. 4.8. UV-visible spectra of MESNA [1.0×10^{-3} M] (A) and complexes: 1 [2.5×10^{-4} M] (B), 2 [1.5×10^{-4} M] (C), 3 [1.6×10^{-4} M] (D), 4 [5.6×10^{-5} M] (E) and 5 [4.2×10^{-5} M] (F) in the absence and presence of CT DNA [$4.6–5.6\times10^{-4}$ M] in Tris-HCl/NaCl (5:50 mM), buffer, pH = 7.2 at 25 °C. Inset is showing linear plots of [DNA]/($\varepsilon_a - \varepsilon_f$) versus [DNA], the arrow indicates the decrease in intensity with increasing concentration of DNA.

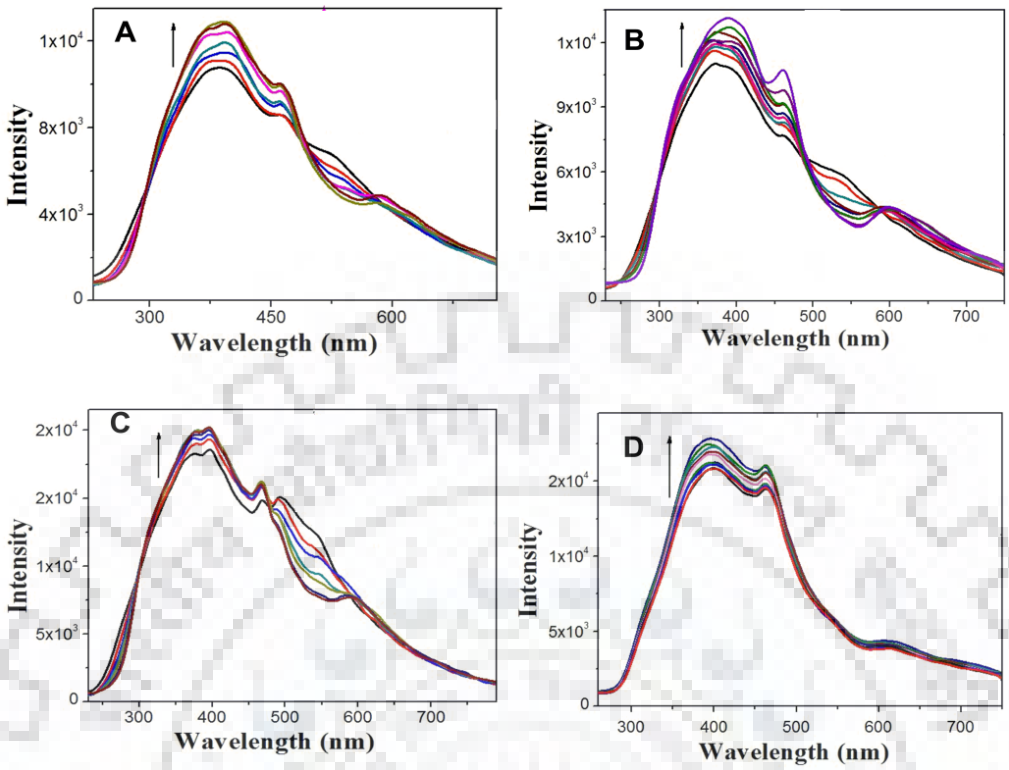

Fig. 4.9. Emission spectra of complexes (100 µM): 2 (A), 3 (B), 4 (C), 5 (D) in the absence and presence of CT DNA (1.3 – 13×10^{-5} M) in Tris-HCl/NaCl (5:50 mM), buffer, pH = 7.2 at 25 °C. Arrow indicates the increase in intensity with increasing concentration of DNA.

Table 4.6. Excitation and emission λ_{max}, and % increase in fluorescence intensity of complexes 2-5 with increasing concentration of CT DNA.

Complex[a]	Excitation λ_{max}	Emission λ_{max}	% Increase in intensity
Complex **2**	201	387	19%
Complex **3**	201	372	14%
Complex **4**	206	366	15%
Complex **5**	226	394	17%

[a]complex number as given in Table 4.1.

4.3.6.3. Ethidium Bromide Quenching Assay

EB displacement assay was carried out in order to explore the binding mode of MESNA and complexes with CT DNA. Being a planar aromatic compound, EB strongly intercalates within the base pairs of DNA. EB shows weak emission spectra in the aqueous solution, due to solvent quenching. However, its intercalation within the hydrophobic environment of DNA causes shielding of EB molecules from the polar solvent molecules, thus makes it strongly emissive [229] in the visible region. Displacement of EB with the addition of MESNA and complexes **1-5** suggests an intercalative mode of binding with CT DNA. In the present case, with successive addition of quenchers, a decrease in emission intensity of CT DNA–EB system (Fig. 4.10) was observed, which is suggestive of the displacement of EB from hydrophobic pockets of DNA by MESNA/complexes **1-5**. Dissociation of EB from CT DNA into the solvent system concomitantly leads to a decrease in fluorescence intensity of the CT DNA–EB system. However, the quenching constants (K_{sv}) calculated for the MESNA and complexes **1-5** are in the order of 10^3 which is quite lower in comparison to that of as obtained for classical intercalators (order of 10^7), which suggests a partial intercalation of MESNA/complexes with CT DNA. Maximum quenching is obtained in case of complex **2** followed by **5** and **4**, which shows a similar trend as observed in absorbance studies. Quenching constant (K_{sv}) and % decrease in fluorescence intensity for MESNA and complexes **1-5** are presented in Table 4.7.

Table 4.7. Quenching constant (K_{sv}), % decrease in fluorescence intensity and R^2 values for MESNA and complexes 1-5.

Ligand/Complex[a]	Decrease in fluorescence Intensity	K_{sv} (M^{-1})	R^2
MESNA	7%	2.38×10^2 (±0.03)	95
Complex **1**	9%	4.70×10^2 (±0.02)	97
Complex **2**	39%	2.80×10^3 (±0.08)	99
Complex **3**	11%	9.22×10^2 (±0.05)	98
Complex **4**	24%	9.44×10^2 (±0.03)	99
Complex **5**	26%	1.19×10^3 (±0.01)	99

[a]complex number as given in Table 4.1; mean ±SD of two independent observations;

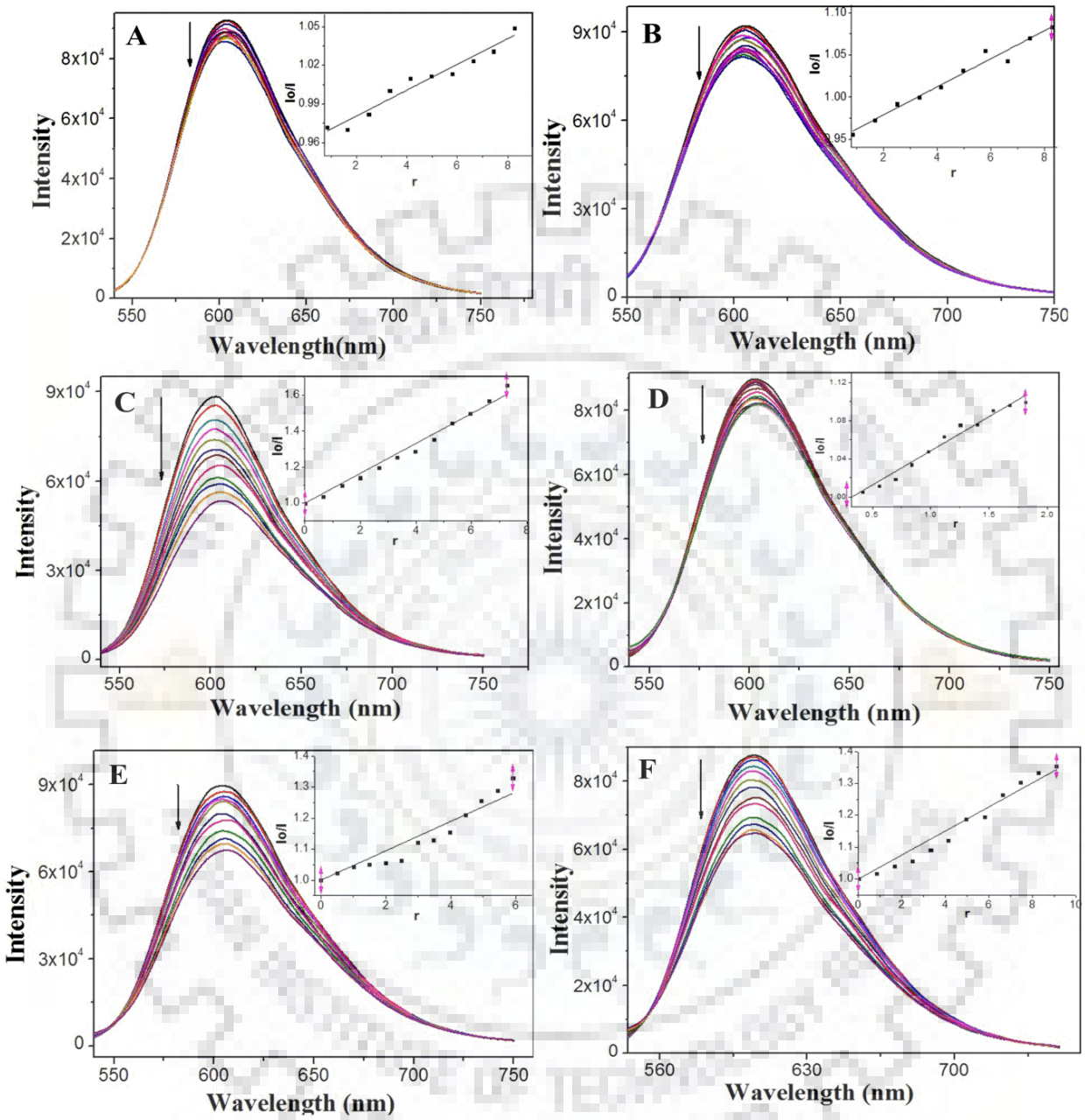

Fig. 4.10. Fluorescence quenching titration spectra of EB–CT DNA ([DNA]/[EB] = 5.3) with successive addition of (2 – 35×10^{-5} M) MESNA (A), 1 (B); 2 (C), 3 (D), 4 (E) and 5 (F), in Tris-HCl/NaCl (5:50 mM) buffer, pH = 7.2 at 25 °C [Excitation λ_{max} at 515 nm]. Inset is showing linear Stern Volmer plots and arrow indicates the decrease in intensity with increasing concentration of MESNA/Complexes.

4.3.6.4. Fluorescence Titration Studies in the Presence of KI

KI is an anionic quencher, having the ability to quench emission intensity of small molecules. Small molecules which can intercalate within the DNA base pairs remains protected inside the helix structure and could not be approached by anionic quenchers due to repulsion experienced by negatively charged phosphate group of nucleotides [230]. Moreover, the molecules which interact with DNA through groove binding or with electrostatic attraction can be easily disturbed by the quencher [231, 232]. In the present study, the fluorescence intensity of complexes, **2**-**5** is effectively quenched with the increasing concentration of KI, in the absence of CT DNA and a high K_{sv} value calculated by Stern-Volmer equation is obtained. However, with increasing amount of KI, the fluorescence intensity of CT DNA complex system was affected to a smaller extent and a substantial decrease in K_{sv} value was observed in comparison to that of latter, which indicates, the complex molecules are interacting with DNA *via* a partial intercalation and remain very less accessible to the quencher. The value of K_{sv} for complexes **2** and **5** are quite high for complex–KI system than that of complex–KI–CT DNA system indicates their strong interaction with CT DNA. However, complexes **3** and **4**, show comparatively less interaction as evident from less decrease in K_{sv} value. These results corroborate with our previous findings as described in sections 4.3.6.2 and 4.3.6.3. Fig. 4.11 indicates the Stern Volmer plots of KI fluorescence quenching titration and Table 4.8 presents the K_{sv} obtained for complex–KI and Complex–KI–CT DNA systems and % reduction in K_{sv}.

Table 4.8. K_{sv} obtained for complex–KI and Complex–KI–CT DNA systems and % reduction in K_{sv}.

Complex[a]	K_{sv} in the absence of DNA (M^{-1})	K_{sv} in the presence of DNA (M^{-1})	Relative reduction in K_{sv} (%)
2	14.7 (±0.1)	2.0 (±0.1)	86
3	1.76 (±0.05)	0.98 (±0.03)	44
4	14.98 (±0.2)	7.88 (±0.2)	47
5	9.2 (±0.1)	2.5 (±0.04)	73

[a]complex number as given in Table 4.1; mean ±SD of two independent observations;

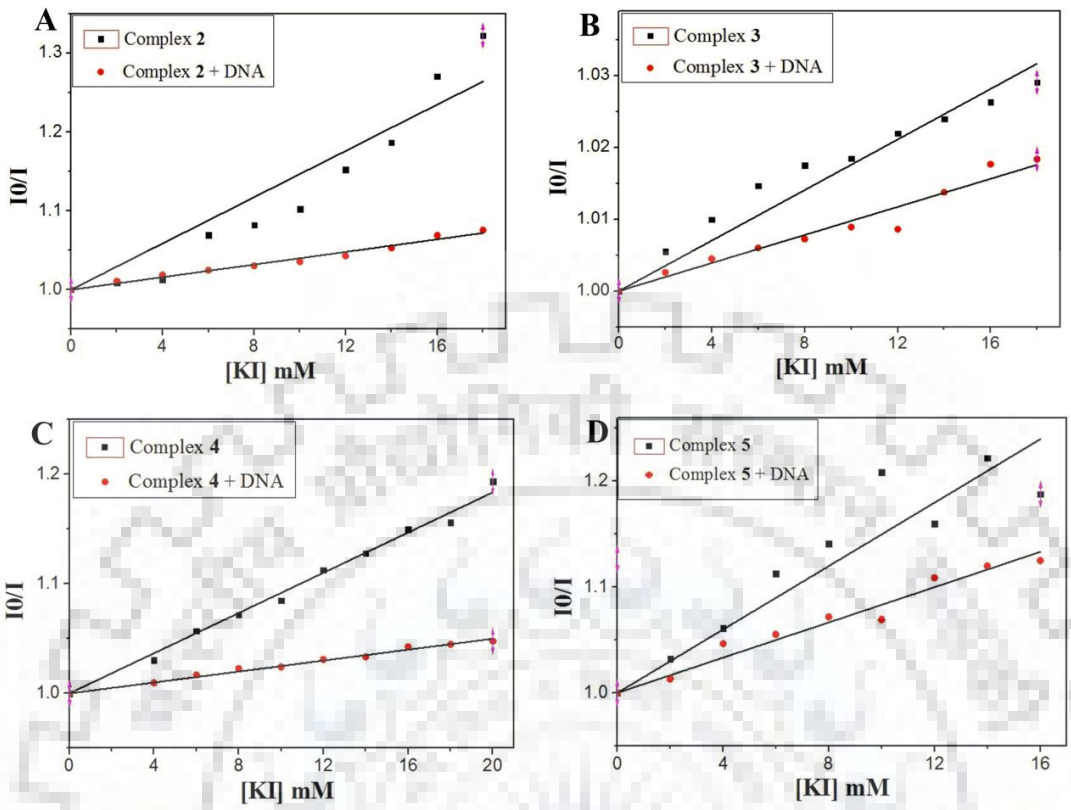

Fig. 4.11. Stern Volmer plots obtained from the fluorescence quenching of complexes (100 µM) 2 (A), 3 (B), 4 (C) and 5 (D), by KI (0–20 mM), in the presence and absence of CT DNA (100 µM) in Tris-HCl/NaCl (5:50 mM) buffer, pH = 7.2 at 25 °C.

4.3.6.5. Circular Dichroism Studies

Binding between DNA and complexes **1-5** can be studied by observing the conformational changes caused by complexes in the DNA helix with the help of circular dichroic (CD) spectroscopic study of DNA in UV region. The CD spectrum of CT DNA exhibited a positive band (279 nm) and a negative band (249 nm) due to the base stacking and helicity, respectively, which is characteristic CD spectrum of DNA in right-handed B form [232]. The changes in CD spectrum of CT DNA with successive addition of MESNA/complexes **1–5** in different concentration ratio ([MESNA] or [Complex]/[CT DNA], r = 0.08-0.25) are shown in Fig. 4.12. A small increase in the positive band and a decrease in negative band intensity of the CT DNA were found with the subsequent addition of MESNA, which indicates a partial intercalative mode of binding with DNA. In the CD spectra of CT DNA, with addition of complexes **3-5**, a moderate to good increase in intensity of positive band was found, which indicates base stacking of these complexes within the base pairs of

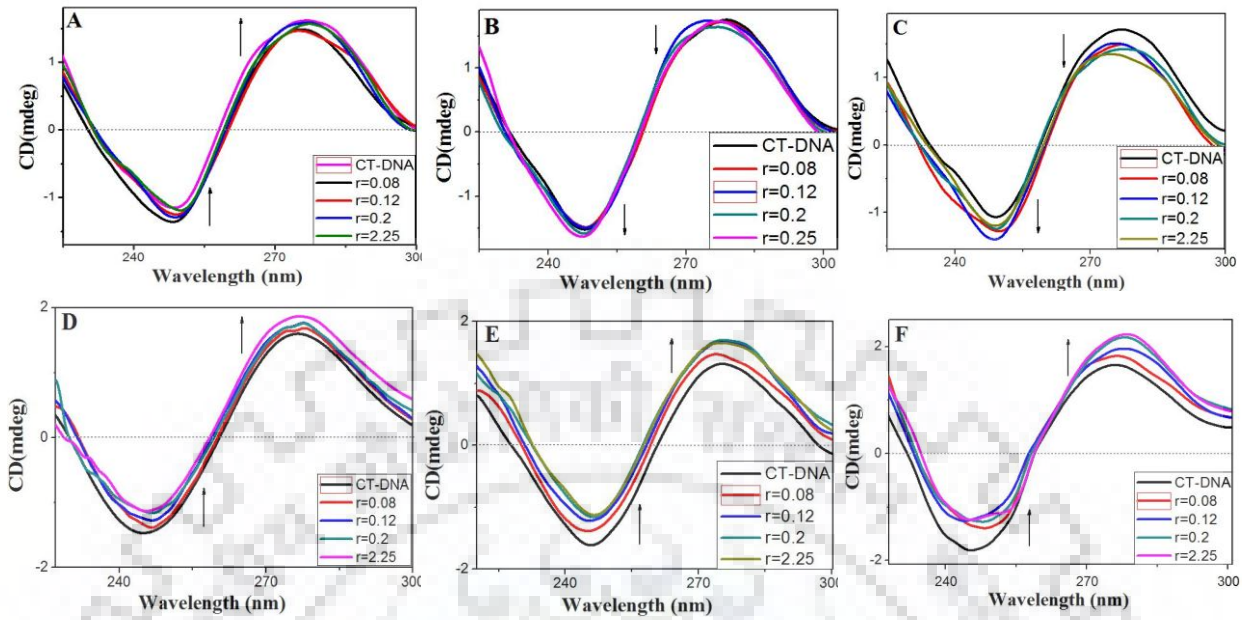

Fig. 4.12. CD spectra of CT DNA in the absence and presence of MESNA (A), 1 (B), 2 (C), 3 (D), 4 (E), 5 (F); ([MESNA] or [Complex]/[CT DNA], [*r* = 0.08-0.25]) in Tris-HCl/NaCl (5:50 mM) buffer, pH = 7.2 at 25 °C. Arrows are indicating the decrease/increase in intensity with increasing concentration of MESNA/Complexes.

DNA [233], on the other hand a decrease in intensities of negative bands of these complexes indicates a disturbance in helix structure of DNA. The decrease in negative band intensity is probably due to the unwinding of the DNA helix upon interaction of complexes and then transformed into other A–like conformations [234]. Complex **2** indicates an increase in the negative band intensities due to a right-handed conformational change of the DNA double helix. An appreciable decrease in the intensity of positive band with the addition of complex **2**, is possibly due to its partial intercalative mode of binding with CT DNA [234]. In contrast, the complex **1** shows a very slight change in the positive and negative band intensities, indicating very less binding of the complex **1** with DNA.

4.3.6.6. Viscosity Measurements

The viscosity of CT DNA is regarded quite sensitive towards any structural change in DNA, hence viscosity measurement is found to be the most critical test which gives a lucid picture of the binding model of DNA with small molecules in solution. The classical intercalation of the

molecule inside the DNA lengthens the helix of DNA. In order to accommodate the bound ligand, separation of base pairs occurs which leads to an increase in viscosity of DNA. However, partial or non-classical intercalators could cause bending or kinking in DNA helix, which results in a reduction of its length and concomitantly, its viscosity [235]. Furthermore, the non-intercalators (electrostatic and grooved binder) cause a less significant change in viscosity of DNA [229]. The specific viscosity (η) was plotted against different concentration ratio of the complex to CT DNA. A decrease in viscosity with increasing complex concentration ascertained that all the complexes are interacting with CT DNA *via* a partial intercalative mode. MESNA is also acting like a partial intercalator but having less binding strength in comparison to that of complexes. It is evident from Fig. 4.13 that more concentration of MESNA is required to cause a similar decrease in viscosity as that of complexes. A very sharp decrease in viscosity of CT DNA was found in case of all complexes which evidenced the only mode of interaction involved is partial intercalation.

All the above observations provide a corroborative evidence for the partial intercalative mode of binding of complexes **2** and **5** with DNA, whereas, for MENSA and complexes **1-3,** other modes of binding too exist along with partial intercalation. These observations are consistent with our data which are obtained from absorption and fluorescence spectroscopic studies. Interaction of metal complex with DNA depends on various factors i.e. size, charge, and geomtry of the complexes. In the present study, it has been found that the complexes have higher potential to bind with DNA in comparison to that of MESNA, which can be inferred from higher K_b, K_{sv}, more pronounced change in circular dichroic spectra of CT DNA and a significant decrease in viscosity upon their addition

4.3.7. Plasmid DNA Cleavage Studies

Organotin complexes have been studied extensively for their ability to cleave supercoiled (SC) pBR322 DNA with the help of agarose gel electrophoresis. Cleavage of one strand results in a slower moving nicked circular (NC) form, however, cleavage of both the strands produce a linear (L) form, which is positioned between nicked and supercoiled forms [235, 236], as the DNA moved under the influence of electric field. The extent of cleavage of plasmid DNA for all the complexes was analyzed with increasing complex concentration and with ascorbic acid, which acts as an activator of cleavage activity. The observed cleavage pattern of plasmid DNA with increasing concentration of MESNA/complexes (25, 50 and 100 μM) is shown in Fig. 4.14, in

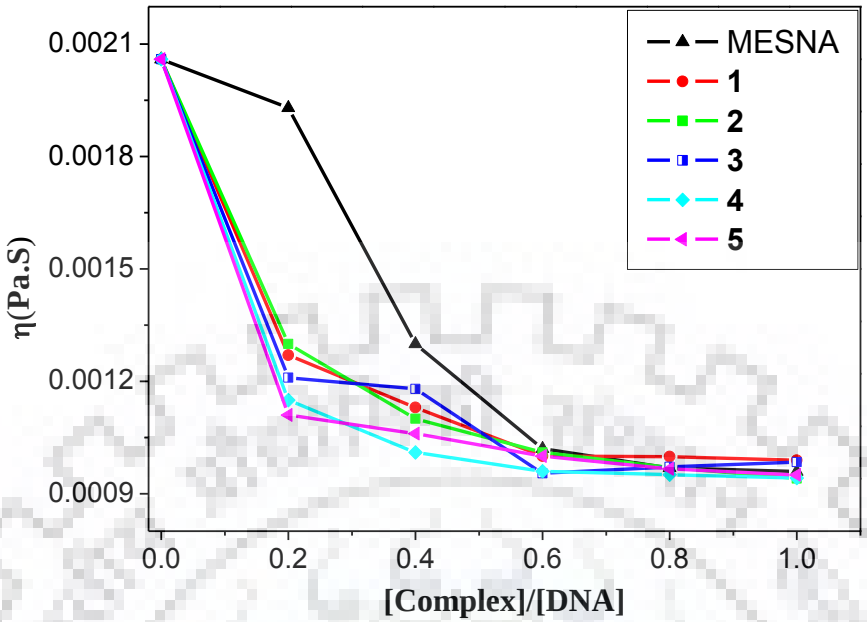

Fig. 4.13. The decrease in viscosity (η) of CT DNA (100 µM) with successive addition of MESNA and complexes 1-5 (0 to 100 µM).

lanes I-III. A little conversion of SC to NC form results in a gradual decrease in the intensity of SC form I with a simultaneous increase in the intensity of the corresponding NC form II. Furthermore, the extent of cleavage in case of MESNA is comparatively smaller than that observed with complexes which indicates that organotin(IV) moieties play an important role and participate in the process of plasmid cleavage. A small amount of adduct is also formed in case of MESNA and complexes **1** and **5,** due to which a mobility of DNA restricted and a band is seen prior to NC form II. The extent of plasmid cleavage was significantly enhanced in the presence of H_2O_2 (lane V, Fig. 4.14), which is a hydoxy radical generator and acts as an activator in plasmid cleavage activity. Ascorbic acid is another activator of plasmid cleavage which also results in a remarkable increase in the form II as shown in lane VII in Fig. 4.14. Furthermore, in order to explore the underlying mechanism of plasmid cleavage by MESNA/complexes, the cleavage pattern of pBR322 plasmid was observed in the presence of $OH^{\cdot}$ radical scavenger, DMSO, 0.2 M (lane V) and singlet oxygen quencher NaN_3, 0.2 M (lane IV). The presence of DMSO (lane VI) along with MESNA/complexes indicate a partial inhibition in the cleavage activity of pBR322 DNA as shown by a small increase in SC and decrease in NC band intensities, which suggests the involvement of hydroxyl radical in the cleavage process, hence suggested a hydrolytic mechanism of DNA cleavage, though the extent of cleavage is small. However, there is no such inhibition in cleavage activity was observed

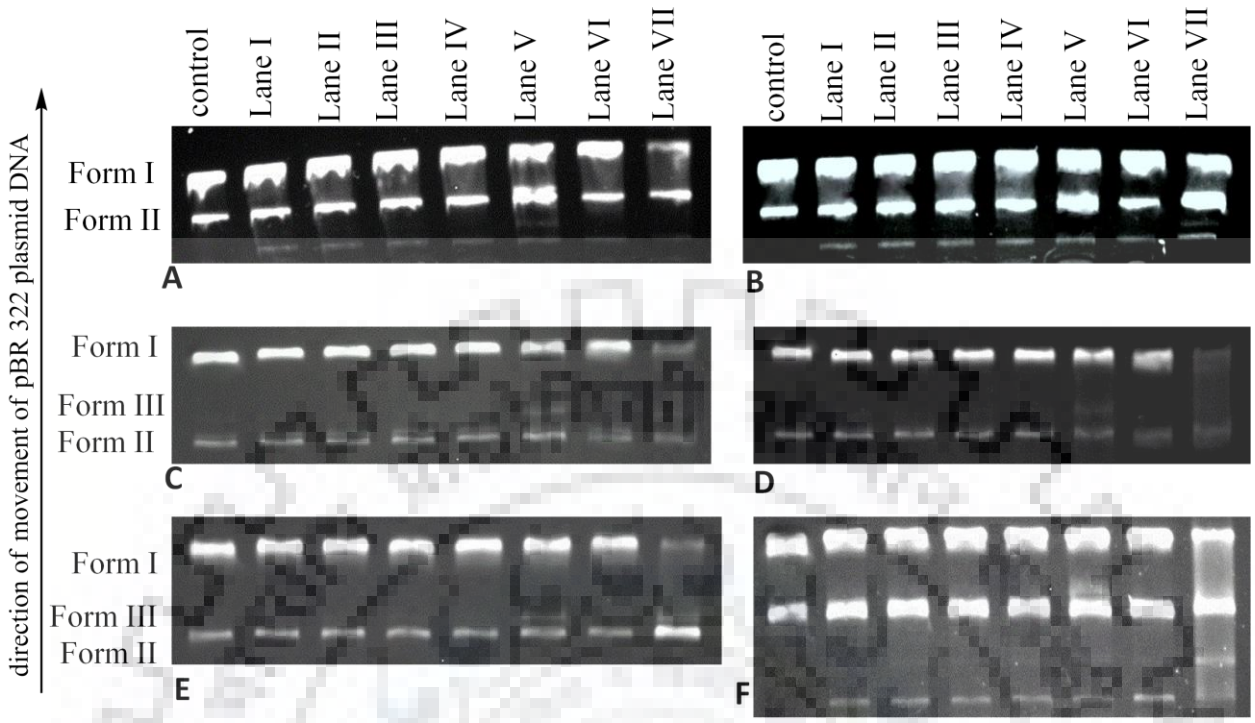

Fig. 4.14. The cleavage pattern of pBR322 plasmid DNA (50 ng) by MESNA (A); complex 1 (B); complex 2 (C); complex 3 (D); complex 4 (E) and complex 5 (F); after incubation for 1h at 37 °C, at different concentration of MESNA/Complexes, Control: DNA; Lane I: [DNA + (25 µM complex/MESNA)]; Lane II: [DNA + (50 µM complex/MESNA)]; Lane III: [DNA + (100 µM complex/MESNA)]; Lane IV: [DNA + (0.2 M NaN_3) + (100 µM complex/MESNA)]; Lane V: [DNA + (100 µM complex/MESNA)+(0.2 M H_2O_2)]; Lane VI: [0.2 M DMSO) + (100 µM complex/MESNA)]; Lane VII: [(0.2 M Ascorbic acid) + (100 µM complex/MESNA)].

in case of NaN_3 (lane IV), which ruled out the involvement of singlet oxygen.

4.3.8. Biological Studies

4.3.8.1. Cytotoxicity Study through MTT Assay

In vitro MTT assay using human cell lines provides important information about the compound cytotoxicity. The cytotoxicity of all the synthesized complexes **1-5**, were estimated through MTT assay against DU145 (prostate cancer), HTC-15 (colon adenocarcinoma) and HeLa (cervical cancer) cell lines and their IC_{50} value along with that of MESNA are listed in Table. 4.9. Calculation of IC_{50} (inhibitory concentration) values are carried out using best linear fit regression model [46, 237, 238] and is an average of two values calculated through two independent

experiments. The literature review revealed that the compounds exhibiting IC_{50} < 1.0 μM, between 1.0–10.0 μM, between 10.0–30.0 μM, > 30.0 < 100.0 μM and > 100.0 μM are considered as highly cytotoxic, considerably cytotoxic, moderately cytotoxic, mildly cytotoxic and non-cytotoxic, respectively [45]. Complexes **4** [Ph_3Sn(MESNA)] and **5** [$Bu_2Sn(MESNA)_2$.Phen] diplayed high cytotoxicity against all the tested cell lines and complex **3** was found moderately active only against colon cancer cell lines, however MESNA and complexes **1** and **2** exhibited very low cytotoxicity against all the tested cancer cell lines. Complex **5** [$Bu_2Sn(MESNA)_2$.Phen] has been found the most cytotoxic among all the test compounds against all the cancer cell lines under observation, which was followed by the Complexes **4** [Ph_3Sn(MESNA)]. Both the displayed potent cytotoxicity against colon cancer cell lines, even exhibited 6–14 times greater activity compared to *cis*-platin and 5-fluorouracil. Complexes **4** and **5** demonstrated considerably high *in vitro* cytotoxicity against DU145 (prostate cancer) cell lines, which possesses intrinsic and acquired resistance to *cis*-platin and also against HeLa (cervical cancer) cell lines, even greater or comparable with that of 5-fluorouracil.

Table: 4.9. Cytotoxic screening results of organotin complexes of MESNA against different cell lines of human origin; IC_{50} value is expressed in μM ± SEM.

Complexes[a]	DU145	HCT-15	HeLa
MESNA	>100	>100	>100
1	>100	>100	>100
2	>100	>100	>100
3	>100	19.22±0.8	>100
4	11.89±0.6	1.69±0.3	3.54±0.2
5	**7.15±0.7**	**0.83±0.1**	**1.85±0.4**
5-FU	15.4±0.8	12.2±0.5	2.08±0.2
Cis-platin	n.d.	5.04±1.4[b]	18[c]

[a]numbers of complexes as given in Table 4.1; [b]reference [237]; [c]reference [57]; n.d.= not determined; 5-FU = 5-fluorouracil; DU145: prostate cancer cells; HTC-15: colon adenocarcinoma cells and HeLa: cervical cancer cell.

The presence of 1,10-phenanthroline moiety makes the other ligand (MESNA) more labile in complex **5** compared to complex **2**, which may be responsible for the generation of active metal species. Moreover, complexes **1** and **2** were more stable in buffer solution at physiological pH compared to other complexes, which could explain their low activity. Further, the electronic and lipophilic character of the complexes may also be responsible for the difference in the activities [239]. The presence of phenyl and butyl groups with high lipophilicity in complex **4** and complex

5, respectively, may responsible for their remarkable cytotoxicity against the prostate cancer, colon adenocarcinoma and cervical cancer cells. Further experiments are needed to be done in order to explore the cause of cytotoxicity and in-depth mechanism.

4.3.8.2. Acridine Orange (AO)/Ethidium Bromide (EB) Staining

This study is an important tool to distinguish between the normal viable cells, early apoptotic cells, late apoptotic cell and necrotic cells. This method is based on the morphological changes occur in the cytoplasmic membranes and nuclear chromatin material of cells during the process of apoptosis. On the basis of fluorescence emission of Acridine Orange (AO)/Ethidium Bromide (EB) stained cells and their chromatin condensation, the cells can be identifies as: A) live/viable cells

with intact nuclei which take up AO dye and appear green and having uniform structures; B) early apoptotic cells can be detected with bright green nuclei with condensed chromatin, but with intact membranes; C) late apoptotic cells stained with EB and appear orange due to their ruptured cell membranes and fragmented chromatin material; D) necrotic cells with normal nuclei and uniform structures look like that of viable cell except the orange-red uniform EB staining [240]. The AO/EB staining of the cancer cells were performed by treating them with the IC_{50} value of the respective test compounds having highest cytotoxicity towards the particular cell line. The morphological changes appeared in the HCT-15, DU145 and HeLa cells when treated with inhibitory concentration (IC_{50}) of the complexes **4** and **5** as illustrated in Fig. 4.15, Fig. 4.16 and Fig. 4.17, respectively. In the control (untreated) and vehicle control (treated with DMSO) all the cells appear uniform with green fluorescing nuclei, however in the cell lines treated with complexes **4** and **5**, cells appear green with condensed chromatin, indicated early apoptotic cells and orange to red coloured cells with condensed or fragmented chromatin material indicated the late apoptosis. Further, a small amount of necrosis with prevalent apoptosis could not be denied. Hence, the involvement of both the apoptosis (majorly) and necrosis are responsible for the cytotoxicity of the complexes.

4.3.8.3. DNA Fragmentation Assay

DNA fragmentation assay is regarded as the hallmark of apoptosis. During apoptosis, Caspase-3 triggers the endonulcease activity which cleave the DNA at the internucleosomal units (where DNA is not wrapped by the histones) and resulted the fragmentation of DNA into different

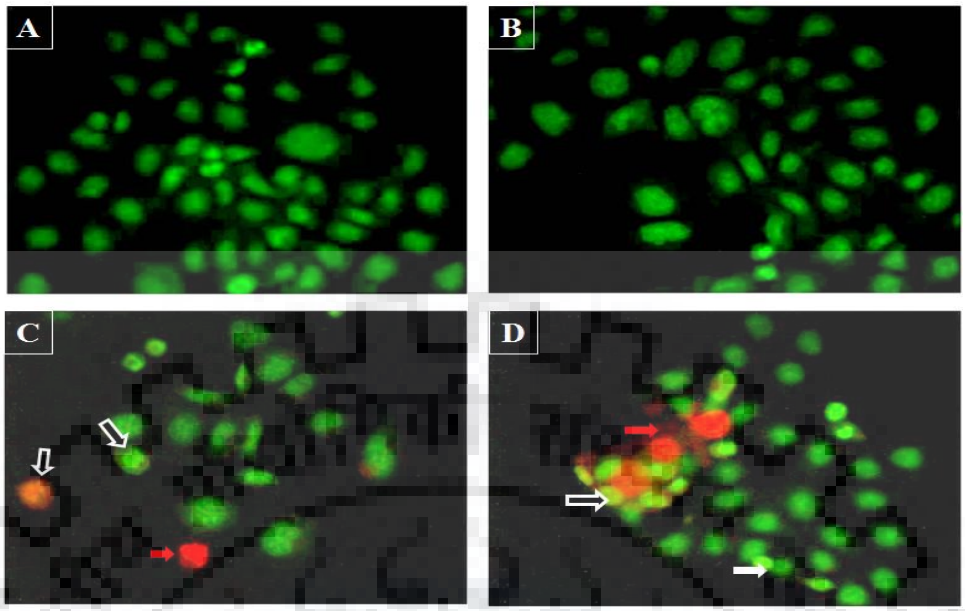

Fig. 4.15. AO/EB staining of HCT-15 cell lines (A) control, (B) vehicle (DMSO) treated cells, (C) cells treated with IC_{50} value of complex 4 and (D) cells treated with IC_{50} value of complex 5. Solid white arrows indicate the early apoptotic, white outlined arrows indicated the late apoptotic and solid red arrows indicated the necrotic cells.

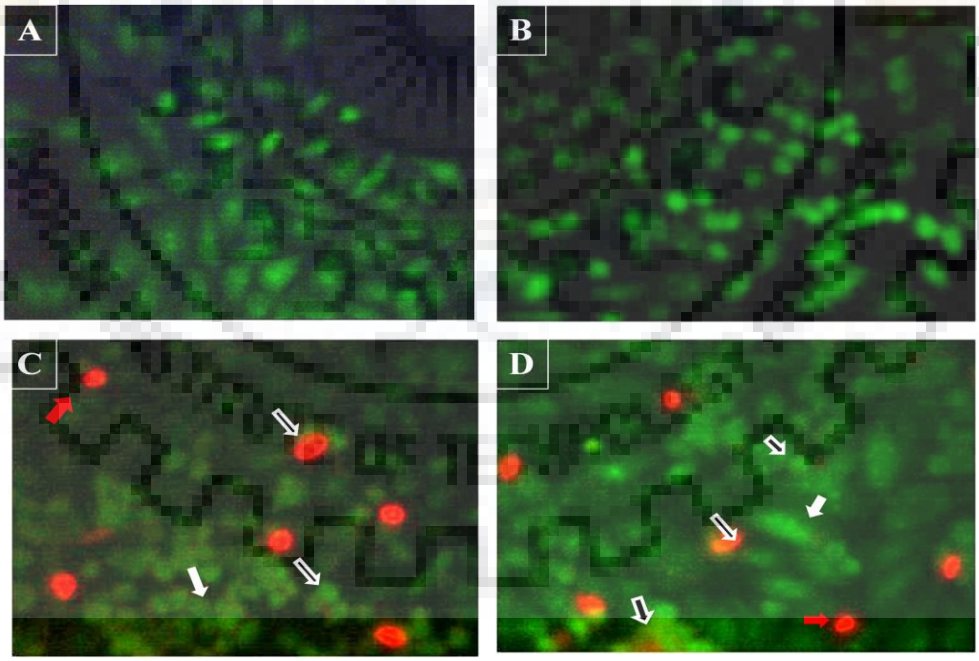

Fig. 4.16. AO/EB staining of DU145 cell lines (A) control, (B) vehicle (DMSO) treated cells, (C) cells treated with IC_{50} value of complex 4 and (D) cells treated with IC_{50} value of complex

5. Solid white arrows indicate the early apoptotic, white outlined arrows indicated the late apoptotic and solid red arrows indicated the necrotic cells.

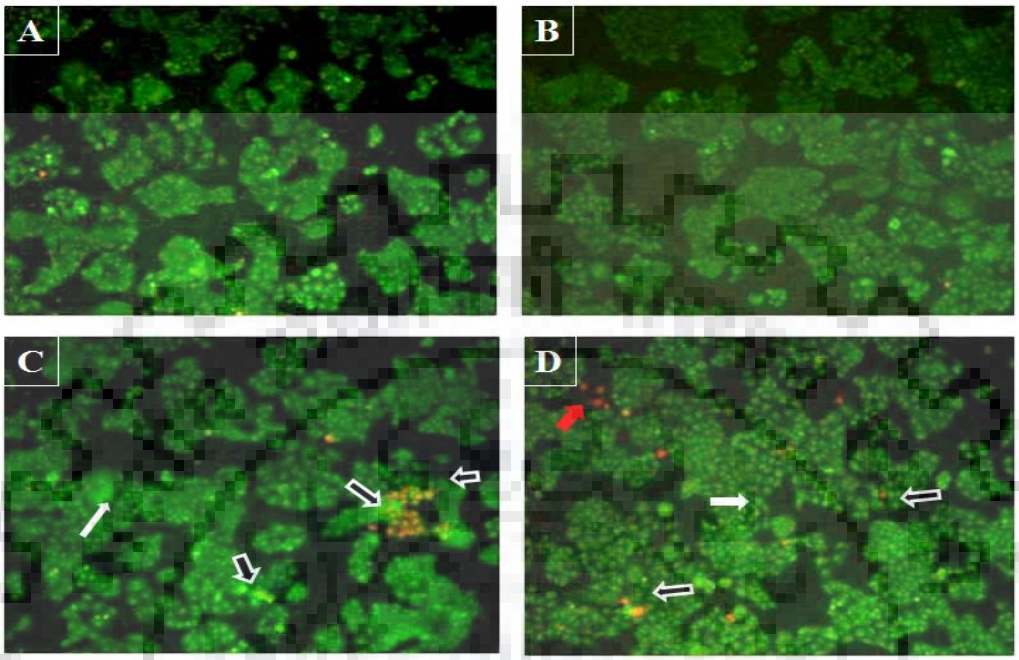

Fig. 4.17. AO/EB staining of HeLa cell lines (A) control, (B) vehicle (DMSO) treated cells, (C) cells treated with IC_{50} value of complex 4 and (D) cells treated with IC_{50} value of complex 5. Solid white arrows indicate the early apoptotic, white outlined arrows indicated the late apoptotic and solid red arrows indicated the necrotic cells.

oligomer units, which looks like a DNA ladder when subjected to agarose gel electrophoresis [241a]. In contrary to apoptotic activity, necrosis leads to appearance of irregular sized DNA bands or DNA smear in agarose gel electrophoresis. However, in some cases single strand cleavage in DNA has been observed in apoptotic phenotypes, which does not form the DNA ladder in gel electrophoresis [241b]. In the present case the DNA (extracted from the DU145 and HCT-15 cells) treated with complex **5** doesn't reveal any fragmentation and look similar as that of vehicle treated DNA control (Fig. 4.18 (A)), which means that apoptosis (as shown in AO/EB staining) and cytotoxicity caused by this complex against DU145 and HCT-15 is caused by methods other than the Caspase-3 activated DNA fragmentation. This may be either due to the single strand scission of the DNA or other changes occur on the cell surface. Furthermore, a ladder formation is seen (Fig.

4.18 (B)) in the fragmentation pattern of DNA extracted from HeLa cells, when treated with the complex **5**, which indicated the apoptosis is the main cause of cytotoxicity against HeLa cell lines.

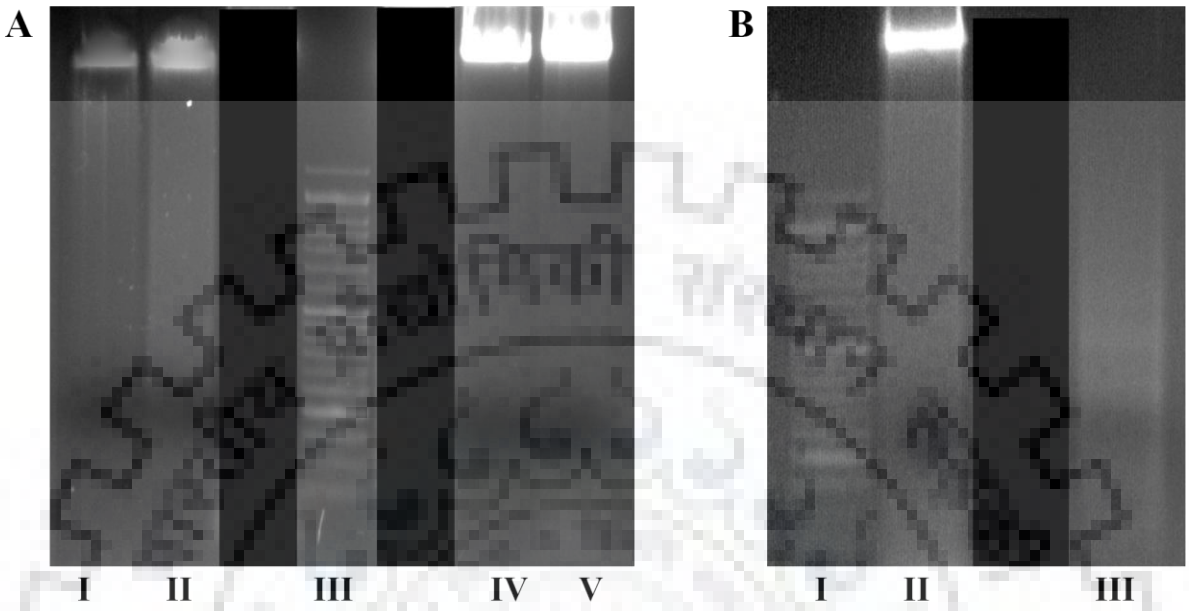

Fig. 4.18. Fragmentation pattern of DNA extracted from cell lines on treatment with complex 5, through agarose gel electrophoresis: (A) lane I: control (DNA extracted from DU145), lane II: DNA extracted from DU145 treated with complex 5; lane III: DNA marker (50 base pairs); lane IV: DNA extracted from HCT-15 treated with complex 5 and lane V: control (DNA extracted from HCT-15) (B) lane 1: DNA marker (50 base pairs); lane II vehicle treated control (HeLa DNA); lane III: DNA extracted from HeLa treated with complex 5

CHAPTER - 5

Tri- and Diorganotin(IV) Derivatives of Non-Steroidal Anti-Inflammatory Drug, Sulindac: Characterization, Electronic Structures (DFT), DNA-Binding, Plasmid Cleavage and *In Vitro* Antitumour Studies.

5.1. INTRODUCTION

Successful applications of metal complexes in the treatment of numerous human diseases have been led to a significant progress in medicinal organometallic chemistry in the past few years, which has been allowing the rational design of novel, non-conventional, platinum compounds, as well as innovative non-platinum metal-based antitumor agents. Organotin(IV) compounds in general and organotin(IV) carboxylates in particular have been emerged potentially biologically active compounds among non-platinum chemotherapeutic metallopharmaceuticals. Organotin corboxylates has been remained the focus of interest in view of their considerable structural diversity and significant biological activities [242, 243].

Non-steroidal anti-inflammatory drugs (NSAIDs) have been found quite effective against various types of cancers *viz.* breast, esophageal, stomach, prostate, bladder, ovarian, lung and colorectal cancers and successfully used in combination therapies with antitumour drugs [244, 245]. A specific group of NSAIDs along with sulindac has been reported to enhance the cytotoxicity of antitumor drugs *viz.* doxorubicin, daunorubicin and epirubicin, teniposide, VP-16 and vincristine, at non-toxic levels [246]. Sulindac sulfide is one of the early NSAID, known to inhibit the activities of cyclooxygenases (COXs), of which COX-1 is constitutively expressed whereas COX-2 is induced by mitogenic and inflammatory stimuli [247]. Sulindac has received extensive attention because of its potential to induce apoptosis and inhibit cancer cell growth [247-251]. Also the effectiveness of sulindac against colorectal cancer has been reported in both humans and animals [252-254]. The effectiveness of sulindac in reducing the number and size of polyps in the patients with familial adenomatous polyposis (a precursor to colorectal cancer) has been studied by Giardiello et al. [255]. It has also been found quite effective against the cell lines derived from oral SCCa [256]. Sulindac's antineoplastic effect on oral cancer cells is mediated through Stat3 (signal transducer and activator of transcription 3) down modulation; treatment with sulindac first leads to a significant decrease in Stat3 phosphorylation and then eventual elimination of Stat3 expression [257].

Synthesis and study of metal complexes with active drugs as ligands is emerging a new area of increasing interest for metallopharmaceutical and medicinal chemistry as an approach to new drug development [258, 259]. Organotin(IV) derivatives of several NSAIDs have been reported as potential antitumor and anti-tuberculosis agents [151, 152, 154, 158, 159, 260, 261].

The complexation of drug with specific metals may improve the activity towards certain diseases and may widen the activity spectrum. In the view of pharmacological importance of sulindac and potential biological activities of organotin(IV) complexes with several NSAIDs increase our quest to explore the chemistry of organotin(IV) derivatives of sulindac. The present chapter describes the complexation of sulindac with a series of organotin(IV) moieties and investigation of their possible modes of DNA binding through photophysical techniques. Further, the antitumour activities of the complexes have been explored against HCT-15 (colon adenocarcinoma), MCF-7 (mammary cancer), HeLa (cervical cancer), and LNCaP (androgen-sensitive prostate adenocarcinoma) cell lines of human origin through MTT assay.

5.2. EXPERIMENTAL SECTION

5.2.1. Synthesis

5.2.1.1. Synthesis of Triorganotin(IV) Complexes of Sulindac by Sodium Salt Method

The solution of sulindac (0.5 mmol, 0.178 g) in 15 mL of specially dried methanol was added to sodium methoxide which was prepared by reacting sodium metal (0.8 mmol, 0.016 g) with 15 mL of dry methanol. The resulting solution was refluxed for 4–5 h with constant stirring. Hot methanol (15 mL) solution of trimethyltin(IV) chloride (0.5 mmol, 0.100 g) or triphenyltin(IV) chloride (0.5 mmol, 0.193 g) or tributyltin(IV) chloride (0.5 mmol, 0.141 mL) was added to the resulting sodium salt solution of the drug. The yellow solution was further refluxed overnight (24–28 h), with constant stirring under dry nitrogen atmosphere. The solution was centrifuged and filtered in order to remove sodium chloride formed during the reaction. The excess solvent was vaporized with reduced pressure and the products then obtained were washed with methanol and *n*-hexane.

5.2.1.2. Synthesis of Dibutyltin(IV) and Dioctyltyltin(IV) Complexes of Sulindac by Azeotropic Removal of Water

Dry and hot methanolic solution of (15 mL) of dibutyltin(IV) oxide (0.5 mmol, 0.124 g) or dioctyltyltin(IV) (0.5 mmol, 0.181 g) oxide was added drop wise into a hot methanolic (15 mL) solution of sulindac (1 mmol, 0.356 g). The solution thus obtained was refluxed for 24–28 h. Water formed in the course of reaction was continuously removed with azeotropic removal of water. The solvent was removed under reduced pressure. Sticky product was obtained, which become solid

after keeping in vacuum for two weeks. The product obtained was washed with methanol–hexane mixture (1:3 v/v).

5.2.1.3. Microwave Assisted Synthesis

Sodium salt of sulindac (1 mmol, 0.356 g) was finely ground with dimethyltin (0.5 mmol, 0.110 g) or diphenyltin(IV) dichloride (1mmol, 0.343 g) to obtain a homogeneous mixture. To this mixture few drops of methanol were added to make a paste which was irradiated in microwave oven at 420 Watt for 1–2 min in a Petri dish, then cooled at room temperature, and again irradiated for 1–2 min; this process was repeated 4 times. A 250 mL beaker filled with water was placed in microwave oven during the whole irradiation time and water was refilled after every irradiation. The resulted product was scratched and washed with petroleum ether (40–60°C).

5.2.2. DNA Binding Studies

Absorption spectral titration experiments were performed in less than 10% DMSO/Tris–HCl/NaCl buffer by preparing appropriate concentrations of metal complex solution and DNA stock solution while maintaining the total volume constant. The working solutions of drug (**Sul**) and complexes **1–7,** were maintained at constant concentrations (3.00×10^{-6}, 0.88×10^{-6}, 1.00×10^{-6}, 1.37×10^{-6}, 0.96×10^{-6}, 1.03×10^{-6}, 0.54×10^{-6}, 0.79×10^{-6} M, respectively) and titrated with DNA. Absorbance was recorded with successive addition of CT DNA (concentration varied from 1.02–14.02 μM), to both the compound solution and the reference solution in order to eliminate the absorbance of the DNA itself. The intrinsic binding constant K_b of the complex to CT DNA was determined by the Wolfe-Shimmer equation [262, 263] as described in Chapter 4.

For fluorometric titrations, Tris–HCl/NaCl buffer was used as a blank to make preliminary adjustments. The excitation wavelength was fixed and the emission range was adjusted before measurements. The experiment was carried out by titrating the fixed amount of ethidium bromide (EB) [5.0 μM for **SUL**, **1**, **3**, **4**, and **5**; 6.25 μM for **2, 6** and **7**]–bound CT DNA [6.03 μM for **SUL**, **1**, **3**, **4**, and **5**; 7.15 μM for **2, 6** and **7**] with successive addition of metal complexes [0–20 μM], in tris HCl–NaCl buffer (pH = 7.2). To increase the solubility 1% DMSO solution of complexes were used. An excitation wavelength of 525 nm was used and the total fluorescence emission was monitored between 540–700 nm. Quenching constant was calculated by Stern-Volmer equation [264] as described in Chapter 4.

Circular dichroism (CD) spectra of CT–DNA (5×10^5 M) in absence and presence of the **Sul** and complexes **1**–**7** were recorded with a 0.1 cm path length cuvette after 10 min incubation at 25 °C in a 50 mM tris–HCl/NaCl buffer (pH = 7.4). The concentration of **Sul** and complexes **1**–**7** used, were in the range from 5–20 μM.

5.2.3. Gel Electrophoresis

DNA cleavage studies were performed using pBR322 E. coli plasmid DNA. The supercoiled DNA was treated with different concentrations of **Sul** and complexes **1**–**7** (*r* = 1–10, where *r* = [complex]/[DNA]) in buffer solution (5:50 mM Tris–HCl, pH 7.2). The samples were incubated at 37 °C for 5 h. After incubation, 2 μL loading buffer (0.05% (w/v) glycerol, 36% (v/v) bromophenol blue) was added to the samples and were loaded onto agarose gel (0.8%) containing EB (0.5 μg/mL). The agarose gel was run in 0.5X TBE buffer at 50 V/cm for 2.5 h till the samples moves ¾ of the gel length.

5.3. RESULTS AND DISCUSSION

5.3.1. Synthetic Aspects

The reaction of sodium salt of sulindac (**Sul**) and triorganotin(IV) chloride(s) (Eq. (5.1)) led to the formation of triorganotin(IV) complexes of **Sul** (1:1 ratio, Eq. (5.2)) and the reaction of diorganotin(IV) dichloride with sodium salt of sulindac led to the formation of dimethyltin(IV) complex of **Sul** (1:2 metal to ligand ratio for Ph_2SnCl_2 Eq. (5.3) and 1:1 metal to ligand ratio for Me_2SnCl_2 Eq.(5.4)). The reaction of diorganotin oxide(s) with sulindac resulted in the formation of diorganotin(IV) carboxylate(s) (1:2 metal to ligand ratio, Eq. (5.5)).

$$HL + MeONa \xrightarrow[MeOH]{1:1} NaL + MeOH \qquad (5.1)$$

L = $C_{20}H_{16}SO_3F$ (Sulindac)

$$R_3SnCl + LNa \xrightarrow[MeOH]{1:1} R_3SnL + NaCl \qquad (5.2)$$

R = Me/ Ph/ n–Bu.

$$R_2SnCl_2 + 2\,LNa \xrightarrow[MeOH]{1:2} R_2SnL_2 + 2NaCl \qquad (5.3)$$

R = Ph

$$2R_2SnCl_2 + 2HL \xrightarrow[MeOH]{1:1} (R_2SnClL)_2 + 2HCl \quad (5.4)$$

R = Me

$$R_2SnO + 2\ HL \xrightarrow[MeOH + C6H6\ mixture]{1:2} R_2SnL_2 + H_2O \quad (5.5)$$

R = *n*–Bu/ *n*–Oct

The reaction in Eq. (5.1) required 4–6 h of refluxing. The reactions given in Eqs. (5.2) and (5.3) required overnight refluxing with constant stirring under an inert atmosphere, and Eq. (5.5) required 24–26 h refluxing. Many attempts were made to synthesize complex **5**, in 1:2 ratio by refluxing method, unfortunately every time, a mixture of complex and ligand was obtained, which could not be purified. Finally, the complex **5** (Eq. (5.4)) was prepared by microwave assisted synthesis which was obtained in 1:1 ratio and reaction was completed in a short period. The resulting products were obtained in 77–89 % yield. Complexes are soluble in methanol, ethanol, chloroform and DMSO, but show low solubility in other organic solvents. The synthetic scheme of complexes along with their proposed structures is shown in Scheme 5.1 and Table 5.1 presents the physical and analytical properties of complexes. The CHNS analysis data was found in accordance to the proposed structures. Complexes were characterized through FTIR, multinuclear NMR and ESI MS spectroscopy and the characteristic data have been tabulated.

5.3.2. X-ray Crystallographic Study of Complex 3, $Bu_3Sn(Sul)$

A good quality yellow coloured, rod shaped crystals were obtained by slow evaporation of methanol at ambient temperature, which were analyzed through single crystal X-ray diffraction study. The crystal structure of complex **3** (CCDC ID - 1522680) is presented in Fig.5.1 (A) in which butyl carbon is having a high thermal parameter (seen by huge ellipsoids). This is because of data collection at room temperature. The refinement of crystal was tried by considering these carbon atoms in two positions with reduced occupancy but no decrease in R value was found and present model is converged satisfactorily. Pertinent crystal refinement parameters are presented in Table. 5.2. Few important bond lengths, bond angles and torsion angles of the molecule obtained from the crystal structure are given in Table.5.3. Fig. 5.1 (B) presents a lucid description of crystal packing in a unit cell. The crystal structure (Fig 5.1 (C)) reveals that the complex **3** exhibit a polymeric

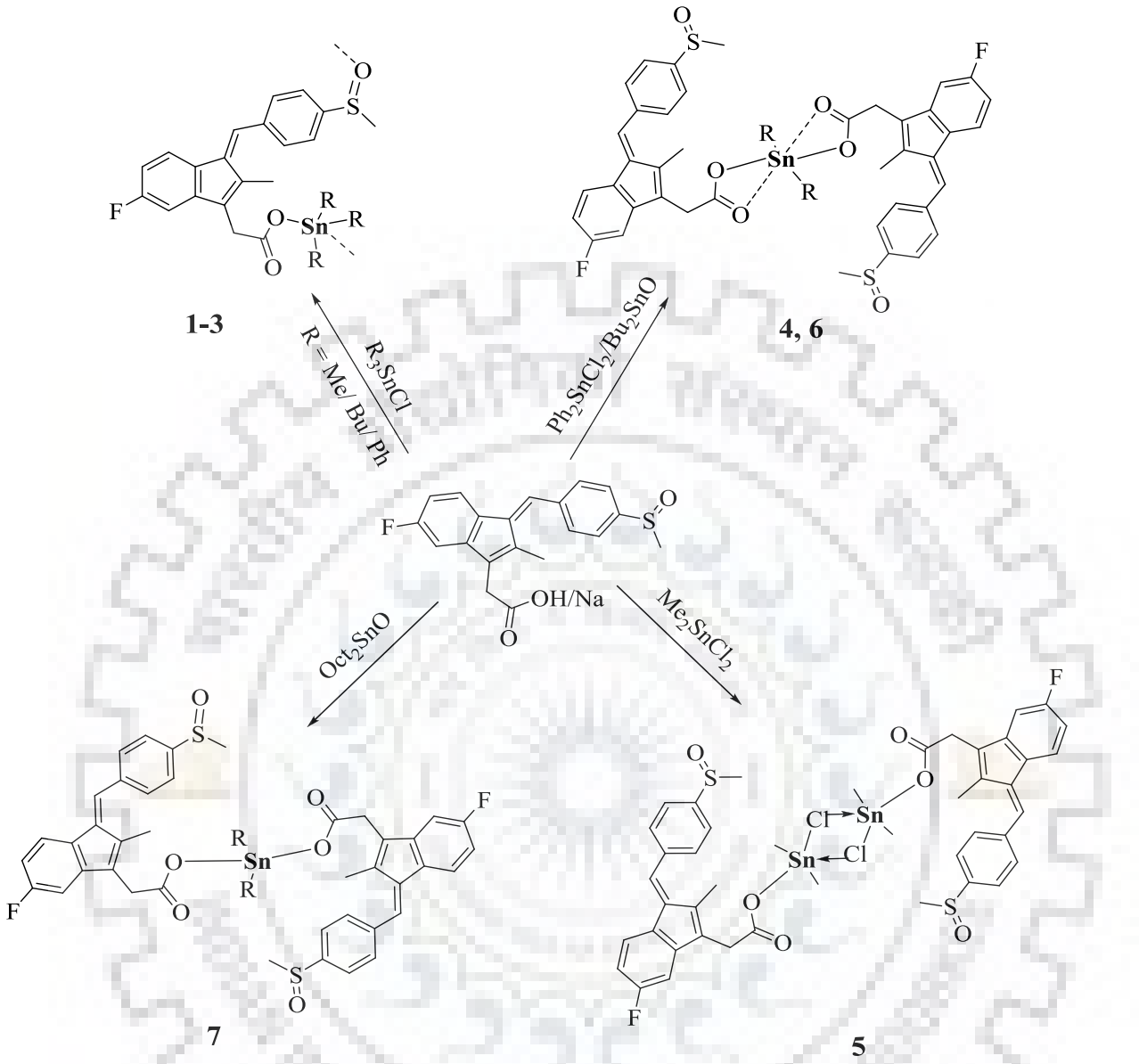

Scheme 5.1. Synthetic scheme of complexes 1-7, with proposed structures.

double chain structure, where oxygen atom of –S=O group (of ligand) of one molecule is coordinated with Sn metal (–[Sn--O]– bond length is 2.549 Å) of next molecule to form a linear chain. Further, two adjacent chains of molecules are stabilized by heteroatom van der Waal interactions between sulphur atom and free oxygen (–[S--O]– = 3.235 Å) of carboxylate group of two adjacent molecules. In this crystal the carboxylate group is acting as a monodentate ligand, in which carbonyl oxygen atom is involved in covalent bonding (2.147 Å) with Sn metal and other free oxygen is involved in weak heteroatom interaction with sulphur atom of other molecule of adjacent chain. The coordination sphere is completed by three butyl groups. The extent of distortion from ideal trigonal bipyramid (TBP) or square pyramidal (SP) geometry can be

quantified by the index of trigonality, τ-value (τ=β–α/60). The measure of τ-value for ideal SP and TBP geometries are 0 and 1, respectively [265]. In this complex the τ-value is 0.8, which indicate a slightly distorted TBP geometry of complex **3**, where axial positions are occupied by two oxygen atoms and three butyl groups occupied the equatorial positions. Further, a covalent bond length of Sn–O (04) is 2.147 Å, which is very close to the value of sum of their covalent radii (2.10 Å) [266], indicating strong covalent bond between two, however, the Sn–O(6) bond length (2.549 Å) is greater than sum of their covalent radii but significantly shorter than the sum of their van der Waal's radii (3.7 Å) [266] and can be regarded as a coordination bond. The Sn–O bond length found in the crystal structure is very close other similar structure found in literature [126, 266, 267].

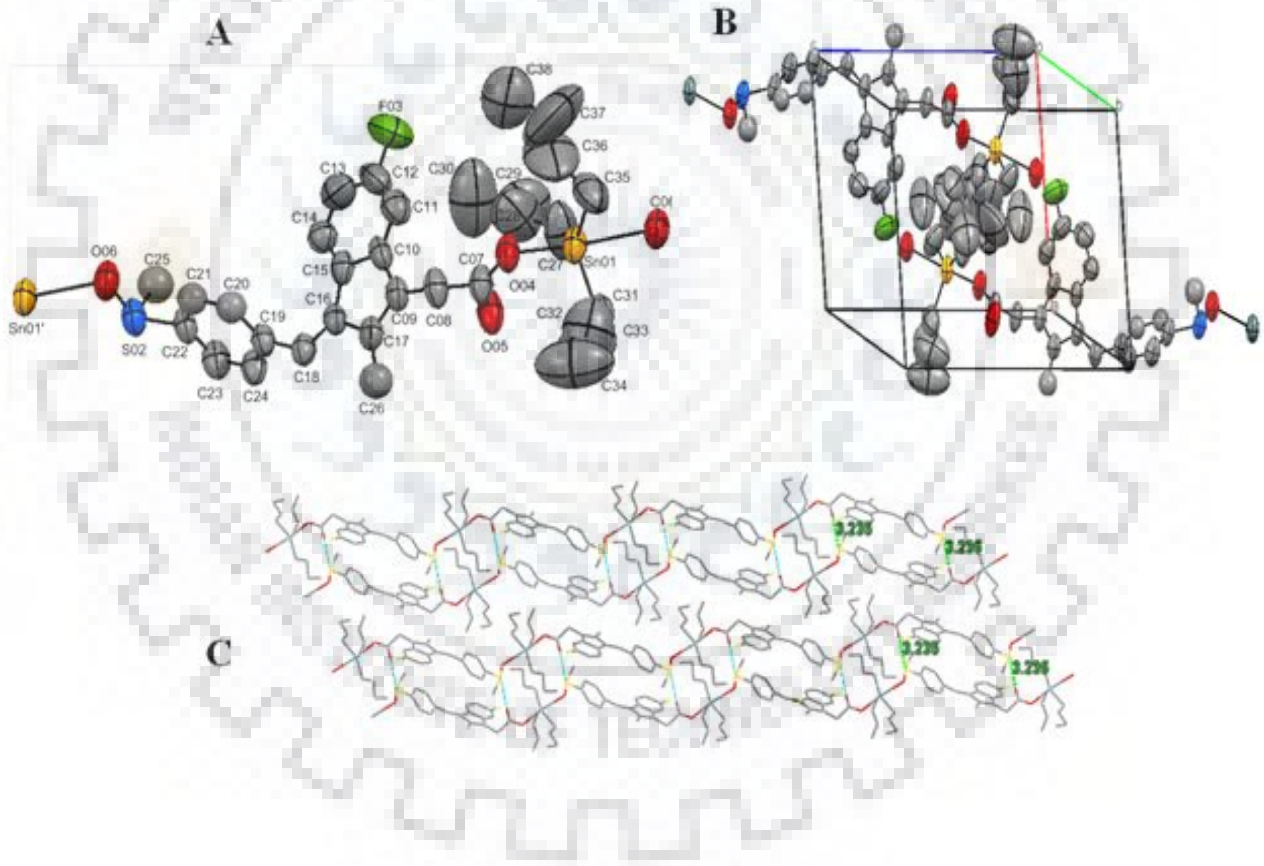

Fig. 5.1. (A) ORTEP diagram of complex 3 with atomic labeling scheme, in 50% ellipsoidal probability level. Hydrogen atoms are omitted for structure clarity: (B) The molecular packing of complex 3, viewed along the crystallographic axis 'b'; (C) 3-D packing of molecules showing polymeric double chain of molecules stabilized by heteroatom –[S--O]– interactions.

Table 5.1. Characteristic physical properties and analytical data of tri- and diorganotin(IV) complexes of sulindac

	Complex (Empirical Formula)	Molecular Weight	Colour & Physical state	Yield (%)	Decomposition/melting temp. (°C)	Analysis (%) Observed (Calculated)			
						C	H	S	Sn
1	**[Me_3Sn(Sul)]** ($C_{23}H_{25}SO_3FSn$)	250.05	Dark yellow solid	73	226	52.83 (53.07)	4.72 (4.86)	5.61 (6.15)	18.99 (20.19)
2	**[Ph_3Sn(Sul)]** ($C_{38}H_{31}SO_3FSn$)	706.10	Yellow solid	76	192	64.09 (64.58)	4.28 (4.39)	5.01 (4.53)	16.03 (16.52)
3	**[Bu_3Sn(Sul)]** ($C_{32}H_{43}SO_3FSn$)	645.50	Pale yellow solid	83	130	59.02 (59.44)	6.41 (6.65)	4.70 (4.95)	17.98 (18.42)
4	**[$Ph_2Sn(Sul)_2$]** ($C_{52}H_{42}S_2O_6F_2Sn$)	984.14	Pale yellow solid	78	80	62.96 (63.41)	4.18 (4.27)	6.02 (6.50)	11.73 (12.09)
5	**[$Me_2SnCl(Sul)]_2$** ($C_{44}H_{44}S_2Cl_2O_6F_2Sn$)	1079.30	Pale yellow solid	69	120	49.93 (48.92)	4.19 (4.07)	5.93 (5.92)	22.18 (22.05)
6	**[$Bu_2Sn(Sul)_2$]** ($C_{48}H_{50}S_2O_6F_2Sn$)	943.74	Pale yellow solid	89	178	60.72 (61.03)	5.11 (5.30)	6.35 (6.78)	12.28 (12.61)
7	**[$Oct_2Sn(Sul)_2$]** ($C_{56}H_{66}S_2O_6F_2Sn$)	1053.21	Dark yellow solid	82	92	63.92 (63.63)	6.33 (6.26)	6.43 (6.06)	11.02 (11.26)

Similar structures have been proposed for complexes [Me_3Sn(Sul)] **1** and [Ph_3Sn(Sul)] **3** in solid state as described by monodentate mode of coordination of carboxylate group and reduction in ν(S=O) stretching frequency upon complexation, on the basis of FTIR study which is being described in next section.

Table 5.6. Crystallographic data and structural refinement parameters for complex 3 [Bu_3Sn(Sul)].

Molecular formula	$C_{32}H_{43}FO_3SSn$
Formula weight	645.43
Temperature:	293 K
Space Group	P-1
Hall group	-P 1
Crystal system	Triclinic
Cell parameter	a=10.0019(4) b=11.8041(4) c=15.9951(5) (Å) α=71.388(1), β=88.153(2), γ=69.339(2)
volume	1667.68(11)
λ (Å) (Mo–Kα)	0.71073
Z	2
Density (g cm^{-3})	1.285
μ (mm^{-1})	0.862
Theta Range (°)	1.3–28.482
F000	668.0
F000'	667.19
h,k,l max	$-13 \leq h \leq 8$, $-15 \leq k \leq 12$, $-21 \leq l \leq 21$
Number of Reflection collected	8331
Data/restraints/parameters	8207/9/323
R1[b] [$I > 2\sigma(I)$]	0.0631
R1 [all data]	0.1157
Data completeness	0.985
GOF[a] on F_2	1.030

Table 5.7. Selected (important) bond lengths (Å) and bond angles (°) obtained for complex 3.

Bond Distances			
Sn(01)–O(04)	2.147(5)	O(04)–C(07)	1.254(9)
Sn(01)–C(31)	2.15(1)	O(05)–C(07)	1.22 (1)
Sn(01)–C(27)	2.11(1)	F(03)–(C12)	1.41(1)
Sn(01)–C(35)	2.12(2)	C(08)–C(07)	1.506 (9)
Sn(01)–O(06)	2.549(5)	C(09)–C(08)	1.489(7)
S(02)–O(06)	1.519(7)	C(17)–C(26)	1.449(9)
S(02)–C(22)	1.796(7)	C–C[a]	1.46

Contd…

S(02)–C(25)	1.790(9)	C–H[a]	0.97
O(06)–Sn(01)	2.549(5)	C=C (aromatic)[a]	1.39

Bond Angles

O(04)–Sn(01)–C(31)	96.9(3)	C(27)–Sn(01)–O(06)	82.9(4)
O(04)–Sn(01)–(C27)	101.9(4)	C(35)–Sn(01)–O(06)	81.9(4)
O(04)–Sn(01)–(C35)	90.6(4)	O(06)–S(02)–C(22)	105.3(3)
O(04)–Sn(01)–O(06)	172.5(2)	O(06)–S(02)–C(25)	104.6(4)
C(31)–Sn(01)–C(27)	117.0(4)	C(22)–S(02)–C(25)	100.0(4)
C(31)–Sn(01)–C(35)	114.7(4)	S(02)–O(06)–Sn(01)	121.4(3)
C(31)–Sn(01)–O(06)	85.8(3)	Sn(01)–O(04)–C(07)	119.9(4)
C(27)–Sn(01)–C(35)	124.5(5)		

Torsion angles

C(22)–S(02)–O(06)–Sn(01)	–126.6(3)	C(09)–C(17)–C(16)–C(18)	–178.2(6)
O(06)–Sn(01)–O(04)–C(07)	–172(1)	C(09)–C(17)–C(16)–C(15)	1.7(6)
O(06)–S(02)–C(22) –C(23)	–2.5(6)	C(17)– C(09)–C(08)–C(07)	106.7(7)
Sn(01)–O(04)–C(07)–O(05)	–0.4(9)	C(26)–C(17)–C(09)–C(08)	–0(1)
Sn(01)–O(04)–C(07) –C(08)	176.6(4)	C(09)–C(08)–C(07)–O(04)	138.3(6)
C(09)–C(08)–C(07)–O(05)	–44.6(9)		

[a]average of similar bond length present in the molecule

5.3.3. Infrared Spectroscopic Studies

The band observed at 1702 cm^{-1} in the spectrum of the free drug (**Sul**) have been assigned to the stretching vibration of the carboxylic –(COOH) carbonyl [268]. The absence of this band in the synthesized complexes indicates coordination through the carboxylate oxygen. The asymmetric stretching of carboxylate group appears in the range 1695–1604 cm^{-1} for organotin(IV) complexes. The spectra of these complexes also show medium to strong intensity bands in the region 1343–1388 cm^{-1}. These bands are absent in the spectrum of **Sul**, which are most likely due to the symmetric vibration of the ligated COO^- group. High magnitude of $\Delta\nu(\nu_{as}COO - \nu_sCOO)$ for **1** (286 cm^{-1})**, 2** (306 cm^{-1}**)** and **3** (287 cm^{-1}) compared to sodium salt of drug (261 cm^{-1}), indicating that the carboxylate group acts as a monodentate donor group and hence the possibility of ionic bonding, bridging and chelation can be excluded [44, 269]. However in **4** and **6** the magnitude of $\Delta\nu$ is 163 and 217 cm^{-1}, respectively, which attributes to the probability of bidentate mode of co-ordination of carboxylate group. Moreover, the monodentate mode of coordination of carboxylate oxygen in **5** and **7** has been displayed by their higher values of $\Delta\nu$ *i.e.* 351 and 287 cm^{-1}, respectively. Appearance of new bands in the region 441-469 cm^{-1} has been assigned to ν(Sn–O), which supports the bonding of carboxylate group to the tin atom [269]. In di–/trialkyltin(IV) derivatives, the observed ν_{as}(Sn–C) and ν_s(Sn–C) frequencies are 595–559 cm^{-1} and 529–536 cm^{-1},

respectively [44]. Characteristic FTIR spectra of complexes **1**, **5** and **6** are given in Fig. 5.2. Table 5.4 presents FTIR data of all complexes along with ligand.

5.3.4. Multinuclear (^{1}H, ^{13}C and ^{119}Sn) NMR Spectroscopic Studies

NMR spectra of studied complexes were recorded in DMSO–d_6 and $CDCl_3$. The number of protons calculated from proposed stoichiometry in all of the complexes found equivalent to the integration curves. Absence of resonance of carboxylic proton at 12.39 ppm suggests the deprotonation of acidic proton upon complexation. Significant downfield shift in proton resonance of $–CH_2$ attached to carboxylic carbon compared to free drug molecule reveals the occurrence of complexation. Similarly, in ^{13}C NMR spectra, a downfield shift in carboxylic carbon resonance supports the complexation between metal and drug. The $^{2}J(^{1}H – ^{119}Sn)$ values calculated for **1** and **3** having well resolved satellites, are 58.36 and 63.17 Hz, respectively, for **2** this magnitude is 65.16 Hz, whereas, $^{1}J(^{13}C–^{119}Sn)$ value could only be calculated for **1**, these values of coupling constants correspond to tetra-coordinated tin atom in **1** and **3**, whereas, penta-coordinated tin for **2** [196, 270]. However, among diorganotin(IV) complexes, $^{2}J(^{1}H – ^{119}Sn)$ values for **5** and **6,** are 110.34 Hz and 83.96 Hz, which reveal hexa-coordination for the respective tin atoms. Further, $^{1}J(^{13}C – ^{119}Sn)$ value (382.11 Hz) in complex **7** reveals tetra-coordinated metal centre [270]. The C–Sn–C angles calculated with the help of $^{2}J(^{1}H–^{119}Sn)$ and $^{1}J(^{13}C–^{119}Sn)$, using Lockhart and Mander's equations [196, 270]. For triorganotin(IV) complexes **1**, **2** and **3**, calculated C–Sn–C angles are 111.2°, 115.75° and 114.45°, respectively, indicating their distorted tetrahedral (td) geometry, which is due to the dissociation of weak intermolecular coordinate bond between sulphoxide oxygen and tin resulting in destruction of polymeric chain like structure and a monomer unit with tetrahedral geometry in solution might have detected. Furthermore, the calculated values of C–Sn–C angles for diorganotin(IV) complexes, **5**, **6** and **7** are 162.10° and 136.07° and 110.27°, respectively, which represent trigonal bipyramedal (tbp) or octahedral (Oh) geometries for **5** and **6** and tetrahedral (td) geometry for **7**. The coordination of DMSO-d_6 with tin metal of complex **5** in solution revealed six-coordination around them. For **4** satellite values could not be resolved, hence no coupling constant could be found. The representative ^{1}H NMR spectra of complexes **5** and **6** and ^{13}C NMR spectra of complexes **3** and **7** are given in Fig 5.3 and Fig 5.4, respectively.

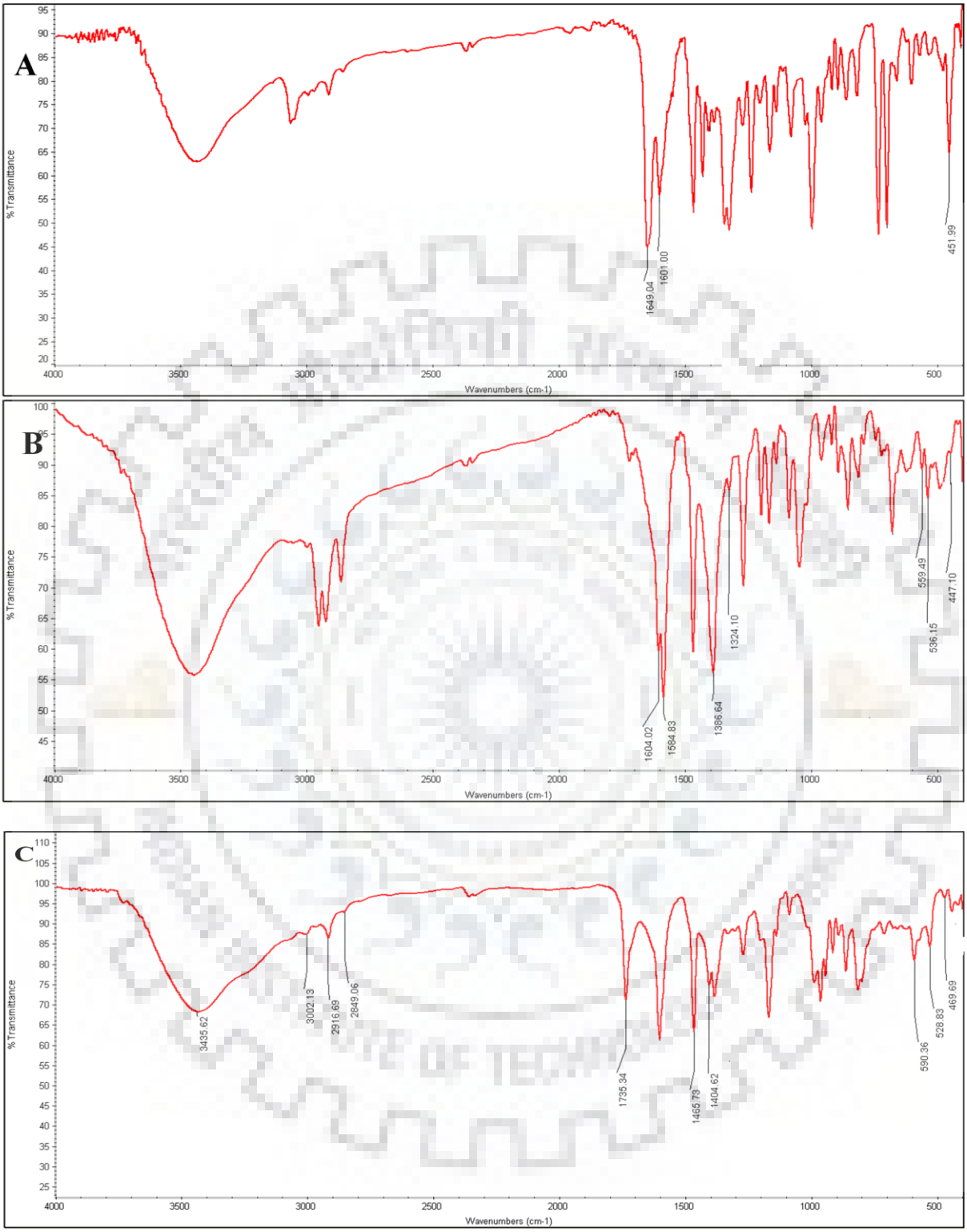

Fig. 5.2. FTIR spectra of complex 1 [$Me_3Sn(Sul)$] (A), complex 6 [$(Bu_2Sn(Sul)_2$] (B) and complex 5 [$Me_2SnCl(Sul)]_2$ (C).

Only one ^{119}Sn resonance was obtained for all studied complexes which ruled out the existence of more than one tin containing species in solution. The values of δ (^{119}Sn) define the co-ordination number of central tin atom thus, the probable geometry of the molecule. For triorganotin(IV) complexes R_3SnL (R = Me, Ph and *n*–Bu), $(Me_2SnL)_2$, and R_2SnL (R = *n*–Bu and Ph), the values of δ ^{119}Sn are 119.60 to 142.48, –102.62 ppm, respectively, which further support their distorted tetrahedral geometries [222, 271]. However the distorted octahedral geometries for **4**, **5** and **6** are evidenced by their δ ^{119}Sn values at –203.17, –240.97, –239.99 ppm, respectively [222], as predicted earlier from the value of observed coupling constants and the calculated C–Sn–C angles. Unfortunately, the δ ^{119}Sn NMR spectra for *n*-Oct_2Sn(IV) could not be recorded. Fig 5.5 presents the characteristic ^{119}Sn NMR spectra of complexes **1**, **2** and **6**. Table 5.5 present the ^{1}H and ^{13}C NMR spectroscopic data. Further, ^{119}Sn NMR chemical shifts are tabulated in Table 5.6.

5.3.5. ESI MS Spectrometry

The ESI MS spectrometric data for organotin(IV) complexes were recorded in the range m/z 200–1200, using acetonitrile as solvent in positive ion mode. All the complexes were characterized by molecular ion peak corresponding to $[M+Na]^+$ and/or $[M+K]^+$, which have been used to determine the molecular weight of the complexes [272], although the base ion peak in all complexes is at m/z = 273 which corresponds to a fragment of drug (**Sul**). Cleavage of the most labile Sn–O bond in organotin carboxylate complexes leads to formation of subsequent ions $[M–L]^+$, where the positive ion part (SnR_3/SnR_2) formed from the molecule is measured in the positive-ion mode [273]. Other peaks, with characteristic isotopic tin pattern have also been obtained by removing other fragments from ligand part of complex, *viz.* $–SOCH_3$, $–SOCH_3$ + F, $–C_6H_5SOCH_3$, $–C_6H_5SOCH_3$ + F, having formula weight 63, 82, 139, and 158, respectively. In some of the complexes some other peaks corresponding to fragments, obtained by defragmentation of –R (alkyl and aryl) groups of organotin moiety from molecular ion, have also been observed [274]. Molecular ion peaks along with few fragmented species of complexes are described in Table 5.7 and representative mass spectra of complexes **1** and **2** are given in Fig. 5.6

Table 5.4. FTIR spectroscopic data of tri- and diorganotin(IV) derivatives of sulindac in KBr (cm^{-1}).

Ligand[a]/ complex	$\nu(OH)_{aromatics}$	$\nu(C–H)$ stretch	$\nu(C=O)$ stretch	$\Delta\nu$ ($\nu_{as}COO – \nu_{s}COO$)	$\nu(C=C)_{ring}$ stretch	$\nu(C–O)$ / $\nu(C–H)_{in\ plane}$	ν (S=O) stretch	$\nu_{outplane}$ (ring)	$\nu_{as}(Sn–C)$ /$\nu_{s}(Sn–C)$	$\nu_{as}(Sn–O)$
HL	3300–2500 m	2915 w,br 3058 w	1702 s	–	1467 s, 1405 sh	1190 m, 1158 w	1269 s	847 w, 890 m	—	—
LNa		2907 w 2854 w	1636 s 1375 s	261	1468 s 1466 s	1169 s 1135 m	1271 m	891 m, 863 m	—	—
1	—	2914 w, 3061 w	1629 s, 1343 s	286	1467 s, 1402 m	1189 m, 1157 w	1259 m	869 m, 893 w	553 w, 474 w	474 m
2	—	2914 m, 3058 w	1649 s, 1427 m	306	1466 m, 1406 m	1162 m, 1137 w	1237 m	858 w, 893 m	—	457 w
3	—	2920w, 3052 w	1632 s, 1345 s	287	1466 m, 1418 m	1157 m, 1133 w	1255 m	891w, 861 m	562 w, 476 w	476 w
4	—	2910 br, 3064 w,	1717 s, 1554 s	163	1466 s, 1403 w	1166 m, 1135 w	1271 w	890w, 855 m	—	441 w
5	—	2914 m, 3005 w	1735 s, 1384 w	351	1466 s, 1402 s	1168 s, 1135 w	1268 w	861 m, 888 w	589 w, 473 w	469 m
6	—	2951 m 3061 w,	1604 s, 1387 s	217	1585 s, 1466 m,	1164 m, 1136 w	1266 m	889 w, 850 m	535 w, 488 w	447 m
7	—	2922m, 2955 w	1635 s, 1348 w,	287	1466 m, 1406 w	1158 m, 1130 w	1271 w	892 w, 841 w	536 w, 482 w	463 w

[a]numbers of complexes as given in Table 5.1; HL= Sulindac; s = strong; br = broad; m = medium; w = weak

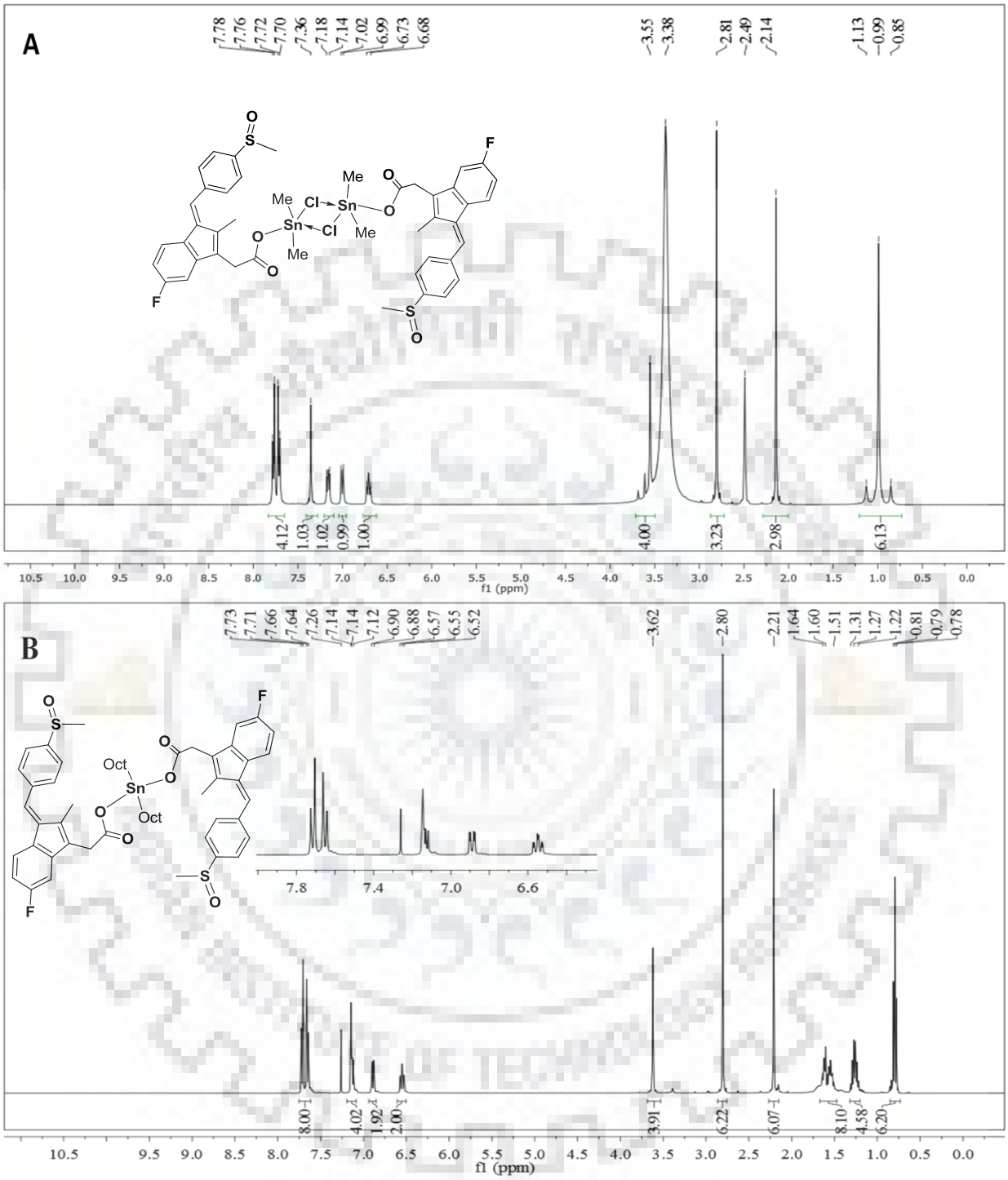

Fig. 5.3. ^{1}H NMR Spectra of complex 5 [($Me_2SnCl.Sul)_2$] in DMSO-d_6 (A) and complex 6 [($Bu_2Sn(Sul)_2$] (B), in $CDCl_3$.

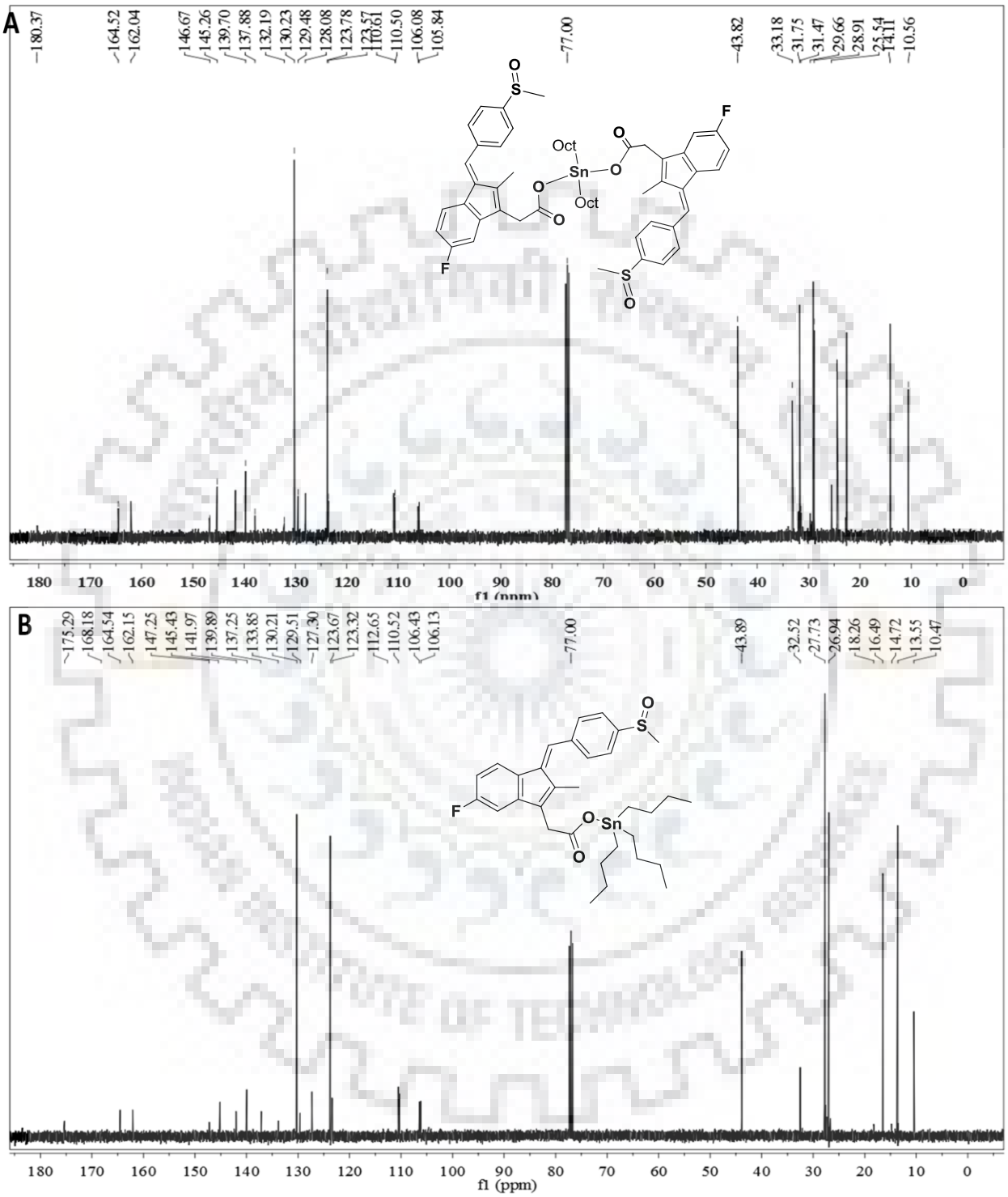

Fig. 5.4. ^{13}C NMR spectra of complex 7 [$Oct_2Sn(Sul)$] (A) and complex 3 [$Bu_3Sn(Sul)$] (B), in $CDCl_3$.

Table 5.5. ^{1}H, and ^{13}C NMR spectroscopic data of organotin(IV) complexes of sulindac in $CDCl_3$/DMSO-d_6.

Ligand/ Complex[a]	^{1}H NMR δ (ppm) (399.78 MHz)
HL (DMSO–d_6)	2.15 (s, 3H, CH_3); 3.57 (s, 2H, CH_2); 6.71–6.72 (td, 1H, H–4); 6.86 (dd, 1H, H–6); 7.17 (q, 1H, H–7); 7.26 (s, 1H, CH); 7.75 (dd, 4H, H–2'/H–3', H–5'/H–6'); 2.81 (s, 3H, CH_3')
LNa (DMSO–d_6)	2.10 (s, 3H, CH_3); 3.18 (s, 2H, CH_2); 6.60–6.65 (td, 1H, H–4); 7.04 (dd, 1H, H–6); 7.10 (q, 1H, H–7); 7.20 (s, 1H, CH); 7.73 (dd, 4H, H–2'/H–3', H–5'/H–6'); 2.80 (s, 3H, CH_3')
Me_3SnL (**1**) ($CDCl_3$)	2.18 (s, 3H, CH_3); 3.55 (s, 2H, CH_2); 6.51–6.56 (td, 1H, H–4); 6.87 (dd, 1H, H–6); 7.13 (q, 1H, H–7); 7.11 (s, 1H, CH); 7.69 (dd, 4H, H–2'/H–3', H–5'/H–6'); 2.81 (s, 3H, CH_3'); 0.55 (s, 9H, Me_3Sn); $^{2}J(^{1}H–^{119}Sn)$ = 58.36 Hz, [θ = 111.20°][b]
Ph_3SnL (**2**) ($CDCl_3$)	2.13 (s, 3H, CH_3); 3.64 (s, 2H, CH_2); 6.52–6.53 (td, 1H, H–4); 6.82 (dd, 1H, H–6); 7.13 (q, 1H, H–7); 7.10 (s, 1H, CH); 7.66–2.70 (dd, 4H, H–2'/H–3', H–5'/H–6'); 2.80 (s, 3H, CH_3'); 7.71–7.64 (br, H_o, Ph_3Sn); 7.41–7.45 (m, $H_{p,m}$, Ph_3Sn); $^{2}J(^{1}H–^{119}Sn)$ = 65.16 Hz, [θ = 115.75°][b]
Bu_3SnL (**3**) ($CDCl_3$)	2.19 (s, 3H, CH_3); 3.54 (s, 2H, CH_2); 6.51–6.54 (td, 1H, H–4); 6.90 (dd, 1H, H–6); 7.13 (q, 1H, H–7); 7.10 (s, 1H, CH); 7.70 (dd, 4H, H–2'/H–3', H–5'/H–6'); 2.80 (s, 3H, CH_3'); 0.86 (t, H_δ, Bu_3Sn); 1.21–1.53 (m, $H_{\beta\gamma}$, Bu_3Sn); 1.52–1.64 (m, H_α, Bu_3Sn); $^{2}J(^{1}H–^{119}Sn)$ = 63.16 Hz, [θ = 114.26°][b]
Ph_2SnL_2 (**4**) ($CDCl_3$)	2.20 (s, 6H, CH_3); 3.60 (s, 4H, CH_2); 6.52–6.56 (td, 2H, H–4); 6.90 (dd, 2H, H–6); 7.1 (q, 2H, H–7); 7.12 (s, 2H, CH); 7.51 (dd, 4H, H–2'/H–3', H–5'/H–6'); 2.81 (s, 6H, CH_3'); 7.36–7.77 (br, 10H, Ph_2Sn)
$(Me_2SnClL)_2$ (**5**) (DMSO–d_6)	2.14 (s, 3H, CH_3); 3.55 (s, 2H, CH_2); 6.69–6.73 (td, 1H, H–4); 7.00 (dd, 1H, H–6); 7.16 (q, 1H, H–7); 7.36 (s, 1H, CH); 7.74 (dd, 4H, H–2'/H–3', H–5'/H–6'); 2.81 (s, 3H, CH_3'); 0.62 (s, 6H, Me_2Sn); $^{2}J(^{1}H–^{119}Sn)$ = 110.34 Hz, [θ = 162.1°][b]
Bu_2SnL_2 (**6**) ($CDCl_3$)	2.21 (s, 6H, CH_3); 3.62 (s, 4H, CH_2); 6.52–6.57 (td, 2H, H–4); 6.89 (dd, 2H, H–6); 7.13 (q, 2H, H–7); 7.14 (s, 2H, CH); 7.68 (dd, 4H, H–2'/H–3', H–5'/H–6'); 2.80 (s, 6H, CH_3'); 0.79 (t, H_δ, Bu_2Sn); 1.22–1.31 (m, H_γ, Bu_2Sn); 1.51–1.64 (m, $H_{\alpha\beta}$, Bu_2Sn); $^{2}J(^{1}H–^{119}Sn)$ = 83.96 Hz, [θ = 136.07°][b]

Contd…

Oct_2SnL_2 (**7**) ($CDCl_3$)	2.20 (s, 6H, CH_3); 3.61 (s, 4H, CH_2); 6.52–6.57 (td, 2H, H–4); 7.87–6.90 (dd, 2H, H–6); 7.15 (q, 2H, H–7); 7.14 (s, 2H, CH); 7.68 (dd, 8H, H–2'/ H–3'/ H–5'/H–6'); 2.81 (s, 6H, CH_3'); 0.843 (t, H_i, Oct_2Sn); 1.17–1.26 (m, $H_{h-\gamma}$, Oct_2Sn); 1.51–1.62 (m, H_β, Oct_2Sn); 1.66–1.84 (br, H_α, Oct_2Sn)
	^{13}C NMR δ (ppm) (100.53 MHz)
HL (DMSO–d_6)	174.72 (COOH); 141.59 (C–1); 138.34 (C–2); 131.49 (C–3); 106.23 (C–4); 164.51 (C–5); 110.91 (C–6); 123.67 (C–7); 130.24 (C–8); 146.59 (C–9); 31.42 (C–10); 10.52 (CH_3); 129.38 (CH); 139.78 (C–1'); 120.19 (C–2'/C–6'); 123.93 (C–3'/C–5'); 145.66 (C–4'); 43.48 (CH_3')
LNa (DMSO–d_6)	172.46 (COOH); 141.34 (C–1); 137.86 (C–2); 134.53 (C–3); 106.91 (C–4); 163.68 (C–5); 109.80 (C–6); 123.91 (C–7); 130.00 (C–8); 148.85 (C–9); 36.57 (C–10); 10.36 (CH_3); 129.79 (CH); 139.08 (C–1'); 127.16 (C–2'/C–6'); 123.91 (C–3'/C–5'); 145.82 (C–4'); 43.15 (CH_3')
Me_3SnL (**1**) ($CDCl_3$)	175.42 (COOH); 141.91 (C–1); 137.32 (C–2); 133.42 (C–3); 106.27 (C–4); 164.53 (C–5); 110.59 (C–6); 123.48 (C–7); 130.26 (C–8); 147.22 (C–9); 32.24 (C–10); 10.51 (CH_3); 129.58 (CH); 139.92 (C–1'); 127.49 (C–2'/C–6'); 123.75 (C–3'/C–5'); 145.08 (C–4'); 43.48 (CH_3'); –2.33 (C–α, Me_3Sn); $^1J(^{13}C–^{119}Sn)$ = 408.13 Hz, [θ=112.56°] [c]
Ph_3SnL (**2**) ($CDCl_3$)	176.38 (COOH); 141.83 (C–1); 137.84 (C–2); 132.99 (C–3); 106.55 (C–4); 164.49 (C–5); 110.60 (C–6); 123.44 (C–7); 130.20 (C–8); 147.00 (C–9); 31.87 (C–10); 10.49 (CH_3); 129.54 (CH); 139.86 (C–1'); 127.57 (C–2'/C–6'); 123.75 (C–3'/C–5');; 145.18 (C–4'); 43.83 (CH_3'); 136.77 (C_i, Ph_3Sn); 136.77 (C_o, Ph_3Sn); 128.89 ($C_{m,p}$ Ph_3Sn)
Bu_3SnL (**3**) ($CDCl_3$)	175.29 (COOH); 141.97 (C–1); 137.25 (C–2); 133.85 (C–3); 106.43 (C–4); 164.54 (C–5); 110.52 (C–6); 123.67 (C–7); 130.21 (C–8); 147.25 (C–9); 32.52 (C–10); 10.47 (CH_3); 129.51 (CH); 139.89 (C–1'); 127.30 (C–2'/C–6'); 123.67 (C–3'/C–5'); 145.43 (C–4'); 43.89 (CH_3'); 13.55 (C_δ, Bu_3Sn); 27.73 (C_γ, Bu_3Sn); 16.49 (C_β, Bu_3Sn); 26.94 (C_α, Bu_3Sn); $^1J(^{13}C–^{119}Sn)$ = 353 Hz, [θ = 107.72°][c]
Ph_2SnL_2 (**4**) ($CDCl_3$)	176.13 (COOH); 141.64 (C–1); 138.46 (C–2); 133.09 (C–3); 106.33 (C–4); 164.53 (C–5); 110.95 (C–6); 123.66 (C–7); 130.29 (C–8); 146.58 (C–9); 31.19 (C–10); 10.55 (CH_3); 129.95 (CH); 139.97 (C–1'); 129.18 (C–2'/C–6'); 124.07 (C–3'/C–5'); 145.34 (C–4'); 43.13 (CH_3'); 135.14 (C_0, Ph_2Sn); 131.50 (C_o, Ph_2Sn); 128.31 ($C_{m,p}$ Ph_2Sn)
$(Me_2SnClL)_2$ (**5**) (DMSO–d_6)	177.27 (COOH); 140.37 (C–1); 137.77 (C–2); 132.76 (C–3); 106.23 (C–4); 163.74 (C–5); 110.54 (C–6); 123.21 (C–7); 130.96 (C–8); 147.16 (C–9); 31.35 (C–10); 10.29 (CH_3); 129.39 (CH); 139.56 (C–1'); 129.96 (C–2'/C–6'); 123.97 (C–3'/C–5');; 146.23 (C–4'); 43.12 (CH_3'); 22.51 (C–α Me_2Sn)

Contd…

Bu_2SnL_2 (**6**) ($CDCl_3$)	180.46 (COOH); 141.67 (C–1); 137.89 (C–2); 132.15 (C–3); 106.11 (C–4); 164.51 (C–5); 110.83 (C–6); 123.65 (C–7); 129.19 (C–8); 146.73 (C–9); 31.43 (C–10); 10.55 (CH_3); 129.53 (CH); 139.68 (C–1'); 127.07 (C–2'/C–6'); 123.79 (C–3'/C–5'); 145.33 (C–4'); 43.85 (CH_3'); 13.39 (C_δ, Bu_2Sn); 26.50 (C_γ, Bu_2Sn); 27.15 (C_β, Bu_2Sn); 25.19 (C_α, Bu_2Sn)
Oct_2SnL_2 (**7**) ($CDCl_3$)	180.37 (COOH); 141.66 (C–1); 137.88 (C–2); 132.18 (C–3); 106.08 (C–4); 164.52 (C–5); 110.50 (C–6); 123.78 (C–7); 130.23 (C–8); 146.76 (C–9); 31.47 (C–10); 10.56 (CH_3); 129.48 (CH); 139.70 (C–1'); 128.78 (C–2'/C–6'); 123.57 (C–3'/C–5'); 145.26 (C–4'); 43.82 (CH_3'); 14.11 (C_i, Oct_2Sn); 22.61 (C_h, Oct_2Sn); 24.41 (C_g, Oct_2Sn); 25.54 (C_f, Oct_2Sn); 28.91(C_δ, Oct_2Sn); 31.75 (C_γ, Oct_2Sn); 33.18 (C_β, Oct_2Sn); 29.66 (C_α, Oct_2Sn); $^1J(^{13}C–^{119}Sn)$ = 382.11 Hz, [θ = 110.27][c]

[a]numbers of complexes as given in Table 5.1; s: singlet; d: doublet; t: triplet; m: multiplet; q; quartet; br: broad; dd: doublet of doublet; [b]determined through Lockhart-Manders equation, Ref. [196]; [c]dertermined through Lockhart-Manders equation, Ref. [270]; HL= Sulindac, (5-flouoro-2–methyl-1-(4-(methylsulfinyl)benzyllidene)-1H-inden-3-yl)acetic acid

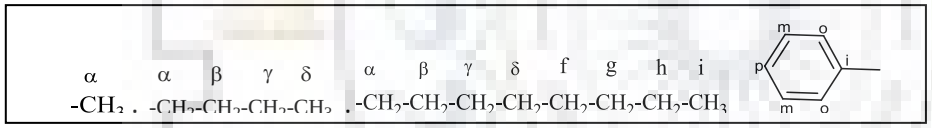

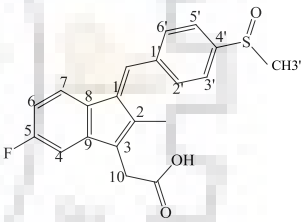

Table 5.6. ^{119}Sn NMR spectroscopic data of organotin(IV) complexes of sulindac.

Ligand/Complex[a]	^{119}Sn NMR δ (ppm)
1 ($CDCl_3$)	142.48
2 ($CDCl_3$)	−102.62
3 ($CDCl_3$)	119
4 ($CDCl_3$)	–203.99
5 (DMSO–d_6)	−240.97
6 ($CDCl_3$)	–239.17

[a]numbers of complexes as given in Table 5.1.

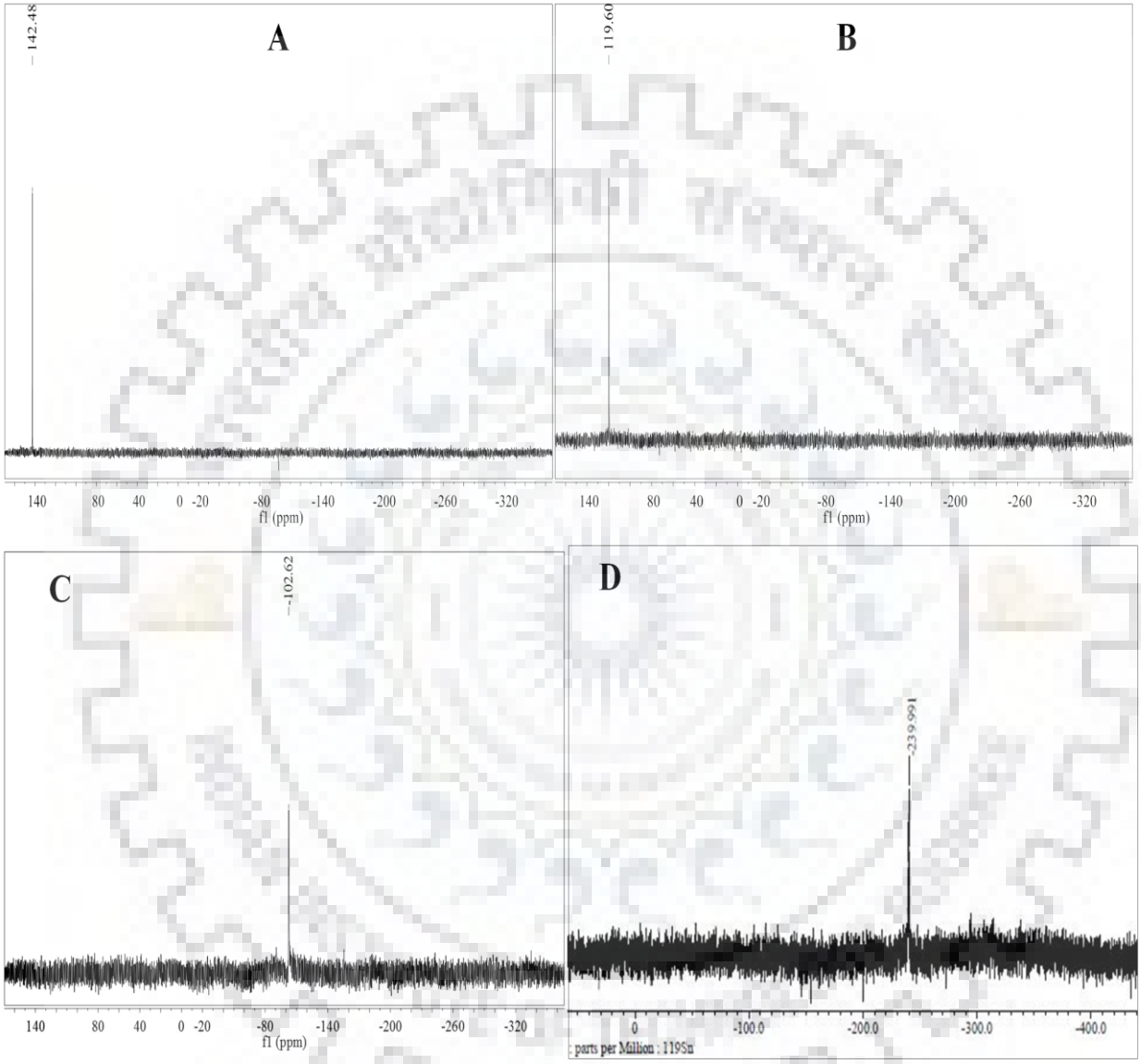

Fig. 5.5. ^{119}Sn NMR spectra of complex 1, [$Me_3Sn(Sul)$] (A); complex 3, [$Bu_3Sn(Sul)$] (B); complex 3, [$Ph_3Sn(Sul)$] and complex 6 [$Bu_2Sn(Sul)_2$] (D), in $CDCl_3$.

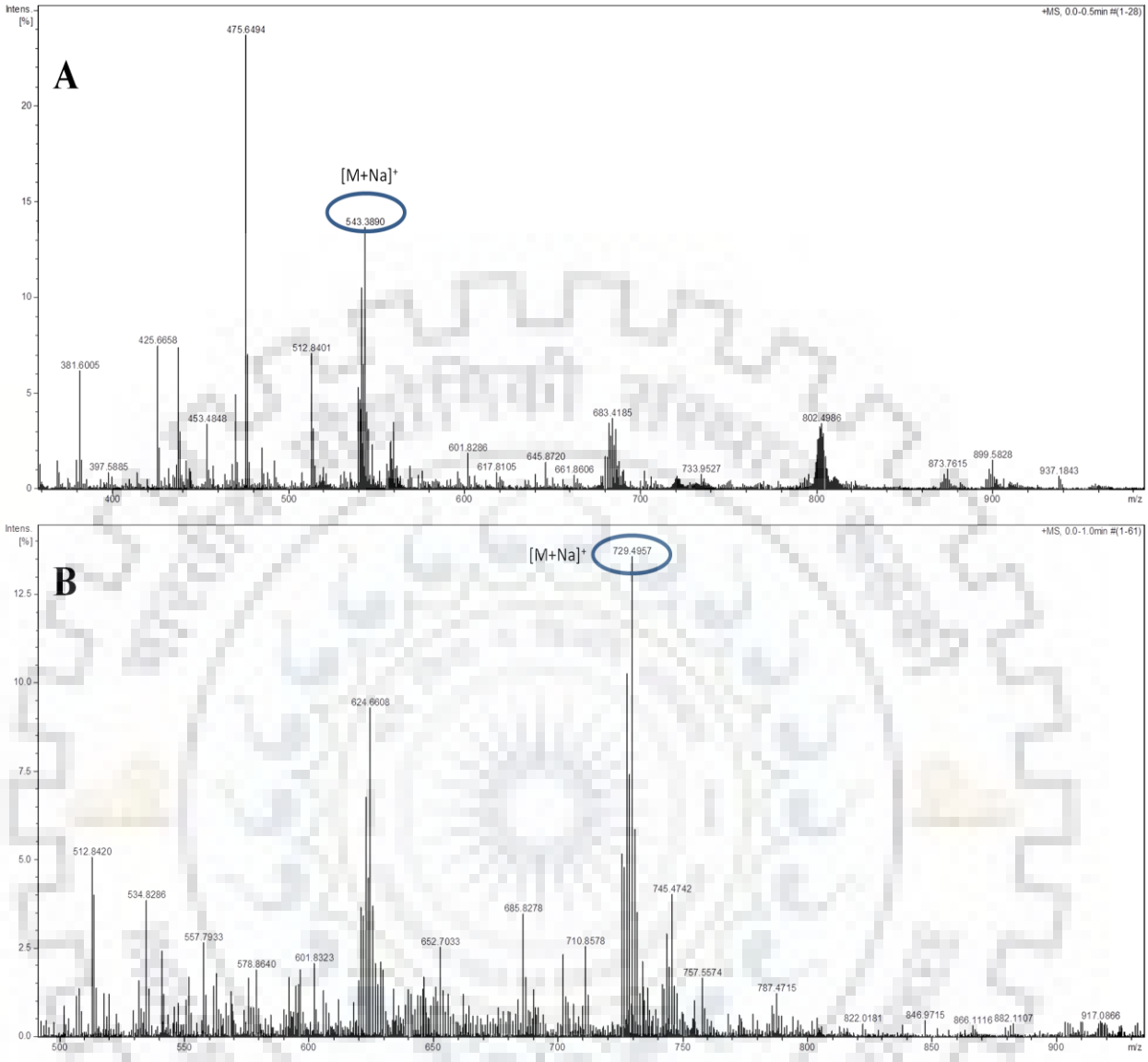

Fig. 5.6. ESI MS mass spectra of complex 1 [$Me_3Sn(Sul)$] (A), complex 2, [$Ph_3Sn(Sul)$] (B).

5.3.6. Geometry Optimization (DFT Calculations)

In order to have better insight into structure of remaining complexes **4**–**7**, we performed full geometry optimizations of ligand (**Sul**) and all complexes Fig. 5.7 using density functional theory (DFT) at B3LYP/6-31G (d, p) and B3LYP/LanL2DZ basis sets [166], respectively. The absence of imaginary frequencies in a harmonic frequency calculation indicates that the calculated geometries are most likely at global minima on the potential energy surface. The optimization of geometries was achieved according to the proposed structures. Complex **5** exhibits distorted trigonal bipyramedal geometry with *trans* methyl groups and complex **7** attained a distorted tetrahedral

Table 5.7. Mass fragmentation pattern of organotin complexes (1–7).

Complex[a]	ESI MS (m/z)
Me_3SnL (**1**)	543.4 $[M + Na]^+$ (13.6%), 437 $[M–(SOCH_3 + F)]^+$, 683 $[M + SnMe_3]^+$
Ph_3SnL (**2**)	729 $[M + Na]^+$ (13.6%), 624 $[M – (SOCH_3 + F)]^+$, 591 $[M –C_6H_5SOCH_3 + H]^+$, 652 $[M – C_6H_5 + Na]^+$, 575 $[M – (2C_6H_5) + Na]^+$
Bu_3SnL (**3**)	669 $[M + Na]^+$ (13.6%), 685 $[M + K]^+$ (2.13%), 606 $[M – SOCH_3 + Na]^+$, 564 $[M – (SOCH_3 + F)]^+$
Ph_2SnL_2 (**4**)	1023 $[M + K]^+$ (0.29%)
$(Me_2SnClL)_2$ (**5**)	1103 $[M + Na]^+$ (1.32%), 563 $[M – SnMe_2LCl + Na]^+$
Bu_2SnL_2 (**6**)	967 $[M + Na]^+$ (0.43%), 862 $[M – (SOCH_3 + F)]^+$
Oct_2SnL_2 (**7**)	1079 $[M + Na]^+$ (0.71%), 701 $[M – L]^+$

[a]numbers of complexes as given in Table 5.1; HL= Sulindac

geometry at lowest energy state where major bond angles and bond lengths were found in good agreement with similar crystal structures reported by Lambert et.al [267]. However **4** and **6** were exhibited highly distorted octahedral geometry, also termed as bicapped tetrahedron with two carboxylate oxygen capping the faces. The carboxylate groups are said to be coordinated in an anisobidentate fashion, with short and long Sn–O bonds 2.038 and 2.89 Å, both of which are significantly shorter than van der Waal's radii [266]. The calculated C–Sn−C angles present in optimized geometries of **4–7** were found in good agreement with angles calculated through Lockhart and Mander's equation from NMR data. Observed bond angles and bond lengths were found in good agreement with similar crystal structures reported [126, 266, 267]. A diagrammatic representation of the HOMO–LUMO orbitals are given in Fig. 5.8, which reveals that HOMO is mostly localized on phenyl ring containing sulphoxide group, whereas in **4–7**, it is shifted to organotin moiety and indene ring of drug, near the carboxyl group. Unlike, LUMO was spread on the whole drug molecule in both free **Sul** and complexed **Sul** (**4–7**)**.** Table 5.8. presents the energy of **Sul** and **4–7** and their HOMO-LUMO energy difference and calculated ∠C–Sn−C. Calculated IR frequencies of **Sul** and **4–7** were found in good agreement with experimental data. Theoretically calculated infrared data of **Sul** and **4–7**, is presented in Table 5.9

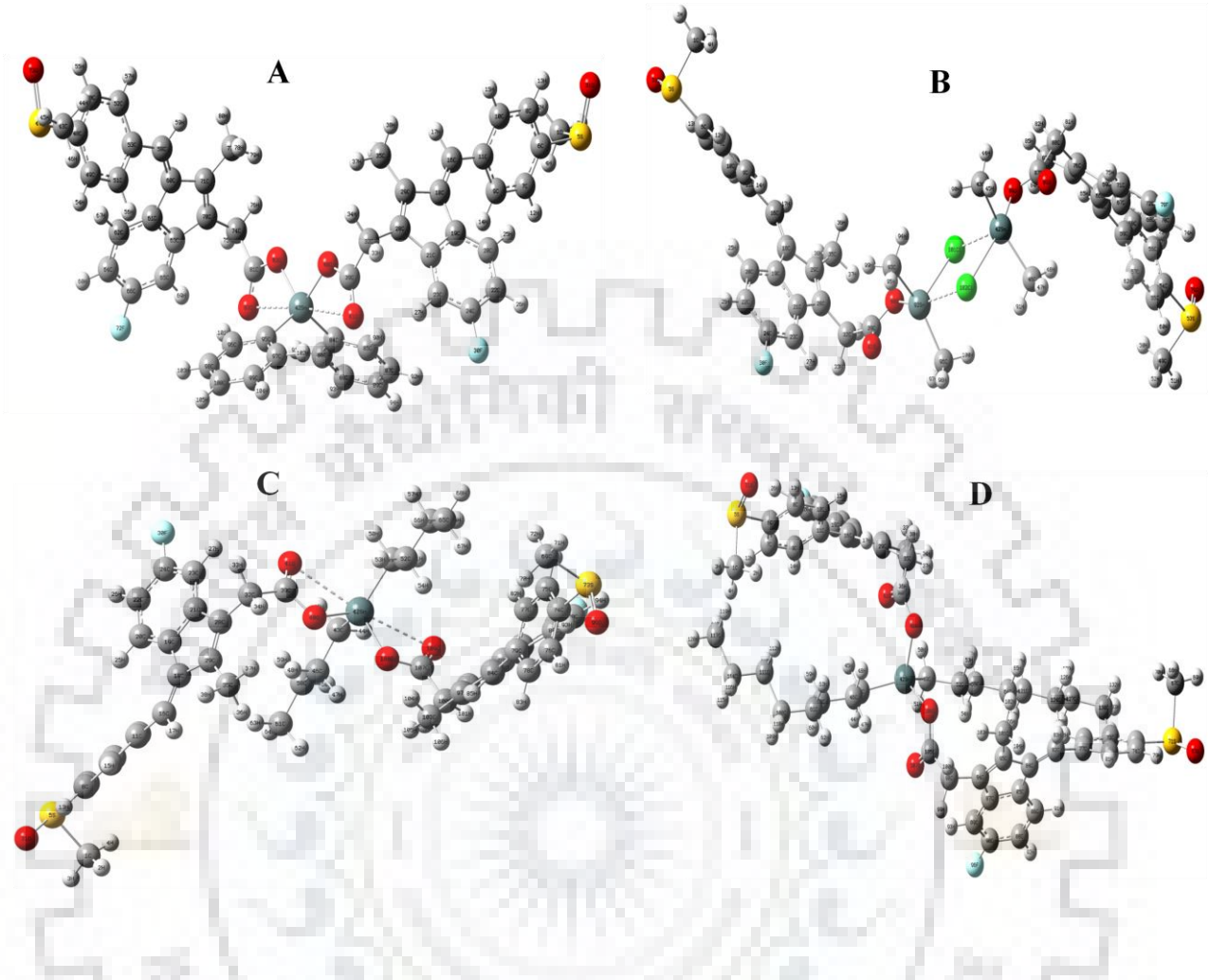

Fig. 5.7. Optimized geometries of complexes distorted tbp geometry of 5 (B), tetrahedral bicapped geometry of 4 (A), 6 (C) and distorted tetrahedral geometry of 7 (D).

5.3.7. DNA Binding Study

5.3.7.1. UV-visible Spectrophotometric Titrations

The absorption spectra of **Sul** and **1– 7** in the absence and presence of CT DNA, are shown in Fig.5.9, where arrow indicates a decrease in absorbance upon increasing the DNA concentration. **Sul** and **1–7** exhibited *n–л** and *л–л** transitions of aromatic chromophore, which showed intense absorption bands at 210, 282 and 328 nm, in the UV region. Among all these transitions, which showed absorption at 210 nm affected the most. With increasing CT DNA concentration (0–1.02 μM) the absorption bands of **Sul** and complexes **1–7,** exhibited a significant hypochromism and moderate red shift of 5, 4, 4, 4, 3, 4, 4 and 3 nm, respectively. Other absorption bands at 256 nm

Table 5.8. Summary of DFT calculations performed on diorganotin(IV) complexes of Sul with B3LYP function, LANL2DZ basis set.

Ligand/ Complex[a]	Energy of optimized geometry (a.u)	∠ C–Sn–C(°) (as calculated from ^1J and ^2J values) in solution	∠ C–Sn–C(°) (as calculated from DFT) in gaseous state	$E_{(HOMO)}$, $E_{(LUMO)}$ (a.u)	$E_{(HOMO)}$− $E_{(LUMO)}$ (a.u)
Sul	–1149.67	–	–	–8.4219 –6.3457	2.0762
4	–2680.65	–	128.20	–9.0886 –9.0750	0.0136
5	–2410.79	162.1	148.16	–9.2600 –9.0777	0.1923
6	–2533.43	126.94	129.04	–9.0777 –9.0750	0.0027
7	–2847.89	110.27	129.01	–9.0777 –9.0750	0.0027

[a]numbers of complexes as given in Table 5.1.

Table 5.9. Theoretical IR frequencies for complexes 4–7, calculated through DFT with B3LYP function, LANL2DZ basis set.

Complex[a]	ν_{as}(COO) (cm^{-1})	ν_s(COO) (cm^{-1})	Δν(COO) (cm^{-1})	ν_{as}(Sn–C) (cm^{-1})	ν_s(Sn–C) (cm^{-1})	ν_s(Sn–O) (cm^{-1})	ν_s(Sn–Cl) (cm^{-1})
4	1684 (m)	1554 (s)	130	356 (m)	–	442(w)	–
5	1684(s)	1389 (s)	295	597	536	465 (w)	258 (w)
6	1593 (s)	1392 (m)	201	559	536	463 (m	–
7	1633 (m)	1357 (s)	276	196	535	462 (w)	–

[a]numbers of complexes as given in Table 5.1.

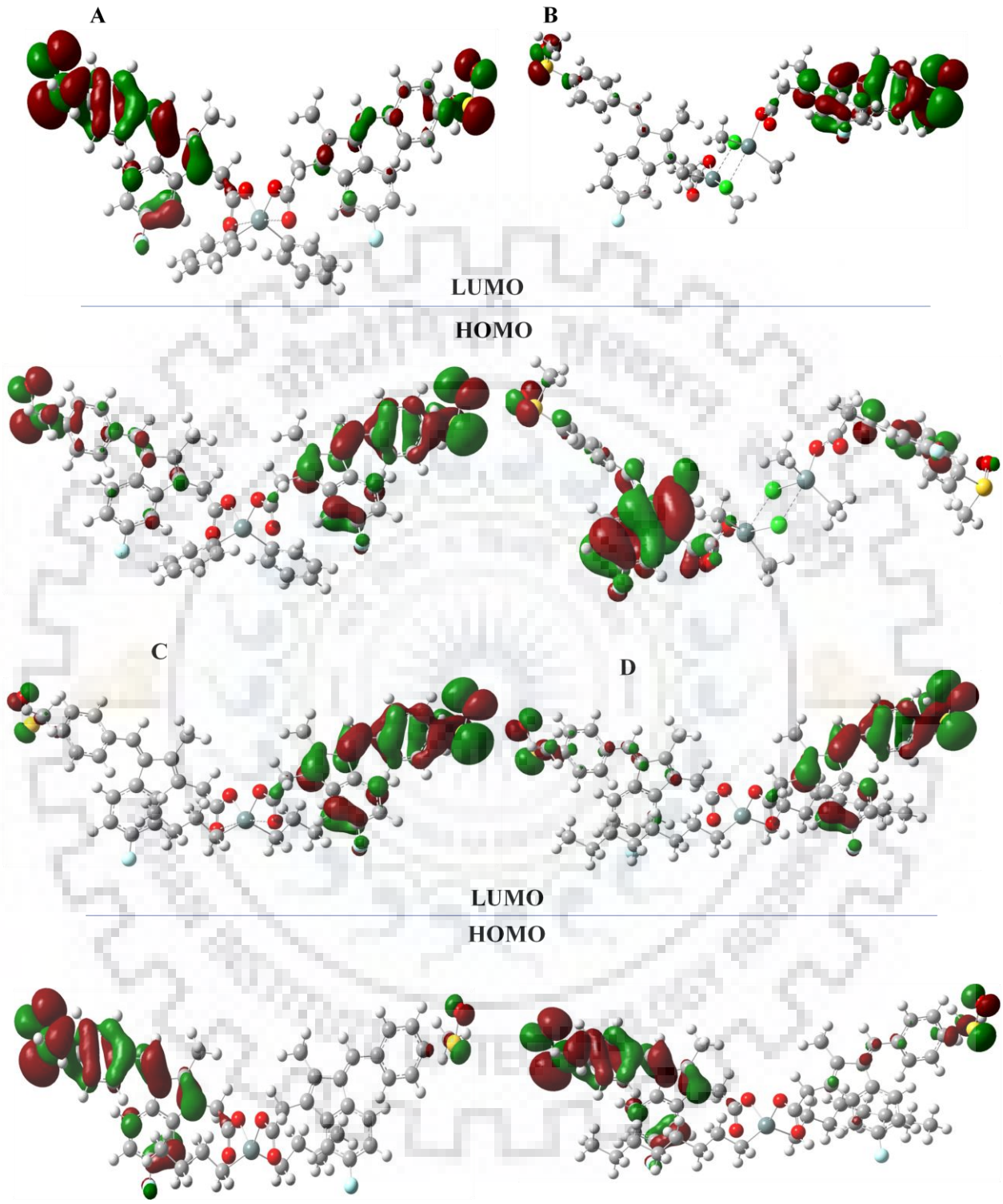

Fig. 5.8. Frontier molecular orbitals (HOMO-LUMO) of complexes 4 (A), 5 (B), 6 (C) and 7 (D) generated at B3LYP level with LANL2DZ basis set.

and 282 nm also exhibit hypochromism to a very small extent in comparison to former band. Hence, main emphasis was given to the absorption band occurred at 210 nm. The hypochromicity is due to the interaction of electronic states of the intercalating chromophore with stacked base pairs of DNA, due to which the probability of *л–л** transitions reduces to much lesser extent [275, 276], whereas red shifts in the absorbance spectra can be described by lowering in *л–л** transition energy of the **Sul**/organotin(IV) complexes due to their organized stacking between the base pairs of DNA during intercalation [126]. The intrinsic binding constants (K_b) have been determined from the plot of [DNA]/($\varepsilon_a - \varepsilon_f$) *vs* [DNA] [262, 263] and values were found to be in the range $7.9 \times 10^3 - 3.69 \times 10^4$ M^{-1}, which is very less in comparison to that of classical DNA intercalators having K_b value is in the order of 10^7 [277]. The K_b value for **Sul** (3.69×10^4 M^{-1}) is about double to that of the studied complexes **1–7,** which indicates its higher binding propensity, and it reveals that there may be a steric prohibition of complete intercalation between a set of adjacent base pairs, but some kind of partial intercalation can be envisioned for **1–7** [233]. The calculated K_b for complexes **1–7** are 7.3×10^3 M^{-1}, 1.14×10^4 M^{-1}, 1.47×10^4 M^{-1}, 1.55×10^4 M^{-1}, 1.49×10^4 M^{-1}, 2.02×10^4 M^{-1}, 1.17×10^4 M^{-1}, respectively, among all, the highest binding affinity was shown by complex **6** followed by **4**, whereas all other complexes showed a comparable binding affinity. The higher DNA binding propensity of dibutyl- and diphenyltin(IV) complexes is due to additional hydrophobic interactions of dibutyl moiety and base stacking interaction of diphenyl moiety [208], with the DNA backbone. In case of dioctyl- and tributytin(IV) complexes, there may be steric reasons which prevent proper intercalation of complex into DNA, it may attribute to lowering of the K_b values. Same reason may be applicable for lowering in binding constant of the studied complexes as compared to that of **Sul**.

5.3.7.2. Ethidium Bromide Displacement Study

To explore DNA binding events further, the competitive binding of ethidium bromide (EB) *vs* **Sul** /complexes **1–7** with CT DNA was examined using fluorescence spectrophotometric studies. Ethidium bromide (EB) shows intense fluorescence emission spectrum when binds with DNA due to its robust intercalation within the base pairs, which prevents it from solvent quenching. The addition of quencher (**Sul** and complexes **1–7**) to EB–DNA mixture leads to reduction in the emission intensity as they replace the EB, indicating competitive DNA binding with EB [278]. The reduction in emission intensity is completely due to the competitive replacement of EB intercalated to DNA, not due to any interaction of EB with **Sul**/complexes **1–7**. This fact has been validated

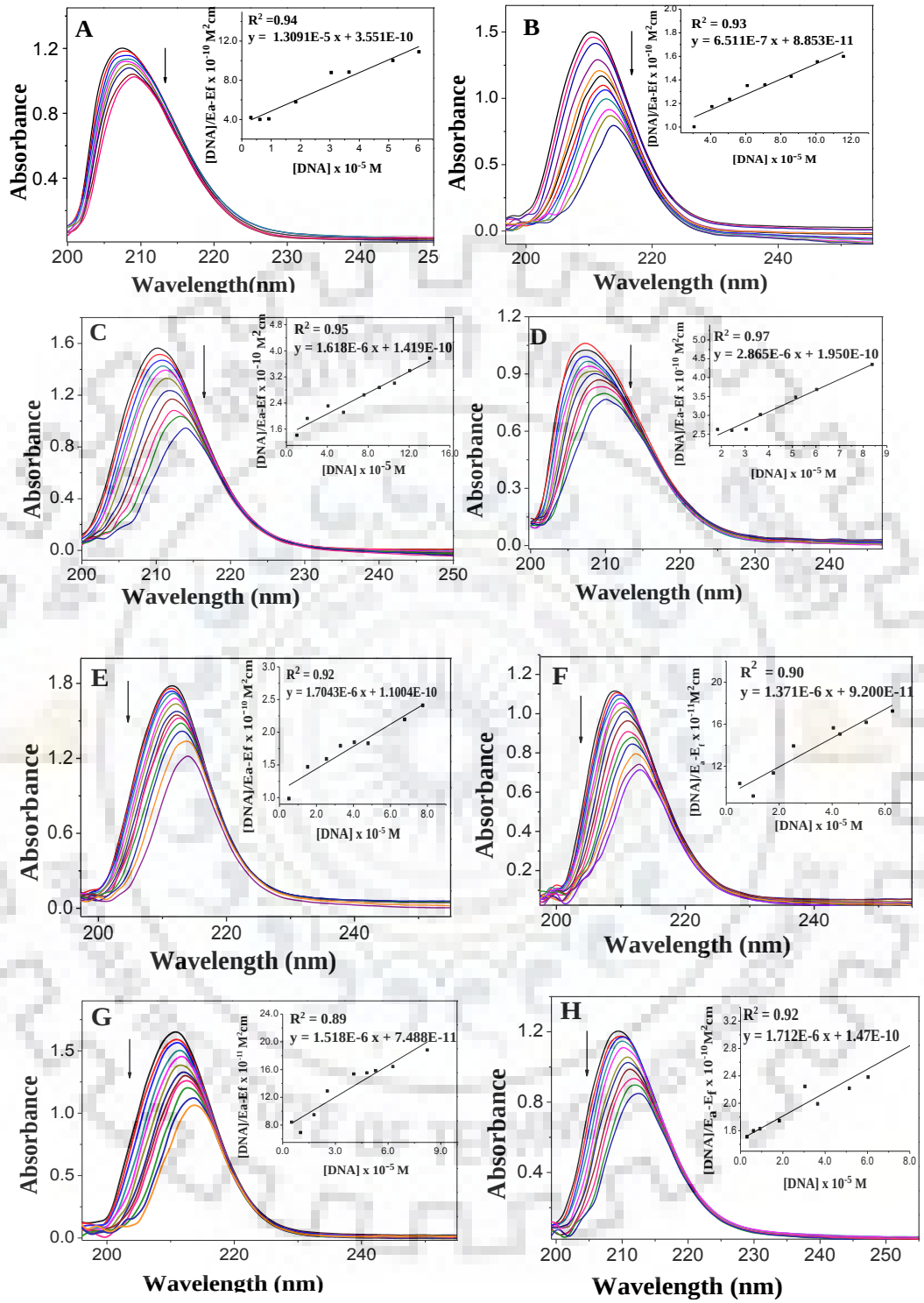

Fig. 5.9. Absorption spectral changes in Sul (A) and complexes 1–7 (B–H, respectively), observed at 210 nm in absence and presence of CT DNA (0–1.02 µM). Inset: plots of DNA *vs* [DNA]/(e_a – e_f) *vs* [DNA].

by examining the change in emission pattern of EB with successive addition of **Sul**/complexes within the same experimental conditions as in case of competitive binding study (spectra have been shown in Fig. 5.12, which indicated a minimal (2–4%) increase in emission intensity of EB (λ_{max}= 613 nm) with increasing concentration of **Sul**/complexes, whereas replacement of intercalated EB from DNA by **Sul**/complexes leads to 14–40% reduction in fluorescence intensity of EB-DNA adduct. The fluorescence quenching curves of ethidium bromide bound to DNA by **Sul** and **1–7** and corresponding Stern-Volmer plots are shown in Fig. 5.10 and Fig. 5.11, where arrow indicates a decrease in fluorescence intensity upon addition of quenchers. The Stern-Volmer quenching constant, K_{sv} values were obtained from the slope of the regression curve and listed in Table 5.10. The extent of ethidium bromide quenching is greater for **Sul** than that of complexes. The calculated values of K_{sv} are consistent with the absorption spectral studies as described above.

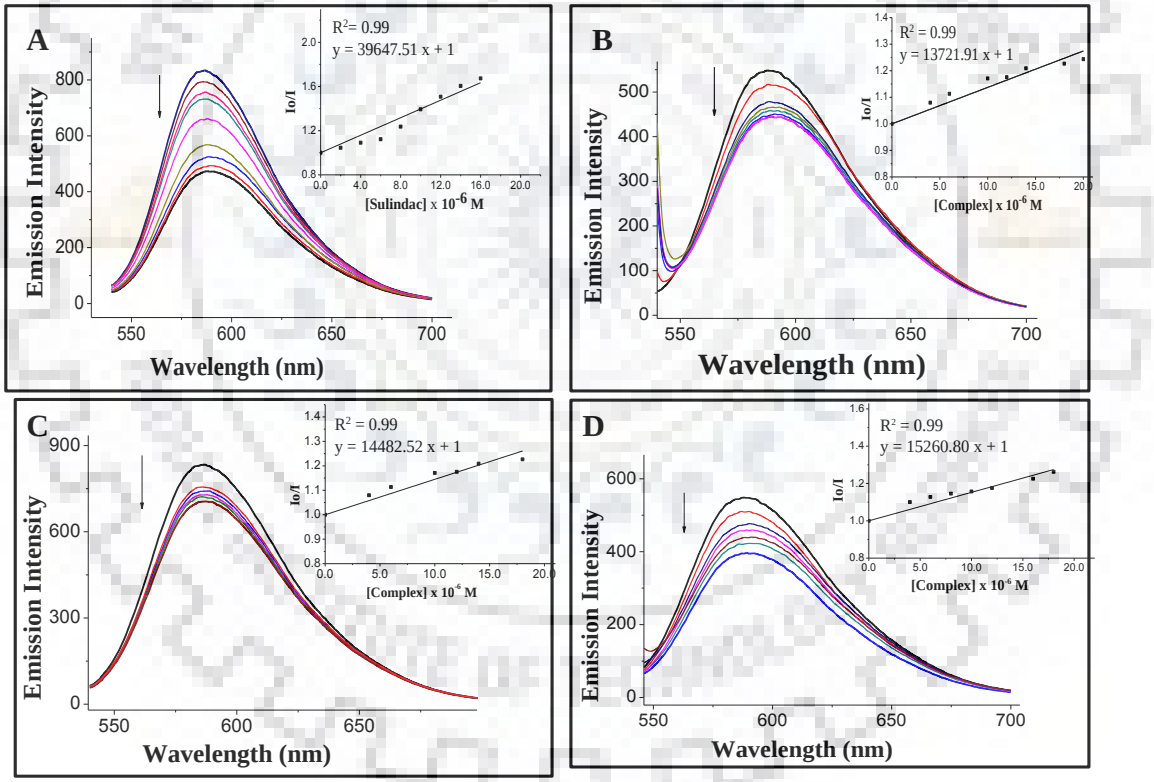

Fig. 5.10. Emission quenching spectra of CT DNA bound ethidium bromide in the absence and presence of Sul (A), complexes 1 (B), 2 (C) and 3 (D) in buffer Tris–HCl/NaCl, pH=7.2 at 25 °C. Arrow shows decrease in intensity with increasing concentration of quencher. Inset: Stern-Volmer plots.

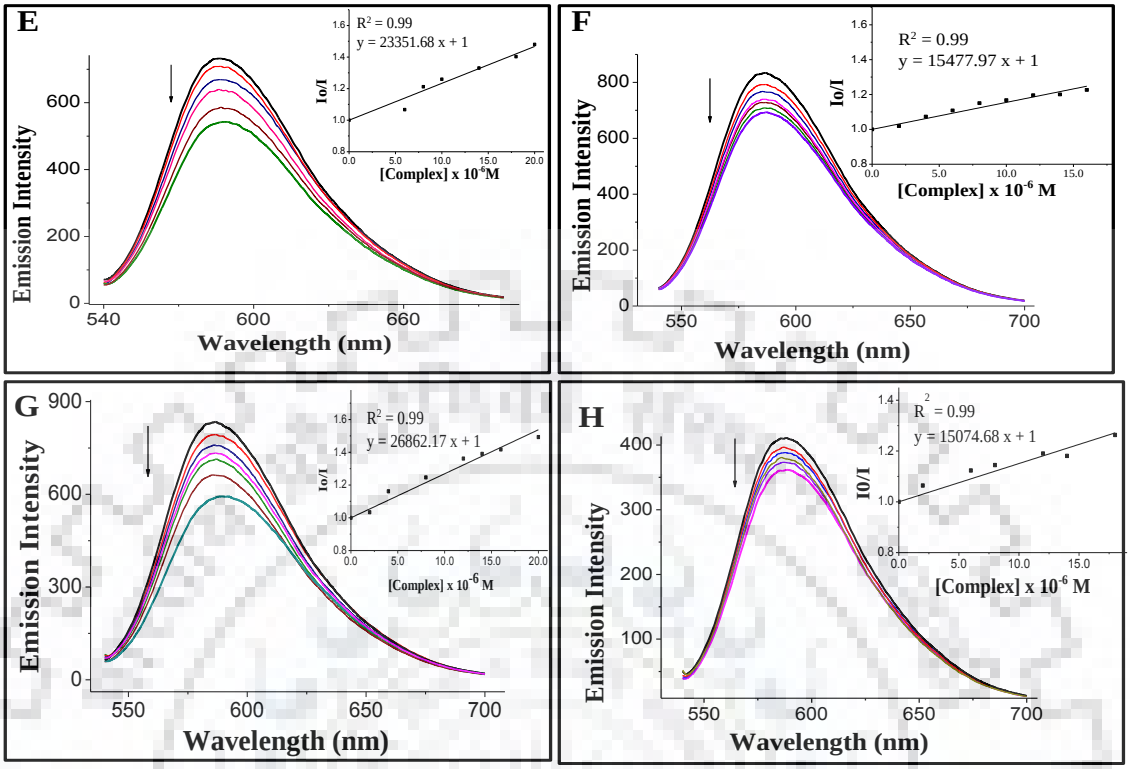

Fig. 5.11. Emission quenching spectra of CT DNA bound ethidium bromide in the absence and presence of 4 (E), complexes 5 (F), 6 (G) and 7 (H) in buffer Tris–HCl/NaCl, pH=7.2 at 25ºC. Arrow shows decrease in intensity with increasing concentration of quencher. Inset: Stren-Volmer plots.

Table 5.10. Stern-Volmer quenching constant, K_{sv} values for Sul and 1-7.

Ligand/complex[a]	K_{sv}
Sul	3.96×10^4
1	1.37×10^4
2	1.45×10^4
3	1.53×10^4
4	2.34×10^4
5	1.55×10^4
6	2.69×10^4
7	1.51×10^4

[a]numbers of complexes as given in Table 5.1.

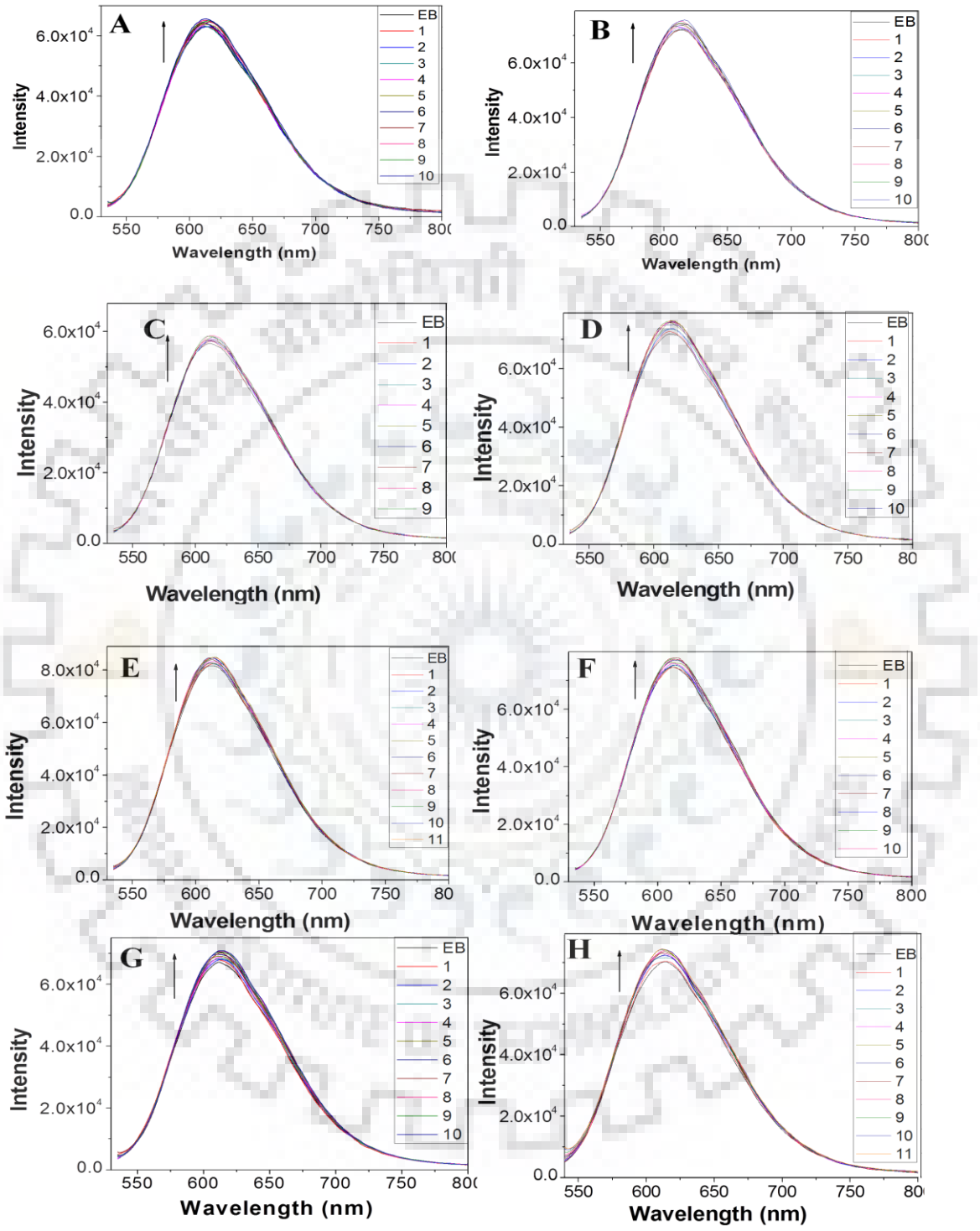

Fig. 5.10. Fluorescence spectra of ethidium bromide in the absence and presence of Sul (A) and complexes 1-7 (B-H). Inset: EB shows emission spectrum of ethidium bromide and 1-10 shows spectra with successive addition of Sul or complexes 2–20 µM, respectively.

5.3.7.3. Circular Dichroism

The CD spectrum in the UV range is particularly informative for the conformational changes of the DNA helix which is very useful for studying DNA–complex binding. The UV circular dichroism spectrum of CT DNA exhibits a positive band at 278 nm due to the base stacking and a negative band at 245 nm due to the helicity, which are characteristics of DNA in right-handed B form [232]. The CD spectra of CT DNA after addition of the **Sul** or complexes **1 –7** at a ratio (DNA/ **Sul** or Complex) r = 10, r = 5 and r = 2.5 are shown in Fig. 5.13. Very small perturbations were found in both bands of CT DNA after successive addition of **1** and **5,** which indicate simple groove binding and electrostatic interaction of the complexes with DNA [279]. However, CD spectra of CT DNA after interaction with **Sul** and complexes **4** and **6** show moderate increase in intensities of both the bands without any red shift indicating intercalation of complexes in DNA strand, however the change is not that remarkable and devoid of any change in wavelength gives indication of comparatively less binding or partial interaction of complexes with CT DNA [279]. Complex **2** shows a slight decrease in the negative and an increase in the positive band intensities when r = 10, and shows reverse results when ratio was decreased to r = 5 and r = 2.5, which suggests its different modes of binding with DNA. In contrast, the complex **3** shows a slight decrease, whereas **7** shows moderate decrease in the band intensities indicating that the complexes can unwind the DNA helix and leads to destabilization of the helical structure of DNA [280]. A decrease in band intensity of positive band upon addition of the complexes is due to a right handed conformational change of the DNA double helix, possibly due to partial intercalative binding of the complexes [233]. Furthermore, the decrease in negative band is probably due to the unwinding of the DNA helix upon interaction of complexes and then transformed into other A–like conformations [232].

Such results suggest that the CD spectral changes are closely correlated with DNA binding affinity. As CD spectroscopy is more sensitive than UV absorbance spectroscopy, hence there is possibility that the complexes could bind with CT DNA through the other suggestive modes, in addition with partial intercalation, as shown by absorption and fluorescence titration results. These data indicate a moderate interaction of complexes **1-7** and **Sul** with DNA and consistent with our data derived from absorption spectral and fluorescence quenching studies. Metal complex and DNA interaction depends on the size, charge and structure of the complexes. Absorption and circular dichroism spectroscopic studies indicated external binding of the complexes; however,

fluorescence studies showed that the K_{sv} values were higher than the external binder but lower than the putative in terms of DNA interaction, it has been found that sulindac itself was more effective as compared to its organotin(IV) derivatives because of its higher K_b and *Ksv* values, and more pronounced change in circular dichroism spectra of CT DNA upon its addition.

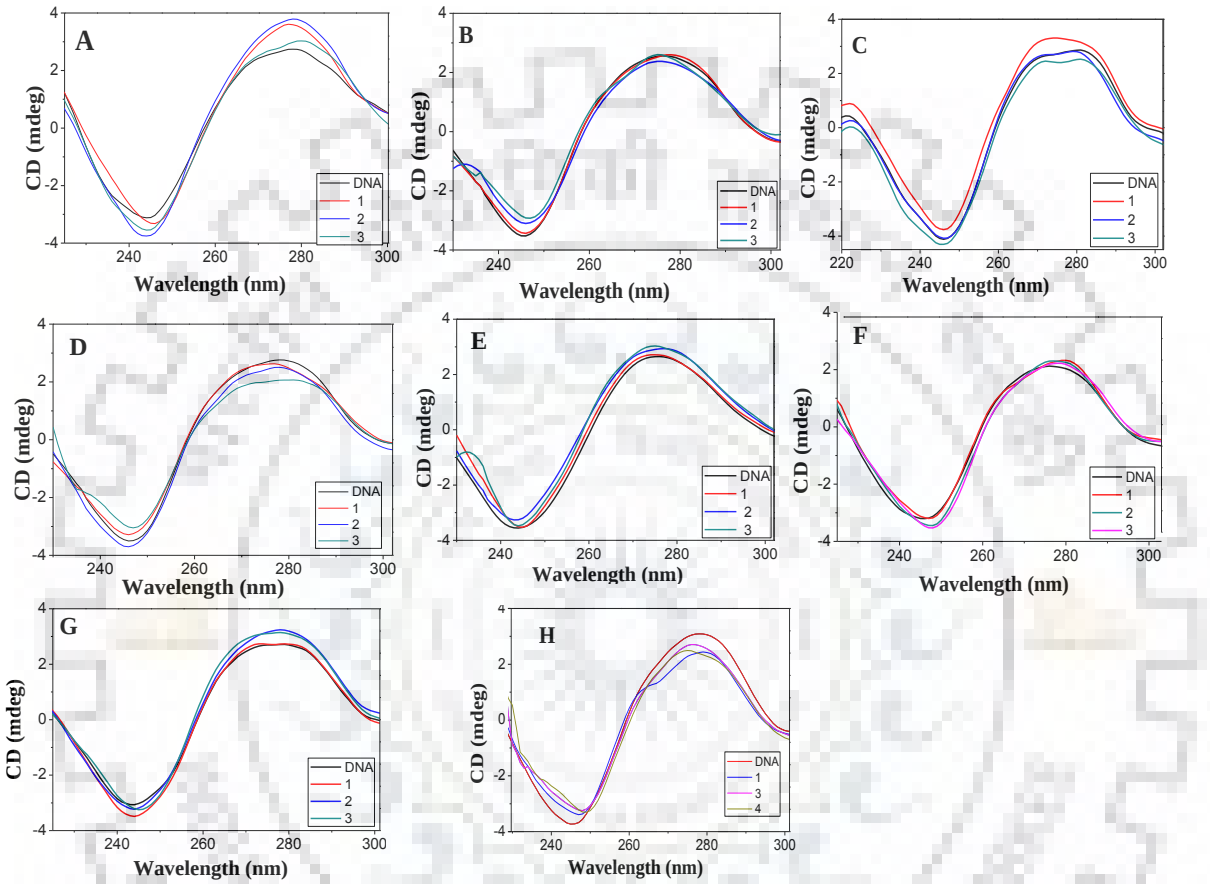

Fig. 5.13. Circular dichroism spectra of CT DNA (5×10^{-5} M) in 5:50 Tris-HCl/ NaCl buffer at pH 7.2 and 25 °C in the absence (DNA) and presence of Sul (A) and complexes 1-7 (B–H) at r = 2.5, 5 and 10.

5.3.8. DNA- Cleavage Studies

The chemistry of DNA strand scission caused by complexes has been investigated by the extent of fragmentation of the supercoiled (SC) form I [281] as mentioned in Chapter 4. Agarose gel electrophoresis gives the distribution of SC, NC and linear forms of DNA which provides a measure of the extent of cleavage of DNA. Gel electrophoretogram of **Sul** and complexes (**1-7**), along with quantification of the all the three forms by using Image J software were depicted in Fig. 5.14. **Sul** and complexes **2, 3, 4, 6** and **7** show an enhancement of the intensity of NC form II upon

increasing the ratio of complex/DNA, *r* = 1 to 10, linear form III is also appeared in complexes **2, 3** and **7** at ratio *r* = 5, *r* = 10 and *r* = 1 onwards, respectively. The results indicate their high binding propensities with DNA as also evidenced by UV, fluorescence and CD studies. The results reveal that complexes **2, 3** and **7** promote conversion of DNA from SC form I to nicked form II along with linear form III**,** whereas **Sul** and complexes **1, 4, 5, 6** trigger the formation of NC form II only with increasing concentration.

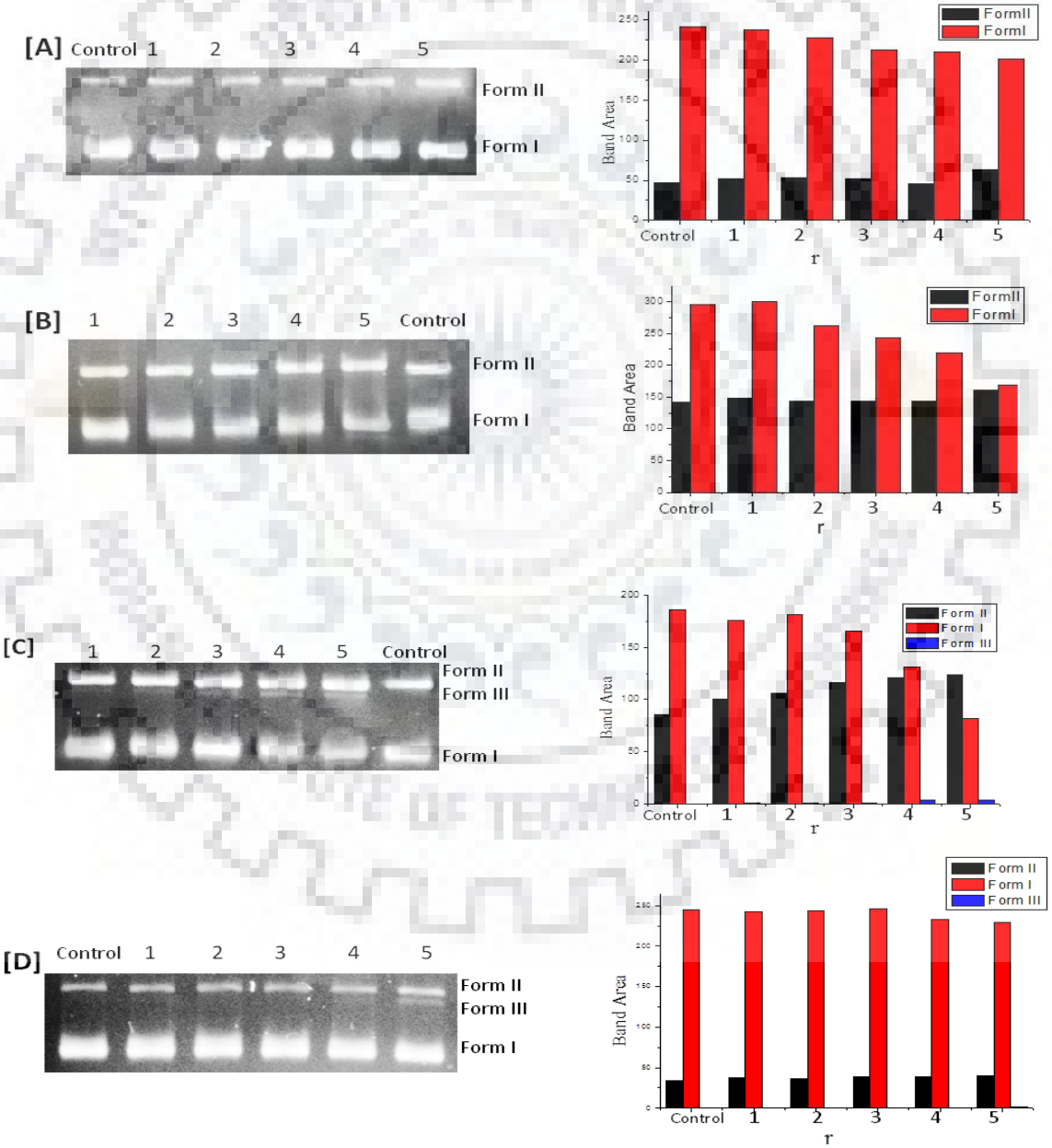

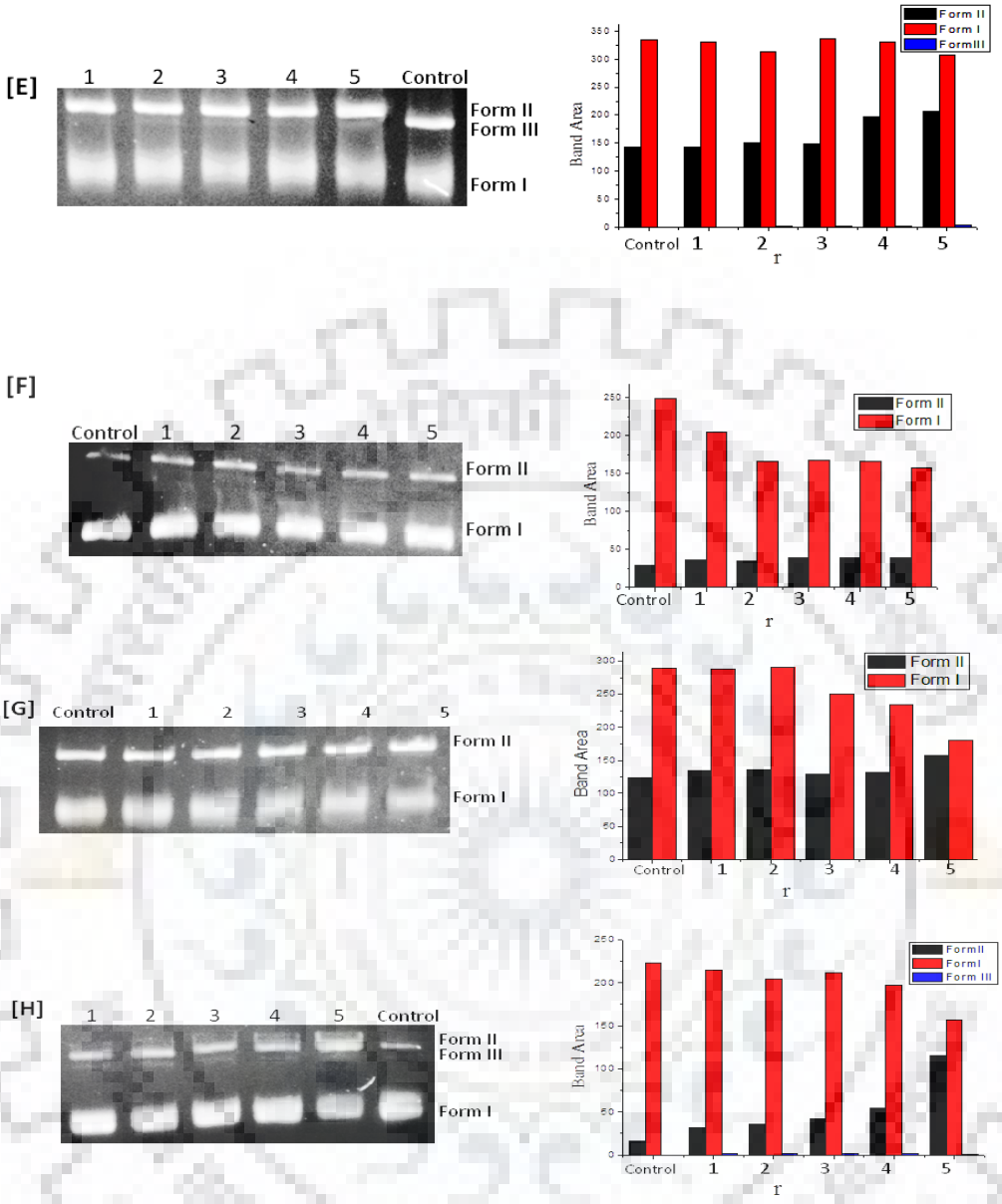

Fig. 5.14. Agarose gel electrophoretic cleavage pattern of pBR 322 DNA by Sul (A) and (1–7) (B–H), after incubation 3 h at 37 °C in 5:50 mM Tris–HCl/NaCl buffer, pH 7.2, along with quantification of band area. (DNA control; lane 1 (*r* = 1); lane 2 (*r* = 2.5); lane 3 (*r* = 5); lane 4 (*r* = 7.5); lane 5 (*r* = 10), where *r* = [complex]/[DNA].

5.3.9. Antitumour Screening through MTT Assay

All the synthesized complexes **1–7** were screened (*in vitro)* for antitumor/cytotoxic activity against HTC-15 (colon adenocarcinoma), MCF-7 (mammary cancer), HeLa (cervical cancer), and LNCaP (androgen-sensitive prostate adenocarcinoma), cell lines of human origin. Calculation of IC_{50}

(inhibitory concentration) values of **Sul** and complexes was carried out using best fit linear regression model [45, 46, 237]. IC_{50} values of all the complexes and **Sul** along with the reference drugs, *cis*-platin and 5-fluorouracil are presented in the Table 5.11. The IC_{50} values in Table 5.11 indicate that the complexes **1–7** as well as **Sul** are showing minimal cytotoxicity towards MCF-7, HeLa and LNCaP cell lines, which may be because of high stability of Sn–O bond and insufficiency to produce active tin species i.e. R_2Sn^{2+} and R_3Sn^{+}, responsible for antitumor activity. Furthermore, all the test compounds were found to induce cytotoxicity towards the HTC-15 cell lines comparable to 5-fluorouracil and *cis*-platin. Moreover, the dibutyltin(IV) complex (complex **6**) showing higher cytotoxicity against MCF-7 and HeLa cell lines. However, triphenyltin(IV) complex, (complex **2**) was able to induce highest cytotoxic effect against HCT-15 cell line. The studies on structure-activity relationship of different organotin complexes towards antitumour activity described that factors like stability of Sn-heteroatom bond, lipophilic and hydrophilic balance in the test compounds, geometry around the tin atom in the test compounds, and stability of Sn-alkyl and Sn-aryl bonds towards hydrolysis, are important to determine their cytotoxicity [44, 46, 282, 283].

Table: 5.11. Cytotoxic screening results of Sul and organotin complexes of Sul against the different cell lines of human origin; IC_{50} value is expressed in µM ± SEM.

Compounds[a]/Reference drugs	H CT-15 (µM)	MCF-7 (µM)	HeLa (µM)	LNCaP (µM)
Sul	14.9±0.9	406±22	179±30	465±15
1	13.8±0.9	>500	250±15	>500
2	**13.2±1.2**	>500	240±10	Very wide
3	14.4±1.8	408±14	157±17	Very wide
4	15.1±0.6	>500	>500	359±14
5	16.2±0.4	388±10	179±11	Very wide
6	14.3±0.4	**301±25**	**149±16**	Very wide
7	14.6±0.8	>500	Very wide	456±22
***cis*-platin**	5.04±1.4[b]	13.98±0.4[b]	18[c]	n.d.
5-Fluorouracil	12.2±0.5	0.48±0.1[b]	2.08±0.2	n.d.

[a]numbers of complexes as givrn in Table 5.1; [b]reference [46]; [c]reference [284] n.d.= not determined ; HCT-15: colon adenocarcinoma; MCF-7: mammary cancer; HeLa: cervical cancer and LNCaP: androgen-sensitive prostate adenocarcinoma.

CHAPTER – 6

Organotin(IV) Complexes of NSAID, Ibuprofen – Interaction with DNA and *In Vitro* Antitumour Studies

6.1. INTRODUCTION

It has been described in literature that several non steroidal anti-inflammatory drugs (NSAIDs) played a crucial role to succumb the tumour activities [285-287] and also used as effective modulators in combination therapies with anticancer drugs *viz.* cyclophosphamide, melphalanor and carmustine [245]. Endo et al. suggested that the ibuprofen is a potential chemotherapeutic agent which might allow lowering in doses of *cis*-platin and may limit the challenges associated with its side effects and development of resistance, by the downregulation of Hsp70 which is a contributor to the process of tumour generation [287]. Ibuprofen is a NSAID and has been known to cure the cancers of colon, protostate, lung and breast [288, 289]. Few literature reports have discussed the DNA binding capacities of aspirin and ibuprofen [229, 290], which might be responsible for their cytotoxicities. Complexes of ibuprofen with different metals have been found to exhibit significant antimicrobial and antitumor activities [291-295]. Ruthenium and copper complexes of ibuprofen have been possessed sufficient antitumour activities *in vitro* against mouse mammary (EMT6) human breast (MDA-MB-231), human prostate (DU145), and human skin melanoma (HT-144) and SKMEl-28 cancer cell lines [294, 295]. Few organotin complexes of ibuprofen were reported to show good antibacterial activities, however none of them was studied for their DNA binding capacity and antitumour activities.

Utilization of the platinum based componds as antitumor drugs had ignited new wave of interest in the synthesis and testing of new metal complex as antitumor agents. But, the side effects, toxicity and drug resistance associated with the platinum based compounds instigate many researchers to look forward for new alternatives with higher potency towards platinum resistant cancer cell with lesser side effects. The organotin carboxylate can be regarded as the best substitute for platinum-based antitumour drugs due to their extensive structural possibilities and wide range biological activities especially high *in vivo* and *in vitro* antitumour activities [163, 164]. Taking into account the importance of ibuprofen and organotin tin carboxylates, this Chapter deals with the synthesis and characterization of five complexes of organotin(IV) moieties with ibuprofen through thermal and microwave methods. The characterization of the synthesized complexes have been carried out through elemental analysis, FTIR, multinuclear NMR and ESI MS analysis and single crystal X-ray crystallography. Since, the organotin complexes were designed to imitate the platinum based drugs, therefore the function of these complexes were presumed to be based on the interaction with DNA, which is regarded as one of the major targets for anticancer candidates [104,

124, 207, 208] so, the DNA binding profile of synthesized complexes have been investigated through various biophysical techniques such as, UV-visible spectroscopic studies, fluorescence emission studies and viscosity measurements of DNA. Further, the DNA cleavage pattern has been investigated using gel electrophoresis technique. In order to correlate, the DNA binding and cleavage potential, with corresponding cytotoxic effect exerted by the compounds under study, their *in vitro* cytotoxicity (MTT assays) were performed with some selected cell lines *viz.* HCT-15 (human colon adenocarcinoma), DU145 (human prostate cancer) and Caco-2 (human colon carcinoma). Further, the underlying cause of cell death was examined through acridine orange(AO)/ethidium bromide (EB) staining of cancer cell lines and DNA fragmentation assay.

6.2. EXPERIMENTAL SECTION

6.2.1. Synthesis

Complexes of triorganotin(IV) and dimethyltin(IV) with IBF were synthesized through thermal method by preparing sodium salt of ibuprofen and dibutyltin(IV)-IBF complex was synthesized through microwave method.

6.2.1.1. Synthesis of Triorganotin(IV)-IBF Complexes, (1-3)

Sodium salt of ibuprofen was prepared by stirring the solution of ibuprofen (5 mM, 1.04 g) in 75 mL methanol and sodium methoxide, which was prepared by reacting sodium metal (5.5 mM, 0.126 g) in 15 mL of dry methanol, for 4 h at ambient temperature. The resulting solution was then evaporated, washed and dried and preserved for further synthesis of complexes.

To a solution of sodium salt of Ibuprofen (0.5 mmol, 0.115 g) in 15 mL of specially dried methanol added a hot methanolic (15 mL) solution of trimethyltin(IV) chloride (0.5 mmol, 0.100 g) or triphenyltin(IV) chloride (0.5 mmol, 0.193 g) or tributyltin(IV) chloride (0.5 mmol, 0.141 mL), the solution thus formed was refluxed with continuous stirring for 4 h. The reaction mixture was continuously supplied with dry nitrogen. The excess solvent was evaporated under reduced pressure. The products thus obtained were washed with a mixture of methanol and n-hexane (1:3, v/v), dried under vacuum and weighed.

6.2.1.2. Synthesis of Dimethyltin(IV)-IBF Complex

To a mixture of Me_2SnCl_2 (0.5 mmol, 0.110 g) and ibuprofen (0.5 mmol, 0.103 g) in 30 mL of

specially dried methanol added NaOH (2M, 1 mL) and the resulting solution was refluxed for 2 h. Further, 3 g of Na_2SO_4 was added in the solution and again refluxed for 4 h. The solution was kept for 2 days at ambient temperature and product started separating out, which was then filtered and washed with methanol and *n*-hexane (1:1, v/v) and dried under vacuum and weighed.

6.2.1.3. Synthesis of Dibutyltin(IV)-IBF Complex by Microwave Assisted Method

Microwave assisted syntheses were carried out in an open glass vessel microwave oven (Magicook 20S (Galaxy) Whirlpool) with a rotating tray and having maximum microwave energy output of 800 W. In order to synthesize complexes **5**, ibuprofen (1 mmol, 0.206 g) and dibutyltin oxide (0.5 mmol, 0.124 g) were finely ground together to obtain a homogeneous mixture. A paste of this mixture was made by adding few drops of methanol and irradiated for 1 min in a microwave oven at 400 Watt, in a Petri dish. The reaction mixture was then allowed to cool at room temperature and again irradiated for 1 minute; this process was repeated 4 times. An oily compound was appeared in Petri dish, which dried after triturating with hexane several times. The resulted product was scratched and washed with *n*-hexane and dried in vacuum.

Syntheses of dioctyltin(IV) and diphenyltin(IV) complexes with IBF have also been tried through microwave and thermal methods, but in both the cases an oily compound was obtained with mixture of product and reactants, which could not be purified. Furthermore, efforts to synthesize the mixed ligand complexes of organotin(IV) with IBF and 1,10-phenanthroline were made, but couldn't succeed.

6.2.2. DNA Binding Studies

To elucidate the mode and extent of binding of IBF/studied complexes towards DNA, biophysical studies were carried out by preparing an appropriate dilution of stock solution (in DMSO) of complexes in Tris–HCl/NaCl buffer (pH 7.2, 5:50 mM), so as the final dilution contains no more than 1% DMSO. Complex **3** $[Ph_3Sn(IBF)]$ precipitated immediately when dissolved in tris buffer and complex **4**, $[(Me_2Sn\text{-}IBF)_2O]_2$ precipitated slowly within half an hour after dissolving in buffer due to its instability in tris buffer, hence DNA binding studies of these complexes could not be performed. In order to avoid degradation and precipitation of the remaining complexes, freshly prepared dilutions were utilized. CT DNA stock solution once prepared was not used after 2 days.

6.2.2.1. UV-Visible Spectrophotometric Titration

The UV-visible spectra of IBF and complexes (**1, 2** and **5)** (6.7×10^{-5}M) were recorded in the absence and presence of CT DNA. Absorbance (A) of IBF and complexes **1-5,** was obtained with successive addition of CT DNA (0.6 μM to 15 μM) while keeping total volume constant. In order to eliminate the absorbance due to CT DNA the reference solution was maintained at equal concentration of CT DNA to that of working solution. As the data doesn't fit in linear regression model when plotted [DNA]/($\varepsilon_a - \varepsilon_f$) vs [DNA] ([DNA] is the concentration of CT DNA, ε_a is the apparent extinction coefficient, ε_f and ε_b correspond to the extinction coefficient of the metal complexes in free and in fully bound form, respectively), thus, K_b could not be determined and further, fluorescence studies were employed to estimate the extent of binding.

6.2.2.2. Fluorescence Titrations and Viscosity Measurement Studies

All the fluorescence emission experiments were carried out by diluting stock solution of the complexes, prepared in 1% DMSO with Tris–HCl/NaCl buffer (pH = 7.2) at 25 °C. IBF and complexes **(1**, **2** and **5)** were excited at 264 nm. Emission spectra were recorded in the range 270 nm to 360 nm with emission maximum at 290 nm. DNA binding experiment was carried out by recording the emission spectra of IBF/complexes (6.7×10^{-5} M) alone and with increasing concentrations (2–20 μM) of CT DNA. In the EB displacement experiment, the emission spectra of a preincubated solution of CT DNA (20 μM) and EB (5 μM) in the absence and presence of increasing concentration of IBF and complexes (2–20 μM), were recorded. The EB–CT DNA adduct ([DNA]/[EB] = 4) was excited at 515 nm and emission spectra were observed in the range 525–700 nm with a slit width of 2 nm. In another experiment iodide quenching was studied in which emission spectra of complexes (6.7×10^{-5} M) were recorded in the absence and the presence of CT DNA (20 μM) with subsequent addition of KI (0–72 mM). Stern-Volmer quenching constants K_{sv} in both the quenching experiments were evaluated using the classical Stern-Volmer equation [264] as described in Chapter 4.

Viscosity of CT DNA (100 μM) was measured in the presence and absence of IBF/complexes (**1, 2** and **5**) (20–100 μM) in Tris–HCl/NaCl buffer (pH = 7.2) at 25 °C.

6.2.3. Gel Electrophoresis

DNA cleavage study was performed using supercoiled pBR322, E. coli plasmid DNA. The supercoiled DNA (100 ng) was treated with varying concentrations of IBF and complexes (20–80 μM) with and without activators or radical quenchers in buffer solution (5:50 mM Tris–HCl/NaCl, pH 7.2) and were incubated for 5 h at 37 °C. Incubated samples were then treated with 2 μL loading buffer (30 mM EDTA, 0.05 % (w/v) glycerol, 36% (v/v) bromophenol blue) and were loaded onto agarose gel (0.8%) containing EB (0.5 μg/mL). The agarose gel was run in 0.5X TBE buffer at 50 V/cm for 3.5 h. Bands formed by moving plasmid DNA were visualized and photographed by Gel documentation system (Bio-Rad, USA).

6.3. RESULTS AND DISCUSSION

6.3.1. Synthetic Aspects

Triorganotin(IV) complexes of ibuprofen (**1-3**) were synthesized by refluxing Me_3SnCl/ Bu_3SnCl/Ph_3SnCl with sodium salt of Ibuprofen (1:1 metal to ligand ratio) in methanol with continuous supply of dry nitrogen as given in Scheme 6.1. (A). NaCl formed during the reaction was removed by washing the complexes with a mixture of MeOH and H_2O (9:1, v/v). Complex **4** was prepared by refluxing Me_2SnCl_2 and ibuprofen with equivalent NaOH, Scheme 6.1 (B), so as to form ibuprofen-dimethyltin hydroxide intermediate which, then further refluxed in the presence of Na_2SO_4 in order to absorb H_2O formed with the course of reaction, which is necessary for reaction completion. Further, complex **5** was synthesized by microwave irradiation (Scheme 6.1 (C)) of a mixture of Bu_2SnO and ibuprofen in 1:2 (metal to ligand) ratio. The reaction proceeded, as the water molecules formed during the course of reaction is evaporated with microwave irradiation. The whole reaction was completed in 5 min and yield was quite high. All the complexes prepared were soluble in methanol, $CHCl_3$, acetonitrile and stable towards air and moisture. The melting point, physical and analytical data of complexes is listed in Table 6.1. The CHNS percentage observed for the proposed structure of the complexes is found very close to their calculated values. The proposed structures and synthetic route opted for the synthesis of all the complexes is given in Scheme 6.1.

Table 6.1. Physical properties and analytical data of Organotin(IV) complexes of ibuprofen.

Ligand/ Complex	Complex (Empirical Formula)	Molecular weight	Colour & Physical state	Yield (%)	Decompos-ition temperature (°C)	Analysis (%) Observed (Calculated)		
						C	H	Sn
IBF	($C_{13}H_{18}O_2$)	206.2	White	–	79	–	–	–
1	**[(Me_3Sn)(IBF)]** ($C_{16}H_{26}O_2Sn$)	370.1	White solid	80	144	51.67 (52.09)	6.93 (7.10)	31.69 (32.16)
2	**[(Bu_3Sn)(IBF)]** ($C_{25}H_{34}O_2Sn$)	496.2	White solid	83	52	60.28 (60.62)	8.44 (8.59)	23.11 (23.97)
3	**[Ph_3Sn(IBF)]** ($C_{31}H_{32}O_2Sn$)	556.1	Off-white solid	78	96	66.68 (67.05)	5.34 (5.81)	20.91 (21.38)
4	**[(Me_2Sn(IBF))$_2$O]$_2$** ($C_{60}H_{92}O_{10}Sn_4$)	1452.3	White solid	63	112	49.70 (49.76)	6.02 (6.40)	32.16 (32.79)
5	**[$Bu_2Sn(IBF)_2$]** ($C_{34}H_{52}O_4Sn$)	644.3	White solid	89	60	63.03 (63.46)	7.99 (8.07)	17.93 (18.45)

IBF= Ibuprofen

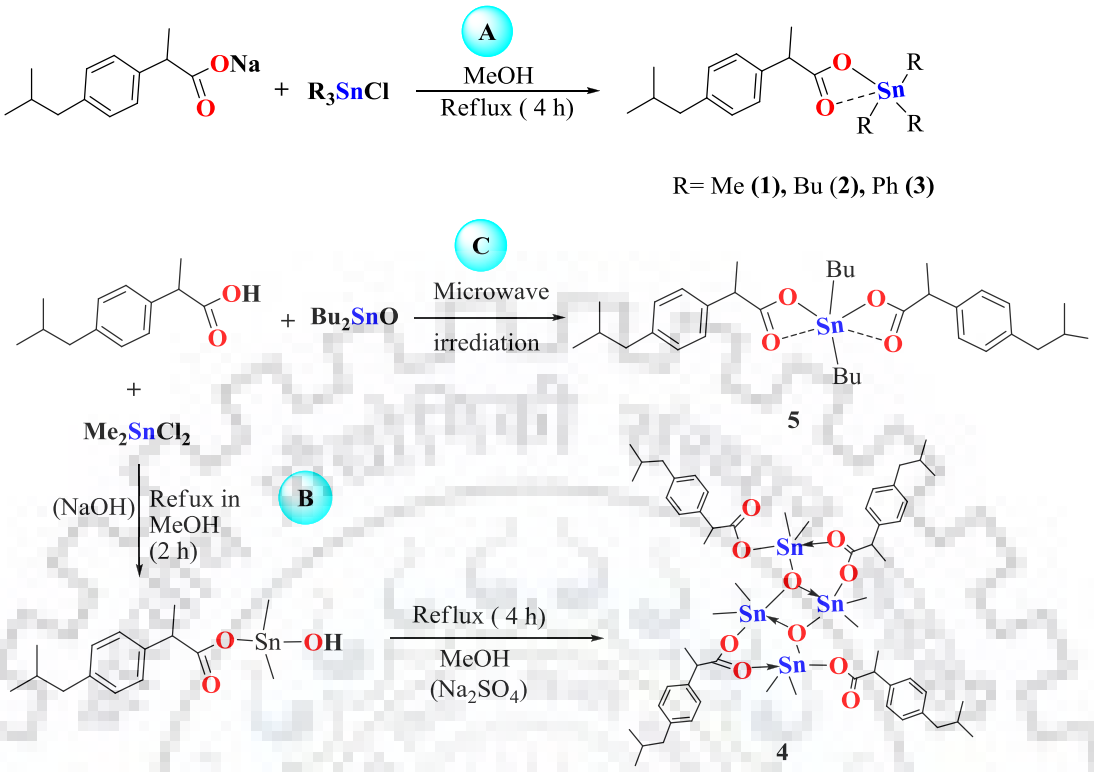

Scheme 6.1. Synthetic routes for complexes 1-5.

6.3.2. X-ray Crystallography of Complex 3 ($Ph_3Sn(IBF)$)

The colourless and rectangular block shaped crystals of complex **3** [($Ph_3Sn(IBF)$] were obtained with very slow evaporation of solvent (chloroform) from the concentrated complex solution filled in a glass tube of small diameter and remained undisturbed at ambient temperature for 5 days. The crystal structure was solved by processing the diffraction data through Direct method with SIR-92 programme [169]. A summary of pertinent crystal data along with other details of structure determination and refinement parameters are depicted in Table 6.2 and the selected bond lengths and bond angles are given in Table 6.3. An ORTEP view of the complex **3** (CCDC ID-1814179) is illustrated in Fig. 6.1. The diffraction data imply that complex is crystallized in a monoclinic crystal system (P 21/n space group). Crystal structure illustrates a monomeric unit of complex **3** where the molecule demonstrates geometry in between tetrahedral geometry (td) and trigonal bipyramedal (TBP) geometries, which is sometimes interpreted as [4+1] coordinated Sn atom. In this molecule the carboxylate group bonded with both oxygen through covalent and coordinate bonds evidenced from observed bond lengths (Å) *viz.* Sn(01)–O)(01) 2.079(2), Sn(01)–O(02) 2.633(2), O(01)–C(22) 1.301(4), O(02)–C(22) 1.224(5). A strong covalent Sn–O bond (2.079 Å) is

present in the complex molecule as equivalent bond lengths has been reported in similar complexes [110, 296, 297], whereas other Sn–O bond (2.633 Å) is much shorter than the van der Waal's radii of corresponding atoms (3.7 Å) [297], is considered a weak coordinate (Sn←O) bond. Owing to the presence of Sn←O bond, the structure of the complex **3** become highly distorted from ideal td to TBP geometry and can be best described as a capped tetrahedron [110]. The extent of distortion from ideal geometry (TBP or td) can be estimated on the basis of observed C–Sn–C angles (108°–119°), O–Sn–C angles (83°–148°) and O–Sn–O angle (54°). Further, the stability of crystal lattice can be described by weak van der Waal forces among the phenyl groups of the adjacent molecules as shown in Fig.6.2.

Table 6.2. Crystallographic data and structural refinement parameters for complex 3, ($Ph_3Sn(IBF)$).

	Complex 3
Molecular formula	$C_{31}H_{32}O_2Sn$
Formula weight	555.28
Space group	P 21/n
Hall group	-P 2yn
Crystal system	Monoclinic
Cell parameters	a=11.423(5), b=9.318(5), c=26.005(5) α=90, β=97.298(5) γ=90
Cell volume ($Å^3$)	2746(2)
Density (gcm^{-3})	1.343
Z	4
Temperature (K)	293
λ (Å) (Mo K_α)	0.71073
μ (mm^{-1})	0.954
F000	1136.0
F000'	1133.77
Theta (θ) range (°)	2.830–28.373
Limiting indices	$-15 \leq h \leq 14$, $-12 \leq k \leq 11$, $-34 \leq l \leq 34$
Total number of reflections	6876
Number of Reflection collected	5777
T_{min},T_{max}	0.795, 0.850
Final R indices(obs data) [I>2σ(I)]	R1=0.0408, WR2=0.0957
Final R indeces [all data]	R1=0.0512 WR2=0.1007
Data/restraints/parameters	6840/1/307
Highest diff. peak/hole ($e.A^{-3}$)	0.770/-0.930
Goodness of fit on F^2	1.147

Space group symmetry operation xyz
'x, y, z';
'-x+1/2, y+1/2, -z+1/2';
'-x, -y, -z'
'x-1/2, -y-1/2, z-1/2'

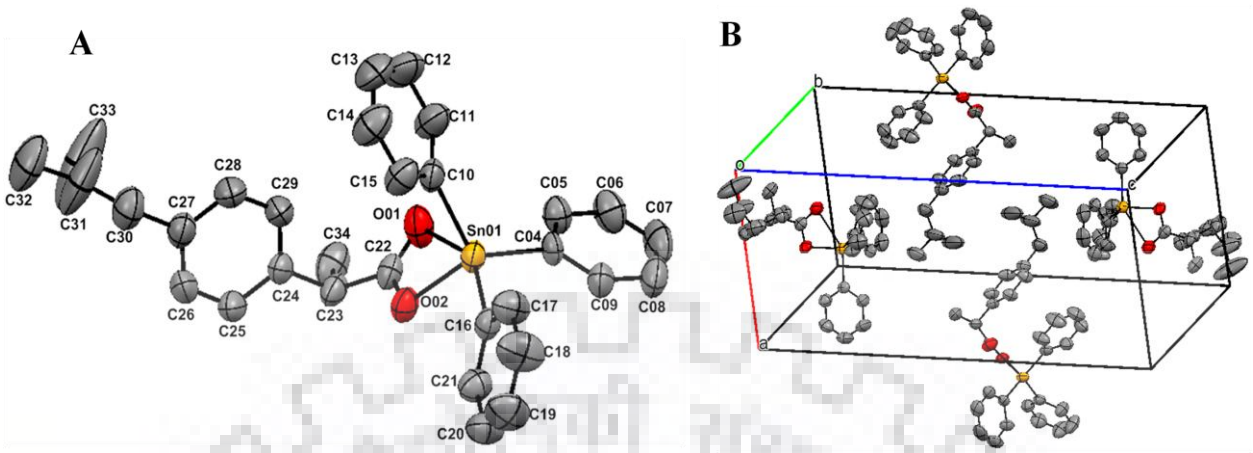

Fig. 6.1. ORTEP diagram of Ph_3Sn(IBF) at thermal ellipsoids (50% probability) with adopted non-hydrogen numbering scheme; H-atoms are omitted for clarity (A) and packing of molecules in a unit cell viewed along crystallographic axis b (B).

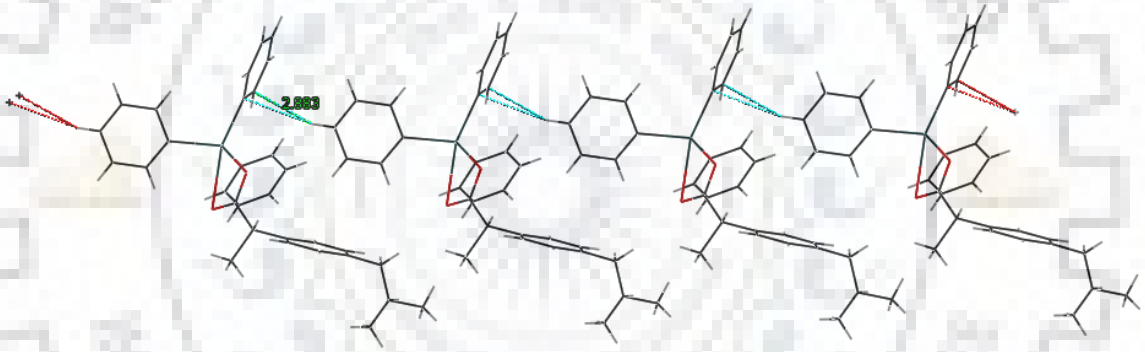

Fig. 6.2. Packing of molecules van der Waal interaction (2.883 Å) between carbon and hydrogen of phenyl groups of adjacent molecules.

Table 6.3. Selected bond angles (θ) and bond lengths (Å) and torsion angles (°) of complex 3.

Bond lengths			
Sn(01)–O)(01)	2.079(2)	O(01)–C(22)	1.301(4)
Sn(01)–O(02)	2.633(2)	O(02)–C(22)	1.224(5)
Sn(01)–C(16)	2.134(4)	C–C 1.513	1.513
Sn(01)–C(10)	2.135(3)	$(C–C)_{aromatic\ ring}$	3.355–3.388
Sn(01)–C(04)	2.137(3)	(C–H)	0.930(1)
Bond angles			
O(01)–Sn(01)–O(02)	53.88(9)	O(02)–Sn(01)–C(04)	85.2(1)
O(01)–Sn(01)–C(16)	104.1(1)	C(16)–Sn(01)–C(10)	112.4(1)
O(01)–Sn(01)–C(10)	94.5(1)	C(16)–Sn(01)–C(04)	119.3(1)

Contd…

O(01)–Sn(01)–C(04)	115.8(1)	C(10)–Sn(01)–C(04)	108.0(1)
O(02)–Sn(01)–C(16)	83.6(1)	Sn(01)–O(01)–C(22)	104.7(2)
O(02)–Sn(01)–C(10)	148.0(1)	Sn(01)–O(02)–C(22)	80.6(2)
Torsion angle			
O(02)–Sn(01)–O(01)–C(22)	3.5(2)	O(01)–Sn(01)–C(10)–C(11)	152.5(3)
O(02)–Sn(01)–C(10)–C(11)	161.0(2)	C(10)–Sn(01)–O(02)– C(22)	14.1(3)
C(10)–Sn(01)–O(01)–C(22)	178.0(2)		

6.3.3. FTIR Spectroscopy

A broad band in the region 2500–3300 cm^{-1} represent the stretching frequency of O–H group of carboxylic acid, its disappearance after complexation to Sn atom reveals the deprotonation of carboxylate oxygen. Weakening of C=O bond after complexation can be explained with a shift in ν(C=O) towards downside frequency. The diagnostic bands for the carboxylate antisymmetric (ν(OCO)as) and symmetric ((OCO)s) stretching vibrations of complexes **1-5**, appeared in the range 1569–1638 cm^{-1} and 1356-1427 cm^{-1}, respectively, which could have not been assigned without the formation of complexes [84, 110, 298, 299]. A measure of difference of ν(OCO)asym and ν(OCO)sym (Δν) is important to estimate the probable mode of binding of carboxylates to Sn metal. In this case, complexes **1-3** and **5** having Δν values 186–206 cm^{-1} which is comparable to the sodium salt of ligand (Ibuprofen) and reveals a bidentate mode of coordination of carboxylate group with metal. However, two different Δν values 231 cm^{-1} and 184 cm^{-1} were observed for complex **4**, which revealed the occurrence of two different mode of binding of carboxylate [300]. Strong to medium intensity bands were appeared in the region 581–444 cm^{-1}, which were assigned to Sn–O and Sn←O stretching frequency, indicate the formation of complexes. Furthermore, the characteristic bands found in the region 635–597 cm^{-1} and 597–503 cm^{-1} could be assigned to ν(Sn–C)as and ν(Sn–C)s modes, respectively [110, 301]. In addition, a sharp band with strong intensity was detected at 635 cm^{-1} which could be assigned to the ν (Sn–O–Sn) mode of complex **4** [84, 301]. Data pertaining to the FTIR studies of complexes, drug and its sodium salt is presented in Table 6.4 and FTIR spectra of complexes **4** and **5** are given as Fig. 6.3.

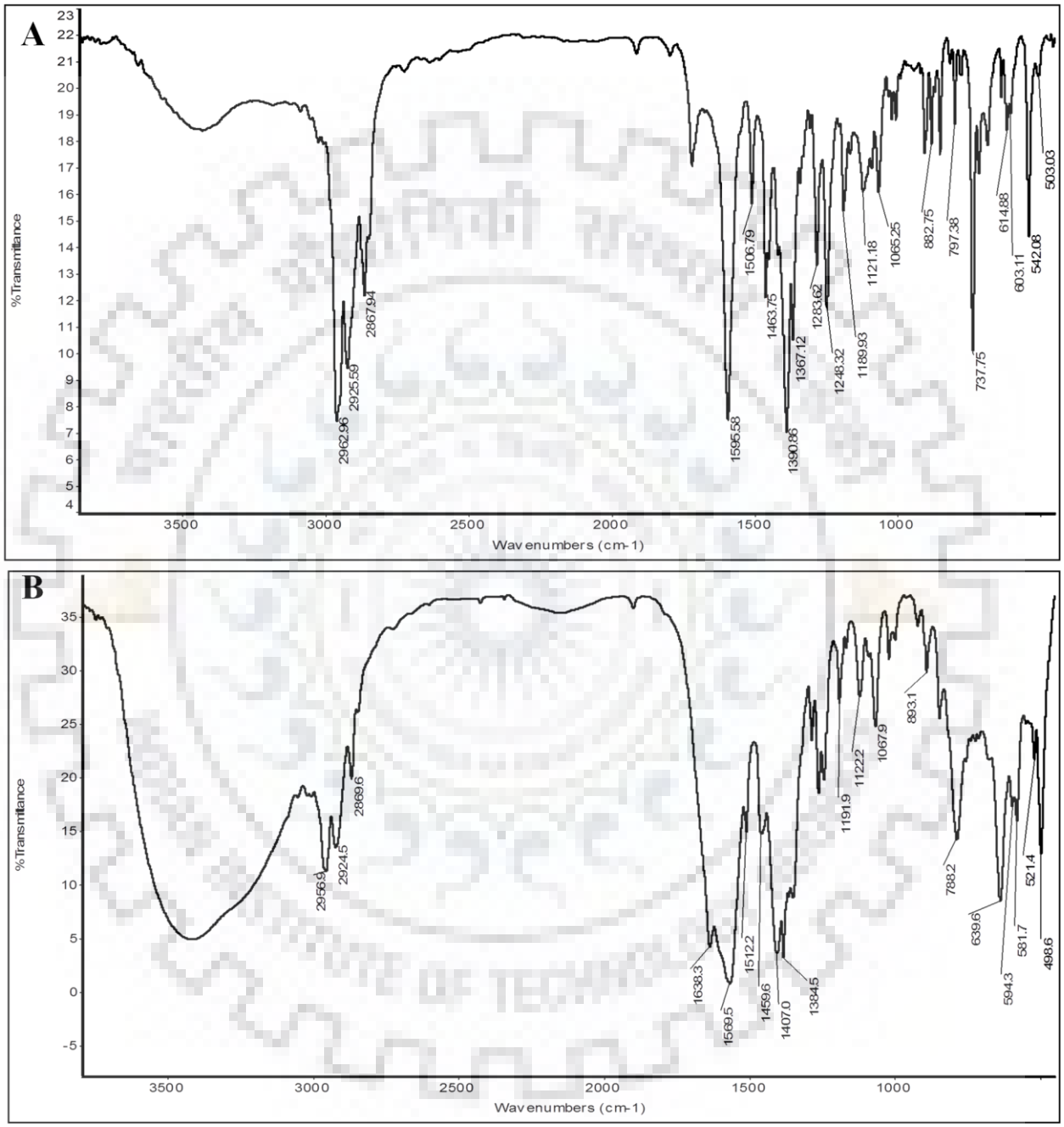

Fig. 6.3. FTIR spectra of complex 5 (A) and complex 4 (B).

Table 6.4. FTIR spectroscopic data of ibuprofen, sodium salt of ibuprofen and organotin(IV) complexes (1-5).

Ligand/ Complex[a]	ν(OH)	ν(OCO)/ ν(OCO)as	ν(C=O)s	Δν= [ν(C=O)as– ν(C=O)s]	ν(C=C)/ν(ring)	$\nu_{inplane}$/ $\nu_{outplane}$ (ring)	ν_{as}(Sn–C) /ν_{s}(Sn–C)	ν(Sn–O), ν(Sn←O)
IBF	2500-3300 br	1707 s	–	–	1636 m, 1563 s, 1465 s	1184 s, 1069 m,1054 s (sp), 949 s, 864 s, 778 s	–	–
IBFNa	–	1550 s	1364 m	186	1635 w, 1474 m	1188 m, 1058 m,847 m, 787 m	–	–
1	–	1577 s	1359 m	218	1560 s, 1506 m, 1453 m,	1186 s 1112 m, 1062 s, 894 w, 777 s	615 m, 597 w	547 s
2	–	1586 s	1391 s	195	1507 s, 1453 m	1183 w, 1118 w, 1068 s, 876 m, 782 m	597 m, 511 w	544 s
3	–	1616 s	1427 s,	189	1506 m, 1474 m, 1450 m	1189 s, 1074 s, 997 s, 788 m		553 m, 444 s
4	–	1638 s, 1569 br	1407 s, 1385 s	231, 184	1512 m, 1459 s	1192 m, 1122 w, 1068 s, 893 m, 788 s	640 s, 594 m, 521 w	581 m, 499s
5	–	1596 s	1389 s,	206	1507 m, 1464 m	1189 m, 1121 m, 1065 m, 883 m, 797 s	603 m, 503 w	542 s

[a]Complex number as given in Table 6.1; IBF = ibuprofen; m=medium; s=strong; w=weak, br= broad

6.3.4. Multinuclear (^{1}H, ^{13}C and ^{119}Sn) NMR Spectroscopic Studies

Characterization and structural estimation of synthesized complexes have been done by multinuclear NMR studies and data of ^{1}H and ^{13}C NMR are listed in Table 6.5 and that of ^{119}Sn NMR in Table 6.6. ^{1}H NMR data reveals right integration of protons as expected according to the plausible structures of complexes **1-5.** A relevant shift is observed in the ^{1}H chemical shifts values of ibuprofen after complexation evidenced the formation of complexes**.** The value of heteronuclear one bond (^{1}J) and two bond coupling (^{2}J) constants plays a significant role in determining the ∠C–Sn–C, thus the predicting the geometry of the complexes. The values of $^{2}J(^{119}\text{Sn}–^{1}\text{H})$ obtained for complexes **1-3** are 57.60 Hz, 55.97 Hz and 51.97/59.98 Hz, respectively, and ∠C–Sn–C calculated form Lockhart and Mander's equation [196, 270] are 110.8°, 109.4 and 108.28–112.15°, respectively, which are in the range of four coordinated tin atom and revealed a tetrahedral geometries for these complexes in solution state [296, 270]. These results are in contrast with the pseudo five or 4+1 type of coordination of Sn atom, revealed on the basis of crystal structure of the complex **3** and similar geometry proposed for complexes **1** and **2** in solid state. This difference in results can be explained by the dissociation of weak coordinate bond between tin and carbonyl oxygen of the drug molecule in solution state. The resolved $^{2}J(^{119}\text{Sn}–^{1}\text{H})$ values for complex **5** is 71.96 Hz and the calculated ∠C–Sn–C is 121.78°, which lie in the range of five coordinated Sn atom [270]. Since, the FTIR data of complex **5** revealed a similar kind of bidentate mode of coordination for both the carboxylate groups attached to Sn, the Sn atom should be hexa-coordinated. Further, five coordination for Sn atom in solution state may be due to the weakening of Sn←O bond. No satellite peaks were resolved for complex **4**, hence ∠C–Sn–C could not be calculated. ^{13}C NMR spectra of complexes reveal a downfield shift in resonance of carboxylate carbon compared to the free ligand due to the drift of electron density towards tin metal. C2 and C3 carbon were also showing significant downfield shift due to similar reason. One bond coupling constant [$^{1}J(^{119}\text{Sn}–^{13}\text{C})$] value for complexes **1** and **3**, 388 Hz and 390.97 Hz and calculated ∠C–Sn–C are 110.8° and 111.05°, respectively, which are similar as calculated form $^{2}J(^{119}\text{Sn}–^{1}\text{H})$ value. Coupling constant and ∠C–Sn–C value for complex **4** are 437.73 Hz and 115.15° respectively, which describe a penta-coordinated geometry around tin metal. Two different resonances observed in ^{13}C NMR spectra of methyl carbon (attached to tin) explained the two different tin environments in the complex [302]. A single resonance observed for carboxylate carbon of this complex can be due to either accidental magnetic equivalence or dynamic

equilibrium between different isomeric structures [302]. ^{119}Sn NMR resonances for complexes **1-3** (136.16 ppm, 110.86 ppm and –109.53 ppm) further support the tetrahedral geometry for these complexes. However, two values of ^{119}Sn resonances at –176.78 ppm and –182.34 ppm for complex **4** suggested a penta-coordinated geometry around tin atom with two different environments, [302-305] which can be justified by tetra-nuclear tin structure as given in Scheme 6.1 (C). For complex **5,** ^{119}Sn NMR chemical shift value is –146.07 which is similar to the other complexes reported in literature [303, 305] for a highly distorted octahedron or bicapped tetrahedron type of geometry. Few representative ^{1}H, ^{13}C and ^{119}Sn NMR spectra of complexes are presented as Fig. 6.4, Fig. 6.4 and Fig. 6.6, respectively.

Table 6.5. ^{1}H, and ^{13}C NMR spectroscopic data of IBF and its organotin(IV) complexes in $CDCl_3$.

Ligand/ Complex[a]	^{1}H NMR δ (ppm) (399.78 MHz)
IBF	3.72 (q, 1H, H-2), 1.51 (d, 3H, H-3), 7.23 (d, 2H, H-5, 5'), 7.11 (d, 2H, H-6, 6'), 2.46 (d, 2H, H-8), 1.85 (m, 1H, H-9), 0.91 (d, 6H, H-10, 10')
1	3.69 (q, 1H, H-2), 1.45 (d, 3H, H-3), 7.20 (d, 2H, H-5, 5'), 7.07 (d, 2H, H-6, 6'), 2.46 (d, 2H, H-8), 1.84 (m, 1H, H-9), 0.89 (d, 6H, H-10, 10'), 0.50 (9H, H-*α*), [^{2}J (^{119}Sn–^{1}H) = 57.6 Hz]; [∠C–Sn–C= 110.8°][b]
2	3.69 (q, 1H, H-2), 1.46 (d, 3H, H-3), 7.22 (d, 2H, H-5, 5'), 7.06 (d, 2H, H-6, 6'), 2.43 (d, 2H, H-8), 1.84 (m, 1H, H-9), 0.90 (d, 6H, H-10, 10'), 0.87 (t, 9H, *δ*-H); 1.18-1.32 (m, 12H, H-*α,β*), 1.49-1.75 (m, 6H, H-*γ*), [^{2}J (^{119}Sn–^{1}H) = 55.97 Hz] [∠C–Sn–C= 109.4°][b]
3	3.83 (q, 1H, H-2), 1.50 (d, 3H, H-3), 7.19 (d, 2H, H-5, 5'), 7.04 (d, 2H, H-6, 6'), 2.44 (d, 2H, H-8), 1.84 (m, 1H, H-9), 0.90 (d, 6H, H-10, 10'), 7.65-7.63 (br, 6H, H_o); 7.42-7.37 (br, 9H, H_{mp}) [^{2}J($^{117/119}$Sn–^{1}H) = 51.97/59.98 Hz] [∠C–Sn–C= 108.28/112.15°][b]
4	3.47 (q, 1H, H-2), 1.36 (d, 3H, H-3), 7.15 (d, 2H, H-5, 5'), 7.06 (d, 2H, H-6, 6'), 2.43 (d, 2H, H-8), 1.83 (m, 1H, H-9), 0.89 (d, 6H, H-10, 10'), 0.47 (6H, br, H-*α*)
5	3.75 (q, 2H, H-2), 1.50 (d, 6H, H-3), 7.23 (d, 4H, H-5, 5'), 7.07 (d, 4H, H-6, 6'), 2.43 (d, 4H, H-8), 1.83 (m, 2H, H-9), 0.89 (d, 12H, H-10, 10'), 0.76 (t, 6H, *δ*-H); 1.25-1.16 (m, 6H, H-*γ*), 1.42-1.56 (m, 8H, H-*α,β*), [^{2}J (^{119}Sn–^{1}H) = 71.96 Hz] [∠C–Sn–C= 121.78°][b]

Contd….

	^{13}C NMR δ (ppm) (100.53 MHz)
IBF	180.03 (C-1), 45.02 (C-2), 18.04 (C-3), 136.93 (C-4), 127.26 (C-5, 5'), 129.38 (C-6, 6'), 140.83 (C-7), 44.95 (C-8), 30.15 (C-9), 22.38 (C-10, 10')
1	180.28 (C-1), 45.73 (C-2), 19.50 (C-3), 139.18 (C-4), 127.06 (C-5, 5'), 129.12 (C-6, 6'), 139.95 (C-7), 45.04 (C-8), 30.14 (C-9), 22.37 (C-10, 10'), –2.49 (C-*α*), [^{1}J (^{119}Sn-^{13}C) = 388 Hz]; [∠C–Sn–C= 110.8][c]
2	180.07 (C-1), 45.91 (C-2), 19.16 (C-3), 139.30 (C-4), 127.10 (C-5, 5'), 129.01 (C-6, 6'), 139.95 (C-7), 45.05 (C-8), 30.17 (C-9), 22.37 (C-10, 10'), 16.37 (C-*α*) 26.92 (C-*β*), 27.71 (C-*γ*), 13.60 (C-*δ*), [^{1}J(^{13}C–$^{117/119}$Sn) = 354.3-500.96], [∠C–Sn–C = 107.8°–120.7°].
3	181.15 (C-1), 45.24 (C-2), 19.24 (C-3), 138.65 (C-4), 127.16 (C-5, 5'), 129.07 (C-6, 6'), 140.10 (C-7), 45.03 (C-8), 30.17 (C-9), 22.38 (C-10, 10'), 128.77, 129.07, 136.69, 138.64 ($C_{i,o,m,p}$), [^{1}J(^{13}C–$^{117/119}$Sn) = 390.97], [∠C–Sn–C = 111.05°][c]
4	180.71 (C-1), 47.00 (C-2), 18.94 (C-3), 138.97 (C-4), 127.11 (C-5, 5'), 129.25 (C-6, 6'), 140.18 (C-7), 45.02 (C-8), 30.17 (C-9), 22.34 (C-10, 10'), 5.87, 8.36 (C-*α*), [^{1}J (^{119}Sn-^{13}C) = 437.73 Hz]; [∠C–Sn–C= 115.15°][c]
5	184.48 (C-1), 45.01 (C-2), 18.70 (C-3), 137.76 (C-4), 127.14 (C-5, 5'), 129.15 (C-6, 6'), 140.49 (C-7), 45.01 (C-8), 30.15 (C-9), 22.35 (C-10, 10'), 24.84 (C-*α*) 26.41 (C-*β*), 26.08 (C-*γ*), 13.42 (C-*δ*)

IBF=ibuprofen; s: singlet; d: doublet; t: triplet; m: multiplet; br: broad; dd: doublet of doublet; q: quartet; [a]complex number as given in Table 6.1; [b]determined through Lockhart Manders equation, Ref. [196]; [c]determined through Lockhart Manders equation, Ref. [270].

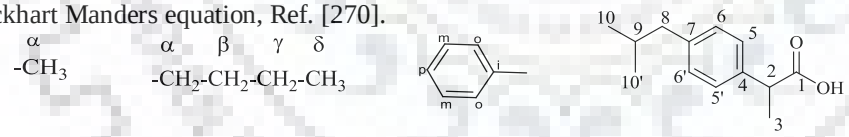

Table 6.6. ^{119}Sn NMR spectroscopic data of organotin(IV) complexes of ibuprofen in $CDCl_3$ (186.50 MHz)

Ligand/ Complex[a]	^{119}Sn NMR *δ* (ppm)
1	136.16
2	110.86
3	–109.53
4	–176.78, –182.34
5	–146.07

[a]Complex number as given in Table 6.1.

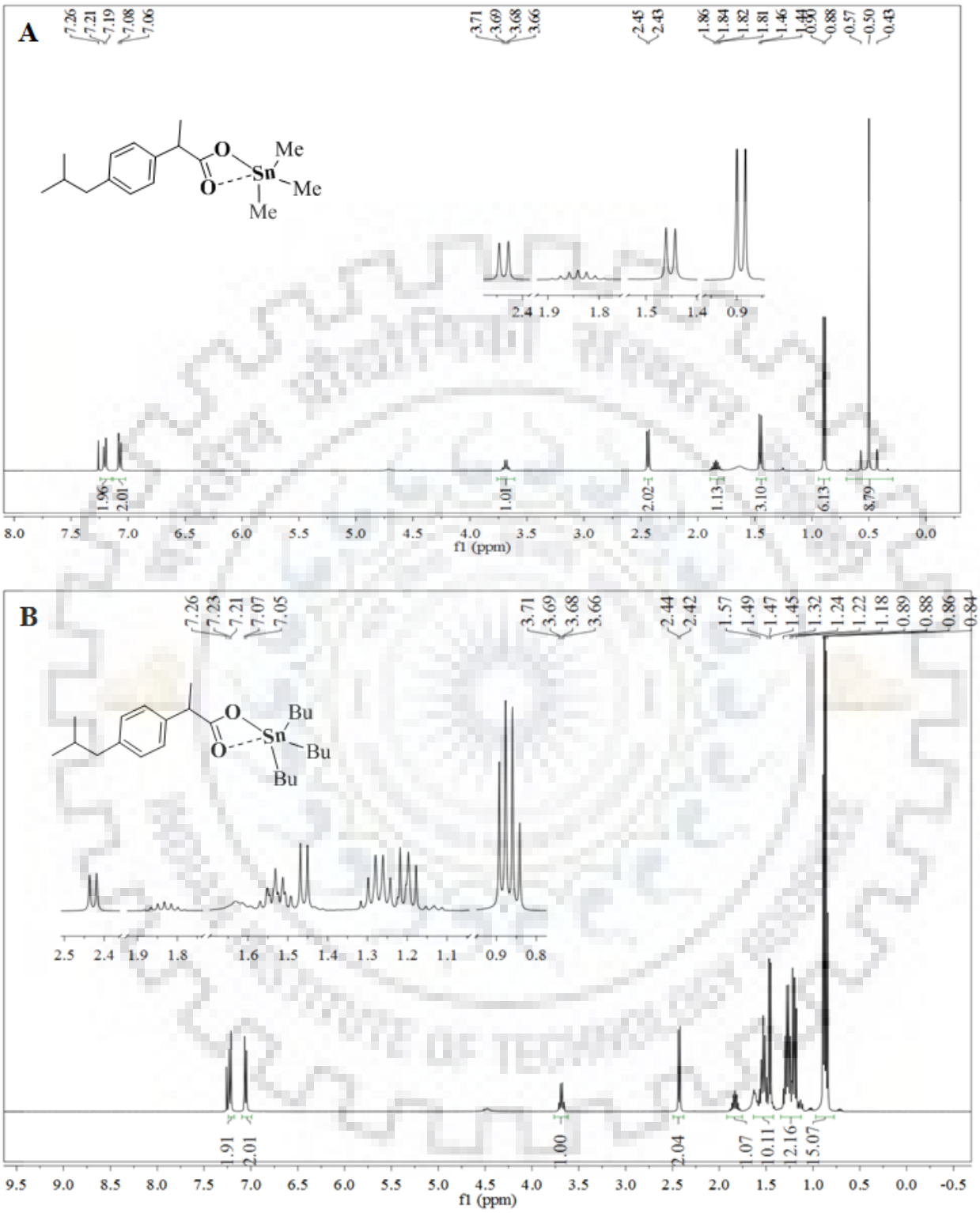

Fig. 6.4. ^{1}H NMR spectra of complex 1 (A) and 2 (B) in $CDCl_3$.

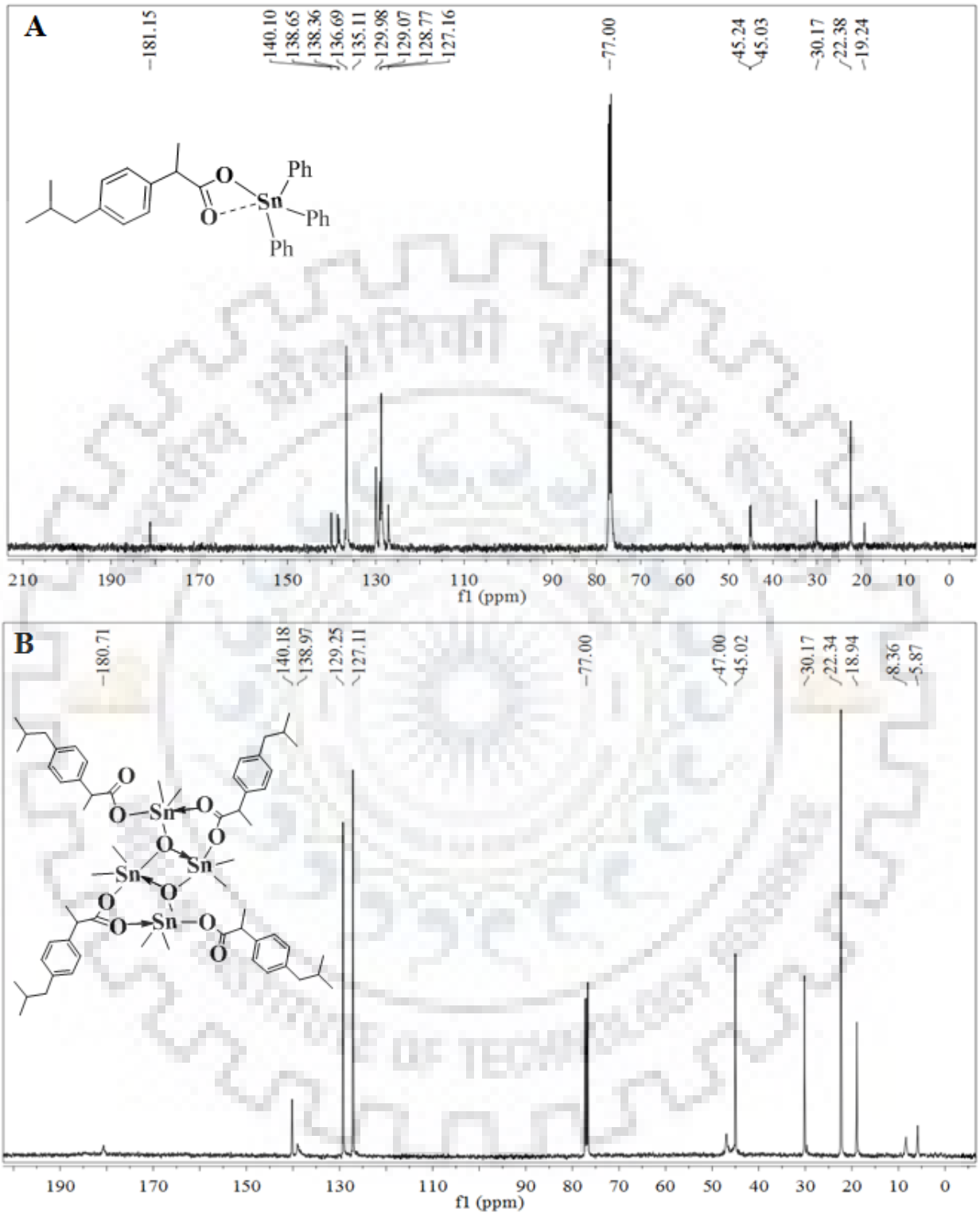

Fig. 6.5. ^{13}C NMR spectra of complex 3 (A) and 4 (B) in $CDCl_3$.

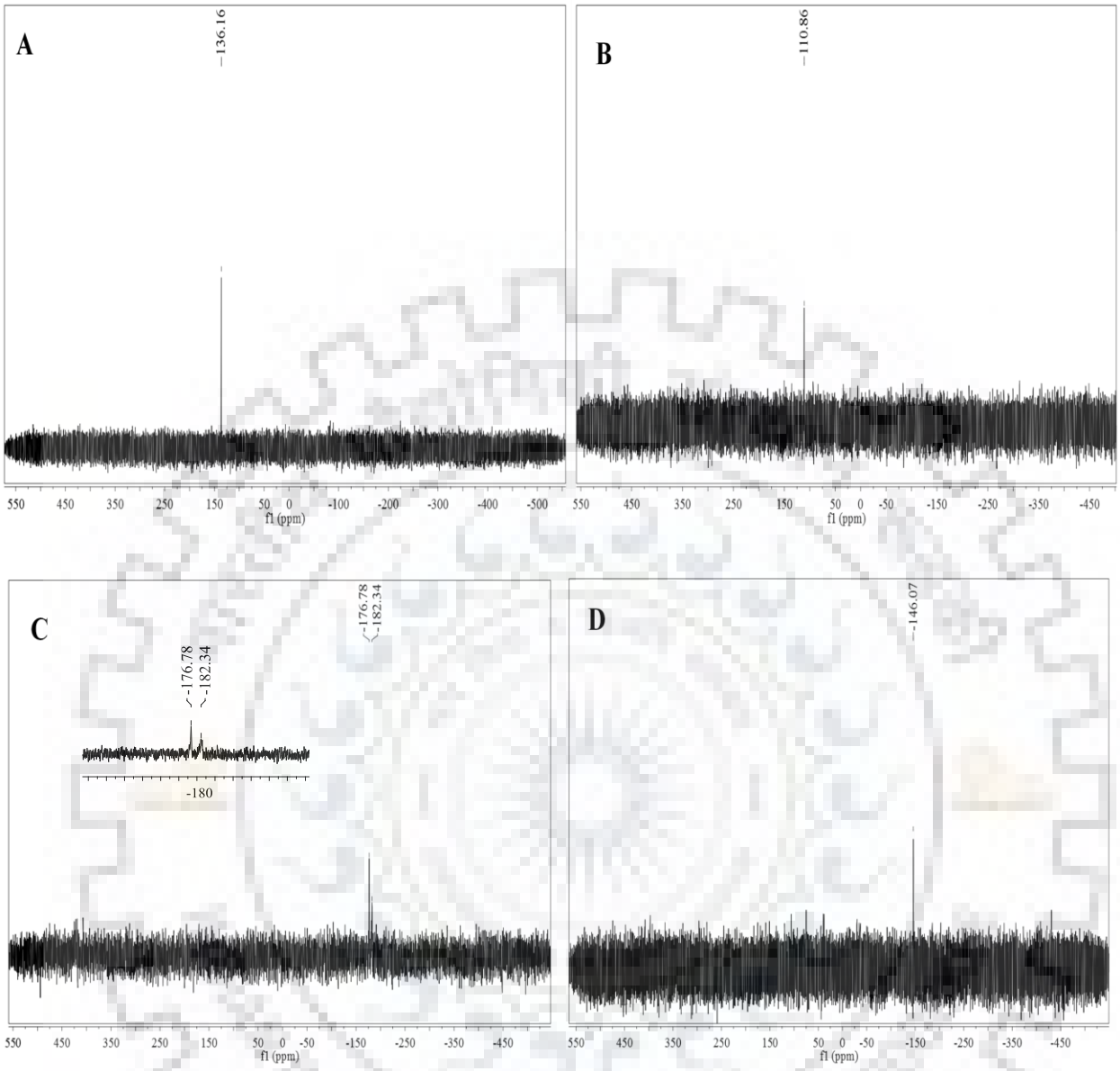

Fig. 6.6. ^{119}Sn NMR spectra of complex 1 (A), 2 (B), 4 (C) and 5 (C) in $CDCl_3$.

6.3.5. ESI–MS Spectrometry

The ESI–MS spectrometric data for synthesized complexes were recorded in the range m/z 200–1500, using acetonitrile solvent (HPLC grade) in positive-ion mode. All the complexes were characterized by molecular ion peaks corresponding to m/z, $[M+Na]^+$ and $[M+K]^+$, where m/z ratio due to $[M+Na]^+$ is always a base peak. Mass spectra of complexes **4** and **5** are given in Fig. 6.7. Isotopic pattern (m/z) due to associated molecules/organotin moieties and fragmented ions found for few complexes are listed in Table 6.7. Fragmentation pattern of complex **4** is illustrated in Scheme 6.2.

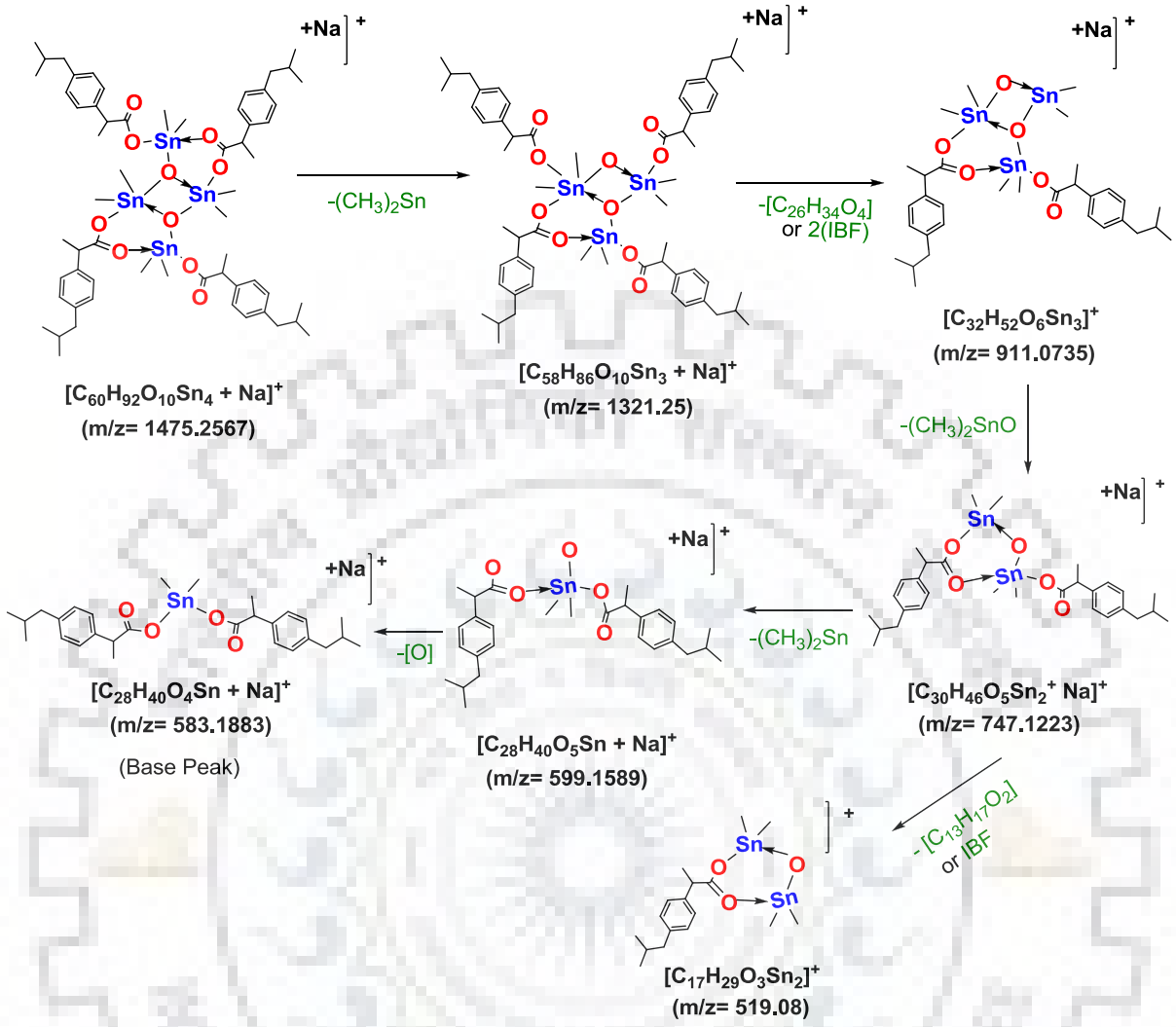

Scheme 6.2. Ions generated by the fragmentation of complex 4 with their respective m/z ratio.

6.3.6. Geometry Optimization through DFT Calculations

Structures of the complexes were designed with the help of Chemcraft software and then subjected to full geometry optimization in the gaseous phase through Gaussian 09 software package [266]. The drug molecule (IBF) and complexes **1-5** were optimized with B3LYP function, and 6-31G (d,p) and LANL2DZ basis set, respectively. All the imaginary frequencies in the harmonic frequency calculation are zero, which implies that the optimized geometries are very likely at global minima on the potential energy surface. Fig. 6.3. presented the optimized structure of IBF

Table 6.7. ESI MS (m/z) pattern of complexes 1-5 and their fragmented or associated pattern.

Complex	ESI– MS (m/z)
$Me_3Sn(IBF)$ (**1**)	393.08 $[M + Na]^+$, 409.05 $[M + K]^+$, 355.07 $[M–CH_3]^+$
$Bu_3Sn(IBF)$ (**2**)	519.23 $[M + Na]^+$, 535.20 $[M + K]^+$, 1013.45 $[2M + Na]^+$
$Ph_3Sn(IBF)$ (**3**)	579.13 $[M + Na]^+$, 595.11 $[M + K]^+$, 1135.26 $[2M + Na]^+$
$[(Me_2SnIBF)_2O]_2$ (**4**)	1475.26 $[M + Na]^+$, 1321.25 $[M–Me_2Sn) + Na]^+$, 911.07 $[(M–Me_2Sn(IBF)_2) + Na]^+$, 747.12 $[(M–(Me_2SnIBF)_2O) + Na]^+$, 599.16 $[(M–(Me_2Sn)_3\ O\ (IBF)_2) + Na]^+$, 583.19 $[(M–(Me_2Sn)_3O_2(IBF)_2) + Na]^+$, 519.08 $[(M–(Me_2Sn)_2\ O\ (IBF)_3)]^+$.
$Bu_2Sn(IBF)_2$ (**5**)	667.28 $[M + Na]^+$, 683.25 $[M + K]^+$

IBF = Ibuprofen; [a]Complex number as given in Table 6.1.

and complexes **1-5**. Triorganotin derivatives of IBF *i.e.* Complexes **1-3** were optimized as distorted tetrahedral geometries, due to weak interaction between the carbonylic oxygen with Sn-atom. The C–Sn–C angles obtained from the optimized geometries were in good agreement with the corresponding calculated angles and presented in Table 6.8. Further, a good agreement between the selected bond lengths and bond angles observed from the crystal structure of complex **3** and its optimized geometry has been found. Compound **4** exhibited a dimer distannoxane, in which the planar Sn_2O_2 core is linked to two exo-cyclic Sn moieties through the bridged oxygen atoms. The coordination geometry for endo Sn atom has a distorted square pyramidal type with O atom of Sn_2O_2 core at the top of the pyramid and two methyl groups *trans* to each other. However, the exo Sn atom has a distorted trigonal bipyramidal geometry having methyl groups *cis* to each other and axial positions occupied with O atoms of two carboxylates as illustrated in Fig.6.8. The bond angle and bond lengths observed are in good approximation with similar reported complexes [303-305]. Complex **5** is optimized as a highly distorted octahedral geometry, sometimes considered as bicapped tetrahedron with two carboxylate oxygen capping the faces. Herein, the carboxylate groups were said to be coordinated in an anisobidentate fashion, with covalent and coordinate Sn–O bonds 2.027 and 2.99 Å, respectively, which are significantly shorter than van der Waal's radii [166, 303, 304]. Frequencies calculated through of DFT for IBF and complexes **1–5** were found in good correlation with that of experimentally obtained for corresponding compounds. Table 6.8. provides the important outcomes of the DFT calculation. Frontier molecular orbitals (HOMO–

LUMO) generated by Gaussian 09 are given in Fig. 6.9. In free ligand HOMO and LUMO are distributed over carboxylic acid group and phenyl ring of IBF, however, with the formation of complexes HOMO remains on ibuprofen part and LUMO is shifted towards the tin metal.

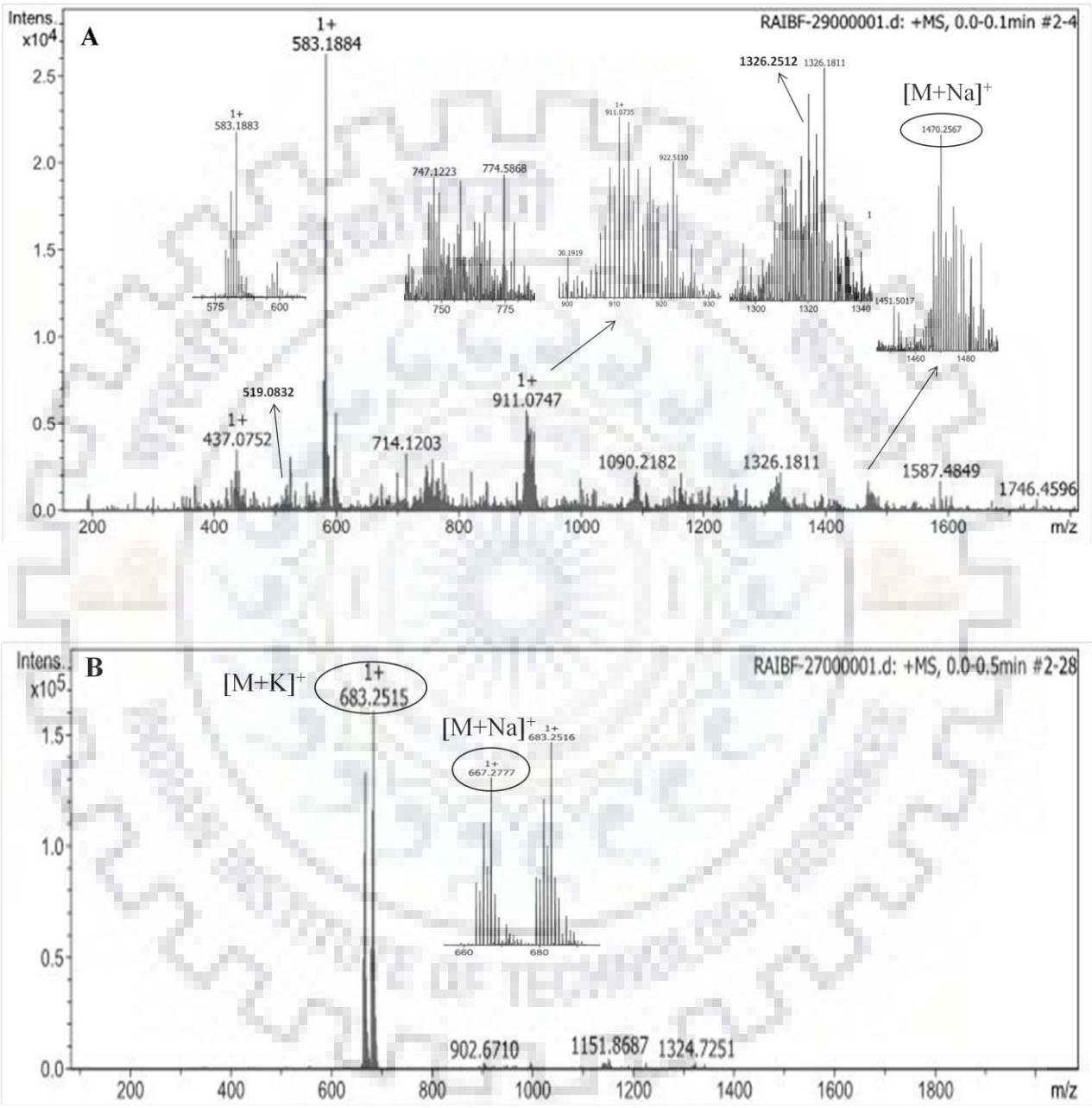

Fig. 6.7. ESI MS mass spectra of complex 4 (A) and 5 (B), showing molecular ion peak and fragments ion peaks.

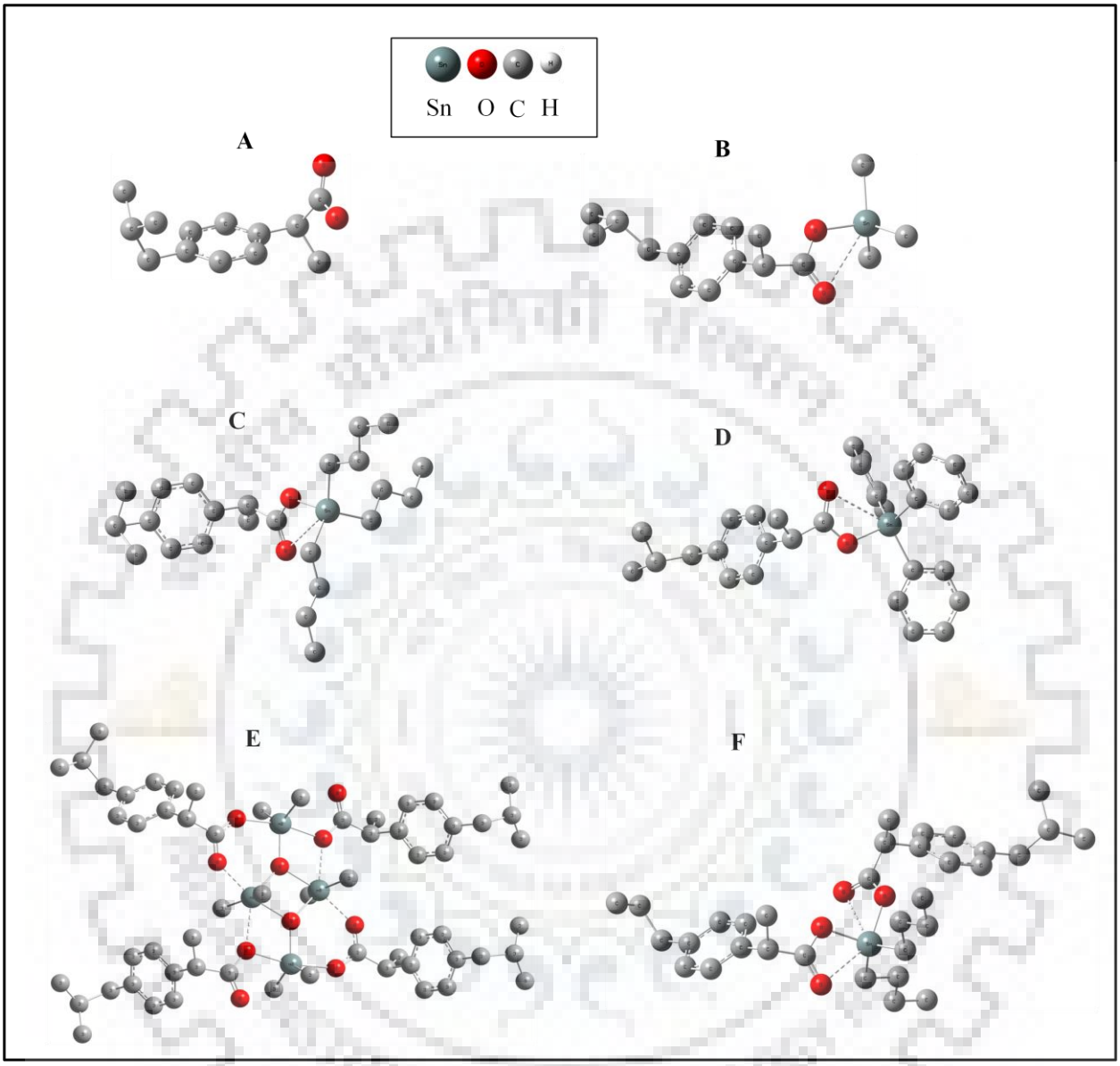

Fig. 6.8. Optimized geometries of IBF (A) and complexes: 1 (B), 2 (C), 3 (D), 4 (E) and 5 (F), with B3LYP function, 6-31g/LANL2DZ basis set; Hydrogen atoms are omitted for clarity.

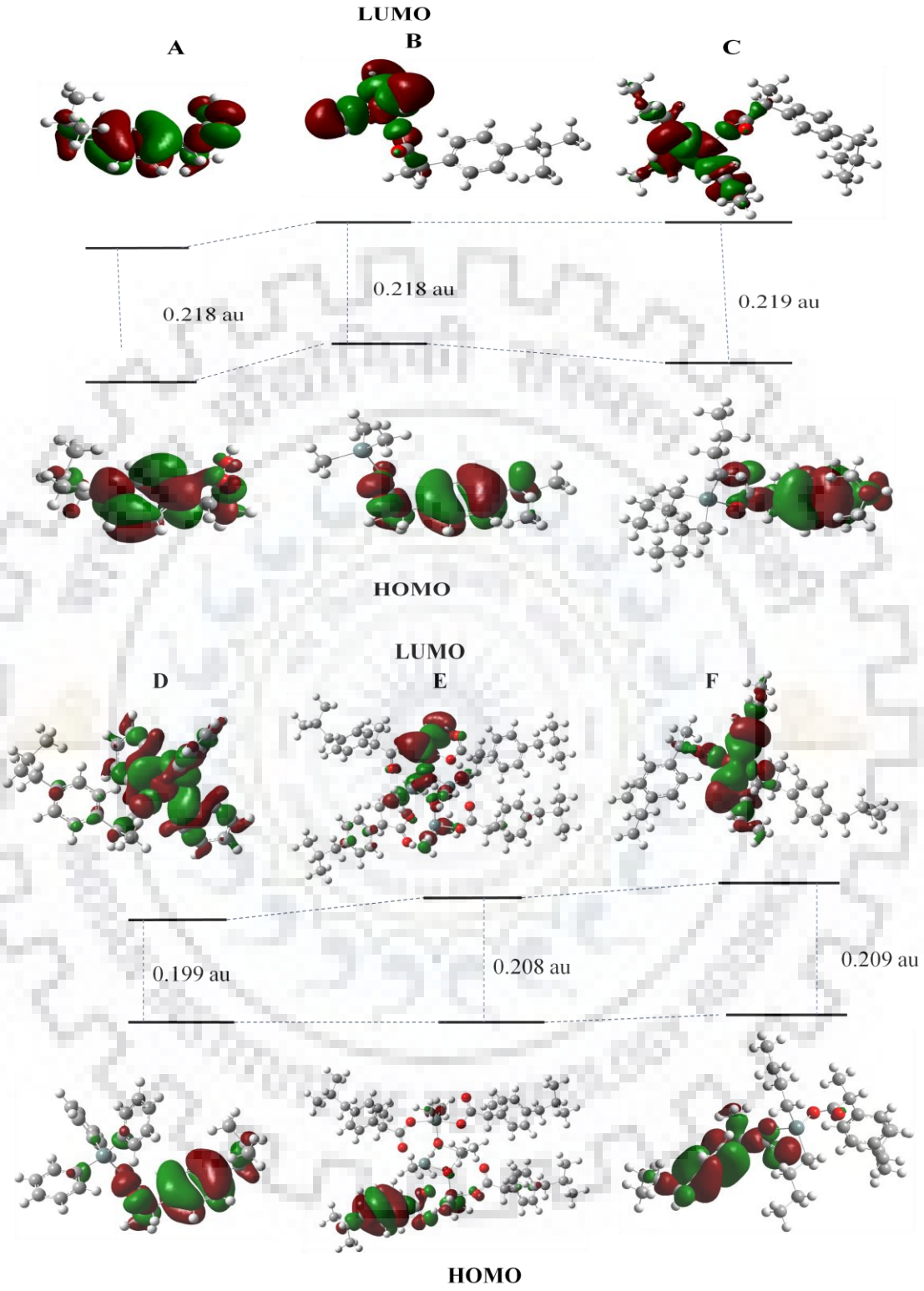

Fig. 6.9. Frontier molecular orbitals (HOMO-LUMO) of complexes IBF (A), 1 (B), 2 (C), 3 (D), 4 (D) and 5 (D) generated at B3LYP level, with 6-31g/LANL2DZ basis set.

Table 6.8. Summary of DFT calculations performed on IBF and complexes 1-5 with B3LYP function, 6-31g/LANL2DZ basis set.

Ligand/ Complex[a]	Energy of optimized geometry (a.u.)	∠ C–Sn–C(°) (calculated from ^2J values)	∠C–Sn–C(°) (calculated from DFT	$E_{(HOMO)}$, $E_{(LUMO)}$ (a.u.)	$E_{(HOMO)}$– $E_{(LUMO)}$ (a.u.)
IBF	–656.52	–	–	–0.236 –0.018	0.218
1	–779.16	111	113, 114, 115	–0.231 –0.013	0.218
2	–1132.91	110	113, 114, 115	–0.231 –0.012	0.218
3	–1354.25	112	111, 112, 115	–0.233 –0.034	0.199
4	–3107.68	–	129[b], 151[c]	–0.233 –0.025 –0.233	0.208
5	–1631.13	122	125	–0.243	0.209

[a]Complex number as given in Table 6.1; [b]∠C–Sn–C for trigonal bipyramidal Sn centre; [c]∠C–Sn–C for square pyramidal Sn centre.

6.3.7. DNA-binding studies

6.3.7.1. UV-Visible Spectrophotometric Studies

Ibuprofen and organotin complexes have been showing UV-visible bands with absorption maximum λ_{max} around 222 nm, 264 nm and 273 nm due to π-π* and n-π* electronic transitions. The bands around $\lambda_{max,}$ 222 and 264 nm are chosen as the specific wavelengths for CT DNA interaction study, because a significant amount of change was associated with them with successive addition of CT DNA. A careful observation of changes in absorbance due to IBF/complexes is insightful to estimate their mode of interaction with DNA. For IBF, a hyperchromic effect in UV bands for first few addition of DNA (till 6 μM), was observed which was followed by a continuous decrease in absorbance shown in Fig 6.10 (A). Similarly, a sudden hyperchromicity followed by a gradual hypochromic effect (Fig. 6.11 (D)) is involved in case of dibutyltin(IV) derivative of IBF i.e. complex **5**. These changes suggested the involvement of

different modes of binding, in case of IBF and complex **5.** For Complex **1** [Me_3Sn(IBF] a significant hyperchromic effect at both bands was observed, whereas the complex **2** [Bu_3Sn(IBF)] was showing a significant increase in the absorbance at λ_{max} 222 and a slight decrease in absorbance at band 263 nm with successive addition of CT DNA. This significant hyperchromism centered at the λ_{max} 222 nm in complexes **1** and **2** (Fig. 6.10 (B) and (C)), is suggestive of a strong interaction of complexes with DNA and the spectral changes indicate the possibility of groove binding or electrostatic interactions [208, 306, 307]. These studies alone are not very insightful for determining the mode of interaction of IBF/complexes with CT DNA, which has been further discussed through fluorescence experiments.

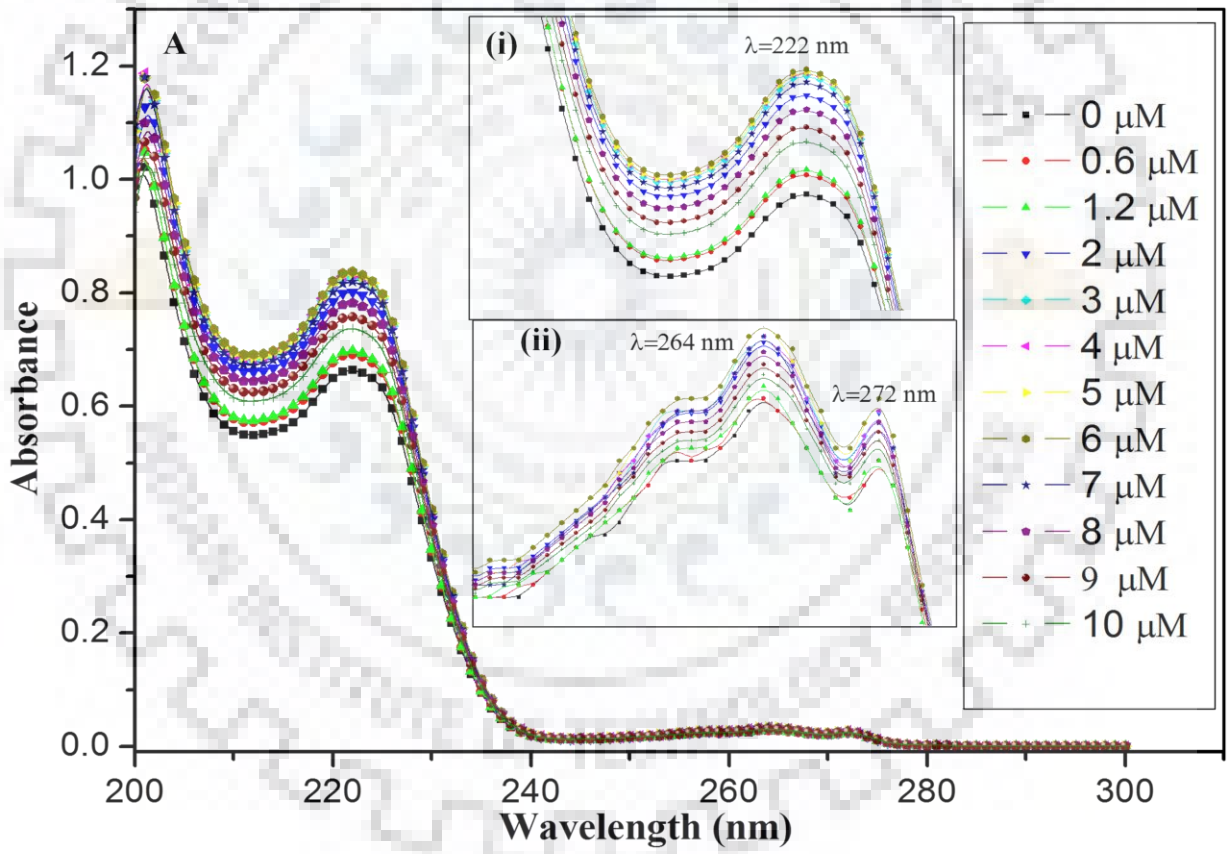

Fig. 6.10. UV-visible spectra of IBF [6.7 × 10^{-5} M] (A), in the absence and presence of CT DNA [0.6–15 µM] in Tris-HCl/NaCl (5:50 mM) buffer, pH = 7.2 at 25 °C; (i) and (ii) show the expanded region of UV bands at λ_{max}, 222 and 264 nm, respectively.

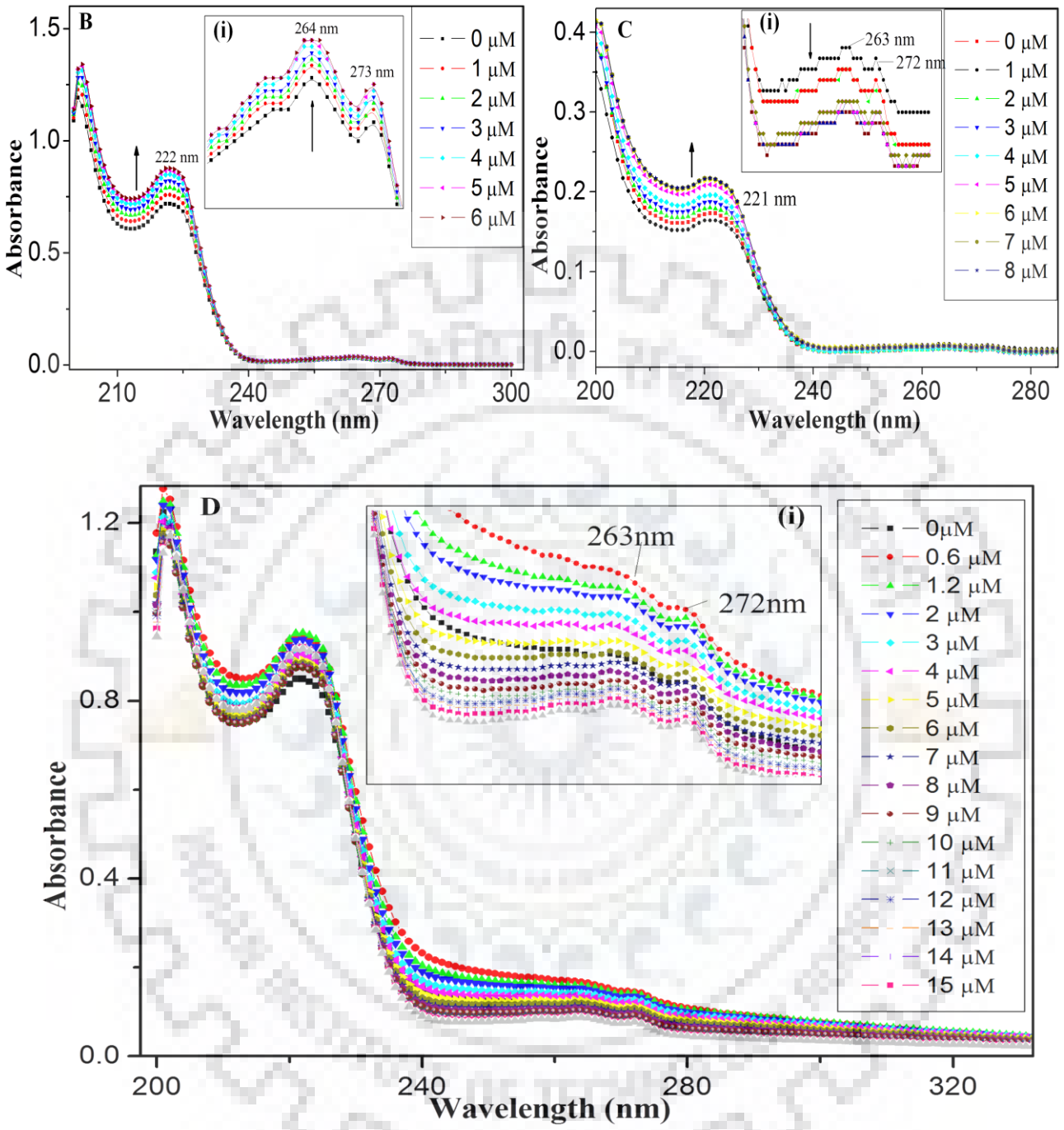

Fig. 6.11. UV-visible spectra of complexes, [6.7 × 10^{-5} M], (B) complex 1; (C) complex 2 and (D) complex 5, in the absence and presence of CT DNA [0.6–15 μM] in Tris-HCl/NaCl (5:50 mM), buffer, pH = 7.2 at 25 °C; (i) and (ii) show the expended region of UV bands at λ_{max}, 221/222 and 263/264 nm, respectively; The arrows indicate the increase/decrease in absorbance with increasing DNA concentration.

6.3.7.2. Fluorescence Titration Studies

The interactions of IBF and complexes with CT DNA were further investigated through fluorescence titrations. Complexes **1**, **2** and **5** were found to exhibit strong emission in the range 270–360 nm (emission maxima around 290 nm). Significant decrease in fluorescence intensity of IBF and complex **5** along with small red shift (2–3 nm), (Fig 6.12) with successive addition of CT DNA (2–20 µM), indicates an intercalation of these molecules within the base pairs of DNA. The intercalation of molecules within the DNA base pairs restricts their rotational motion which favours the deactivation of the excited states through radiationless processes [290], which are generally associated with quenching of the fluorescence intensity as in case of IBF and complex **5**. The increase in fluorescence intensity with minimal red shift (1–2 nm) was observed for complexes **1** and **2**, which indicate the possibility of the groove binding or electrostatic interactions. Further, the partial intercalative mode of binding could not be ruled out for these complexes.

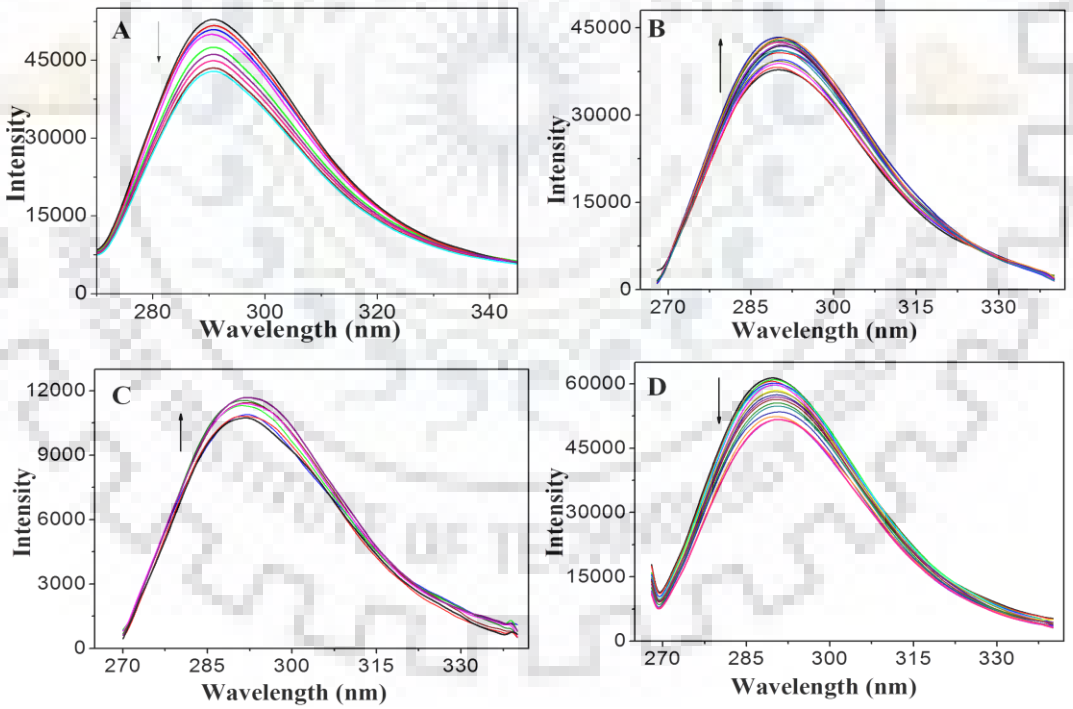

Fig. 6.12. Emission spectra of IBF (66.7 µM) (A) and complexes (66.7 µM); 1 (B), 2 (C), 5 (D) in the absence and presence of CT DNA (2–20 µM) in Tris-HCl/NaCl (5:50 mM) buffer, pH = 7.2 at 25 °C. Arrows indicate the increase/decrease in emission intensity with increasing concentration of DNA.

6.3.7.3. Ethidium Bromide Quenching Assay

Being a planar aromatic compound, ethidium bromide (EB) intercalates strongly within the base pairs of DNA. EB shows weak emission spectra in the aqueous solution, however, its emission intensity increases many fold after intercalation within the hydrophobic environment of DNA. This is because of shielding of EB molecules from the polar solvent which reduce its quenching [229]. In order to have insight into the binding mode of IBF and complexes with CT DNA, EB displacement experiment was performed. The results of the experiment (Fig. 6.13) reveal a continuous decrease in emission intensity of EB-DNA adduct with subsequent addition of IBF and complexes **1**, **2** and **5**, which suggest that the molecules are able to displace the EB from the intercalated sites of DNA and set it free in the solvent, which leads to a decrease in its emission intensity. The quenching constant (K_{sv}) (given in Table 6.9) are in the order of 10^3–10^4 for IBF and complexes. The results reveal that the IBF and the complex **5** competes strongly with EB for the available intercalation sites in DNA compared to the complexes **1** and **2**. The above findings suggest that IBF and complex **5** bind with DNA through moderate intercalation [84, 307]. However, a lesser decrease in emission intensity of EB-DNA adduct wih the addition of complexes **1** and **2** indicate that the complexes may bind through either non intercalative (groove binding or electrostatic interaction) or a partial interacalative mode of interaction.

Table 6.9. Quenching constant (K_{sv}), % decrease in fluorescence intensity and R^2 values for IBF and complexes.

Ligand/Complex[a]	Decrease in fluorescence Intensity	K_{sv}	[b]R^2
IBF	23%	2.05×10^4 (±0.03)	99
Complex **1**	9%	5.59×10^3 (±0.09)	98
Complex **2**	14%	1.01×10^4 (±0.1)	99
Complex **5**	25%	2.21×10^4 (±0.05)	98

[a]Complex number as given in Table 6.1; [b]R^2 is the correlation coefficient; mean ±SD of two independent observations.

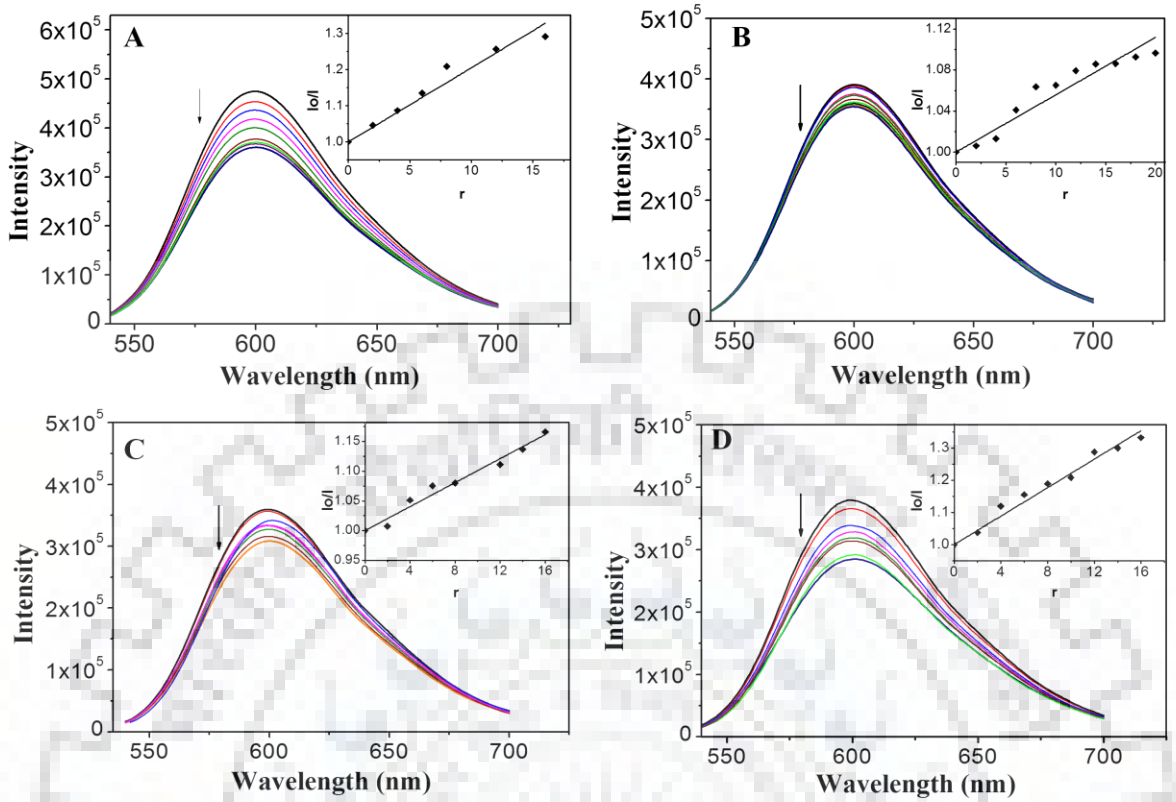

Fig. 6.13. Fluorescence quenching titration spectra of EB–CT DNA ([DNA]/[EB] = 4) with successive addition of (2 – 20 µM) IBF(A), 1 (B); 2 (C) and 5 (D), in Tris-HCl/NaCl (5:50 mM) buffer, pH = 7.2 at 25 °C [Excitation λ_{max} at 515 nm]. Inset is showing linear Stern Volmer plots and arrow indicates a decrease in intensity with increasing concentration of quenchers.

6.3.7.4. Fluorescence Studies in the Presence of KI

KI is an anionic quencher, which can quench the emission intensity of small molecules. However, it cannot quench the emission of molecules, which intercalate within the DNA base pairs, because of the repulsion experienced by negatively charged phosphate group of nucleotides [230]. However, the groove binders or electrostatic binders can be easily disturbed by the quencher [231, 232]. The present study, reveals a significant reduction in fluorescence intensity of IBF and complexes **5** in the presence of DNA compared to in the absence of DNA**,** which indicate the intercalation of these molecules inside the DNA which protect them from being quenched. Complexes **1** and **2** show a very insignificant change in emission intensity in the presence and absence of DNA as revealed from Fig. 6.14. The listed K_{sv} values calculated by Stern-Volmer

equation in Table 6.10, suggest a non intercalative type of interaction for complexes **1** and **2**. These results corroborate with our previous findings as described in section 6.3.7.3.

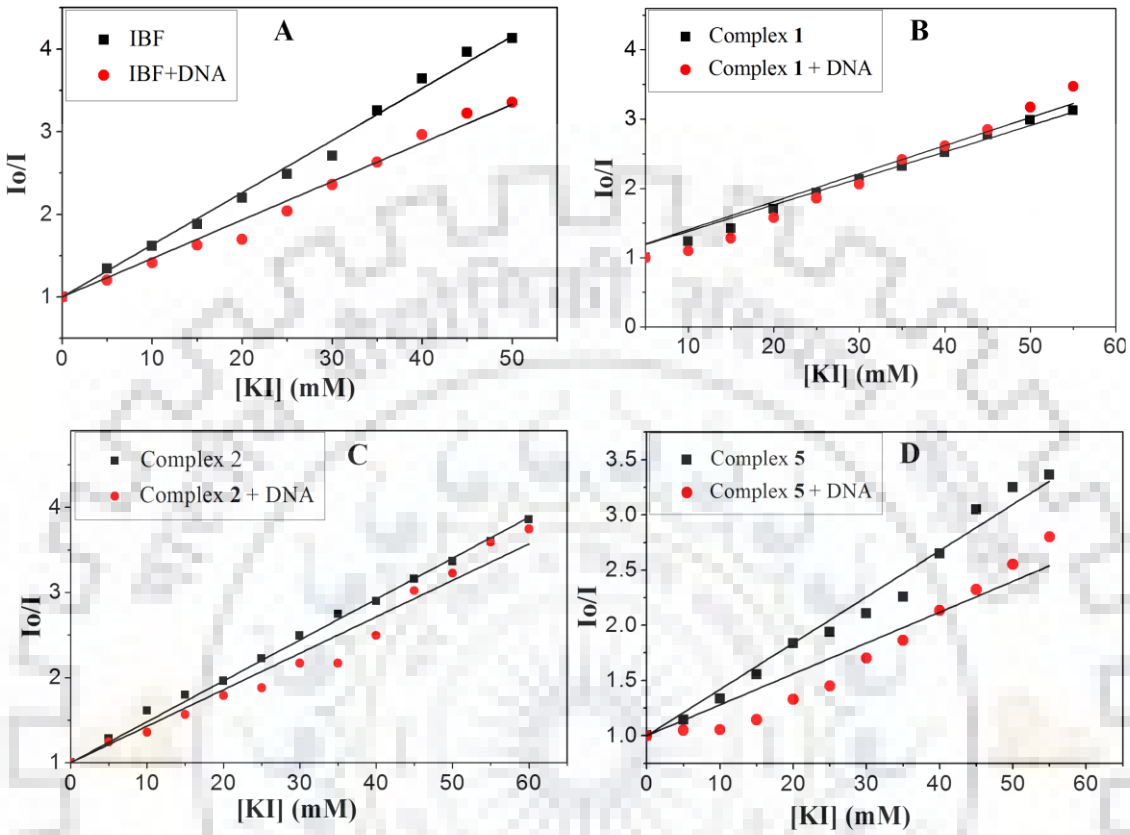

Fig. 6.14. Stern-Volmer plots obtained from fluorescence quenching of IBF (66.7 µM) (A) and complexes (66.7 µM); 1 (B); 2 (C); 5 (D) by KI (0–72 mM), in the presence and absence of CT DNA (20 µM) in Tris-HCl/NaCl (5:50 mM) buffer, pH = 7.2 at 25 °C.

Table 6.10. Value of K_{sv} obtained for complex–KI and Complex–KI–CT DNA systems and % reduction in K_{sv}.

Complex[a]	K_{sv} in the absence of DNA (M^{-1})	K_{sv} in the presence of DNA (M^{-1})	Relative reduction in K_{sv} (%)
IBF	63.1 (±0.2)	46.6 (±0.1)	~26
1	39.8 (±0.3)	40.5 (±0.2)	~2
2	48.0 (±0.1)	42.9 (±0.08)	~11
5	41.0 (±0.08)	27.0 (±0.06)	~34

[a]Complex number as given in Table 6.1; mean ±SD of two independent observations.

6.3.7.5. Viscosity Measurements

The viscosity of CT DNA is regarded quite sensitive towards any structural change in DNA, hence viscosity measurement of DNA with different concentrations of compounds in solution gives a lucid picture of their binding model with DNA. The classical intercalation of the molecule in DNA lengthens the helix of DNA. In order to accommodate the bound ligand, separation of base pairs occurs which leads to an increase in viscosity of DNA. However, partial or non-classical intercalators could cause bending or kinking in DNA helix, which results in a reduction of its length and concomitantly, its viscosity [235]. Furthermore, the non-intercalators (electrostatic and groove binder) cause a less significant change in viscosity of DNA [229]. Fig. 6.15 illustrates a change in the specific viscosity (η) with different concentration ratio of the complex to CT DNA. A remarkable increase in DNA viscosity with increasing concentration of IBF and complex **5** reveal an intercalative mode of binding of these complexes with DNA. A groove binding or external interactions with DNA was suggested for complexes **1** and **2** as they caused a very little change in the viscosity of DNA.

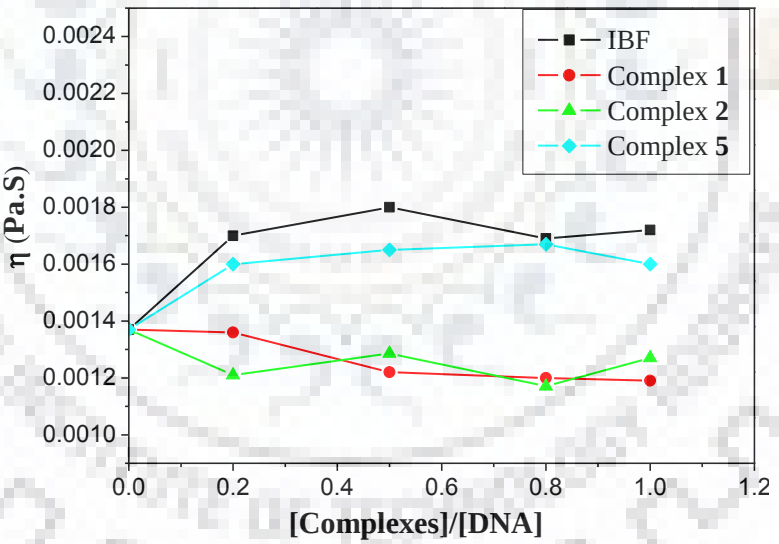

Fig. 6.15. Change in viscosity (η) of CT DNA (100 µM) with successive addition of MESNA and complexes 1-5 (0–100 µM), in Tris-HCl/NaCl (5:50 mM) buffer, pH = 7.2 at 25 °C.

All the experimental observations evidenced the occurrence of different modes of binding for different complexes with CT DNA. An intercalative mode of binding of IBF with DNA was suggested, which is in accordance with literature report [290]. Complex **5** also interacts with DNA through intercalative mode, but slightly higher than the ibuprofen, as evidenced from the K_{sv} value

in EB displacement experiment and fluorescence experiment with KI. A slight increase in the binding propensity can be explained on the basis of the presence of dibutyltin moieties in complex **5** which may facilitate the intercalation of ibuprofen inside the base pairs by providing additional hydrophobic interaction with DNA. A groove binding or external binding of complexes **1** and **2** with DNA was revealed from UV-visible, fluorescence and viscosity measurements.

6.3.8. Plasmid Cleavage Activities

DNA cleavage activities with organotin complexes have been extensively studied because of their potential to cleave supercoiled (SC) pBR322 DNA. One strand cleavage of circular supercoiled DNA results in a slow moving nicked circular (NC) form, and cleavage of both strands produce a linear (L) form, which positioned itself between nicked and supercoiled forms, [235, 236] as the DNA moves under the influence of electric field. The cleavage pattern of plasmid DNA due to IBF and complexes **1**, **2** and **5** was analyzed with their increasing concentrations (20, 40, 60 and 80 μM) in successive lanes and in the presence of activator (ascorbic acid). Bands *viz.* Form I (SC), Form II (NC) and Form III (L) formed by the cleavage of plasmid DNA and the corresponding normalized area occupied by the different forms are presented in Fig. 6.16, which clearly illustrate a continuous increase in cleavage activity with increasing concentration of IBF and complexes in lanes I-IV. A gradual decrease in SC form (Form I) associated with moderate increase in NC form (Form II) and (Form III) revealed a significant cleavage activity of IBF and complexes. Moreover, the presence of H_2O_2, (lane VI) which is a hydroxy radical generator and acts as activator in the DNA cleavage activity, enhance the cleavage activity significantly in all the cases. The maximum cleavage activity observed for the dibutyltin derivative of ibuprofen (complex **5**), which shows the importance of organotin moiety in the process of DNA cleavage. Further, to explore the underlying mechanism of cleavage activity by compounds under study, the cleavage experiment was run in the presence of a singlet oxygen quencher NaN_3, (lane VII) and hydroxy radical scavenger, DMSO, (lane VIII). In the presence of DMSO a partial inhibition in the cleavage activity of pBR322 DNA was observed for IBF and complexes **2** and **5**, as shown by a decrease in NC and L band intensities in lane VIII compared to lane V (having same IBF/complex concentrations) as clearly illustrated in Fig. 6.16. These findings suggest the involvement of hydroxyl radical in DNA cleavage process. However, no much difference was observed for complex **1** in the presence of DMSO, but a little decrease in NC form in the presence of NaN_3 could not be denied, which suggest the possibility of DNA cleavage through the involvement of reactive oxygen species for complex **1**. However, for

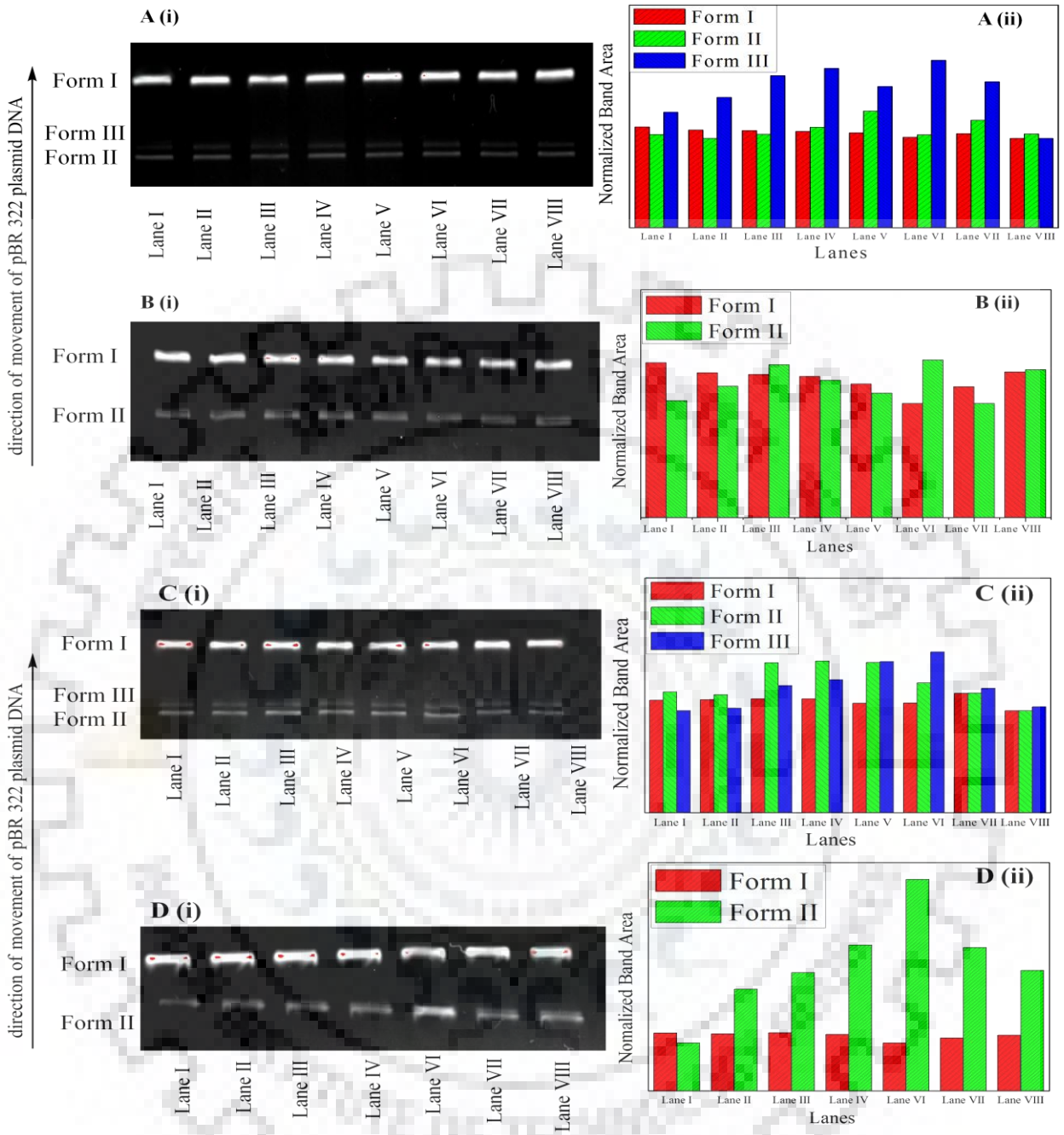

Fig. 6.16. The cleavage pattern of pBR322 plasmid DNA (100 ng) by IBF (A); complex 1 (B); complex 2 (C); complex 5 (D), after incubation for 5 h at 37 °C, at different concentration of IBF/Complexes, in Tris-HCl/NaCl (5:50 mM), buffer, pH = 7.2 at 25 °C. Lane I: Control (DNA): Lane II: [DNA + (20 µM complex/IBF)]; Lane III: [DNA + (40 µM complex/IBF)]; Lane IV: [DNA + (60 µM complex/IBF)]; Lane V: [DNA + (80 µM complex/IBF)]; Lane VI: [DNA + (0.2 M H_2O_2) + (60 µM complex/IBF)]; Lane VII: [DNA + (60 µM complex/IBF)+(2 mM NaN_3)]; Lane VIII: [DNA+ (60 µM complex/IBF)] + (2 µL DMSO)].

IBF and complexes **2** and **5** no such inhibition is seen which ruled out the involvement of singlet oxygen.

6.3.9. Biological Studies

6.3.9.1. Cytotoxicity Study (MTT Assay)

IBF and complexes **1-5** were screened *in vitro* for cytotoxicity against human cancer cell lines *viz.* DU145 (prostate cancer), HCT-15 (colon adenocarcinoma) and Caco-2 (colorectal adenocarcinoma. IC_{50} values for all the tested compounds and reference drugs are listed in Table 6.11. The results indicate that the complexes display different activities against different cell lines. Ph_3Sn(IBF) (complex **3**) displayed the maximum activity towards the colorectal cancer, exhibiting IC_{50} value (1.21 μM) many fold lesser than that of *cis*-platin; followed by Bu_3Sn(Ibf) (complex **2**, IC_{50} = 2.48 μM) and $[(Me_2Sn(IBF))_2O]_2$ (complex **4**, IC_{50} = 13.38 μM). All complexes except complex **1** (Me_3Sn(IBF)) induce cytotoxicity among the tested cancer cell lines. Further, the ligand (IBF) indicated potent cytotoxicity only against prostare cancer cell lines and very low cytoxicity (IC_{50} > 100 μM) against HCT-15 and Caco-2 cell lines. Complexes **4** and **5** displayed about 2.5 to 4 times higher activity against prostate cancer cells in terms of their IC_{50} value, comapred to 5-fluorouracil. Complex **5** also displayed good cytotoxicity against colon cancer cell lines, whereas complex **5** showed around 6 and 2 times less IC_{50} values compared to 5-fluorouracil and *cis*-platin, respectively. Hence, complex **4** is highly cytotoxic and displayed maximum cytotoxicity against prostate and colon cancer cell lines among the all complexes, while complex **3** is highly regressive against colorectal cancer cell lines.

Huber et al. [57] has explained the activity of the metal complexes on the basis of availablity of co-ordination postions around tin metal, relative stability of tin-ligand bond and balance between hyphilicity and lipophilicity in order to cross the cell membranes. On carefully examining the structure-activity relationship of the tested compounds the higher cytotoxicity of Ph_3Sn(IBf) (complex **3**) and Bu_3Sn(IBF) (complex **2**) against colorectal cancer can be explained due to their tetrahedral structure and higher lipophilicity of the phenyl and butyl groups. Further, the good cytotoxic effect of the complex **4**, $[(Me_2Sn(IBF))_2O]_2$, can be explained on the basis of synergistic effect of organotin(IV) moieties present in the tetranuclear complex. Further, the moderate activity of the complex **5**, $Bu_2Sn(IBF)_2$ is due to lesser availability of the coordination positions in this

complex, which is eventually compensated by the higher lipophilicity of the butyl moieties present in the same.

Table. 6.11. Cytotoxic screening results of organotin complexes of IBF against the different cell lines of human origin; IC_{50} value is expressed in µM ± SEM.

Complexes[a]	DU145	HCT-15	Caco-2
IBF	1.65±0..5	>100	>100
1	>100	>100	>100
2	>100	>100	2.48±0.1
3	19.22±0.8	>100	**1.21±0.84**
4	**3.97±0.81**	**2.188±0.67**	13.38±1.5
5	5.92±1.54	32.32±2.1	>100
5-FU	15.4±0.8	12.2±0.5	n.d.
Cis-platin	n.d.	5.04±1.4[b]	96.38 ± 32.03[c]

[a]numbers of complexes as given in Table 6.1; [b]reference [48]; [c]reference [308] n.d.= not determined; 5- FU = 5-fluorouracil; DU145: prostate cancer cells; HTC-15: colon adenocarcinoma cells and Caco-2: colorectal adenocarcinoma cells.

6.3.9.2. Acridine Orange (AO)/Ethidium Bromide (EB) Staining

As mentioned in previous Chapter also, this study is an important tool to distinguish between the viable, early apoptotic, late apoptotic and necrotic cells. This method is based on the morphological changes occur in the cytoplasmic membranes and nuclear chromatin material of cells during the process of apoptosis [240]. On the basis of fluorescence emission of acridine orange (AO)/ethidium bromide (EB) stained cells and their chromatin condensation, the cells can be identified as viable, apoptotic and necrotic as explained in the Chapter 4. The morphological changes appeared in the Caco-2, HCT-15 and DU145 cells on treatment with inhibitory concentration (IC_{50}) of the test compounds (showing highest activity against certain cell line) are illustrated in Fig. 6.17 – Fig. 6.19. In the control and vehicle treated cell lines, all the cells remained viable which appear uniform and green in colour, however in the case of HCT-15 cell lines treated with complex **4**, Caco-2 cell lines treated with complex **2** and DU145 cell lines treated with IBF and complex **4**, cells appear green with condensed chromatin indicated early apoptotic cells and orange to red coloured cells with condensed or fragmented chromatin material indicated the late apoptosis. Further, a small amount of necrosis was also found in all the stained cell lines.

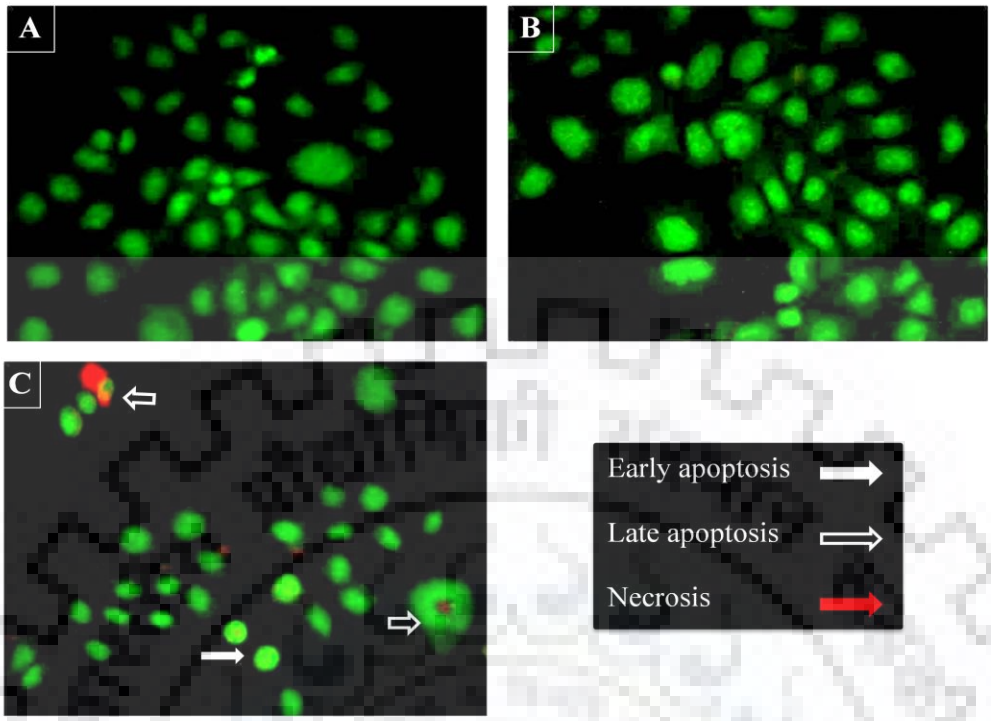

Fig. 6.17. AO/EB staining of HCT-15 cell lines (A) control, (B) vehicle (DMSO) treated cells and (C) cells treated with IC_{50} value of complex 4.

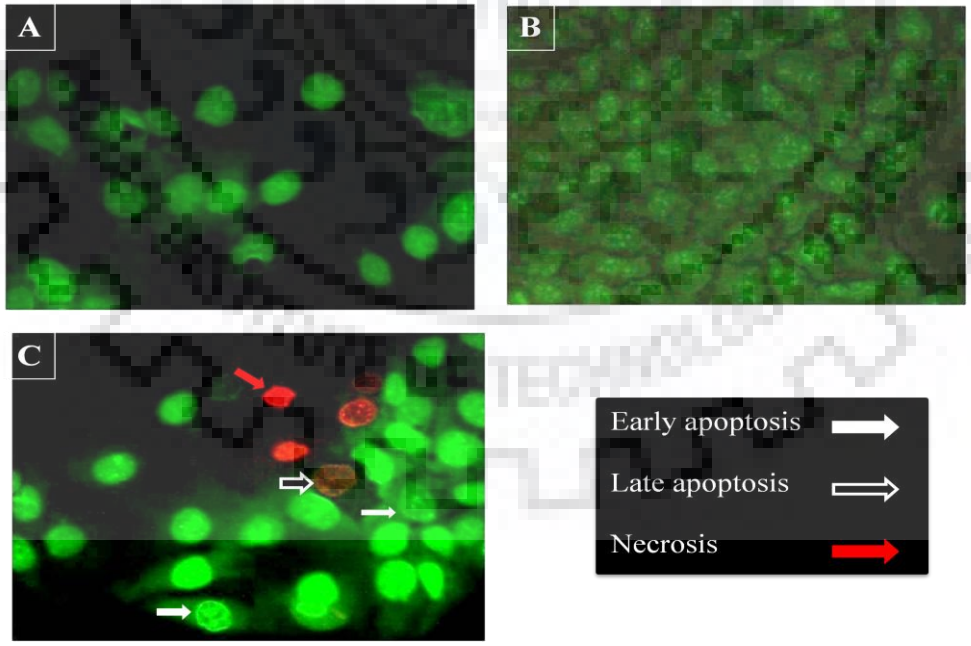

Fig. 6.18. AO/EB staining of Caco-2 cell lines (A) control, (B) vehicle (DMSO) treated cells, (C) cells treated with IC_{50} value of complex 2.

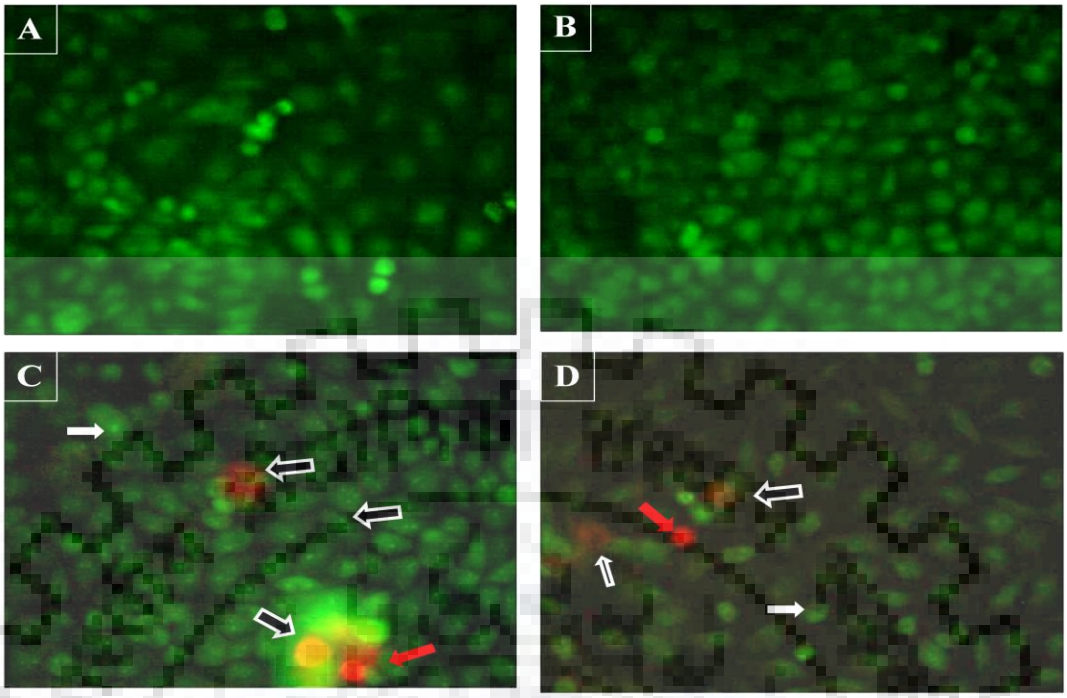

Fig. 6.19. AO/EB staining of DU145 cell lines (A) control, (B) vehicle (DMSO) treated cells, (C) cells treated with IC_{50} value IBF and (D) cells treated with IC_{50} value of complex 4. Solid white arrows indicate the early apoptotic, white outlined arrows indicated the late apoptotic and solid red arrows indicated the necrotic cells.

6.3.9.3. DNA Fragmentation Assay

DNA fragmentation assay is reliable method to distinguish between the apoptotic and necrotic activities. During apoptosis, the endonulcease activity cleave the DNA and resulted the fragmentation of DNA into different oligomer units, which looks like a DNA ladder when subjected to agarose gel electrophoresis [241]. In contrary to apoptotic activity necrosis leads to appearance of irregular sized DNA bands or DNA smear in agarose gel electrophoresis. However, in some cases single strand cleavage in DNA has been observed in apoptotic phenotypes, which does not form the DNA ladder in gel electrophoresis [241b]. (Fig. 6.20 (A)), DNA (extracted from the DU145 and HCT-15 cells) treated with complex **4** doesn't reveal any fragmentation, which means that apoptosis (as shown in AO/EB staining) and cytotoxicity caused by this complex against DU145 and HCT-15 may be due to the activities other than the Caspase-3 activated DNA fragmentation. This may be either due to the single strand scission of the DNA or other changes

occur on the cell surface. Furthermore, a ladder formation is seen (Fig. 6.20 (B)) in the fragmentation pattern of DNA extracted from HeLa cells, when treated with the complex **4**, which indicated the apoptosis is the main cause of cytotoxicity against HeLa cell lines.

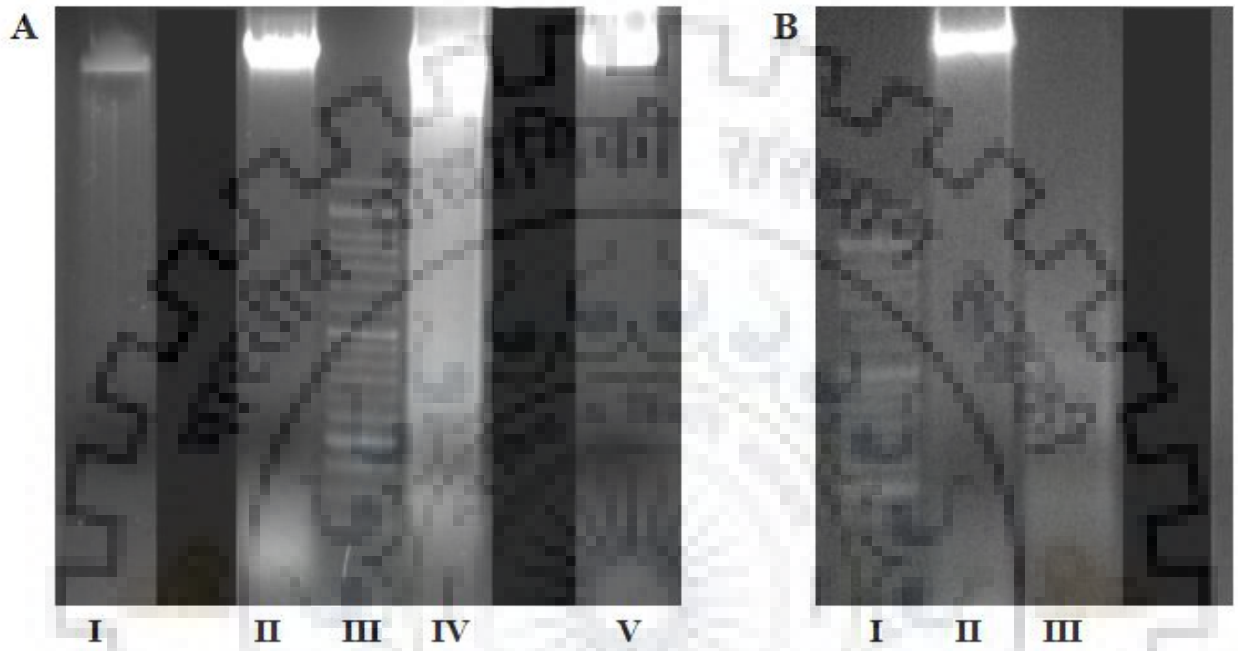

Fig. 6.20. Fragmentation pattern of DNA extracted from cell lines on treatment with complex 5, through agarose gel electrophoresis: (A) lane I: control (DNA extracted from DU145), lane II: DNA extracted from DU145 treated with complex 4; lane III: DNA marker (50 base pairs); lane IV: DNA extracted from HCT-15 treated with complex 4 and lane V: control (DNA extracted from HCT-15). (B) lane 1: DNA marker (50 base pairs); lane II vehicle treated control (HeLa DNA); lane III: DNA extracted from HeLa treated with complex 4.

CHAPTER - 7

Novel Trimethyltin(IV) and Tributyltin(IV) Complexes of Anticoagulant, WARFARIN – DNA Binding, Plasmid Cleavage and Cytotoxic Agents

7.1. INTRODUCTION

Warfarin (WR) has been used most widely as an oral anticoagulant in the world after fourteen years of its crystallization by Karl Link in 1940 [309, 310]. In 2006, it was estimated that in the UK alone, approximately 1% of the total population and 8% of population aged over 80 years are using WR as oral anticoagulant drug [311]. Over the last two decades, a tremendous increase in its use can be traced due to its obvious effectiveness to prevent embolic strokes in patients with atrial fibrillation and valvular heart disease [312]. Besides, the ability of WR and other coagulants to decrease thromboembolic events, various reports in the literature suggest the possibility of their antitumor benefits [313-317]. The laboratory experiments and clinical trials on animals with WR, heparin and vitamin K have been successful in treating and preventing the hematogenous metastasis, and helpful in the survival prolongation in cancer patients. These drugs are able to suppress the development of metastases and primary tumors, and also diminish the occurrence of thromboembolic diseases [317]. All these results indicate that the WR may favorably modify the course of some human cancer types; small cell carcinoma of the lung is one among them. Furthermore, the trial by Levine et al. at stage IV in breast cancer patients during chemotherapy, evaluated a low dose of WR for prevention of thromboembolism [318].

The organotin complexes, with remarkable antimicrobial, antituberculosis and potent antitumor activities [23, 36, 319-321], can act as the best substitute for the platinum based antitumor drugs owing ameliorating side effects such as nephrotoxicity and Wilson's disease [322-324]. Since long, the complexation with WR and its derivatives with transition metals and lanthanides have been remaining a focus of research for their fascinating antiproliferative properties [325-327]. Besides, the interesting biological activities of the WR and coumarin metal complexes, the coordination chemistry of WR is also a matter of attention which has been investigated collectively by the theoretical and experimental means, where the metal ions co-ordinate with WR through either i) the oxygen anion of the phenolic group by losing the proton and the oxygen atoms of two carbonyl groups, or ii) the oxygen anion of the phenolic group and one of the carbonyl group [22]. WR itself exhibits an interesting chemistry by existing as cyclic hemiketal form (Scheme 7.1a), with one –C=O group (coumarin carbonyl group), in free state and as an open chain conformer with two –C=O groups (coumarin carbonyl and side chain keto carbonyl groups) (Scheme 7.1b), upon complexation with metal ions [328, 329].

The present Chapter explored the coordination chemistry of warfarin within its triorganotin(IV) complexes and scrutinizes their DNA-binding ability through photophysical techniques, along with their cytotoxic activities against few human cancer cell lines *viz.* HCT-15, MCF-7, HeLa and LNCaP cell lines of human origin.

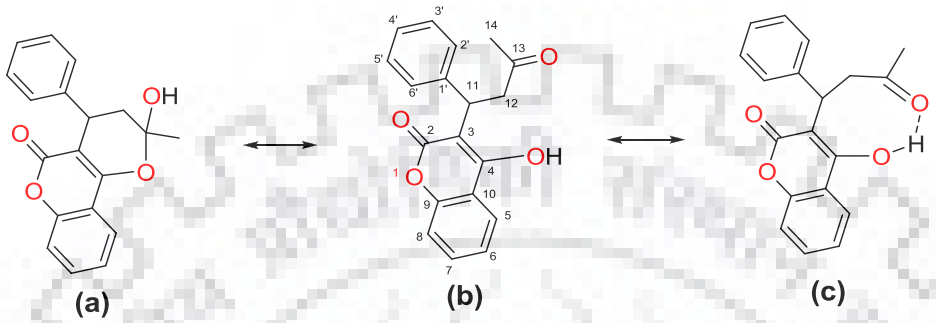

Scheme 7.1. Different forms of warfarin (a) cyclic hemiketal for, (b) open chain conformer with numbering scheme, (c) intramolecular hydrogen bonded open chain form.

7.2. EXPERIMENTAL SECTION

7.2.1. Syntheses

7.2.1.1. Synthesis of Trimethyltin(IV) Derivative of WR

Methanolic solution of Me_3SnCl (100 mg, 0.5 mmol) was added to sodium salt of WR (prepared *in situ* by stirring a solution of WR (154 mg, 0.5 mmol) in specially dried methanol with equivalent sodium methoxide, for 4 h) and resulting solution was stirred for 12 h in an inert atmosphere. A crude product was obtained by slow evaporation of solvent which was washed with chloroform first to remove any unreacted ligand and then recrystallized from petroleum ether to obtain pure and white powder, which was collected for further characterization.

7.2.1.2. Synthesis of Tributyltin(IV) Derivative of WR

To methanolic solution of WR (154 mg, 0.5 mmol), one equivalent of sodium methoxide was added and resulting solution was stirred for four hours which leads to the *in situ* formation of sodium salt of WR. To the sodium salt prepared, methanolic solution of Bu_3SnCl (162.74 mg, 0.5 mmol) was added and then allowed to stir for 10–12 h, resulting a clear solution. By slow evaporation of this solution at room temperature a sticky product was obtained which was washed

with chloroform to dissolve unreacted matter and further triturated with petroleum ether several times, and then re-crystallized to obtain a white coloured compound. Product was soluble in methanol and DMSO. Scheme 7.2 represents the reaction method opted for the synthesis of complexes **1** and **2**. The physical and analytical data is listed in Table 7.1, and FTIR and NMR (^{1}H and ^{13}C) spectroscopic data of WR, sodium salt of WR and complexes **1** and **2** are presented in Table 7.2 and Table 7.3, respectively.

7.2.2. DNA Binding and Plasmid Cleavage Studies

The studies which elucidate the mode and extent of WR and its organotin(IV) complexes towards DNA, were carried out by preparing the appropriate dilution of their stock solution (in DMSO) in Tris–HCl/NaCl buffer (pH 7.2, 5:50 mM), so as the final dilution contains no more than 1% DMSO. All the dilutions prepared were utilized within 3 days while storing at 25 °C, in order to avoid the degradation or precipitation of the complexes.

The absorption spectral studies of WR (2.6 μM) and complexes **1** and **2** (0.94 μM and 0.75 μM, respectively) were carried out in the absence and presence of CT DNA. The absorption spectra of WR and complexes **1** and **2**, were recorded with successive addition of CT DNA (2.6–52.9 μM) while keeping the total volume constant. The intrinsic binding constant (K_b) of the complex to CT DNA was determined by using Wolfe-Shimmer equation [218], as described in Chapter 4. The viscosity measurement experiments were performed by keeping the CT DNA concentration at 100 μM while varying complex concentrations (0 to 100 μM) in Tris–HCl/NaCl buffer (pH = 7.2). The emission spectra of a pre-incubated solution of CT DNA (7.2 μM) and EB (6.3 μM) in the absence and presence of increasing concentration of WR and complexes **1** and **2** (2–20 μM), were recorded. The pre-incubated EB–CT DNA adduct ([DNA]/[EB] = 1.14) was excited at 525 nm and the emission spectra were observed in the range 540–700 nm with a slit width 3 nm. The quenching constants (K_{sv}) were evaluated using the classical Stern-Volmer equation [219], as described in Chapter 4.

DNA cleavage study was performed using supercoiled pBR322, E. coli plasmid DNA. The supercoiled DNA (100 ng) was treated with varying concentrations of WR or complexes **1** and **2** (r = 1–10; where r = [complex]/[DNA]) in buffer solution (5:50 mM Tris–HCl/NaCl, pH 7.2) and were incubated for 3 h at 37 °C. Further, procedure was followed, as mention in Chapter 4.

Table 7.1. Characteristic physical properties and analytical data of triorganotin(IV) derivatives of warfarin.

	Complex (Empirical Formula)	Molecular weight	Colour & Physical state	Yield (%)	Decomposition/melting temp. (°C)	Analysis (%) Observed (Calculated)		
						C	H	Sn
Wr Na	**[WrNa]** ($C_{19}H_{15}NaO_4$)	330.32	White solid	94	160	68.83 (69.09)	4.52 (4.58)	–
1	**[Me_3Sn(Wr)]** ($C_{22}H_{24}SnO_4$)	472.07	white solid	62	214	55.47 (55.92)	4.96 (5.08)	24.05 (25.41)
2	**[Bu_3Sn(Wr)]** ($C_{31}H_{42}SnO_4$)	598.21	White solid	66	82	61.96 (62.18)	6.92 (7.02)	19.36 (20.05)

Table 7.2. FTIR spectroscopic data of triorganotin(IV) derivatives of warfarin in KBr (cm^{-1})

Ligand / complex[a]	ν(OH)	$\nu(C=O)_{coum}$	$\nu(C=O)_{keto}$	$\nu(C–C)_{coum}$ + $\delta(CCH)_{coum}$	$\nu(C–CH)_{coum}$	δ (COH) + ν(C–CH)	ν(C–O)	$\delta(C–CH)_{coum}$	ν (Sn–O)	$\nu_{as}(Sn–C)$ /$\nu_s(Sn–C)$
WR	3279 m	1681 s	1616 s,	1571 s, 1493 m	1452 m	1381 s	1162	1104 m	–	–
Wr Na	–	1704	1640s, 1601 s	1601 s, 1451 s	1412 m	1386 s 1351 m	1174	1107 m	–	–
1	–	1716, 1692 m (sp)	1621, 1600 s (sp)	1600 s 1444 m	1414 s,	1351 s	1182	1108 m	417 w	549 s, 462 m
2	–	1705 m	1623, 1600 s (sp)	1600 s (sp) 1447 s	1413 s	1374 m, 1353 w	1178	1104 m	411 m	530 m, 465 m

WR= warfarin; Wr Na=sodium salt of warfarin; [a]complex number as given in Table 7.1

Table 7.3. ^{1}H and ^{13}C NMR data of warfarin and its complexes recorded in DMSO-d_6.

Complex[a]/ lignad	^{1}H NMR Chemical shift, δ (ppm), DMSO-d_6
Wr	1.62/1.56 (s, 3H, CH_3); 1.85–2.34 (m, 2H, CH_2); 3.95–4.00 (t, 1H, CH); 7.30 (t, 1H, H-6); 7.62 (q, 2H, H-5/H-7); 7.83–7.81 (s, 1H/H-8); 7.12–7.20 (m, 3H, H-2'/ H-4'/H-6'); 7.24 (t, 2H, H-3'/H-5')
Wr Na	2.02 (s, 3H, CH_3); 3.24–3.28 (dd, 2H, CH_2); 4.85 (t, 1H, CH); 7.30 (t, 1H, H-6); 7.35–7.37 (q, 2H, H-5/H-7); 7.76–7.77 (s, 1H, H-8); 6.97–7.05 (m, 3H, H-2'/H-4'/ H-6'); 7.11 (t, 2H, H-3'/H-5')
1	2.03 (s, 3H, CH_3); 3.24–3.28 (dd, 2H, CH_2); 4.86 (t, 1H, CH); 7.28 (t, 1H, H-6); 7.35–7.37 (q, 2H H-5/ H-7); 7.76–7.78 (s, 1H, H-8); 6.97–7.06 (m, 3H, H-2'/H-4'/ H-6'); 7.11 (t, 2H, H-3'/H-5'); 0.46 (s, 9H, Me_3Sn); $^{2}J(^{1}H–^{119}Sn)$ = 68.76 Hz, θ = 117.10°.
2	2.02 (s, 6H, CH_3); 3.26 (t, 4H, CH_2); 4.86 (t, 2H, CH); 7.28 (t, 2H, H-6); 7.35–7.37 (q, 4H, H-5/H-7); 7.76–7.78 (s, 2H, H-8); 6.96–7.05 (m, 6H, H-2'/H-4'/H-6'); 7.11 (t, 4H, H-3'/H-5'); 0.841 (t, H_δ, Bu_3Sn); 1.64–1.49 (m, H_β, Bu_3Sn); 1.22–1.31 (m, H_γ, Bu_3Sn); 1.05 (t, H_α, Bu_3Sn); $^{2}J(^{1}H–^{119}Sn)$ = 76.35 Hz, θ = 122.60°.
	^{13}C NMR Chemical shift, δ (ppm), DMSO-d_6
Wr	158.39, 158.79 (C-2); 103.34, 101.93, (C-3); 160.23, 160.68 (C-4), 123.68, 123.91 (C-5); 123.60, 123.02 (C-6); 127.85, 128.22 (C-7); 116.15 (C-8); 152.29 (C-9); 116.61, 115.48 (C-10); 27.67, 25.78 (C-11); 41.52, 42.82 (C-12); 101.35, 99.64 (C-13); 36.03, 35.17 (C-14); 143.93, 143.82 (C-1'); 128.22, 127.85 (C-2', C-6'); 131.90 (C-4'); 127.04, 127.27 (C-3', C-5').
WrNa	163.81 (C-2); 98.94 (C-3); 172.00 (C-4); 121.29 (C-5); 123.63 (C-6); 127.24 (C-7); 98.94 (C-8); 153.72 (C-9); 115.15 (C-10); 29.76 (C-11); 46.42 (C-12); 209.04 (C-13); 35.72 (C-14); 146.98 (C-1'); 129.16 (C-2', C-6'); 124.60 (C-3', C-5'); 124.79 (C-4').
1	163.81 (C-2); 99.43 (C-3); 171.94 (C-4); 121.37 (C-5); 123.55 (C-6); 127.27 (C-7); 99.24 (C-8); 153.68 (C-9); 115.20 (C-10); 29.78 (C-11); 46.40 (C-12); 209.10 (C-13); 35.66 (C-14); 146.91 (C-1'); 129.24 (C-2', C-6'); 124.81 (C-3', C-5'); 127.67 (C-4'); 2.90 (C-α).
2	163.86 (C-2); 99.06 (C-3); 172.06 (C-4); 121.37 (C-5); 123.64 (C-6); 127.29 (C-7); 99.06 (C-8); 153.73 (C-9); 115.21 (C-10); 29.80 (C-11); 46.43 (C-12); 209.14 (C-13); 35.72 (C-14); 146.98 (C-1'); 129.26 (C-2'/C-6'); 124.84 (C-3'/C-5'); 13.77 (C_δ); 27.90 (C_γ), (C_β); 26.68 (C_α).

[a]complex number as given in Table 7.1; s: singlet; d: doublet; t: triplet; m: multiplet; q; quartet; ∠C–Sn–C (θ) calculated from Lockhart and Mander's equations, Ref. [196, 270].

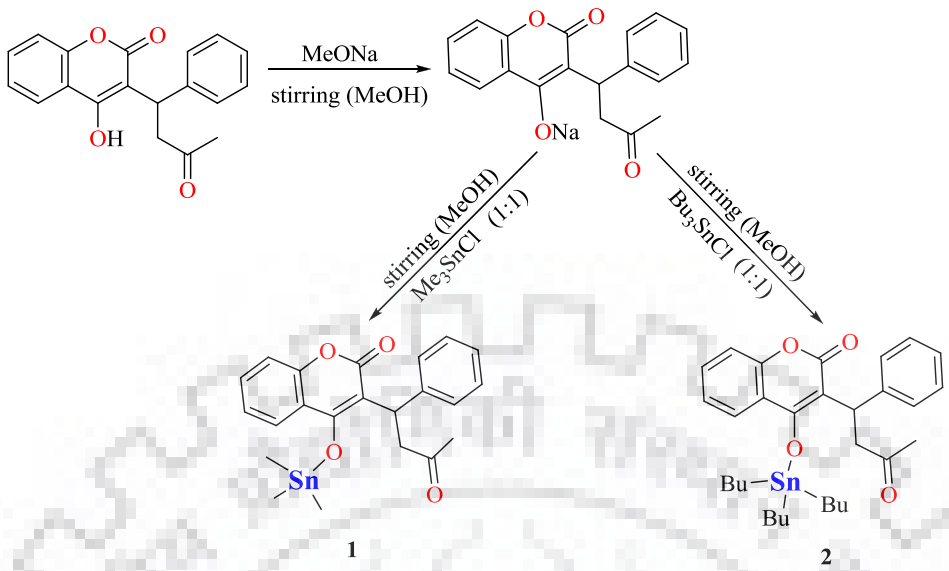

Scheme 7.2. Reaction schemes representing the syntheses of complexes 1 and 2.

7.3. RESULTS AND DISCUSSION

7.3.1. FTIR Spectroscopy

Kostova *et al.* reported a detailed comparison of experimental and theoretical (DFT modeling based) FTIR spectrum of the WR by assuming its different structures in the solid state, which reveals the existence of WR as a dimer of its cyclic hemiketal form, in which two molecules are coupled through intermolecular –C=O---H–O– hydrogen bonds [329, 330]. The dimer formation as well as hemiketal form in the solid state influenced the positions of the two carbonyl groups. Moreover, a cautious comparison of FTIR spectra of WR, sodium salt of WR, and synthesized complexes reveals the information about the fact that the oxygen atom of the hydroxyl group is involved in bonding with tin metal. A strong band around 3279 cm^{-1} in the FTIR spectrum of the WR is assigned to the intermolecularly hydrogen bonded O–H stretching vibrational mode, whereas, this band is absent in the FTIR spectra of both the complexes and sodium salt which indicates the occurrence of the coordination of deprotonated warfarin with tin metal. The ν(C=O) band (1681 cm^{-1}) of lactone group of coumarin appeared at lower frequency than its usual position due to hydrogen bonding, and the IR band for keto group in hemiketal form appeared at 1616 cm^{-1} in the solid state. However, in the sodium salt and complexes **1** and **2**, the ν(C=O) band shifted to 1704–1715 cm^{-1}. A shift of about 24 cm^{-1} indicates the loss of hydrogen bonding on complexation. It was already reported in the literature that after deprotonation the cyclic hemiketal form of WR converts to an open chain form [328, 330, 331]. An increase in the $\nu(C=O)_{keto}$ group from 1616

cm^{-1} in free ligand to 1640 cm^{-1} in its sodium salt indicates the existence of sodium salt in open chain form. However, the complexation with tin decreases the $\nu(C=O)_{keto}$ to 1621 and 1623 cm^{-1} in **1** and **2**, respectively (in comparison to Wr Na), which signifies the involvement of $(C=O)_{keto}$ group in weak interaction with tin metal. The weak bands around 417–411 cm^{-1} due to ν(Sn–O) stretching and 549–530 cm^{-1} and 462–465 cm^{-1} due to asymmetric and symmetric ν(Sn–C) stretching reveals the formation of complexes. Fig. 7.1 illustrated the comparative FTIR spectra of complexes with WR and its sodium salt.

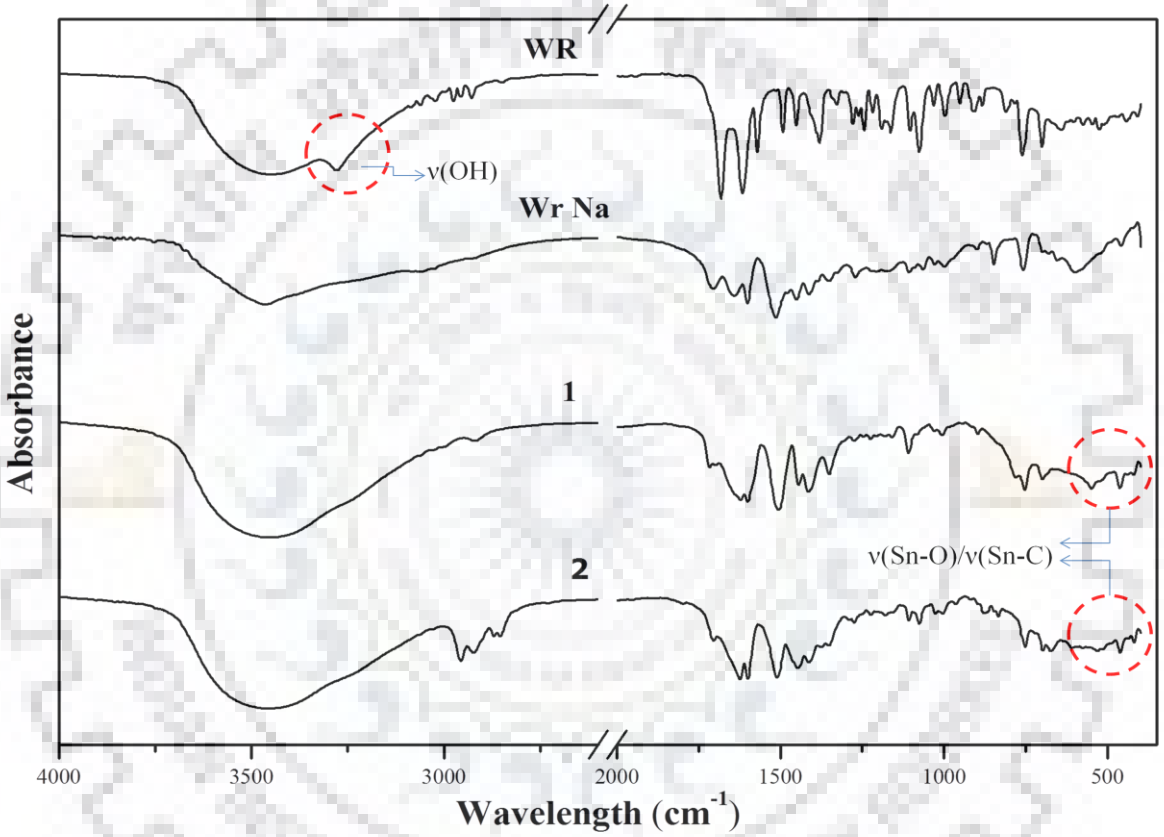

Fig 7.1. FTIR spectra of WR, sodium salt of WR (Wr Na) and complexes 1 and 2.

7.3.2. Multinuclear (^{1}H, ^{13}C and ^{119}Sn) NMR Spectroscopy

The NMR studies performed to elucidate the structure of WR indicate the existence of a dynamic equilibrium between two cyclic hemiketal diastereomeric forms of WR [330, 332]. It has been reported that in the $CDCl_3$ solution three structures of WR, two diastereomeric cyclic hemiketal and one minor intermediate in open chain exists as represented in Scheme 7.1, whereas in DMSO-d_6 solvent, the two cyclic forms were observed in 1:3 ratio [332]. It was observed from the ^{1}H and ^{13}C NMR spectroscopic data of WR in DMSO-d_6 that one proton/carbon gives different (more than

one) values of chemical shift which corresponds to the two cyclic hemiketal isomeric forms. This reveals that the WR exists in two different forms in the solution as already reported in the literature [332]. The ^{1}H NMR data revealed a significant downfield shift in methyl (H-14), methylene (H-12) and methyne (H-11) protons with respect to the WR, which indicate the presence of WR in sodium salt and two complexes **1** and **2** as an open chain form. In the complexes **1** and **2** the methyl protons resonate at 2.02 ppm whereas methylene and methyne protons show chemical shift value at 2.24–3.28 and 4.85 ppm, respectively, which indicate the presence of open chain form irrespective of any cyclic hemiketal isomeric form of WR. The resonance of methyl protons at 0.46 ppm and butyl protons around 0.85–1.64 ppm flanked with the satellite peaks corresponds to the methyl and butyl (attached to tin) moieties of the complexes **1** and **2**, respectively. The integration of the protons in ^{1}H NMR spectra of complexes reveals the 1:1 stoichiometry of the ligand and organotin moiety in the complexes. The ^{13}C NMR spectrum of WR in DMSO-d_6 is quite complicated because of the presence of two cyclic forms which can be revealed due to the presence of more than one signals for WR carbons, similar as that of the ^{1}H NMR. The resonance in ^{13}C NMR spectrum of WR, due to C-13 is observed at 99.64 ppm which is shifted to 209.04 ppm in its sodium salt and synthesized complexes **1** and **2**, which clearly signifies that the ligand does not retain the cyclic hemiketal form after complexation as in free-state but converts to its open chain form with one ketone group. Similarly, a downfield shift in C-4 from 160.23 to 172.00±0.1 ppm shows a similar effect on WR after its complexation. All the ^{13}C NMR resonances due to carbons of WR unit were assigned according to the reports available in the literature [332-334]. A downfield shift in the resonance of C-3 from 98.94 ppm to 99.06 and 99.43 ppm in the complexes **1** and **2**, respectively, with respect to WrNa clearly indicates the co-ordination through deprotonated hydroxyl group of WR. A negligible shift in the resonance of C-13 in complexes **1** and **2** with respect to WrNa from 209.04 ppm to 209.02 and 209.14 ppm, respectively, is observed. Furthermore, a negligible shift in the ^{13}C NMR resonance of C-2 from 163.81 ppm in WrNa salt to 163.81 and 163.86 ppm in complexes **1** and **2**, respectively, indicated very less or no chances of coordination through carbonyl oxygen of lactone group of WR. The similar coordination sites (Scheme 2) as described by Kostova et al. in promithium complexes are proposed with a co-relation of the detailed theoretical calculation and FTIR spectrometry, where deprotonated hydroxy group and carbonyl oxygen of keto group are the most probable coordinating sites [329]. Theoretical C–Sn–C angle calculated for the complexes **1** and **2** by the Lockhart and Mander's equation [196], is 117.1° and 122.6°, respectively, which clearly indicated distorted tetrahedral (td)

or distorted trigonal bipyramidal (TBP) geometry around the tin metal in these complexes. The probable coordination of solvent (DMSO-d_6) molecule to tin in these complexes may also be possible. The value of chemical shift in ^{119}Sn NMR spectra of **1** and **2** are –27.33 and –82.36 ppm, which shows the coordination of tin metal can be 4 or 5 for these complexes [198]. ^{1}H, and ^{13}C NMR spectra of the complexes are given as Fig 7.2 and Fig. 7.3, respectively.

7.3.3. ESI MS Mass Spectrometry

Furthermore, the formation of complexes was also confirmed with the help of ESI MS spectra (positive ion mode), where the synthesized complexes were characterized by their usual molecular ion peaks ($[M+Na]^+$). For complex **1** a cluster of peaks corresponding to mononuclear tin compound was observed at 495.39 m/z ratio with 100% intensity. The complex **2** is characterized with a molecular ion peaks $[M]^+$ at 597.59 m/z ratio (100% intensity) and $[M+Na]^+$ at 621.58 m/z ratio (40% intensity). Furthermore, a very less intense isotopic pattern corresponding to peaks for binuclear tin and trinuclear tin was observed for **2**, which may be due to the association of fragments formed. The representative spectra of the complexes **1** and **2** are given in Fig. 7.4.

7.3.4. DFT Calculations

To further support the proposed structures of the complexes a full geometry optimization and simple harmonic frequency calculations in gaseous phase were performed as explained in the experimental section. All the imaginary frequencies in the harmonic frequency calculation are zero, which implies that the optimized geometries are very likely at global minima on the potential energy surface. Fig.7.5 represents the optimized structure of two complexes, where both the complexes with distorted tetrahedral geometries are showing the lowest energy of molecule and the highest match towards the experimentally obtained FTIR data. The ∠C–Sn–C obtained from the geometries are 117.8° and 116.0° for complexes **1** and **2**, respectively, the value is fairly close for the complex **1** and nearly close for the complex **2** obtained in solution (DMSO-d_6). The energy of WR and complexes in the gaseous state, HOMO–LUMO energy gap and calculated ∠C–Sn−C are presented in Table 7.6. The frontier molecular orbitals (HOMO–LUMO) generated by Gaussian 09 are given as Fig. 7.6. HOMO of the complexes is mainly located on coumarin ring and keto of the WR and LUMO is localized on the whole coumarin moiety.

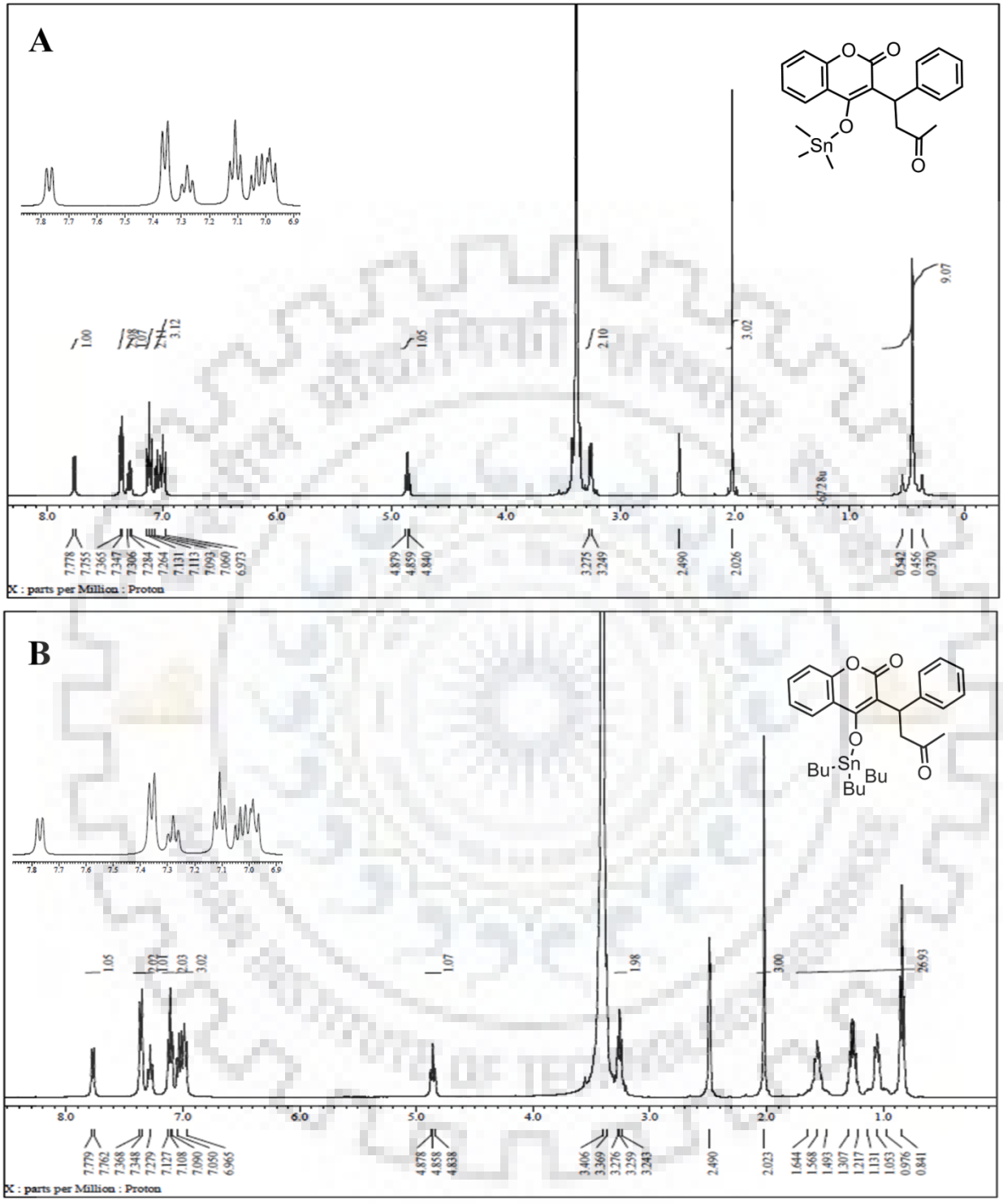

Fig. 7.2. ^{1}H NMR spectra of organotin complexes of warfarin; (A) 1, (B) 2, in DMSO-d_6.

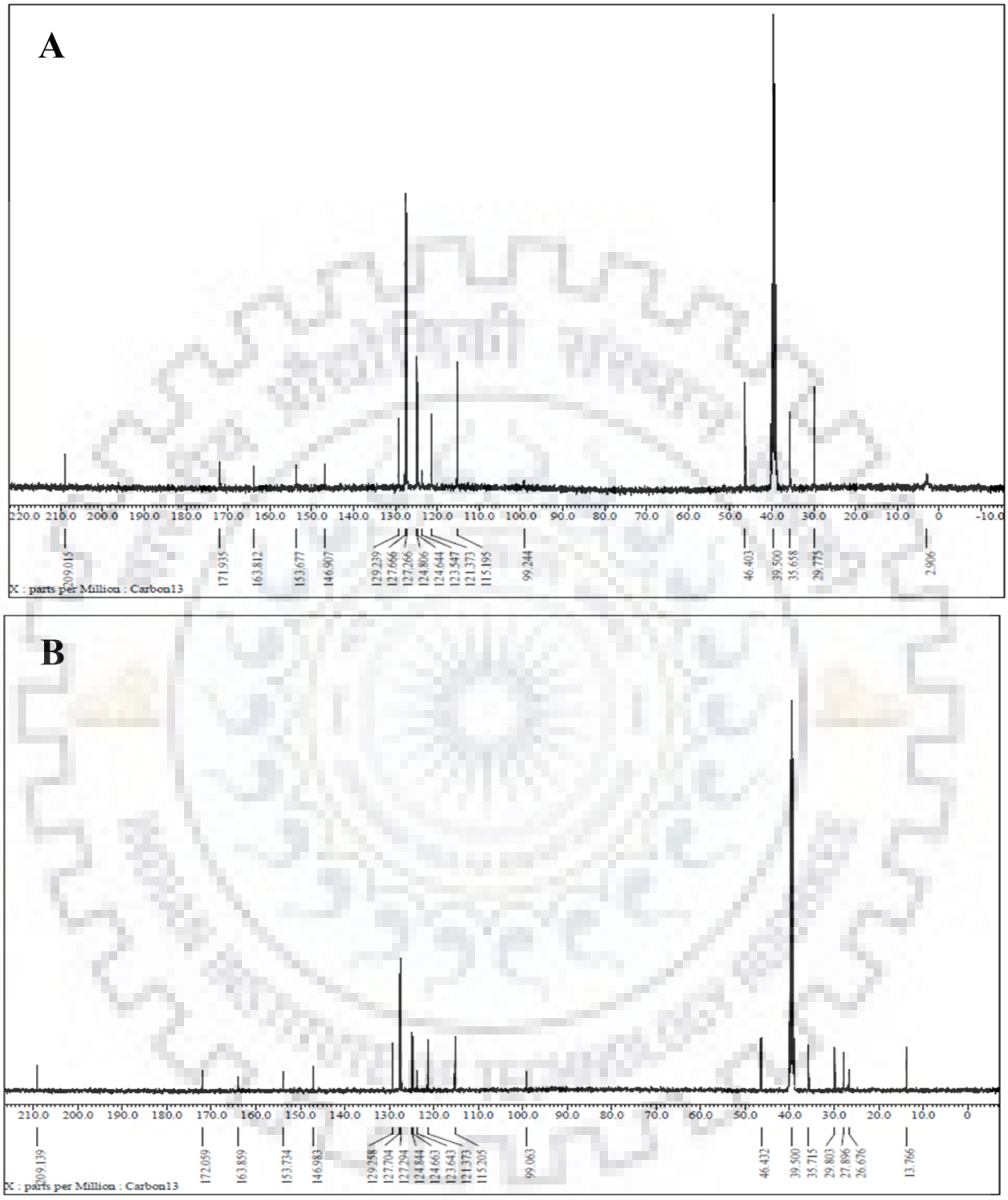

Fig. 7.3. ^{13}C NMR spectra of organotin complexes of warfarin; (A) 1, (B) 2, in DMSO-d_6.

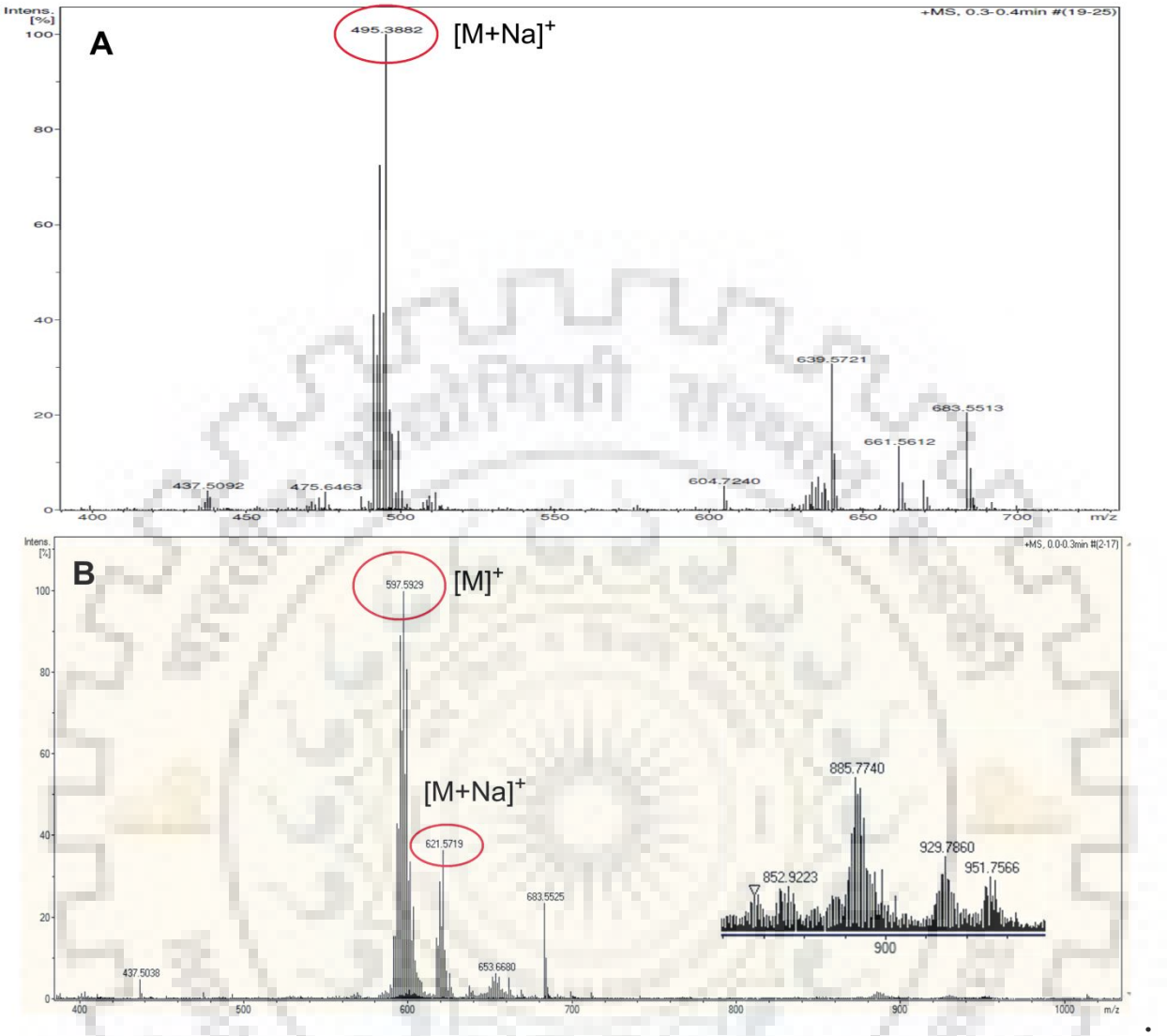

Fig. 7.4. ESI MS spectra of organotin complexes of warfarin; (A) 1, (B) 2, in acetonitrile.

Table 7.4. Summary of DFT calculations performed on triorganotin(IV) complexes 1 and 2 with B3LYP function, LANL2DZ basis set.

Complex[a]	Energy of optimized geometry (eV)	∠ C–Sn–C(°) (calculated from ^2J values)	Angle C–Sn–C(°) (calculated from DFT	$E_{(HOMO)}$, $E_{(LUMO)}$ (eV)	$E_{(HOMO)}$– $E_{(LUMO)}$ (eV)
1	–31564.83	117	118	–6.261 –1.867	4.394
2	–41109.17	122	116	–5.858 –1.682	4.175

[a]Complex number as given in Table 7.1.

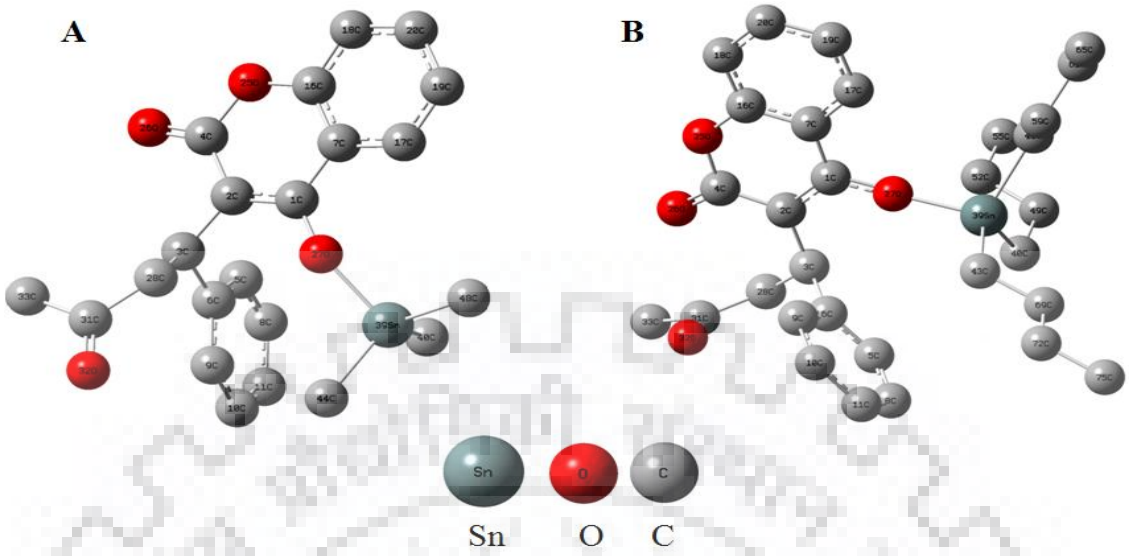

Fig. 7.5. Optimized structures of the complexes 1 (A) and 2 (B) generated by Gaussian 09 at B3LYP/LANL2DZ level, showing distorted tetrahedral geometries.

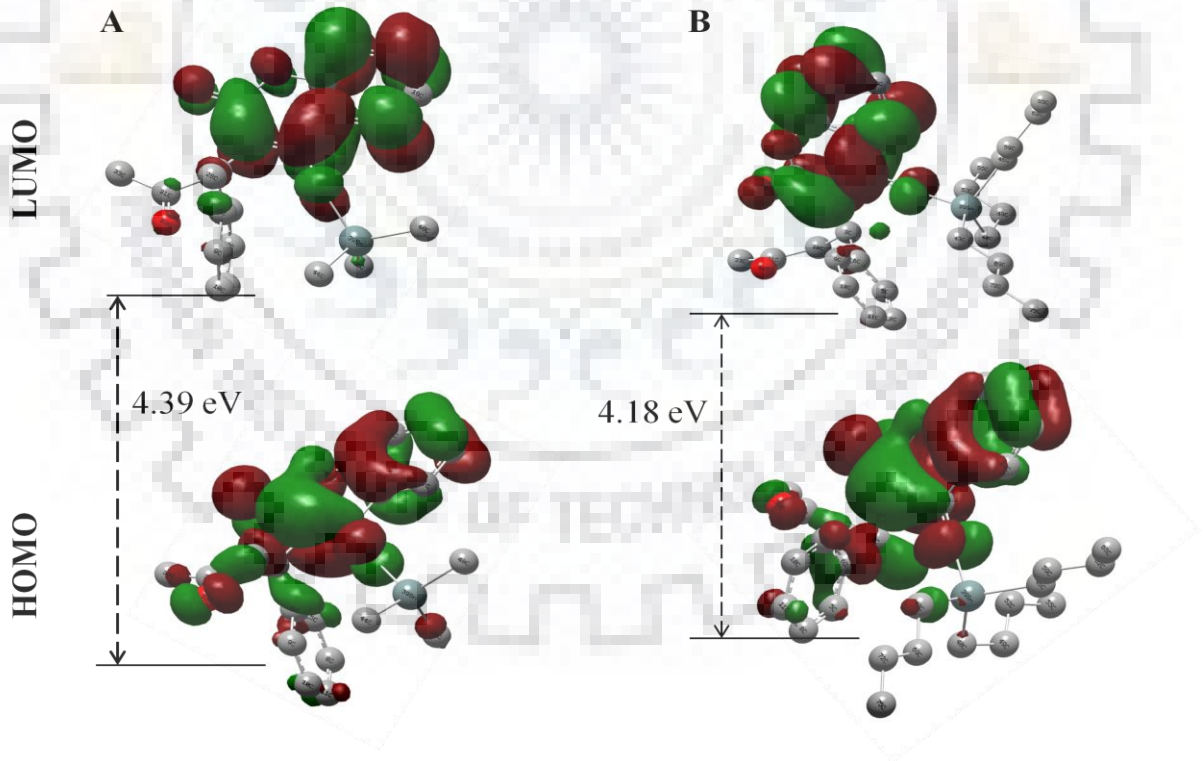

Fig. 7.6. Frontier molecular orbitals HOMO-LUMO of complex 1 (A); complexes 2 (B), derived from DFT calculation using B3LYP/LANL2DZ level of theory.

7.3.5. DNA Interaction Studies

7.3.5.1. UV-visible Spectrophotometric Studies

The mode and extent of DNA binding of the WR and complexes **1** and **2** were studied with the help of UV-visible and fluorescence spectrophotometric titrations. UV-visible spectra of the warfarin and the complexes have a characteristic low intensity band at λ_{max} 307 nm and 249 nm and a high intensity band at 204 nm due to intraligand n-π^* and π- π^* transitions, respectively. This high intensity band at 204 nm, shifted to 207 nm, in case of both the complexes. On continuous addition of CT DNA (2.6–52.9 μM) to the standard solutions of the WR and complexes **1** and **2**, an appreciable hypochromic shift was observed (Fig. 7.7) in the most intense band of WR at 204 nm and of the complexes at 207 nm. However a very small shift was observed for the other band, so for the binding constant calculation the former band was considered. A hypochromic shift accompanied with red shift of around 2-4 nm is suggestive of the intercalation of complexes between the DNA strands. The intercalation causes the coupling of π^* orbitals of intercalator with partially filled π orbitals of base pairs which results in a decrease in the probability of transition and concomitantly leads to the hypochromism in UV-spectra [87, 335, 336]. The coupling of the orbitals decreases the HOMO–LUMO energy gap, which leads to a red shift in spectra after intercalation [87]. The intercalation of the WR and complexes **1** and **2** into the base pairs of DNA can be explained on the basis of planar structure of coumarin moiety of the warfarin which easily gets inserted in-between the base pairs. Furthermore, to evaluate the extent of binding between the WR/complexes and CT DNA, the intrinsic binding constant (K_b) was calculated which comes out to be $1.25 \times 10^4\ M^{-1}$, $4.51 \times 10^4\ M^{-1}$ and $6.90 \times 10^4\ M^{-1}$ for WR, complex **1** and **2**, respectively. The values of K_b indicate that the complexes **1** and **2** combine more efficiently to CT DNA as compared to the WR, where tributyltin(IV) derivative of WR showed the highest binding affinity. This is due to the more hydrophobic nature of the butyl moiety, which contributes towards the efficient interaction with hydrophobic pockets of the DNA.

7.3.5.2. Fluorescence Spectrophotometric Studies

To support the findings from UV-visible study, further EB displacement assay was performed with fluorescence titrations. As from the various reports available in the literature it is clear that EB is a planar molecule and strongly intercalates within the DNA base pairs; due to this EB remains

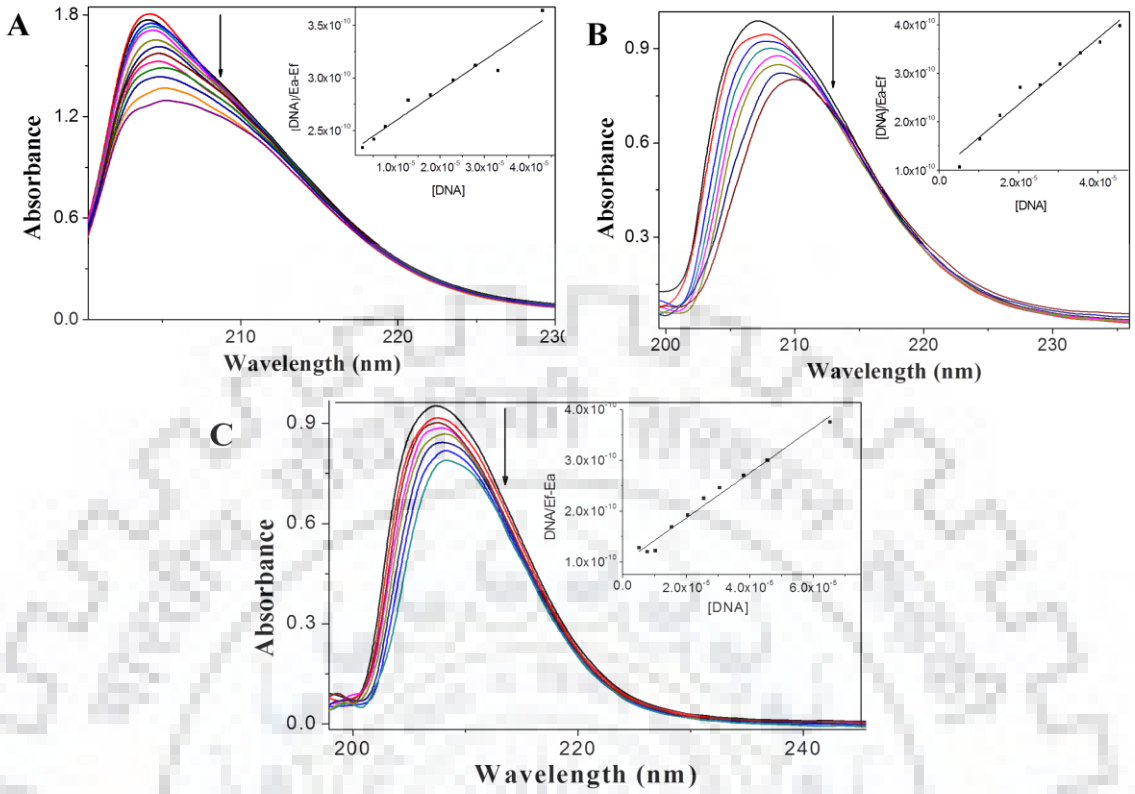

Fig. 7.7. UV-visible spectra of WR [2.6 µM] (A) and complexes: 1 [0.9 µM] (B); 2 [0.8 µM] (C), in the absence and presence of CT DNA [2.6–52.9 µM] in Tris-HCl/NaCl (5:50 mM), buffer, pH = 7.2 at 25 °C. Inset is showing linear plots of [DNA]/($\varepsilon_a - \varepsilon_f$) versus [DNA], the arrow indicates the decrease in intensity with subsequent addition of DNA.

protected from the solvent quenching and emits strongly in the UV-region in comparison to that of free EB in the solvent [337]. When quenchers (WR/complexes **1**/complex **2**) were added successively in the EB-DNA solution (already incubated), a steady decrease in the fluorescence intensity was observed as shown in Fig. 7.9, which can be explained with successive replacement of the EB from the EB-DNA adduct by WR and complexes **1** and **2.** These quenchers replace the EB form the EB-DNA adduct, set it free into the solution and with each successive addition a concomitant decrease in the fluorescence intensity was observed. The results clearly show the existence of intercalative mode of binding of WR, **1** and **2** with CT DNA. However, the value of quenching constants (K_{sv}) evaluated are 1.0×10^4, 1.75×10^4 and 2.58×10^4 M^{-1} for WR and complexes **1** and **2**, respectively, which is quite less as obtained for the classical intercalators (usually in the order of 10^7 M^{-1}). This suggests that a kind of partial intercalation played a role in this case.

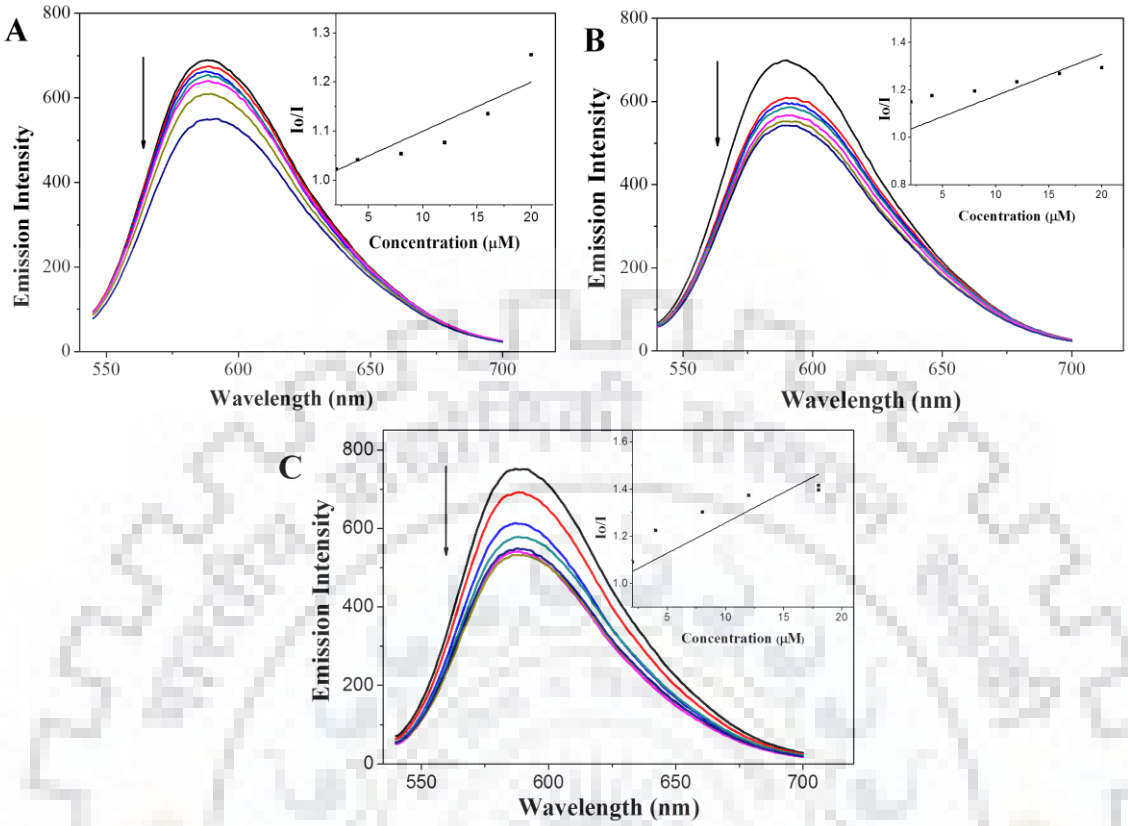

Fig. 7.8. Fluorescence quenching titration spectra of EB (6.3 μM)–CT DNA (7.2 μM) [([DNA]/[EB] = 1.14)] with successive addition of (2–20 μM) WR (A), 1 (B) and 2 (C) in Tris-HCl/NaCl (5:50 mM) buffer, pH = 7.2 at 25 °C [Excitation λ_{max} at 525 nm]. Inset is showing linear Stern-Volmer plots and arrow indicates the decrease in fluorescence intensity with increasing concentration of WR/Complexes 1, 2.

7.3.5.3. Viscosity Measurements

To further explore the mode of binding, the viscosity measurement experiment was performed, which is regarded as the most reliable test to get a clear idea of the changes involved during the binding of any molecule to DNA helix [338]. The classical intercalators, separate the base pairs of DNA in order to accommodate the bound ligand, which increases the viscosity of DNA. However, the partial intercalators cause the bending or kinking of DNA helix, which reduces its length and concomitantly its viscosity [339]. A decrease in viscosity of the DNA with addition of WR and complexes **1** and **2** (Fig. 7.9) gives a clear indication of the partial intercalation of the WR and synthesized complexes into the DNA base pairs.

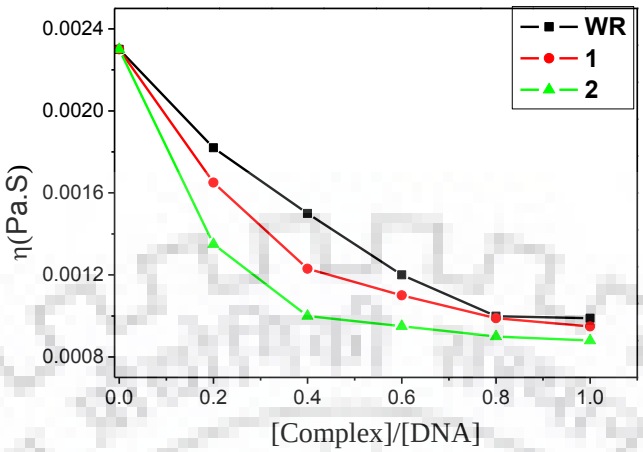

Fig. 7.9. Decrease in viscosity (η) of CT DNA (100 µM) with successive addition of WR and complexes 1 and 2 (0–50 µM).

7.3.5.4. Plasmid Cleavage by Agarose Gel Electrophoresis

WR and synthesized complexes **1** and **2** were also tested for their plasmid cleavage ability with the help of agarose gel electrophoresis. One strand cleavage of plasmid results in nicked circular (NC) form, which moves slowly in comparison to that supercoiled (SC) form, however, a linear (L) form, which moves faster than NC but slower than SC form, is produced by the cleavage of both the strands of the plasmid DNA [235, 236]. The cleavage activity of plasmid DNA due to the complexes **1**, **2** and WR was analyzed with their increasing concentration. The cleavage patterns of plasmid DNA due to WR and complexes **1** and **2** are shown in Fig. 7.10 (A, C, E). With increasing concentration of WR form r = 1 to 10 (r = [complex]/[DNA], a very little effect on the SC and NC band intensity with respect to the control was observed, on the other hand there is an increase in NC and a decrease in the SC band intensity with increasing the complexes concentration. The third linear form is also appeared at r = 10 in complex **1** and at r = 5 in complex **2,** which again witnessed the high cleavage activity of the complex **2** at lower concentration, among the tested compounds. The quantification of cleavage activity by assessing the band area with the help of image J software has been done which is shown as bar diagram in Fig. 7.10 (B, D, F), clearly indicating the extent of cleavage to compare the nuclease cleavage activity of tested compounds.

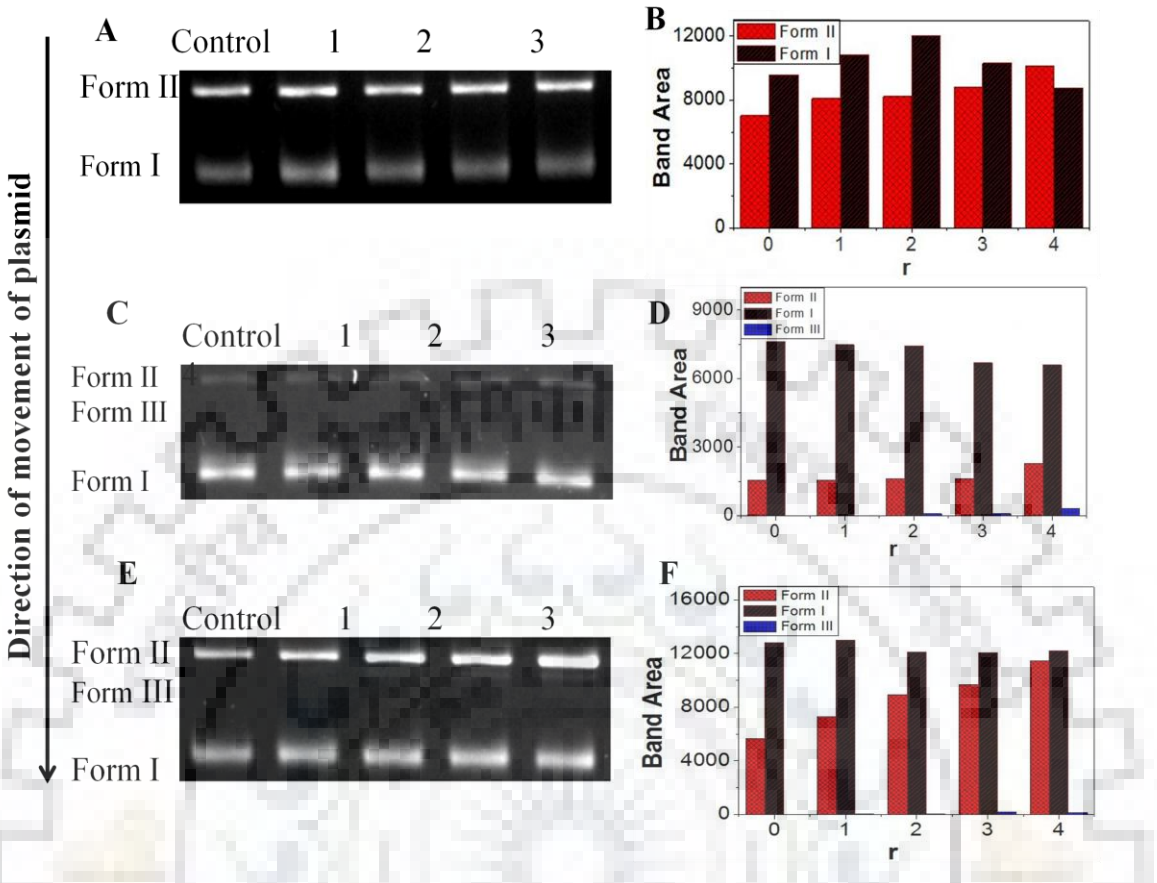

Fig. 7.10. The cleavage pattern of pBR322 plasmid DNA (100 ng) by WR (A); complex 1 (C) and complex 2 (E); after incubation for 1h at 37°C, at different concentration of WR/Complexes. Control (100 ng DNA); Lane I (DNA + 100 µM WR/Complexes); Lane II (DNA + 75 µM WR/Complexes); Lane III (DNA+ 50 µM WR/Complexes); Lane IV (DNA + 25 µM WR/Complexes).

7.3.6. Antitumour Screening through MTT Assay

Complexes and WR were screened (*in vitro)* for anti-tumor/cytotoxic activity against HCT-15 (colon adenocarcinoma), MCF-7 (mammary cancer), HeLa (cervical cancer), and LNCaP (androgen-sensitive prostate adenocarcinoma), cell lines of human origin. Calculation of IC_{50} (inhibitory concentration) values of WR and complexes were carried out using best fit linear regression model [45, 46, 237] as in previous Chapters. IC_{50} values of complexes and WR along with *cis*-platin and 5-fluorouracil are presented in the Table 7.5. WR and complexes **1–2** were found non-cytotoxic towards MCF-7, HeLa and LNCaP cell lines, this may be because of high stability of complexes which may not be able to produce active tin species i.e R_3Sn^+. However,

both the test compounds were exhibited considerable cytotoxicity towards the HCT-15 cell line which is comparable to *cis*-platin and 5-fluorouracil. In comparison to WR, both the complexes were exhibited considerably good cytotoxicity towards HCT-15 cell lines. Tributytin(IV)-WR complex exhibited more activity compared to the trimethyltin(IV)-WR complex, which may be due to the higher lipophilicity of the butyl groups attached to the tin atom.

Table. 7.5. Cytotoxic screening results of WR and its triorganotin complexes against the different cell lines of human origin; IC_{50} value is expressed in μM ± SEM.

Complex[a]/Reference drugs	HTC-15 (μM)	MCF-7 (μM)	HeLa (μM)	INCaP (μM)
WR	16.2±0.8	>500	375±25	>500
1	14.8±3.2	Very wide	>500	>500
2	**14.5±0.8**	**479±16**	**251±14**	>500
***cis*-platin**	13.98±0.4[b]	13.98±0.4[b]	n.d.	n.d.
5-Fluorouracil	12.2±0.5	0.48±0.1[b]	2.08±0.2	n.d.

[a]complex number as given in Table 7.1; [b]reference [46]; HCT-15 (colon adenocarcinoma); MCF-7 (mammary cancer); HeLa (cervical cancer) and LNCaP (androgen-sensitive prostate adenocarcinoma).

CHAPTER - 8

Conclusions

8.1. CONCLUSIONS

The study of equilibrium involved in the formation of different species of organotin(IV) compounds in aqueous media is important to understand the behavior of these compounds in chemical, biological and environmental system. Inside the physiological system the different organotin(IV) species may interact with biomolecules and drug molecules having sulphur donor sites. In order to understand these interactions and species formation along with their coordination chemistry in solution state, the potentiometric study of di- and triorganotin(IV) moieties with a sulphur donor prodrug, sodium 2-mercaptoethane sulfonate (MESNA) was performed. On the basis of the amount of different complex and mixed ligand-hydroxo complex species *viz.* $[Me_2SnL]^+$ ~ 62% , $[Me_2Sn(L)(OH)]$ ~ 89.9% and $[Me_2Sn(L)_2OH]^-$ ~ 39% in dimethyltin(IV)–(HL) and $[Me_3SnL]$ ~ 57.4%, $[Me_3Sn(L)(OH)]^-$ ~ 46.5% and $[Me_3Sn(L)_2OH]^{2-}$ ~ 1.6% in trimethyltin(IV)–(HL), formed in the equilibrium mixture, it is concluded that the extent of interaction of –SH group of MESNA is greater for Me_2SnCl_2 as compared to Me_3SnCl. The present study inferred the inability of thiol group to suppress the hydrolysis of organotin cations completely, despite having a strong tendency of complexation with Me_2Sn^{2+}/Me_3Sn^+. In general, it was appeared that the extent of formation of complex and mixed ligand-hydoxo complex species is more for 1:2 (metal:ligand) concentration set as compared to 1:1 system. This showed the extent of reaction between metal and ligand is dependent on the concentration of the ligand present. At physiological pH ~ 7.0, $[Me_2SnL]^+$ (~64.3%) in 1:1, $[Me_2SnL]^+$ (~89.9%) in 1:2, $[Me_3Sn(OH)]$ (~58.7%) in 1:1 and $[Me_3SnL]$ (~57.4%) in 1:2, di/trimethyltin(IV)–(HL), systems, are the major species. Possible geometries for different species i.e. distorted octahedral for $[Me_2SnL]^-$, distorted trigonal bipyramidal/distorted octahedral for $[Me_2Sn(L)OH]$, and distorted tetrahedral/distorted trigonal-bipyramidal geometry for $[Me_2Sn(OH)_2]$, in dimethyltin(IV)–(HL) were proposed on the basis of multinuclear NMR spectroscopic investigations. Whereas, in case of trimethyltin(IV)–(HL) a distorted trigonal-bipyramidal/distorted tetrahedral geometry was proposed for $[Me_3SnL]$ and $[Me_3SnOH]$. Furthermore, it is observed that MESNA acts as a potential sulphur donor which strongly interacts with $R_nSn^{(4-n)+}$ and forms stable species at physiological pH (~7.0). Therefore, $R_nSn^{(4-n)+}$ (n = 2 and 3) species may effectively disturb the DNA duplication by interacting with the thiol group of the protein and can be further studied as an antitumor agent.

Further, the interaction of MESNA with diorganotin(IV) compounds was studied in solid state. Four diorganotin(IV) complexes with MESNA, *viz.* **1** $[Me_2Sn(MESNA)_2]$, **2**

$[Bu_2Sn(MESNA)_2]$, **3** $[Oct_2Sn(MESNA)_2]$, **4** $[Ph_2Sn(MESNA)_2]$, and a mixed ligand complex of dibutyltin(IV) with MESNA and 1,10-phenanthroline, **5** $[Bu_2Sn(MESNA)_2.Phen]$ were successfully synthesized. The FTIR data and multinuclear NMR data depicted that all the single ligand complexes having slightly distorted tetrahedral and mix ligand complex having octahedral geometry in solid as well as solution state. The structures of the complexes were also confirmed by the geometry optimization of complexes through DFT calculations in gaseous state. The UV-visible and fluorescence spectroscopic studies of all the complexes and MESNA revealed that the interaction of synthesized complexes with CT DNA is specifically through partial intercalation, however, other modes of interactions were also envisioned. The extent of binding of these complexes with DNA was estimated from K_b and K_{sv} values obtained from absorbance and emission titrations, which followed the order as: $[Bu_2Sn(MESNA)_2]$ > $[Bu_2Sn(MESNA)_2.Phen]$ > $[Ph_2Sn(MESNA)_2]$ > $[Oct_2Sn(MESNA)_2]$ > $[Me_2Sn(MESNA)_2]$ > MESNA. The $[Bu_2Sn(MESNA)_2]$ and $[Bu_2Sn(MESNA)_2.Phen]$ showed the maximum binding towards CT DNA due to the additional hydrophobic interaction of butyl moiety. The CD spectroscopic analysis and viscosity experiments further supported the partial intercalative mode of binding of complexes with CT DNA. All the organotin complexes demonstrated a higher binding propensity towards CT DNA in comparison to MESNA. The agarose gel electrophoresis of pBR322 DNA with all the complexes suggested that the cleavage of plasmid DNA is mediated through the involvement of hydroxyl radical. Furthermore, the cytotoxicity study of the synthesized complexes depicted the remarkable cytotoxicity (many folds higher than 5-fluorouracil and *cis*-platin) of the $[Ph_2Sn(MESNA)_2]$ and $[Bu_2Sn(MESNA)_2.Phen]$ against the prostate cancer, colon cancer and cervical cancer cells. The activities of these complexes vary dramatically irrespective of their structures which can be explained on the basis of structure-activity relationship described by Saxena and Huber. The lipophilicity of butyl and phenyl groups plays a major role in the transportation of the respective complexes across the cell membranes and thereafter, which interfere with cellular functions eventually leads to cell death. The higher cytotoxicity of $[Bu_2Sn(MESNA)_2.Phen]$ compared to $[Bu_2Sn(MESNA)_2]$ can be explained with the greater stability of $[Bu_2Sn(MESNA)_2]$ in buffer system at physiological pH, which may unable to produce active metal species, when required. The extent of DNA binding abilities and cytotoxicities of the complexes are related to some extent. Moreover, the ligand (MESNA) is found inactive towards these cancer cell lines, indicating that the combination of MESNA with some organotin(IV) compounds led to increase in cytotoxicity manyfold. AO/EB staining of cancer cell lines with the

IC_{50} values of the complexes revealed that the apoptosis is the major cause of the induction of the cytotoxicity for complexes $[Ph_2Sn(MESNA)_2]$ and $[Bu_2Sn(MESNA)_2.Phen]$. However, the DNA fragmentation assay revealed that some other processes along with Casapase-3 induced DNA cleavage may also involved for the induction of apoptosis. Hence, the synthesized organotin complexes with MESNA can find the applications in the field of cancer chemotherapy, as they can successfully bind with and cleave the DNA and show the remarkable *in vitro* cytotoxicities by inducing programmed cell death along with some extent of necrosis.

Organotin complexes of NSAID, Sulindac (**Sul**), (**1–7**) *viz.* $[Me_3Sn(Sul)]$, $[Ph_3Sn(Sul)]$, $[Bu_3Sn(Sul)]$, $[Ph_2Sn(Sul)_2]$, $[Me_2SnCl(Sul)]_2$, $[Bu_2Sn(Sul)_2]$ and $[Oct_2Sn(Sul)_2]$ were designed, characterized thoroughly, and their *in vitro* DNA binding profile was studied, with an aim to develop new chemotherapeutic agents. The X-ray crystallographic study of $[Bu_3Sn(Sul)]$ revealed a trigonal bipyramedal geometry aroud tin, where three equitorial positions were occupied by the butyl groups and oxygen atoms from carboxylate and sulphoxide groups occupied the axial positions. However, the weak bond present between tin and sulphoxide oxygen dissociated in the solution due to which a four coordiantion for tin is revaeled from NMR studies. Similar structures are proposed for $[Me_3Sn(Sul)]$ and $[Ph_3Sn(Sul)]$. A highly distorted octahedral geometry, more precisely a tetrahedral bicapped geomtry for $[Ph_2Sn(Sul)_2]$ and $[Bu_2Sn(Sul)_2]$, a dinuclear clorine-bridged structure with trigonal bipyramidal geometry around tin in solid state and a distorted octahedral geometry in solution (in DMSO-d_6) for $[Me_2SnCl(Sul)]_2$, and a distorted tetrahedral geometry for $Oct_2Sn(Sul)_2]$ are proposed, on the bases of optimized structures obtained through DFT calculations and multinuclear NMR and ESI MS studies. Furthermore, the corroborative results from DNA binding experiments suggested the binding of complexes occurs with CT DNA preferably through partial intercalation. **Sul** and complexes $[Bu_2Sn(Sul)_2]$ and $[Ph_2Sn(Sul)_2]$ displayed higher binding propensity towards CT DNA as compared to other complexes. CD experimental results depicted other modes of interaction along with the existence of partial intercalation, for some complexes. The pBR322 plasmid cleavage activity of **Sul** /complexes was carried out by gel electrophoretic mobility assay which showed a moderate cleavage activity. Interestingly, $[Oct_2Sn(Sul)_2]$ presented an efficient cleavage activity of plasmid DNA converting Form I to Form II and ultimately leading to the formation of linearized Form III. All the complexes displayed good *in vitro* antitumour activity towards the HCT-15 (colon adenocarcinoma) and very low cytotoxicity towards HeLa (cervix cancer) cells whereas, these complexes seemed non-

cytotoxic towards MCF-7 (mammary cancer) and LNCaP (androgen sensitive prostate) cell lines. The lesser activities of these complexes irrespective of their geometry may be because of the higher stability of Sn–O bond strength which refrain the complexes from producing active organotin species. Moreover, the cytotoxicities of the complexes are highly dependable on the nature of the cell line.

Since the role of the anti-inflammatory drugs in the combination chemotherapy with other antitumour drugs is a well known fact, thus we were eager to explore the effect of combination of organotin(IV) moieties with a very simple and well known NSAID ibuprofen. A successful syntheses of di- and triorganotin(IV) complexes of ibuprofen (IBF) with thermal and microwave methods were described in this thesis. The synthesized complexes **1-5** *viz.* [$(Me_3Sn)(IBF)$], [$(Bu_3Sn)(IBF)$], [$(Ph_3Sn)(IBF)$], [$(Me_2Sn(IBF))_2O]_2$ and [$(Bu_2Sn)(IBF)_2$], respectively, were characterized through various techniques in order to confirm the purity of the compounds. The single crystal X-ray determination of [$Ph_3Sn(IBF)$] revealed an intermediate geometry (between td and TBP geometries) around tin metal, where carboxylate group of IBF is coordinated with bidentate mode. Similar geometries were proposed for the triorganotin(IV) complexes in solid state. A distannoxane structure for [$(Me_2Sn(IBF))_2O]_2$ and a highly distorted octahedral structure or tetrahedral bicapped structure with two carboxylate group coordinating through bidentate mode, were proposed for [$(Bu_2Sn)(IBF)_2$], which were further validated by optimization of complexes geometries through DFT calculations in gaseous state. Further, the major stretching frequencies calculated from DFT and obtained from experimental FTIR spectra were found in good agreement. However, these complexes lose their bidentate mode of coordination in solution state, which have been revealed by multinuclear NMR studies. As we were eager to explore the biological utility of the complexes, so we perform the DNA binding and DNA cleavage studies of these complexes. The binding studies through various photophysical techniques and viscosity measurement of DNA depicted the intercalation of IBF and [$(Bu_2Sn)(IBF)_2$], within the base pairs of DNA, however an external binding (electrostatic or groove binding) were revealed for the complexes **1** and **2**. Further, the cleavage activity of these complexes including IBF specifies them as potential DNA cleaving agents, which displayed a concentration dependent cleavage of DNA. A hydrolytic mechanism of cleavage was revealed for the IBF and complexes except complex **1**, though the involvement of reactive oxygen radical in the cleavage activity could not be ruled out. Furthermore, the *in vitro* cytotoxicity studies for these complexes highlight their good cytotoxic

effect, particularly of complexes [(Bu_3Sn)(IBF)] and [(Ph_3Sn)(IBF)], [($Me_2Sn(IBF))_2O]_2$ and [(Bu_2Sn)$(IBF)_2$] against DU145 (prostate cancer), HCT-15 (colon adenocarcinoma) and Caco-2 (colorectal adenocarcinoma). [(Ph_3Sn)(IBF)] demonstrated a remarkable cytotoxicity towards Caco-2 (IC_{50} = 1.21 μM) approx 8 times to that of *cis*-platin. [(Bu_2Sn)$(IBF)_2$] displayed a high cytotoxicity against colon and prostate cancer. The higher activity of [Bu_3Sn(IBF)] and [(Ph_3Sn)(IBF)] complexes against colorectal cancer can be explained on the basis of their tetrahedral structure and higher lipophilicity of the butyl and phenyl groups. Further, the cytotoxicity of the complex **4**, $[(Me_2Sn(IBF))_2O]_2$, can be described by the synergistic effect of oragnotin(IV) moieties due to tetranuclear complex structure. The prostate cancer cell line (DU145) is resistant towards *cis*-platin, hence these complexes can be further studied in order to make them suitable for clinical trials. It was evidenced from the AO/EB staining of the cells and DNA fragmentation assay that the major cause of cell death is apoptosis, however necrosis in few cases could not be excluded. A number of commercially used antitumour drugs i.e. doxorubicin, 5-fluorouracil, *cis*-platin and cladribine exhibit necrotic and apoptotic effects together. It is concluded that the organotin(IV) complexes exert their cytotoxic effects due to their dual capability of inducing apoptosis to the greater extent and necrosis to minor extent.

Two triorganotin(IV) derivatives of an anticoagulant drug, warfarin ([Me_3Sn(WR)], [Bu_3Sn(WR)]) were synthesized. A detailed structural characterization revealed distorted td geometry in the solid state and distorted tbp geometry in solution (DMSO-d_6), for these complexes. In order to get an insight into the chemotherapeutic probabilities of synthesized complexes, DNA binding and cleavage experiments were performed, which revealed their better abilities to bind with and to cleave DNA compared to WR. These activities highlights the importance of organotin(IV)-warfarin derivatives and their potential to induce DNA damage which may be responsible for the antitumor activity. The MTT assay results displayed a good antitumour activity of these complexes towards colon cancer cell lines, which is comparable to *cis*-platin and 5-fluorouracil. Further, the order of cytotoxicity as obtained from the their IC_{50} values is [Bu_3Sn(Wr)] > [Me_3Sn(Wr)] > WR, which is in accordance of their DNA binding abilities.

From the above mentioned analysis it is concluded that the metallation of drugs with dibutyl-, dipheny-, triphenyl- and tributyltin(IV) moieties increases their cytotoxicity and DNA binding capacities manyfold. The introduction of 1,10-phenantholine moiety in the organotin-drug complexes increases the *in vitro* antitumour activity of the complexes. [$Bu_2Sn(MESNA)_2$.Phen]

displayed the maximum antitumour activity (IC_{50} = 0.83±0.1 μM) against HCT-15 and HeLa cell lines (IC_{50} = 1.85±0.4) among all the synthesized complexes. $[(Me_2Sn(IBF))_2O]_2$ displayed the highest antitumor activity against DU145 cancer cell line (3.97±0.81) and $[(Ph_3Sn)(IBF)]$ demonstrated the maximum activity against Caco-2 cell lines. IBF and complexes, $[Bu_2Sn(MESNA)_2.Phen]$, $[(Me_2Sn(IBF))_2O]_2$ and $[(Bu_2Sn)(IBF)_2]$ displayed remarkable cytotoxicities against DU145 cell lines which is resistant to *cis*-platin, hence can be tested further. It has been analyzed that different cell lines displayed different behavior towards similar complexes as their cytotoxicities are concerned. Furthermore, the DNA binding ability and DNA cleavage activity of the compounds, alone may not describe the antitumour effect of the compounds completely. Therefore, the antitumour activities of the organotin(IV) compounds would be controlled by other factors along with the DNA binding and cleavage abilities.

8.2. FUTURE PROSPECTS

- It is inferred from the above discussion that NSAIDs and other drugs with small structure with potential binding sites such as carboxylate, thiol and hydoxy groups on metallation showing high antitumour activities, which can be developed as innovative non platinum based antitumour drugs with further *in vivo* experimentation.
- As the incorporation of 1,10-phenanthroline moiety increases the cytotoxicity of single ligand complexes many fold, so the mixed ligand organotin(IV) complexes with drug molecule and 1, 10-phenanthroline must be synthesized and their biological studies should be carried out.
- It has been seen that many organotin complexes dissociate when dissolved in buffer system, hence efforts should be made to increase their solubility in water based buffers, which can be achieved through the incorporation of polar substituents *viz.* fluorine, sulphydryl and hydroxyl groups in the drug molecules.
- Furthermore, to draw out the clarity of mode of action of organotin(IV) compounds through which they induce the cytotoxicity, other mechanistic biological experiments have to be done. Analysis of enzyme assays such as lipid peroxidase, glutathione peroxidase/reductase, lactate dehydrogenase assays, cell cycle arrest (through flow cytometry), caspse-9 expression, expression of antiapoptotic (Bcl-x and Bcl) and proapoptotic proteins (Bax and Bak) are required to be done to clarify various apoptotic pathways related to the cytotoxicity of the organotin complexes.

REFERENCES

(1) Riordan, J. F. The Role of Metals in Enzyme Activity. *Ann. Clin. Lab. Sci.* **1977**, *7*, 119–129.

(2) Holm, R. H.; Kennepohl, P.; Solomon, E. I. Structural and Functional Aspects of Metal Sites in Biology. *Chem. Rev.* **1996**, *96*, 2239–2314.

(3) Ainscough, E. W.; Brodie, A. M. The Role of Metal Ions in Proteins and other Biological Molecules. *J. Chem. Educ.* 156–158.

(4) Mu, J. Functional Metal Ions in Nucleic Acids. *Metallomics* **2010**, *2*, 318–327.

(5) Huang, R.; Wallqvist, A.; Covell, D. G. Anticancer Metal Compounds in NCI's Tumor-Screening Database: Putative Mode of Action. *Biochem. Pharmacol.* **2005**, *69* (7), 1009–1039.

(6) Kumar, A.; Singh, J. D. An Organoselenium-Based Highly Sensitive and Selective Fluorescent "Turn-On" Probe for the Hg^{2+} Ion, *Inorg. Chem.* **2012**, *51*, 772−774.

(7) Manjare S. T.; Singh, H. B.; Butcher, R. J. Synthesis and Glutathione Peroxidase-like Activity of N-heterocyclic Carbene Derived Cationic Diselenides, *Tetrahedron* **2012**, *68*, 10561–10566.

(8) Singh, J. D.; Maheshwari, M.; Khana S.; Butcher R. J. Sterically Encumbered Hexakis(alkylseleno)benzenes: Conformational Behavior of Hexakis(iso-propylselenomethyl)benzene Toward Hg^{2+} Ions on Selective Recognition, *Tetrahedron Lett.* **2008**, *49*, 117–121.

(9) Gasser, G.; Metzler-Nolte, N. The Potential of Organometallic Complexes in Medicinal Chemistry. *Curr. Opin. Chem. Biol.* **2012**, *16*, 84–91.

(10) Coogan, M. P.; Dyson, P. J.; Bochmann, M. Introduction to the Organometallics in Biology and Medicine Issue. *Organometallics* **2012**, *31* (16), 5671–5672.

(11) Chavain, N.; Biot, C. Organometallic Complexes : New Tools for Chemotherapy. *Curr. Med. Chem.* **2010**, *17*, 2729–2745.

(12) Pettinari, C.; Marchetti, F.; Pettinari, R.; Martini, D.; Drozdov, A.; Troyanov, S. The Interaction of Organotin(IV) Acceptors with a Benzoic acid Containing Two Pyrazolone Groups. *J. Chem. Soc.dalt. Trans.* **2001**, 1790–1797.

(13) Marchetti, F.; Pettinari, C.; Cingolani, A.; Pettinari, R.; Rossi, F.; M.; Caruso, F. Organotin(IV) Derivatives of Novel β-Diketones Part V. Synthesis and Characterization of Di- and Triorganotin(IV) Derivatives of 4-acyl-5-pyrazolones Modified in Position 3 of the Pyrazolone Group. Crystal Structure of (1,3-Diphenyl-4-Benzoyl-Pyrazolono-5-ato)triphenyltin(IV). *J. Organomet. Chem.* **2002**, *645*, 134–145.

(14) Timerbaev, A. R.; Hartinger, C. G.; Aleksenko, S. S.; Keppler, B. K. Interactions of Antitumor Metallodrugs with Serum Proteins : Advances in Characterization Using Modern Analytical Methodology. *Chem. Rev.* **2006**, *106*, 2224–2248.

(15) Atilla-gokcumen, G. E.; Williams, D. S.; Bregman, H.; Pagano, N.; Meggers, E.

Organometallic Compounds with Biological Activity: A Very Selective and Highly Potent Cellular Inhibitor for Glycogen Synthase Kinase 3. *Chem. Bio. Chem.* **2006**, *7*, 1443–1450.

(16) Debreczeni, J. É.; Bullock, A. N.; Atilla, G. E.; Williams, D. S.; Bregman, H.; Knapp, S.; Meggers, E. Ruthenium Half-Sandwich Complexes Bound to Protein Kinase Pim-1. *Angew. Chem.* **2006**, *45*, 1580–1585.

(17) Meggers, E. Targeting Proteins with Metal Complexes. *Chem.Comm.* **2009**, 1001–1010.

(18) Lewis, W. R.; Hedges, E. S. Applications of Organotin Compounds. In *Metal-Organic Compounds*; Advances in Chemistry; American Chemical Society, 1959; Vol. 23, pp 17–190.

(19) Hartinger, G. C.; Dyson, P. J. Bioorganometallic Chemistry–From Teaching Paradigms to Medicinal Applications. *Chem. Soc. Rev.* **2009**, *38*, 391–401.

(20) Michael, J. S. G; Michael, F.; Lappert, F.; Stuart. J. M.; Power, P. P. Ready Oxidative Addition of an Alkyl or Aryl Halide to a Tin(II) Alkyl or Amide ; Evidence for a Free-Radical Pathway. *J. Chem. Soc. Chem. Comm.* **1976**, 256, 256–257.

(21) Michael, J. S. G; Michael, F.; Lappert, F.; Stuart. J. M.; Power, P. P. Catalysis and Solvent Participation in Organometallic Oxidative Additions ($Pt^{0}\rightarrow Pt^{I1}$ and $Sn^{II}\rightarrow Sn^{IV}$). *J. Chem. Soc. Chem. Comm.* **1978**, *3*, 192–193.

(22) Nicholson, J. W. The Early History of Organotin Chemistry. *J. Chem. Educ.* **1899**, *66*, 621–622.

(23) Iqbal, H.; Ali, S.; Shahzadi, S.; Antituberculosis Study of Organotin (IV) Complexes : A Review, *Cogent Chem.* **2015**, *104* (1), 1029–1039.

(24) Lewis, W. R.; Hedges, E. S. Applications of Organotin Compounds, in Metal Organic Compounds. *Am. Chem. Soc.* 1959, 190–203.

(25) Yasuda, M.; Chiba, K.; Baba, A. An Ab Initio Computational Study on the Reaction of Organotin Enolates: Comparison of Highly Coordinated Tin Reagent with Noncoordinated Reagent. *J. Am. Chem. Soc.* **2000**, *122*, 7549–7555.

(26) Penninks, A. H.; Bol-Schoenmakers, M.; Seinen, W. Cellular Interactions of Organotin Compounds in Relation to Their Antitumor Activity BT- Tin-Based Antitumour Drugs; Gielen, M., Ed.; Springer Berlin Heidelberg: Berlin, Heidelberg, 1990; pp 169–190.

(27) Tsangaris, J. M.; Williams, D. R. Tin in Pharmacy and Nutrition. *Appl. Organomet. Chem.* **1992**, *6*, 3–18.

(28) Crowe, A. J. Tin Compounds and Their Potential as Pharmaceutical Agents BT- Tin-Based Antitumour Drugs; Gielen, M., Ed.; Springer Berlin Heidelberg: Berlin, Heidelberg, 1990; pp 69–114.

(29) Ross, A. Industrial Applications Of Organotin Compounds. *Ann. N. Y. Acad. Sci.* **1965**, *125*, 107–123.

(30) Piver, W. T. Organotin Compounds : Industrial Applications and Biological Investigation. *Environ. Health Perspect.* **1973**, 61–79.

(31) Omae, I. *Applications of Organometallic Compounds*; John Wiley & Sons, 1998.

(32) Evans, C. J. Industrial Uses of Tin Chemicals BT - Chemistry of Tin; Smith, P. J., Ed.; Springer Netherlands: Dordrecht, 1998; pp 442–479.

(33) Davies, A. G. Organotin Compounds in Technology and Industry. *J. Chem. Res.* **2010**, *34*, 181–190.

(34) Van der Kerk, G. J. M. Organotin Compounds: New Chemistry and Applications. In *Organotin Compounds: New Chemistry and Applications*; Zuckerman, Ed.; Washington, DC, 1976; pp 1–25.

(35) Omae, I. Organotin Antifouling Paints and Their Alternatives. *Appl. Organomet. Chem.* **2003**, *17*, 81–105.

(36) Hadjikakou, S. K.; Hadjiliadis, N. Antiproliferative and Anti-Tumor Activity of Organotin Compounds. *Coord. Chem. Rev.* **2009**, *253*, 235–249.

(37) Wu, W.; Yu, L. H.; Ma, B.; Xu, M. J. The Inhibitory Effect of Doxycycline on *Cis*-platin-Sensitive and Resistant Epithelial Ovarian Cancer. *PLoS One* **2014**, *9*, *e*89841.

(38) Nath, M. Toxicity and the Cardiovascular Activity of Organotin Compounds: A Review. *Appl. Organomet. Chem.* **2008**, 22, 598–612.

(39) Nath, M.; Singh, H.; Eng, G.; Song, X. Synthesis , Structure–Activity Relationship of Some New Triorganotin (IV) Derivatives of Dipeptides as Anti-Inflammatory Agents. *Phosphorus. Sulfur. Silicon Relat. Elem.* **2013**, *188*, 755–767.

(40) Nath, M.; Jairath, R.; Eng, G.; Song, X.; Kumar, A. New Organotin (IV) Ascorbates: Synthesis, Spectral Characterization, Biological and Potentiometric Studies. *Spectrochim. Acta Part A* **2005**, *61*, 77–86.

(41) Nath, M.; Kompelli, N. Speciation and NMR Spectrometric Studies of Interaction of Di- and Tri-organotin(IV) Moieties with 5′-Guanosine Monophosphate and Guanosine in Aqueous Solution. *J. Solution Chem.* **2014**, *43* (6), 1184–1204.

(42) Nath, M.; Kumar, P.; Kumar, A. New Di- and Triorganotin (IV) Complexes of Tripodal Schiff Base Ligand Containing Three Imidazole Arms : Synthesis, Structural Characterization, Anti-Inflammatory Activity and Thermal Studies. *J. Organomet. Chem.* **2010**, *695*, 1353–1362.

(43) Nath, M.; Pokharia, S.; Eng, G.; Song, X.; Kumar, A. New Triorganotin (IV) Derivatives of Dipeptides as Models for Metal–Protein Interactions : Synthesis, Structural Characterization and Biological Studies. *Spectrochim. Acta Part A* **2006**, *63*, 66–75.

(44) Nath, M.; Pokharia, S.; Eng, G.; Song, X.; Kumar, A. New Triorganotin (IV) Derivatives of Dipeptides as Anti-Inflammatory–Antimicrobial Agents. *Eur. J. Med. Chem.* **2005**, *40*, 289–298.

(45) Nath, M.; Vats, M.; Roy, P. Design and Microwave-Assisted Synthesis of Tri- and dialkyltin(IV) Hippurates, Characterization, in Vitro Anti-Cancer and in Vivo Anti-Inflammatory Activities. *Med. Chem. Res.* **2015**, *24* (1), 51–62.

(46) Nath, M.; Vats, M.; Roy, P. Tri- and Diorganotin (IV) Complexes of Biologically Important Orotic Acid: Synthesis, Spectroscopic Studies, in Vitro Anti-Cancer, DNA Fragmentation , Enzyme Assays and in Vivo Anti-inflammatory Activities. *Eur. J. Med. Chem.* **2013**, *59*, 310–321; and references cited therein.

(47) Cancer Facts & Figures 2017. *Cancer Facts Fig. 2017* **2017**.

(48) News, I. Over 17 Lakh New Cancer Cases in India by 2020: ICMR. 1–2 (2016).

(49) Rosenberg, B.; VavCamp, L.; Trosko, J. E.; Mansour, V. H. Platinum Compounds: A New Class of Potent Antitumour Agents. *Nature* **1969**, *222*, 385–386.

(50) Tabassum, S.; Yadav, S.; Arjmand, F. Exploration of Glycosylated-Organotin(IV) Complexes as Anticancer Drug Candidates. *Inorganica Chim. Acta* **2014**, *423*, 38–45.

(51) Wheate, N. J.; Walker, S.; Craig, G. E.; Oun, R. The Status of Platinum Anticancer Drugs in the Clinic and in Clinical Trials. *Dalton Trans.* **2010**, *39*, 1471–1485.

(52) Ellahioui, Y.; Prashar, S.; Gómez-ruiz, S. Anticancer Applications and Recent Investigations of Metallodrugs Based on Gallium, Tin and Titanium. *Inorganics* **2017**, *5*, 4–29.

(53) Reedijk, J. Why Does *Cis*-platin Reach Guanine-N7 with Competing S-Donor Ligands Available in the Cell ? *Chem. Rev.* **1999**, *99*, 2499–2510.

(54) Tabassum, S.; Pettinari, C. Chemical and Biotechnological Developments in Organotin Cancer Chemotherapy. *J. Organomet. Chem.* **2006**, *691*, 1761–1766.

(55) Pellerito, C.; Agati, Paolo, D.; Fiore, T.; Mansueto, C.; Mansueto V.; Stocco, G.; Nagy, pellerito L. Synthesis, Structural Investigations on Organotin(IV)chlorin-e_6 Complexes, Their Effect on Sea Urchin Embryonic Development and Induced Apoptosis. *J. Inorg. Biochem.* **2005**, *99*, 1294–1305.

(56) A. J. Crowe, Smith, P. J.; Atassi, G. Investigations into the Antitumour Activity of Organotin Compounds. I. Diorganotin Dihalides and Di-Pseudohalide Complexes. *Chem. Biol. Interact.* **1980**, *32*, 171–178.

(57) Saxena, A. K.; Huber, F.; Organotin Compounds and Cancer Chemotherapy. *Coord. Chem. Rev.* **1989**, *95*, 109–123.

(58) Gielen, M. Tin Based Antitumour Drugs. *Coord. Chem. Rev.* **1996**, *151*, 41–51.

(59) Williams, J. L.; Lewis-alleyne, L. C.; Solomon, M.; Nguyen, L.; Johnson, R.; Vital, J.; Ji, P.; Durant, J.; Cooper, C.; Cagle, P.; Martin, P.; Van-Derveer, D.; Jarrett, W. L.; Holder, A. A. An In Vitro Study on the Effect of Synthesized Tin(IV) Complexes on Glioblastoma, Colorectal, and Skin Cancer Cell Lines. *Biomed. Res. Clin. Prac.* **2016**, *1*, 7–15.

(60) Gielen, M.; Tiekink, E. R. T. 50 Sn Tin Compounds and Their Therapeutic Potential. In *Metallotherapeutic Drugs and Metal-Based Diagnostic Agents*; John Wiley & Sons, Ltd, 2005; pp 421–439.

(61) Gielen, M.; Wiilem, S. R.; Biesemans, M.; Bouiilam, M.; Khloufi, A. E. Exceptionally High in Vitro Antitumor Activity of Substituted Triphenyltin Benzoates Including Salicylates against a Human Mammary Tumor, MCF-7, and a Colon Carcinoma, WiDr. *Appl. Organomet. Chem.* **1992**, *6*, 287–291.

(62) Gielen, M.; El, A.; Biesemans, M.; Bouhdid, A.; Vos, D. De; Mahieu, B.; Willem, R. Synthesis, Characetrization and High in Vitro Antitumour Activity of Novel Triphenyl Carboxylates. *Met. Based Drugs* **1994**, *1*, 305–309.

(63) Girasolo, M. A.; Rubino, S.; Portanova, P.; Calvaruso, G.; Ruisi, G.; Stocco, G. New Organotin(IV) Complexes with $_{L}$-Arginine, Nα-t-Boc-$_{L}$-Arginine and $_{L}$-Alanyl-$_{L}$-Arginine: Synthesis, Structural Investigations and Cytotoxic Activity. *J. Organomet. Chem.* **2010**, *695*, 609–618.

(64) Nishikimi, A.; Kira, Y.; Kasahara, E.; Sato, E. F.; Kannou, T.; Tsumi, K.; Inoue, M. Tributyltin Interacts with Mitochondria and Induces Cytochrome c Release. *Biochem. J.* **2001**, *626*, 621–626

(65) Das, K. V. G. Main Group Elements and Their Compounds Perspectives in Materials Science, *Chemistry and Biology*; Das, K. V. G., Ed.; Springer-Verlag Berlin Heidelberg, 1996.

(66) Williams, J. L.; Lewis-alleyne, L. C.; Solomon, M.; Nguyen, L.; Johnson, R.; Vital, J.; Ji, P.; Durant, J.; Cooper, C.; Cagle, P.; et al. An *In Vitro* Study on the Effect of Synthesized Tin (IV) Complexes on Glioblastoma, Colorectal, and Skin Cancer Cell Lines. *Biomed. Res. Clin. Pract. Res.* **2016**, *1*, 7–15.

(67) Pellerito, C.; Pellerito, B. N. L.; Szorcsik, A. Biological Activity Studies on Organotin (IV)$^{N+}$ Complexes and Parent Compounds. *J. Organomet. Chem.* **2006**, *691*, 1733–1747.

(68) Ohhira, S.; Enomoto, M.; Matsui, H. In Vitro Metabolism of Tributyltin and Triphenyltin by Human Cytochrome P-450 Isoforms. *Toxicol.* **2006**, *228*, 171–177.

(69) Samuel, P. M.; Roy, S.; Jaiswal, K. A.; Rao, J. V. Differential Effects of Organometallic Tin Compounds on Na^+ /K^+ -ATPase Activity. *J. Appl. Toxicol.* **1998**, *18*, 383–386.

(70) Moosavi-movahedi, A. A.; Golchin, A. R.; Nazari, K.; Chamani, J.; Saboury, A. A.; Bathaie, S. Z.; Tangestani-nejad, S. Microcalorimetry, Energetics and Binding Studies of DNA–Dimethyltin Dichloride Complexes. *Thermochim. Acta* **2004**, *414*, 233–241.

(71) Barone, G.; Terenzi, A.; Lauria, A.; Almerico, A. M.; Leal, J. M.; Busto, N.; García, B. DNA-Binding of nickel(II), copper(II) and zinc(II) Complexes: Structure-Affinity Relationships. *Coord. Chem. Rev.* **2013**, *257*, 2848–2862.

(72) Camm, K. D.; McGowan, P. C. Rhodium– and Tin–DNA Interactions and Applications. In *Metal Complex–DNA Interactions*; John Wiley & Sons, Ltd, 2009; pp 301–315.

(73) Silvestri, C.; Brodbelt, J. S. Tandem Mass Spectrometry for Characterization of Covalent Adducts of DNA With Anticancer Therapeutics. *Mass Spectrom. Rev.* **2013**, *32*, 247–266.

(74) Ni, Y.; Lin, D.; Kokot, S. Synchronous Fluorescence, UV–Visible Spectrophotometric, and Voltammetric Studies of the Competitive Interaction of Bis-(1,10-Phenanthroline) Copper(II) Complex and Neutral Red with DNA. *Anal. Biochem.* **2006**, *352*, 231–242.

(75) Shui, X.; Peek, M. E.; Lipscomb, L. A.; Gao, Q.; Ogata, C.; Roques, P.; Garbay-jaureguiberry, C.; Wilkinson, A. P.; Williams, D. L. Effects of Cationic Charge on Three-Dimensional Structures of Intercalative Complexes : Structure of a Bis-Intercalated DNA Complex Solved by MAD Phasing. *Curr. Med. Chem.* **2000**, *7*, 59–71.

(76) Bauer, W.; Vinograd, J. The Interaction of Closed Circular DNA with Intercalative Dyes: III. Dependence of the Buoyant Density upon Superhelix Density and Base Composition. *J. Mol. Biol.* **1970**, *54*, 281–298.

(77) Neidle, S.; Abraham, Z. Structural and Sequence-Dependent Aspects of Drug Intercalation Into Nucleic Acid. *Crit. Rev. Biochem.* **1984**, *17* (1), 73–121.

(78) González-Bulnes, L.; Gallego, J. Indirect Effects Modulating the Interaction between DNA and a Cytotoxic Bisnaphthalimide Reveal a Two-Step Binding Process. *J. Am. Chem. Soc.* **2009**, *131*, 7781–7791.

(79) Liu, H.; Sadler, P. J. Metal Complexes as DNA Intercalators. *Acc. Chem. Res.* **2011**, *44*, 349–359.

(80) Arjmand, F.; Parveen, S.; Tabassum, S.; Pettinari, C. Organotin Antitumor Compounds: Their Present Status in Drug Development and Future Perspectives. *Inorganica Chim. Acta* **2014**, *423*, 26–37.

(81) Liu, K.; Yan, H.; Chang, G.; Li, Z.; Niu, M.; Hong, M. Organotin(IV) Complexes Derived from Hydrazone Schiff Base: Synthesis, Crystal Structure, *In Vitro* Cytotoxicity and DNA/BSA Interactions. *Inorganica Chim. Acta* **2017**, *464*, 137–146.

(82) Hong, M.; Chang, G.; Li, R.; Niu, M. Anti-Proliferative Activity and DNA/BSA Interactions of Five Mono- or Di-Organotin(iv) Compounds Derived from 2-hydroxy-N'-[(2-hydroxy-3-methoxyphenyl)methylidene]-benzohydrazone. *New J. Chem.* **2016**, *40*, 7889–7900.

(83) Sirajuddin, M.; Mckee, V.; Tariq, M.; Ali, S. Newly Designed Organotin(IV) Carboxylates with Peptide Linkage : Synthesis, Structural Elucidation, Physicochemical Characterizations and Pharmacological Investigations. *Eur. J. Med. Chem.* **2018**, *143*, 1903–1918.

(84) Mridula; Nath, M. Conventional and Microwave-Assisted Synthesis, Characterization, DFT Calculations, in Vitro DNA Binding and Cleavage Studies of Potential Chemotherapeutic Diorganotin(IV) Mandelates. *J. Photochem. Photobiol. , B Biol.* **2016**, *162*, 348–360.

(85) Yang, Y.; Hong, M.; Xu, L.; Cui, J.; Chang, G.; Li, D.; Li, C. Organotin(IV) Complexes Derived from Schiff Base N'-[(1E)-(2-Synthesis, *In Vitro* Cytotoxicities and DNA/BSA Interaction. *J. Organomet. Chem.* **2016**, *804*, 48–58.

(86) Arjmand, F.; Yousuf, I. Synthesis , Characterization and *In Vitro* DNA Binding of Chromone Schiff Base Organotin(IV) Complexes. *J. Organomet. Chem.* **2013**, *743*, 55–62.

(87) Sirajuddin, M.; Ali, S.; Mckee, V.; Sohail, M.; Pasha, H. Potentially Bioactive Organotin(IV) Compounds : Synthesis, Characterization, *In Vitro* Bioactivities and Interaction with SS-DNA. *Eur. J. Med. Chem.* **2014**, *84*, 343–363.

(88) Lee, S.; Chung, J.; Won, H.; Lee, D.; Lee, Y. Analysis of Antifouling Agents after Regulation of Tributyltin Compounds in Korea. *J. Hazard. Mater.* **2011**, *185*, 1318–1325.

(89) Ventrella, V.; Nesci, S.; Trombetti, F.; Bandiera, P.; Pirini, M.; Borgatti, A. R.; Pagliarani, A. Comparative Biochemistry and Physiology, Part C Tributyltin Inhibits the Oligomycin-Sensitive Mg-ATPase Activity in Mytilus Galloprovincialis Digestive Gland Mitochondria. *Comp. Biochem. Physiol. Part C* **2011**, *153* (1), 75–81.

(90) Girasolo, M. A.; Di, C.; Schillaci, D.; Barone, G.; Silvestri, A.; Ruisi, G. Synthesis, Characterization, and in Vitro Antimicrobial Activity of Organotin(IV) Complexes with Triazolo-Pyrimidine Ligands Containing Exocyclic Oxygen Atoms. *J. Organomet. Chem.* **2005**, *690*, 4773–4783.

(91) Xanthopoulou, M. N.; Kourkoumelis, N.; Hadjikakou, S. K.; Hadjiliadis, N.; Kubicki, M.; Karkabounas, S.; Bakas, T. Structural and Biological Studies of Organotin(IV) Derivatives with 2-Mercapto-Benzoic Acid and 2-Mercapto-4-Methyl-Pyrimidine. *Polyhedron* **2008**, *27*, 3318–3324.

(92) Xanthopoulou, M. N.; Hadjikakou, S. K.; Hadjiliadis, N.; Milaeva, E. R.; Gracheva, J. A.; Tyurin, V. Y.; Christoforidis, N.; Christoforidis, K. C.; Metsios, A. K.; Karkabounas, S. K. C. Biological Studies of New Organotin(IV) Complexes of Thioamide Ligands. *Eur. J. Med. Chem.* **2008**, *43*, 327–335.

(93) Hansch, C.; Verma, R. P. Larvicidal Activities of Some Organotin Compounds on Mosquito Larvae: A QSAR Study. *Eur. J. Med. Chem.* **2009**, *44*, 260–273.

(94) Kashif, M.; Khan, S.; Shah, A.; Butler, I. S. Anticancer Activity of Organotin(IV) Carboxylates. *Inorganica Chim. Acta* **2014**, *423*, 14–25.

(95) Affan, A.; Wan Foo, S.; Jusoh, I.; Hanapi, S.; Tiekink, E. R. T. Inorganica Chimica Acta Synthesis, Characterization and Biological Studies of Organotin(IV) Complexes with Hydrazone Ligand. *Inorganica Chim. Acta* **2009**, *362*, 5031–5037.

(96) Arjmand, F.; Sayeed, F. Synthesis, Characterization and DNA-Binding Studies of Mono and Heterobimetallic Complexes Cu-Sn_2/Zn-Sn_2 and Their DNA Cleavage Activity. *J. Mol. Struct.* **2010**, *965*, 14–22.

(97) Alama, A.; Tasso, B.; Novelli, F.; Sparatore, F. Organometallic Compounds in Oncology: Implications of Novel Organotins as Antitumor Agents. *Drug Discov. Today* **2009**, *14* (9-10), 500–508.

(98) Hynes, M. J.; Keely, J. M.; McManus, J. Investigation of the Hydrolysis of $[Sn(CH_3)_3(H_2O)_2]^+$ in Aqueous Solution by Sn-119 Nuclear Magnetic Resonance Spectroscopy. *J. Chem. Soc. Dalt. Trans.* **1991**, 3427–3429.

(99) Nath, M.; Sulaxna Potentiometric and Multinuclear NMR Investigations of Di-/trimethyltin(IV) Cations with Some Heterocyclic Thiones in Aqueous Media. *New J. Chem.* **2007**, *31*, 418.

(100) De Robertis, A.; Gianguzza, A.; Giuffrè, O.; Pettignano, A.; Sammartano, S. Interaction of methyltin(IV) Compounds with Carboxylate Ligands. Part 1: Formation and Stability of methyltin(IV)-Carboxylate Complexes and Their Relevance in Speciation Studies of Natural Waters. *Appl. Organomet. Chem.* **2006**, *20*, 89–98.

(101) Shoukry, M. M.; Hassan, S. S. Speciation Studies of Diorganotin(IV) Complexes with 3, 3-Bis(1-Methylimidazol-2-yl)propionate. Displacement Reaction by DNA Constituents. *Sci. J.* **2013**, *2013*, 1–7.

(102) Barbieri, R.; Silvestri, A. The Hydrolysis of $Me_2Sn(IV)$ and $Me_3Sn(IV)$ Moieties Monitored through ^{119}Sn Mössbauer Spectroscopy. *Inorganica Chim. Acta* **1991**, *188*, 95–98.

(103) Cigala, R. M.; Stefano, C. De; Giacalone, A.; Gianguzza, A.; Sammartano, S. Hydrolysis of Monomethyl, Dimethyl, and Trimethyltin(IV) Cations in Fairly Concentrated Aqueous Solutions at I = 1 $MolL^{-1}$ ($NaNO_3$) and T=298.15 K. Evidence for the Predominance of Polynuclear Species. **2011**, *56*, 1108–1115.

(104) Pellerito, L.; Nagy, L. Organotin(IV)$^{n+}$ Complexes Formed with Biologically Active Ligands: Equilibrium and Structural Studies, and Some Biological Aspects. *Coord. Chem. Rev.* **2002**, *224*, 111–150.

(105) Mukerjee, G. N.; Chattopadhyay, S. K.; Sarkar, S. Metal Complexes of some Model Peptides Derivatives. 11. Mixed Ligand Complexes Formation of Copper(II) with Salicyloyglycine and Typical Lignads, *J. Indian Chem. Soc.* **1994**, *71*, 45–48.

(106) Hussain, M.; Ahmad, M. S.; Altaf, M.; Stoeckli-evans, H.; Ali, S. Structural and Biological Studies of New Monomeric, Tetrameric, and Polymeric Organotin(IV) Esters of 3-(Benzo[D][1,3] dioxol-4-yl) Propanoic Acid. *J. Coord. Chem.* **2013**, *66*, 868–880.

(107) Sedaghat, T.; Tarassoli, A.; Ansari-asl, Z.; Motamedi, H. Water Soluble Organotin (IV) Complexes with Girard-T Reagent-Based Hydrazones : Synthesis, Spectral Characterization, and Antibacterial Activity. *J. Coord. Chem.* **2013**, *66*, 2549–2557.

(108) Singh, H. L.; Singh, J.; Chauhan, S. S.; Mukherjee, A.; Dewa, T. Research Article Synthetic, Structural, Theoretical and Biological Study of Triorganotin(IV) Schiff Base Complexes Derived from Amino Acids. *J. Chem. Pharm. Res.* **2014**, *6*, 248–257.

(109) Sirajuddin, M.; Ali, S.; Ali, F. S.; Shah, F. A.; Ahmad, M.; Tahir, N. M. Potential Bioactive Vanillin–Schiff Base Di- and Tri-Organotin(IV) Methoxyphenol : Synthesis , Characterization and Biological Screenings. *J. Iran. Chem. Soc.* **2014**, *11*, 297–313.

(110) Shah, F. A.; Sabir, S.; Fatima, K.; Ali, S.; Qadri, I.; Rizzoli, C. Organotin(IV) Based Anti-HCV Drugs: Synthesis, Characterization and Biochemical Activity. *Dalt. Trans.* **2015**, *44*, 10467–10478.

(111) Shah F. A.; Fatima, K.; Sabir, S.; Ali, S.; Qadri, I.; Din, N. Ud. Design, Synthesis, Structure Information and Biochemical Activity of New Fluoro Substituted Organotin(IV) Carboxylates. *J. Photochem. Photobiol. B Biol.* **2016**, *154*, 99–107.

(112) Barreiro, S.; Duran-Carril, M. L.; Viqueira, J.; Sousa-Pedrares, A.; García-Vazquez, J. A.; Romero, J. Structural Studies and Bioactivity of Diorganotin (IV) Complexes of Pyridin-2-thionato Derivatives. *J. Organomet. Chem.* **2015**, *791*, 155–162.

(113) Salam, M. A.; Arafath, A.; Hussein, M. A.; Basri, R. Organotin(IV) Complexes with 2-ethylthiosemicarbazone : Synthesis, Characterization, and in Vitro Antibacterial Activity. *Phosphorus, Sulfur, and Silicon* **2016**, *191*, 1101–1107.

(114) Khandani, M.; Sedaghat, T.; Erfani, N.; Reza, M.; Khavasi, H. R. Synthesis, Spectroscopic Characterization, Structural Studies and Antibacterial and Antitumor Activities of Diorganotin Complexes with 3-methoxysalicylaldehyde thiosemicarbazone. *J. Mol. Struct.* **2013**, *1037*, 136–143.

(115) Devi, J.; Kumari, S.; Asijaa, S.; Malhotra, R. Synthetic, Spectroscopic, and Biological Aspects of Triorganosilicon(IV) Complexes of Tridentate Schiff Bases. *Phosphorus, Sulfur, and Silicon* **2012**, *187*, 1409–1417.

(116) Devi, J.; Devi, S.; Kumar, A. Synthesis, Characterization, and Quantitative Structure–Activity Relationship Studies of Bioactive Dehydroacetic Acid and Amino Ether Schiff Base Complexes. *Heteroat. Chem.* **2016**, 361–371.

(117) Chohan, Z. H.; Scozzafava, A.; Supuran, C. T. Zinc Complexes of Benzothiazole-Derived Schiff Bases with Antibacterial Activity. *J. Enzyme Inhib. Med. Chem.* **2003**, *18*, 259–263.

(118) Singh, H. L.; Singh, J. B.; Bhanuka, S. Synthesis, Spectroscopic Characterization, Biological Screening, and Theoretical Studies of organotin(IV) Complexes of Semicarbazone and Thiosemicarbazones Derived from (2-hydroxyphenyl)(pyrrolidin-1-yl)methanone. *Res. Chem. Intermed.* **2016**, *42*, 997–1015.

(119) Gholivand, K.; Asghar, A.; Gholami, A.; Dusek, M.; Eigner, V.; Abolghasemi, S. Synthesis, Characterization, Crystal Structures, QSAR Study and Antibacterial Activities of Organotin Bisphosphoramidates. *J. Organomet. Chem.* **2016**, *806*, 33–44.

(120) Barbosa, S. A. L.; Guedes, de J. S.; Silva, R. D. da; Meneghetti, M. S. P.; Meneghetti, M. R.; Silva, E. A. da; Araujo, M. V. de; Moreira, M. S. A.; Aquino, T. M. de; Jr. Siqueria, J. P. de S.; et al. Synthesis and Evaluation of the Antibiotic and Adjuvant Antibiotic Potential of Organotin(IV) Derivatives. *J. Inorg. Biochem.* **2018**, *180*, 80–88.

(121) Mahanty, S.; Raghav, D.; Rathinasamy, K. Chemosphere *In Vitro* Evaluation of the Cytotoxic and Bactericidal Mechanism of the Commonly used Pesticide Triphenyltin hydroxide. *Chemosphere* **2017**, *183*, 339–352.

(122) Bom, L. F. O.; Oliveira, M. R. L.; Miranda, L. D. L.; Vidigal, A. E. C.; Guilardi, S.; Souza, R. A. C.; Ellena, J.; Rubinger, M. M. M. Syntheses , Characterization and Antifungal Activity of Novel Dimethylbis(N-R-sulfonyldithiocarbimato)stannate(IV) Complexes. *J. Mol. Struct.* **2017**, *1129*, 60–67.

(123) Tabassum, S.; Ahmad, R.; Arjmand, F.; Sen, S.; Kayal, J.; Juvekar, A. S.; Zingde, S. M. Synthesis and Characterization of Glycoconjugate Tin(IV) Complexes: *In Vitro* DNA Binding Studies, Cytotoxicity, and Cell Death. *J. Organomet. Chem.* **2011**, *696*, 1600–1608.

(124) Tabassum, S.; Mathur, S.; Arjmand, F.; Mishrab, K.; Banerjee, K. Design, Synthesis, Characterization and DNA-Binding Studies of a Apoptosis Inducer: In Vitro and in Vivo Assessment of Induction of Apoptosis by GATPT. *Metallomics* **2012**, *4*, 205–217.

(125) Khan, R. A.; Yadav, S.; Hussain, Z.; Arjmand, F.; Tabassum, S. Human Topoisomerase I α Inhibitor and Their Antiproliferative Effects against the Human Cell Line. *Dalton Trans.* **2014**, *43*, 2534–2548.

(126) Shang, X.; Meng, X.; Alegria, E. C. B. A.; Li, Q.; Guedes, C.; Kuznetsov, M. L.; Pombeiro, A. J. L. Syntheses, Molecular Structures, Electrochemical Behavior, Theoretical Study, and Antitumor Activities of Organotin(IV) Complexes Containing 1-(4-chlorophenyl)-1-cyclopentanecarboxylato Ligands. *Inorg. Chem.* **2011**, *50*, 8158–8167.

(127) Shang, X.; Ding, N.; Xiang, G. European Journal of Medicinal Chemistry Novel Di-*n*-Butyltin(IV) Derivatives : Synthesis , High Levels of Cytotoxicity in Tumor Cells and the Induction of Apoptosis in KB Cancer Cells. *Eur. J. Med. Chem.* **2012**, *48*, 305–312.

(128) Pruchnik, H.; Lis, T.; Latocha, M.; Zielińska. A.; Pruchnik, F. P. Novel Organotin Complexes Containing the 2,2-bipyridine-3,3,6,6-tetracarboxylate. Helical Supramolecular Structure and Cytostatic Activity. *J. Organomet. Chem.* **2015**, *777*, 81–87.

(129) Arjmand, F.; Sharma, S.; Usman, M.; Leu, B. M.; Hu, M. Y.; Toupet, L.; Gosztola, D.; Tabassum, S. Vibrational Dynamics (IR, Raman, NRVS) and a DFT Study of a New Antitumor Tetranuclearstannoxane Cluster, Sn((IV)-oxo-{di-o-vanillin}dimethyl dichloride. *Phys. Chem. Chem. Phys.* **2016**, *18*, 17805–17809.

(130) Shpakovsky, D. B.; Banti, C. N.; Beaulieu-Houle, G.; Kourkoumelis, N.; Manoli, M. J.; Manos, Tasiopoulos, A. J.; Hadjikakou, S. K.; Milaeva, E. R.; Charalabopoulos, K.; Bakas, T.; et al. Synthesis, Structural Characterization and *In Vitro* Inhibitory Studies Against Human Breast Cancer Of The Bis-(2,6-di-tert-butylphenol)tin(IV) dichloride and its Complexes. *Dalt. Trans.* **2012**, *41*, 14568–14582.

(131) Basu, T. S.; Dutta, D.; Duthie, A.; Guchhait, N.; Rocha, B. G. M.; Guedes, M. F. C.; Mokhamatam, R. B.; Raviprakash, N.; Manna, S. K. New Dibutyltin(IV) Ladders: Syntheses, Structures and, Optimization and Evaluation of Cytotoxic Potential Employing A375 (Melanoma) and HCT116 (Colon Carcinoma) Cell Lines in Vitro. *J. Inorg. Biochem.* **2017**, *166*, 34–48.

(132) Tsanaktsidis, I.; Batistatou, A.; Zelovitis, J.; Simos, Y. V; Ragos, V.; Karkabounas, S.; Peschos, D. Chemistry, Cytotoxic Effect, Antitumour Activity and Toxicity of Organotin Derivatives with Ortho- or Para-Hydroxy-benzoic Acids. *Med. Chem. Res.* **2011**, *7*. DOI 10.1007/s00044-018-2135-7

(133) Wang, H.; Hu, L.; Du, W.; Tian, X.; Zhang, Q.; Hu, Z.; Luo, L.; Zhou, H.; Wu, J.; Tian, Y. Two-Photon Active Organotin(IV) Carboxylate Complexes for Visualization of Anticancer

Action. *ACS Biomater. Sci. engneering* **2017**, *3*, 836–842.

(134) Navakoski, K.; Oliveira, D.; Andermark, V.; Onambele, L. A.; Dahl, G.; Prokop, A.; Ott, I. Organotin Complexes Containing Carboxylate Ligands with Maleimide and Naphthalimide Derived Partial Structures : TrxR Inhibition, Cytotoxicity and Activity in Resistant Cancer Cells. *Eur. J. Med. Chem.* **2014**, *87*, 794–800.

(135) Xiao, X.; Liang, J.; Xie, J.; Liu, X.; Zhu, D.; Dong, Y. Organotin(IV) Carboxylates Based on 2-(1,3-dioxo-1H-benzo[de]isoquinolin-2(3H)-yl)acetic acid : Syntheses, Crystal Structures, Luminescent Properties and Antitumor Activities. *J. Mol. Struct.* **2017**, *1146*, 233–241.

(136) Rojas-oviedo, I.; Camacho-camacho, C.; Sánchez-sánchez, L.; Cárdenas, J.; López-muñoz, H.; Eugenio-robledo, H.; Velázquez, I.; Alfredo, R. Synthesis and Characterization of Tributyltin Derivatives from 4-Oxo-4-(arylamino)butanoic acids and their in vitro Biological Activity against Cervical Cancer Cell Lines. *Appl. Organomet. Chem.* **2014**, *28*, 884–891.

(137) Shpakovsky, D. B.; Banti, C. N.; Mukhatova, E. M.; Osipova, V. P.; Berberova, N. T.; Albov, D. V; Antonenko, T. A.; Milaeva, E. R.; Hadjikakou, S. K. Synthesis, Antiradical Activity and in Vitro Cytotoxicity of Novel Organotin Complexes Based on 2,6-di-tert-butyl-4-mercaptophenol. *Dalt. Trans.* **2014**, *43*, 6880–6890.

(138) Xu, L.; Hong, M.; Yang, Y.; Cui, J.; Li, C. Synthesis, Structural Characterization, *In Vitro* Cytotoxicities, and BSA Interaction of Diorganotin(IV) Complexes Derived from Salicylaldehyde Nicotinoyl Hydrazone. *J. Coord. Chem.* **2016**, *8972*, 1–12.

(139) Salam, M. A.; Hussein, M. A.; Ramli, I.; Islam, S. Synthesis , Structural Characterization, and Evaluation of Biological Activity of Organotin(IV) Complexes with 2-hydroxy-5-methoxybenzaldehyde-N(4)-methylthiosemicarbazone. *J. Organomet. Chem.* **2016**, *813*, 71–77.

(140) Yang, Y.; Hong, M.; Xu, L.; Cui, J.; Chang, G.; Li, D.; Li, C. Z. Organotin(IV) Complexes Derived from Schiff Base N'-[(1E)-(2-Hydroxy-3-Methoxyphenyl) methylidene]pyridine-3-Carbohydrazone: Synthesis, *In Vitro* Cytotoxicities and DNA/BSA Interaction. *Eur. J. Med. Chem.* **2014**, *86*, 550–561.

(141) Jankovics, H.; Nagy, L.; Kele, Z.; Pettinari, C.; D'Agati, P.; Mansueto, C.; Pellerito, C.; Pellerito, L. Coordination Properties of the ACE Inhibitor Captopril towards $Me_2Sn(IV)^{2+}$ in Aqueous Solution, and Biological Aspects of Some dialkyltin(IV) Derivatives of this Ligand. *J. Organomet. Chem.* **2003**, *668* (1-2), 129–139.

(142) Nath, M.; Sulaxna,; Song, X.; Eng, G. New Di- and Triorganotin(IV) Tyrosylalaninates as Models for Metal-Protein Interactions: Synthesis, Structural Characterization, and Potentiometric Studies of Tyrosylalanine, Glycyltyrosine, and Glycylisoleucine with Di- and Trimethyltin(IV) Moieties in Aqueous Medium. *ISRN Spectrosc.* **2012**, *2012*, 1–13.

(143) Shoukry, M. M. Equilibrium Studies of the diorganotin(IV) Complexes with Some Amino Acids and Related Compounds. *Talanta* **1996**, *43*, 177–183.

(144) Jancsó, A.; Nagy, L.; Moldrheim, E.; Sletten, E. Potentiometric and Spectroscopic Evidence for Coordination of Dimethyltin. *J. Chem. Soc., Dalt. Trans.* **1999**, 1587–1594.

(145) Danish, M.; Raza, M. A.; Ilyas, T.; Sharif, A.; Anjum, N. Metal Complexes and Organotin(IV) Compounds of Cefixime and their Biological Study. *Med. Chem.* **2015**, *5*, 373–377.

(146) Roy, S.; Hagen, K. D.; Maheswari, P. U.; Lutz, M.; Spek, A. L.; Reedijk, J.; Van Wezel, G. P. Phenanthroline Derivatives with Improved Selectivity as DNA-Targeting Anticancer or Antimicrobial Drugs. *Chem. Med. Chem.* **2008**, *3*, 1427–1434.

(147) Garza-ortiz, A.; Camacho-camacho, C.; Sainz-espuñes, T.; Rojas-oviedo, I.; Gutiérrez-lucas, L. R.; Carrillo, A. G.; Ramirez, M. A. V. Novel Organotin(IV) Schiff Base Complexes with Histidine Derivatives : Synthesis, Characterization, and Biological Activity. *Bioinorg. Chem. Appl.* **2013**, *2013*, 1–12.

(148) Stefano, R. Di; Scopelliti, M.; Pellerito, C.; Casella, G.; Fiore, T.; Stocco, G. C.; Vitturi, R.; Colomba, M.; Ronconi, L.; Sciacca, I. D.; et al. Organometallic Complexes with Biological Molecules. XVIII. Alkyltin(IV) Cephalexinate Complexes: Synthesis, Solid State and Solution Phase Investigations. *J. Inorg. Biochem.* **2004**, *98* (3), 534–546.

(149) Stefano, R. Di; Scopelliti, M.; Pellerito, C.; Fiore, T.; Vitturi, R.; Colomba, M. S.; Gianguzza, P.; Stocco, G. C.; Consiglio, M.; Pellerito, L. Organometallic Complexes with Biological Molecules XVII. Triorganotin(IV) Complexes with Amoxicillin and Ampicillin. *J. Inorg. Biochem.* **2002**, *89*, 279–292.

(150) Pellerito, A.; Fiore, T.; Pellerito, C.; Fontana, A.; Di Stefano, R.; Pellerito, L.; Cambria, M. T.; Mansueto, C. Organometallic Complexes with Biological Molecules, VI. Diorganotin(IV) and Triorganotin(IV) Ampicillin and Methicillin Derivatives: Spectroscopic Investigations in the Solid State. *J. Inorg. Biochem.* **1998**, *10*, 2–4.

(151) Kovala-demertzi, D.; Kourkoumelis, N.; Koutsodimou, A. Synthesis and Spectroscopic Studies of Diorganotin Derivatives with Tolfenamic Acid. Crystal and Molecular Structure of the First complex of tolfenamic acid, 1,2:3,4-di-μ_2-2-[(3-chloro-2-methylphenyl)amino]-benzoato-*O,O*-1,3-bis-2-[(3-chloro-2-methylphenyl)amino] benzoato-*O*-1,2,4:2,3,4-di-μ_3-oxo-tetrakis[di-*n*-butyltin(IV)]. *J. Organomet. Chem.* **2001**, *620*, 194–201.

(152) Kourkoumelis, N.; Demertzis, M. A.; Kovala-demertzi, D.; Koutsodimou, A.; Moukarika, A. Preparations and Spectroscopic Studies of Organotin Complexes of Diclofenac. *Spectrochim. Acta Part A* **2004**, *60*, 2253–2259.

(153) Kovala-demertzi, D.; Dokorou, V.; Ciunik, Z.; Kourkoumelis, N.; Demertzis, M. A. Organotin Mefenamic Complexes Preparations, Spectroscopic Studies and Crystal Structure of a Triphenyltin Ester of Mefenamic Acid: Novel Anti-Tuberculosis Agents. *Appl. Organomet. Chem.* **2002**, *16*, 360–368.

(154) Kovala-demertzi, D.; Dokorou, V. N.; Jasinski, J. P.; Opolski, A.; Wiecek, J.; Zervou, M.; Demertzis, M. A. Organotin Flufenamates : Synthesis, Characterization and Antiproliferative Activity of Organotin Flufenamates. *J. Organomet. Chem.* **2005**, *690*, 1800–1806.

(155) Dokorou, V.; Primikiri, A.; Kovala-demertzi, D. The Triphenyltin(VI) Complexes of NSAIDs and Derivatives. Synthesis, Crystal Structure and Antiproliferative Activity. Potent Anticancer Agents. *J. Inorg. Biochem.* **2011**, *105*, 195–201.

(156) Galani, A.; Demertzis, M. A.; Kubicki, M.; Kovala-Demertzi, D. Organotin-Drug Interactions. Organotin Adducts of Lornoxicam, Synthesis and Characterisation of the First Complexes of Lornoxicam. *Eur. J. Inorg. Chem.* **2003**, *2003*, 1761–1767.

(157) Kovala-demertzi, D. Recent Advances on Non-Steroidal Anti-Inflammatory Drugs, NSAIDs: Organotin Complexes of NSAIDs. *J. Organomet. Chem.* **2006**, *691*, 1767–1774.

(158) Kovala-demertzi, D.; Dokorou, V.; Primikiri, A.; Vargas, R.; Silvestru, C.; Russo, U.; Demertzis, M. A. Organotin Meclofenamic Complexes : Synthesis, Crystal Structures and Antiproliferative Activity of the First Complexes of Meclofenamic Acid–Novel Anti-Tuberculosis Agents. *J. Inorg. Biochem.* **2009**, *103*, 738–744.

(159) Galani, A.; Kovala-demertzi, D.; Kourkoumelis, N.; Koutsodimou, A.; Dokorou, V.; Zbigniew, C.; Russo, U.; Demertzis, M. A. Organotin Adducts of Indomethacin : Synthesis, Crystal Structures and Spectral Characterization of the First Organotin Complexes of Indomethacin. *Polyhedron* **2004**, *23*, 2021–2030.

(160) Georgiou, E.; Ganiatsou, F.; Manos, M.; Tasiopoulos, A. J.; Karkabounas, S.; Hadjikakou, S. K. Biological Study of Diorganotin IV) Complex [Bu_2Sn $(Naproxen)_2$] with the Anti-Inflammatory Naproxen as Ligand . *12th Eurasia Conf. Chem. Sci. Greece* **2012**, 10.

(161) Gupta, M. K.; Singh, H. L.; Varshney, S.; Varshney, A. K. Synthetic and Spectroscopic Characterization of Organotin(IV) Complexes of Biologically Active Schiff Bases Derived from Sulpha Drugs. *Bioinorg. Chem. Appl.* **2003**, *1*, 309–320.

(162) Kaur, H.; Dhir, K.; Kaur, J.; Mittu, B.; Chuhan, A. Synthesis and Evaluation of diorganotin(IV) and triorganotin(IV) Derivatives of Aspirin, Paracetamol and Metronidazole as Antimicrobial Agents. *Am. J. Drug Discov. Dev.* 2013, *3*, 13–22.

(163) Shahzadi, S.; Shahid, K.; Ali, S.; Mazhar, M.; Badshah, A.; Ahmed, E.; Malik, A. Non-Steroidal Anti-Inflammatory Drugs (NSAIDs) as Donor Ligands in organotin(IV) Derivatives: Synthesis, Spectroscopic Characterization and Biological Applications. *Turk. J. Chem.* **2005**, *29*, 273–287.

(164) Jalal, A.; Shahzadi, S.; Shahid, K.; Ali, S.; Badshah, A.; Mazhar, M.; Khan, K. M. Preparation, Spectroscopic Studies and Biological Activity of Mono-Organotin(IV) Derivatives of Non-Steroidal Anti-Inflammatory Drugs. *Turk. J. Chem.* **2004**, *28*, 629–644.

(165) Reicmann, M. E.; Rice, S. A.; Thomas, C. A.; Doty, P. A Further Examination of the Molecular Weight and Size of Desoxypentose Nucleic Acid. *J. Am. Chem. Soc.* **1954**, *76*, 3047–3053.

(166) Frisch, M. J.; Trucks, G. W.; Schlegel, H. B.; Scuseria, G. E.; Robb, M. A.; Cheeseman, J.R.; Scalmani, G.; Barone, V.; Mennucci, B.; Petersson, G. A.; Nakatsuji, H.; Caricato, M;. Li, X.; Hratchian, H. P.; Izmaylov, A. F.; Blno, J.; Zheng, G.; Sonnenberg, J. L.;

Hada, M.; Ehara, M. et. al., Gaussian 09, (Revision A.02), Gaussian, Inc., Wallingford, CT, **2009**.

(167) Hay, P. J.; Wadt, W. R. Ab Initio Effective Core Potentials for Molecular Calculations. Potentials for K to Au Including the Outermost Core Orbitals. *J. Chem. Phys.* **1985**, *82*, 299–310.

(168) Poller, R. C. "The Chemistry of Organotin Compounds, *Logos Press Limited, London,* **1970**, 1-315; and references cited therein.

(169) Altomare, A.; Cascarano, G.; Giacovazzo, C.; Guagliardi, A.; Burla, M. C.; Polidori, G.; Camalli, M. SIRPOW.92. A Program for Automatic Solution of Crystal Structures by Direct Methods Optimized for Powder Data, *J. Appl. Crystallogr*. **1994,** *27*, 435–436.

(170) Sheldrick, G. M. SHELX-97, Program for the Solution and Refinement of Crystal Structures. *University of Göttingen, Germany*, **1997**.

(171) Mosmann, T. Rapid Colorimetric Assay for Cellular Growth and Survival: Application to Proliferation and Cytotoxicity Assays. *J. Immunol. Meth.* **1983**, *65*, 55–63.

(172) Takahashi, A.; Matsumoto, H.; Yuki, K.; Yasumoto, J. I.; Kajiwala, A.; Aoki, M.; Furusawa, Y.; Ohnishi, K.; Ohnishi, T. High-LET Radiation Enhanced Apoptosis but not Necrosis Regardless of p53 Status. *Int. J. Radiat. Oncol. Biol. Phy.* **2004**, *60*, 591–597.

(173) Sánchez-Alcázar, J. A.; Khodjakov, A.; Schneider, E. Anticancer Drugs Induce Increased Mitochondrial Cytochrome c Expression that Proceeds Cell Death. *Cancer Res*. **2001**, *61*, 1038–1044.

(174) Sánchez-Alcázar, J. A.; Ruíz-Cabello, J; Hernández-Muñoz, I.; Pobre, P. S.; De La Torre, P.; Siles-Rivas, E.; García, I.; Kaplan, O.; Moñoz-Yagüe, M. T.; Solís-Herruzo, J. A.; Tumor Necrosis Factor-α Increases ATP Content in Metabolically Inhibited L929 Cells Proceeding Cell Death. *J. Biol. Chem.* 1997, 272, 30167–30177.

(175) Kotsakis, D.; Hatzidaki, L.; Vamvakas, L.; Vardakis, N.; Kalykaki, A.; Bozionelou, V.; Androulakis. N.; Kalbakis, K.; Saridaki, Z.; Georgoulias, V.; Agelaki, S. A. Retrospective Analysis of Non-Platinum Based First- and Second-Line Chemotherapy in Patients with Advanced Non-Small Cell Lung Cancer. *Anticancer Res.* **2010**, *30*, 4335–4342.

(176) Nath, M.; Pokharia, S.; Yadav, R. Organotin(IV) Complexes of Amino Acids and Peptides. *Coord. Chem. Rev*. **2001**, *215*, 99–149.

(177) Gielen, M. Organotin Compounds and Their Therapeutic Potential: A Report from the Organometallic Chemistry Department of the Free University of Brussels. *Appl. Organomet*. **2002**, *16*, 481–494.

(178) Nath, M.; Eng, G.; Song, X.; Beraldo, H.; De Lima, G. M.; Pettinari, C.; Marchetti, F.; Whalen, M. M.; Beltrán, H. I.; Santillan, R.; Farfán, N. Medicinal/Biocidal Applications of

Tin Compounds and Environmental Aspects. In: Davies, A. G.; Gielen, M.; Pannell, K. H.; Tiekink, E. R. T.; Tin Chemistry Fundamentals, Frontiers, and Applications, Wiley, London, 2008.

(179) Natsume, T.; Aizawa, S.; Hatano, K.; Funahashi, S. Hydrolysis, Polymerization, and Structure of Dimethyltin(IV) in Aqueous Solution. Molecular Structure of the Polymer $[(SnMe_2)_2(OH)_3]ClO_4$. *J. Chem. Soc. Dalton Trans.* **1994**, 2749–2753.

(180) Al-Najjar, A. A.; Shehata, M. R.; Mohamed, M. M. A.; Shoukry, M, M. Equilibrium Studies of Organotin (IV) Complexes of Peptides. *Main Group Met. Chem*. **1999**, *22*, 253–261.

(181) Musmeci, M. T.; Madonia, G.; Giudice, M. T. L.; Silvestri, A.; Ruisi, G.; Barbieri, R. Interactions of Organotins with Biological Systems. *Appl. Organometal. Chem*. **1992**, *6*, 127–138.

(182) Obrocea, M. M.; Nassim, M. A.; Molepo, M. J.; Shirazi, F. H. Gallant, G.; Dulud, H.; Vincent M. D.; Stewart, D. J.; Goel, R. *In vitro* Carboplatin-MESNA Interaction in Aqueous Solution, Human Plasma and Urine. *Oncol. Rep*. **1998**, *5*, 1493–1498.

(183) Leeuwenkamp, O. R.; Neijt, J. P.; Van der Vijgh, W. J.; Pinedo, H. M. Reaction Kinetics of Cis-platin and its Monoaquated Species with the Modulating Agents DiMesna and Thiosulphate, *Eur. J. Cancer* **1991**, *27*, 1243–1247.

(184) Petrov, A. I.; Golovnev, N. N.; Dergachev, I. D.; Leshok, A. A. Complex Formation of Bismuth(III) with 2-mercaptoethanesulfonic and 3-mercaptopropanesulfonic Acids: Experimental and Theoretical Study. *Polyhedron* **2013**, *50*, 59–65.

(185) Capitran-Vallvey, L. F.; Mirron, M. C. V.; Acosta, R. A. Chemiluminescence Determination of Sodium 2-mercaptoethane sulfonate by Flow Injection Analysis Using Cerium(IV) Sensitized by Quinine. *Talanta* **2000**, *51*, 1155–1161.

(186) Martin, D.; Piera, C.; Mazzi, U.; Rossin, R.; Solans, X.; Font-Bardiad, M.; Suades, J. Rhenium and Technetium-99m Complexes with Coenzyme M (MESNA), *Dalton Trans.* **2003**, 3041–3045.

(187) El-Sherif, A. A. Solution Coordination Chemistry of Organotin(IV) Cations with Bio-Relevant Ligands. *J. Solution Chem.* **2012**, *41*, 1522–1554.

(188) Takahashi, A.; Natsume, T.; Koshino, N.; Funahashi, S.; Inada, Y.; Takagi, H. D. Speciation of Trimethyltin(IV): Hydrolysis, Complexation Equilibria, and Structures of Trimethyltin(IV) Ion in Aqueous Solution, *Can. J. Chem*. **1997**, *75*, 1084–1092.

(189) Mohamed, M. M. A.; Shoukry, M. M. Interaction of Diphenyltin(IV) Dichloride With Some Selected Bioligands. *Chem. Pharm. Bull*. **2001**, *49*, 253–257.

(190) Mridula, Nath, M. Equilibrium and Multinuclear NMR Spectroscopic Studies of Di- And Trimethyltin(IV) Moieties with Hydroxycarboxylic Acids in Aqueous Medium. *J. Solution Chem.* **2016**, *45*, 445–462.

(191) Nath, M.; Jairath, R.; Mukherjee, G. N.; Das, A. Speciation of Dimethyltin(IV) and Trimethyltin(IV) Cations with Some Biologically Important Ligands in Aqueous Medium: A Potentiometric Investigation. *Indian J. Chem*. **2005**, *44A*, 1602–1607.

(192) Buck-Koehntop, B. A.; Porcelli, F.; Lewin, J. L.; Cramer, C. J.; Veglia, G. Biological Chemistry of Organotin Compounds: Interactions and Dealkylation by Dithiols. *J. Organomet. Chem.* **2006**, *691*, 1748–1755.

(193) Danehy, J. P.; Parameswaran, K. N. Acidic Dissociation Constants of Thiols. *J. Chem. Eng. Data*, **1968**, *13*, 386–389. **doi:** 10.1021/je60038a025.

(194) De Stefano, C.; Foti, C.; Gianguzza, A.; Martino, M.; Pellerito, L.; Sammartano, S. Hydrolysis of $(CH_3)_2Sn^{2+}$ in Different Ionic Media: Salt Effects and Complex Formation. *J. Chem. Eng. Data* **1996**, *41*, 511–515.

(195) De Stefano, C.; Foti, C.; Gianguzza, A.; Millero, F. J. Sammartano, S. Hydrolysis of $(CH_3)_3Sn^{+}$ in Various Salt Media. *J. Solution Chem.* **1999**, *28*, 959–972.

(196) Lockhart, T. P.; Manders, W. F. Structure Determination by NMR Spectroscopy. Correlation of $[^{2}J(^{119}Sn\text{-}^{1}H)]$ and the Me–Sn–Me Angle in Methyltin(IV) Compounds. *Inorg. Chem.* **1986**, *25*, 892–895.

(197) Surdy, P.; Rubini, P.; Buzás, N.; Henry, B.; Pellerito, L.; Gajda, T. Interaction of Dimethyltin(IV)$^{2+}$ Cation with Gly-Gly, Gly-His, and Some Related Ligands. A New Case of a Metal Ion Able to Promote Peptide Nitrogen Deprotonation in Aqueous Solution. *Inorg. Chem.* **1999**, *38*, 346–352.

(198) Holeček, J.; Nádvorník, M.; Handlíř, M.; Lyčka, A. ^{13}C and ^{119}Sn NMR Spectra of di-n-butyltin(IV) Compounds. *J. Organomet. Chem*. **1986**, *315*, 299–308.

(199) Jankovics, H.; Nagy, L.; Buzas, N.; Pellerito, L.; Barbieri, R. Coordination Properties of adenosine-5'-monophosphate and Related Ligands Towards $Me_2Sn(IV)^{2+}$ in Aqueous Solution. *J. Inorg. Biochem.* **2002**, *92*, 55–64.

(200) Hynes, M. J.; O'Dowd, M. Interaction of Trimethyl(IV) Cation With Carboxylic Acid, Amino Acid and Related Ligands. *J. Chem. Soc. Dalton Trans.* **1987**, 563–566.

(201) Noffke, A.L.; Habtemariam, A.; Pizarro, A. M.; Sadler, P. J. Designing Organometallic Compounds for Catalysis and Therapy. *Chem. Commun.* **2012**, *48*, 5219–5246.

(202) Yadav, S.; Yousuf, I.; Usman, M.; Ahmad, M.; Arjmand, F.; Tabassum S. Chemical and Biotechnological Developments in Organotin Cancer Chemotherapy. *RSC Adv*. **2015**, *5*, 50673–50690.

(203) Samuel, M. P.; Vos, de D.; Raveendra, D.; Sarma, J. A. R. P.; Roy, S. 3-D QSAR Studies on New Dibenzyltin(IV) Anticancer Agents by Comparative Molecular Field Analysis (CoMFA). *Bioorg. Med. Chem. Lett.* **2002**, *12*, 61–64.

(204) Siegmann-Louda, W. D.; Carraher, E. C., Jr.; Pflueger, F.; Coleman, J.; Harless, S.; Luing, H. Functional Condensation Polymers, *Polym. Mater. Sci. Eng.* **2000**, *82*, 83–88.

(205) Xanthopoulou, M. N.; Hadjikakou, S. K.; Hadjiliadis, N.; Kourkoumelis, N.; Milaeva, E. R. Gracheva, Yu. A.; Tyurin, Yu V.; Verginadis, I.; Karkabounas, S.; Baril, M.; Butler, I. S. Biological Studies of Organotin(IV) Complexes with 2-mercaptopyrimidine. *Russ. Chem. Bull.* **2007**, *56*, 767–773.

(206) Hadjikakou, S. K.; Ozturk, I. I.; Xanthopoulou, M. N.; Zachariadis, P.C.; Zartilas, S.; Karkabounas, S.; Hadjiliadis, N. Synthesis, Structural Characterization and Biological Study of New Organotin(IV), Silver(I) and Antimony(III) Complexes with Thioamides. *J. Inorg. Biochem.* **2008**, *102*, 1007–1015.

(207) Al-Allaf, T. A. K.; Rashan, L. J.; Stelzner, A.; Powell, D.R. Organotin(IV) Complexes with Various Donor Ligands and their Cytotoxicity Against Tumour Cell Lines. Part(I): R_2SnCl_2 With Schiff Bases; Unusual C=N Bond Cleavage of the Bases and X-Ray Structures of the Ionic Products Formed. *Appl. Organomet. Chem.* **2003**, *17*, 891–897.

(208) Sirajuddin, M.; Ali, S.; Badshah, A. Drug–DNA Interactions and their Study by UV–Visible, Fluorescence Spectroscopies and Cyclic Voltammetry. *J. Photochem. Photobiol. B, Biol.* **2013**, *124*, 1–19.

(209) Aluise, C. D.; Miriyala, S. Noel, T.; Sultana, R.; Jungsuwadee, P.; Taylor, T. J.; Cai, J.; Pierce, W. M.; Vore, M.; Moscow, J. A.; St Clair, D. K.; Butterfield, D. A. 2-mercaptoethane sulfonate Prevents Doxorubicin-Induced Plasma Protein Oxidation and TNF-A Release: Implications for the Reactive Oxygen Species-Mediated Mechanisms of Chemobrain. *Free Radic. Biol. Med.* **2011**, *50*, 1630–1638.

(210) Li, X.; Yang, S.; Lv, X.; Sun, H.; Weng, J.; Liang, Y.; Zhou, D. The Mechanism of Mesna in Protection from Cisplatin-Induced Ovarian Damage in Female Rats. *J. Gynecol. Oncol.* **2013**, *24*, 177–185.

(211) Ypsilantis, P.; Tentes, I.; Lambropoulou, M.; Anagnostopoulos, K.; Papadopoulos, N.; Kortsaris, A.; Simopoulos, C. Prophylaxis With Mesna Prevents Oxidative Stress Induced by Ischemia Reperfusion in the Intestine *via* Inhibition of Nuclear Factor-Kappa β-Activation. *J. Gastroenterol. Hepatol.* **2008**, *23*, 328–335.

(212) Ludwig, U.; Riedel, M. K.; Backes, M.; Imhof, A.; Muche, R.; Keller, F. MESNA (Sodium 2-Mercaptoethanesulfonate) for Prevention of Contrast Medium-Induced Nephrotoxicity. *Clin. Nephrol.* **2011**, *75*, 302–308.

(213) Miller, R. P.; Tadagavadi, R. K.; Ramesh, G.; Reeves, W. B. Mechanisms of Cisplatin Nephrotoxicity. *Toxins* **2010**, *2*, 2490–2518.

(214) Amirshahrokhi, K.; Khalili, A. R. Gastroprotective Effect of 2-Mercaptoethane sulfonate Against Acute Gastric Mucosal Damage Induced by Ethanol. *Int. Immunopharmacolo.* **2016**, *34*, 183–188.

(215) Bergstrom, D. E.; Lin, X.; Wood, T.D.; Witvrouw, M. M.; Ikeda, S.; Andrei, G.; Snoeck, R.; Schols, D.; De Clercq, E. Polysulfonates Derived from Metal Thiolate Complexes as Inhibitors of HIV-1 and Various Other Enveloped Viruses *In Vitro*. *Antivir. Chem. Chemother*. **2002**, *13*, 185–189.

(216) Huber, F.; Roge, G.; Carl, L. Studies on the Anti-Tumour Activity of Di- and Tri-Organotin(Iv) Complexes of Amino Acids and Related Compounds, of 2-Mercaptoethanesulphonate and of Purine-6-thiol. *J. Chem. Soc. Dalton Trans.* **1985**, 523–527.

(217) Barbieri, R.; Silvestri, A.; Huber, F. A ^{l19}Sn Mössbauer Spectroscopic Study on Complexes of Di- and Tri-Organotin(1V) Moieties with 2-mercaptoethanesulfonates, in the solid state and in aqueous solution. *Appl. Organomet. Chem.* **1988**, *2*, 457–461.

(218) Wolfe, A.; Shimer, G. H. Jr.; Meehan, T. Polycyclic Aromatic Hydrocarbons Physically Intercalate into Duplex Regions of Denatured DNA. *Biochem.* **1987**, *26*, 6392–6396.

(219) Lakowicz, J. R.; Weber, G. Quenching of Fluorescence by Oxygen. A Probe for Structural Fluctuations in Macromolecules. *Biochem.* **1973**, *12*, 4161–4170.

(220) Li, Y. S.; Wang, Y.; Church, J. S.; Garzena, F.; Zhang, Z.; An, D. Vibrational Spectroscopic Studies of Mesna and Dimesna. *Spectrochim. Acta Part A* **2003**, *59*, 1791–1798.

(221) Honnick, W. D.; Hughes, M. C. Jr.; C. D.; Schaeffer, Zuckerman, J. J. Tin-119 Mössbauer, Infrared, Nuclear Magnetic Resonance, Equilibrium, and Thermodynamic Measurements on Complexes of Dimethyltin dichloride with Substituted 1,l0-phenanthrolines and 2,2'-bipyridine. *Inorg. Chem.* **1976**, *15*, 1391–1396.

(222) Otera, J. ^{119}Sn Chemical Shifts in Five and Six Coordinate Organotin Chelates. *J. Organometal. Chem.* **1981**, *221*, 57–61.

(223) Arshad, F.; Farooqi, S.; Bhatti, M. H.; Saleem, S.; Mirza, B. Electrochemical and Spectroscopic Investigations of Carboxylic Acid Ligand and its Triorganotin Complexes for their Binding with Ds.DNA: *In Vitro* Biological Studies. *J. Photochem. Photobiol. B: Biology* **2013**, *125*, 70–82.

(224) Nath, M.; Mridula; Kumari, R. Microwave-assisted Synthesis of Mixed Ligands Organotin(IV) Complexes Of 1,10-Phenanthroline and $_{L}$-Proline: Physicochemical Characterization, DFT Calculations, Chemotherapeutic Potential Validation by *In Vitro*

DNA Binding and Nuclease Activity. *J. Photochem. Photobiol. B: Biology* **2017**, *174*, 182–194.

(225) Lepecq, J. B.; Paoletti, C. A Fluorescent Complex Between Ethidium Bromide and Nucleic Acids. Physical-Chemical Characterization. *J. Mol. Biol.* **1967**, *27*, 87–106.

(226) Arshad, N.; Abbas, N.; Bhatti, M. H.; Rashid, N.; Tahir, M. N.; Saleem, S.; Mirza, B. Synthesis, Crystal Structure, DNA Binding and *In Vitro* Biological Studies of Ni(II), Cu(II) and Zn(II) Complexes of N-phthaloylglycine. *J. Photochem. Photobiol. B: Biology* **2012,** *117*, 228–239.

(227) Tabassum, S.; Amir, S.; Arjmand, F.; Pettinari, C.; Marchetti, F.; Masciocchi, N.; Lupidi, G.; Pettinari, R. Mixed-ligand Cu(II) Vanillin Schiff Base Complexes; Effect of Ligands on their DNA Binding, DNA Cleavage, SOD Mimetic and Anticancer Activity. *Eur. J. Med. Chem.* **2013**, *60*, 216–232.

(228) Cao, Y.; He, X. W. Studies of Interaction Between Safranine T and Double Helix DNA by Spectral Methods, *Spectrochim. Acta, Part A* **1998**, *54*, 883–892.

(229) Husain, M. A.; Ur Rehman, S.; Ishqi, H. M.; Sarwar, T.; Tabish, M. Spectroscopic and Molecular Docking Evidence of Aspirin and Diflunisal Binding to DNA: A Comparative Study. *RSC Adv.* **2015**, *5*, 64335–64345.

(230) Li, X. L.; Hu, Y. J.; Wang, H.; Yu, B.Q.; Yue, H. L. Molecular Spectroscopy Evidence of Berberine Binding to DNA: Comparative Binding and Thermodynamic Profile of Intercalation. *Biomacromol.* **2012**, *13*, 873–880.

(231) Sahoo, D.; Bhattacharya, P.; Chakravorti, S. Quest for Mode of Binding of 2-(4 (Dimethylamino)styryl)-1-methylpyridinium Iodide with Calf Thymus DNA. *J. Phys. Chem. B*, **2010**, *114*, 2044–2050.

(232) Karidi, K.; Garoufis, A.; Tsipis, A.; Hadjiliadis, N.; den Dulk, H.; Reedijk, J. Synthesis, Characterization, *In Vitro* Antitumor Activity, DNA-Binding Properties and Electronic Structure (DFT) of the New Complex *cis*-(Cl,Cl)[Ru(II)Cl_2(NO^+)(terpy)]Cl. *Dalton Trans.* **2005,** 1176–1187.

(233) Arjmand, F.; Sayeed, F.; Parveen, S. *In vitro* Binding Studies of Organotin(IV) Complexes of 1,2-bis-(1H-benzimidazol-2-yl)ethane-1,2-diol with CT-DNA and Nucleotides (5′-GMP and 5′-TMP): Effect of the Ancillary Ligand on the Binding Propensity. *J. Organomet. Chem.* **2011**, *696*, 3836–3845.

(234) Ramakrishnan, S.; Palaniandavar, Interaction of rac-$[Cu(diimine)_3]^{2+}$ and rac-$[Zn(diimine)_3]^{2+}$ Complexes with CT DNA: Effect of Fluxional Cu(II) Geometry on DNA Binding, Ligand-Promoted Exciton Coupling and Prominent DNA Cleavage. M. *Dalton Trans.* **2008**, 3866–3878.

(235) Tabassum, S.; Asim, A.; Khan, R. A.; Arjmand, F.; Rajakumar, D.; Balaji, P.; Akbarsha, M. A. A Multifunctional Molecular Entity Cu^{ii}–Sn^{iv} Heterobimetallic Complex as a Potential Cancer Chemotherapeutic Agent: DNA Binding/Cleavage, SOD Mimetic, Topoisomerase Iα Inhibitory and *In Vitro* Cytotoxic Activities. *RSC Adv.* **2015**, *5*, 47439–47450.

(236) Silva, P. P.; Guerra, W.; Silveira, J. N.; da, A. M.; Ferreira, C.; Bortolotto, T.; Fischer, F.L.; Terenzi, H.; Neves, A.; Pereira-Maia, E. C. Two New Ternary Complexes of Copper(II) with Tetracycline or Doxycycline and 1,10-phenanthroline and their Potential as Antitumoral: Cytotoxicity and DNA Cleavage. *Inorg. Chem.* **2011**, *50*, 6414–6424.

(237) Nath, M.; Vats, M.; Roy, P. Mode of Action of Tin-Based Anti-Proliferative Agents: Biological Studies of Organotin(IV) Derivatives of Fatty Acids, *J. Photochem. Photobiol. B* **2015**, *148*, 88–100.

(238) Moshi, M. J.; Innocent, E.; Magadula, J. J.; Otieno, D. F.; Weisheit, A.; Mbabazi, P. K.; Nondo, R. S. O. Brine Shrimps Toxicity of Some Plants Used as Traditional Medicines in Kagera Region, North Western Tanzania. *Tanz. J. Health Res.* **2010**, *12*, 63–67.

(239) Larasati, Y. A.; Putri, D. D. P.; Utomo, R. Y.; Hermawan, A.; Meiyanto, E. Combination of Cisplatin and Cinnamon Essential Oil Inhibits HeLa Cells Proliferation through Cell Cycle Arrest, *J.App.Pharm.* **2014,** *4*,14–19.

(240) Leite, M.; Quinta-Costa, M.; Leite P. S.; Guimarães, J. E. Critical Evaluation of Techniques to Detect and Measure Cell Death -Study in a Model of UV Radiation of the Leukaemic Cell Line HL60, *Anal. Cell. Pathol.* **1999**,*19*, 139–151.

(241) **(a)** Matassov, D.; Kagan, T.; Leblanc, J.; Sikorska, M.; Zakeri, Z. Measurement of Apoptosis by DNA Fragmentation. In *Apoptosis Methods and Protocols*; Brady, H. J. M., Ed.; Humana Press: Totowa, NJ, **2004**; pp 1–17. **(b)** Tomei, D. L.; Shapiro, P. J.; Cope, O. F. Apoptosis in C3H/10T1/2 mouse embryonic cells: Evidence for internucleosomal DNA modification in the absence of double-strand cleavage. *Proc. Natl. Acad. Sci. U. S. A.* **1993**, *90*, 853– 857.

(242) Holmes, R. R. Organotin Cluster Chemistry. *Acc. Chem. Res.* **1989**, *22*, 190–197.

(243) Prabusankar, G.; Murugavel, R.; Murugavel, Hexameric Organotincarboxylates with Cyclic and Drum Structures. *Organomet.* **2004**, *23*, 5644–5647 and references therein.

(244) Ciolino, H. P.; Bass, S. E.; MacDonald, C. J.; Cheng, R. Y. S.; Yeh, G. C. Sulindac and its Metabolites Induce Carcinogen Metabolizing Enzymes in Human Colon Cancer Cells. *Int. J. Cancer* **2008**, *122*, 990–998.

(245) Thicher, B. A.; Korbut, T. T.; Menon, K.; Holden, S. A.; Ara, G. Cyclooxygenase and Lipoxygenase Inhibitors as Modulators of Cancer Therapies. *Cancer Chemother. Pharmacol.* **1994**, *33*, 515–522.

(246) Duffy, C. P.; Elliott, C. J.; O'Connor, R. A.; Heenan, M. M.; Coyle, S.; Cleary, I. M.; Kavanagh, K.; Verhaegen, S.; O'Loughlin, C. M.; Nic Amhlaoibh, R.; Clynes, M. Enhancement of Chemotherapeutic Drug Toxicity to Human Tumour Cells *In Vitro* by a Subset of Non-steroidal Anti-inflammatory Drugs (NSAIDs). *Eur. J. Cancer* **1998**, *34*, 1250–1259.

(247) Haanen, C. Sulindac and its Derivatives: A Novel Class of Anticancer Agents. *Curr. Opin. Investig. Drugs* **2001**, *2*, 677–683.

(248) Yamamoto, Y.; Yin, M. J.; Lin, K. M.; Gaynor, R. B. Sulindac Inhibits Activation of the NF-kappaB Pathway. *J. Biol. Chem.* **1999**, *274*, 27307–27314.

(249) Zhang, L.; Yu, J.; Park, B. H.; Kinzler, K. W.; Vogelstein, B. Role of BAX in the Apoptotic Response to Anticancer Agents. *Science* **2000**, *290*, 989–992.

(250) Goldberg, Y.; Nassif, I. I.; Pittas, A.; Tsai, L. L.; Dynlacht, B. D.; Rigas, B.; Shiff, S. J. The Antiproliferative Effect of Sulindac and Sulindac Sulfide on HT-29 Colon Cancer Cells: Alterations in Tumor Suppressor and Cell Cycle-Regulatory Proteins. *Oncogene* **1996**, *12*, 893–92.

(251) Piazza, G. A.; Rahm, A. K.; Finn, T. S.; Fryer, B. H.; Li, H.; Stoumen, A. L.; Pamukcu, R.; Ahnen, D. J. Apoptosis Primarily Accounts for the Growth-Inhibitory Properties of Sulindac Metabolites and Involves a Mechanism that is Independent of Cyclooxygenase Inhibition, Cell Cycle Arrest, and p53 Induction. *Cancer Res.* **1997**, *57*, 2452–2459.

(252) Kishimoto, Y.; Yashima, K.; Morisawa, T.; Ohishi, T.; Marumoto, A.; Sano, A.; Idobe-Fujii, Y.; Miura, N.; Shiota, G.; Murawaki, Y.; Hasegawa, J. Effects of Long-Term Administration of Sulindac on APC mRNA and Apoptosis in Colons of Rats Treated With Azoxymethane. *J. Cancer Res. Clin. Oncol.* **2002**, *128*, 589–595.

(253) Winde, G.; Schmid, K. W.; Schlegel, W.; Fischer, R.; Osswald, H.; Bunte, H. Complete Reversion and Prevention of Rectal Adenomas in Colectomized Patients with Familial Adenomatous Polyposis by Rectal Low-dose Sulindac Maintenance Treatment: Advantages of a Low-dose Non-steroidal Anti-inflammatory Drug Regimen in Reversing Adenomas Exceeding 33 Months. *Dis. Colon Rectum* **1995**, *38*, 813–830.

(254) Pepin, P.; Bouchard, L.; Nicole, P.; Castonguay, A. Effects of Sulindac and Oltipraz on the Tumorigenicity of 4-(methylnitrosamino)1-(3-pyridyl)-1-butanone in A/J Mouse Lung. *Carcinogenesis* **1992**, *13*, 341–348.

(255) Cruz-Correa, M.; Hylind, L. M.; Romans, K. E.; Booker, S. V. Giardiello, F. M. Long-term Treatment with Sulindac in Familial Adenomatous Polyposis: A Prospective Cohort Study. *Gastroenterol.* **2002**, *122*, 641–645.

(256) Giardiello, F. M.; Offerhaus, J. A.; Tersmette, A. C. Hylind, L. M.; Krush, A. J.; Brensinger, J. D.; Booker, S. V.; Hamilton, S. R. Sulindac Induced Regression of

Colorectal Adenomas in Familial Adenomatous Polyposis: Evaluation of Predictive Factors. *Gut* **1996**, *38*, 578–581.

(257) Nikitakis, G. N.; Hamburger, A. W.; Sauk, J. J. The Non Steroidal Anti-Inflammatory Drug Sulindac Causes Down-Regulation of Signal Transducer and Activator of Transcription 3 in Human Oral Squamous Cell Carcinoma Cells. *Cancer Res.* **2002**, *62*, 1004–1007.

(258) Ronconi, L.; Sadler, P. J. Using Coordination Chemistry to Design New Medicines. *Coord. Chem. Rev.* **2007**, *251*, 1633–1648.

(259) Abrams, M. J.; Murrer, B.A. Metal Compounds in Therapy and Diagnosis. *Science* **1993**, *261*, 725–730.

(260) Tian, L.; Yu, Q.; Zheng, X.; Shang, Z.; Liu, X.; Qian, B. Synthesis, Characterization and *In Vitro* Antitumour Activity of Di- and Tri-Organotin Derivatives of Fenbufen. *Appl. Organometal. Chem.* **2005**, *19*, 672–676.

(261) Demertzis, M. A.; Hadjikakou, S. K.; Kovala-Demertzi, D.; Koutsodimou, A.; Kubicki, M. Organotin-Drug Interactions. Organotin Adducts of Tenoxicam: Synthesis and Characterization of the First Organotin Complex of Tenoxicam. *Helv. Chem. Acta* **2000**, *83*, 2787–2808.

(262) Dang, X. J.; Tong, J.; Li, H. L. The Electrochemistry of the Inclusion Complex of Anthraquinone with β-cyclodextrin Studied by means of OSWV. *J. Inclusion Phenom.* **1996**, *24*, 275–286.

(263) Ibrahim, M. S.; Shehatta, I. S.; Al-nyeli, A. A. Voltammetric Studies of the Interaction of Lumazine with Cyclodextrins and DNA. *J. Pharm. Biomed. Anal.* **2002**, *28*, 217–225.

(264) Kumar, C. V.; Barton, J. K.; Turro, N. J. Photophysics of Ruthenium Complexes Bound to Double Helical DNA. *J. Am. Chem. Soc.* **1985**, *107*, 5518–5523.

(265) Zhao, R.; Zhang, W.; Li, J. K.; Zhang, L. Y. (E)-2-hydroxy-3-methoxybenzaldehyde thiosemicarbazone. *Acta Crystallogr. E* **2008**, 1113.

(266) Lockhart, T. P.; Calabrese, J. C.; David, F. The Mössbauer Recoil-free Fraction and Structure. Part 3. Triorganotin arylazo benzoates. *Organomet.* **1987**, *6*, 2419–2483.

(267) Harrison, P. G.; Lambert, K.; King, T. J. Structural Studies of Diorganotin(IV) Carboxylates. X-Ray and NMR Structures of $Me_2Sn(OAc)$, and a 7-Coordinate Tin Anion, $Me_2Sn(OAC)^-NMe_4^+$. $2CHCl_3$. *J. Chem. Soc. Dalton Trans.* **1983**, 363–369.

(268) Masood, H.; Ali, S.; Mazhar, M.; Shahzadi, S.; Shahid, K. ^1H, ^{13}C, ^{119}Sn NMR, Mass, Mössbauer and Biological Studies of Tri-, Di- and Chlorodiorganotin(IV) Carboxylates. *Turk. J. Chem.* **2004**, *28*, 75–85.

(269) Xiao, X.; Shao, K.; Yan, L.; Mei, Z.; Zhu, D.; Xua, L. A Novel Macrocyclic Organotin Carboxylate Containing a Nona-nuclear Long Ladder. *Dalton Trans.* **2013**, 15387–15390.

(270) Lockhart, T. P.; Manders, W. F.; Zuckerman, J. J. Structural Investigations by Solid-state ^{13}C NMR. Dependence of $|^{1}J$ (^{119}Sn, $^{13}C|$ on the Me-Sn-Me Angle in Methyltin(IV)s. *J. Am. Chem. Soc*. **1985**, *107*, 4547–4548.

(271) Willem, R.; Verbruggen, I.; Gielen, M.; Biesemans, M.; Mahieu, B.; Baul, T. S. B.; Tiekink, E. R. T. Correlating Mössbauer and Solution and Solid-State ^{119}Sn NMR Data with X-Ray Diffraction Structural Data of Triorganotin 2-[(*E*)-2-(2-hydroxy-5-methylphenyl)-1-diazenyl]benzoates. *Organomet.* **1998**, *17*, 5758–5766.

(272) Baul, T. S. B.; Mizar, A.; Song, X.; Eng, G.; Jirásko, R.; Holčapek, M.; Willem, R.; Biesemans, M.; Verbruggen, I.; Butcher, R. Dibenzyltin(IV) Complexes of the 5-[(E)-2-(Aryl)-1-diazenyl]quinolin-8-olates: Synthesis and an Investigation of Structures by X-Ray Diffraction, Solution and Solid-State Tin NMR, ^{119}Sn Mössbauer and Electrospray Ionization MS. *J. Organomet. Chem.* **2006**, *691*, 2605–2613.

(273) Lycka, A.; Ruzicka, A.; Vanecek, J.; Ceslová, L. Structural Study of Di- and Triorganotin(IV) Dicarboxylates Containing One Double Bond. *J. Organomet. Chem.* **2010**, *695*, 2493–2498.

(274) Baul, T. S. B.; Singh, K. S.; Holčapek, M.; Jirásko, R.; Rivarola, E.; Linden, A. Synthesis, Characterization and Crystal Structures of Polymeric and Dimeric Triphenyl-tin(IV) of 4-[((E)-1-{2-hydroxy-5-[(E)-2-(2-carboxyphenyl)-1-diazenyl]phenyl}-methylidene)-amino]-aryls. *J. Organomet. Chem.* **2005**, *690*, 4232–4242.

(275) Yang, X.; Shen, G. L.; Yu, Ru-Q. Studies on Intramolecular Charge Transfer Fluorescence Probe and DNA Binding Characteristics. *Microchem. J.* **1999**, *62*, 394–404.

(276) Shujha, S.; Shah, A.; Rehman, Z.; Muhammad, N.; Ali, S.; Qureshi, R.; Khalid, N.; Meetsma, A. Diorganotin(IV) Derivatives of ONO Tridentate Schiff Base: Synthesis, Crystal Structure, *in vitro* Antimicrobial, Anti-leishmanial and DNA Binding Studies. *Eur. J. Med. Chem.* **2010**, *45*, 2902–2911.

(277) Ghosh, K.; Kumar, P.; Tyagi, N.; Singh, U. P.; Goel, N. Synthesis, Structural Characterization and DNA-Interaction Studies on a Mononuclear Copper Complex: Nuclease Activity *via* Self-activation. *Inorg. Chem. Com.* **2011**, *14*, 489–492.

(278) Wu, H.; Yuan, J.; Bai, Y.; Kou, F.; Jia, F.; Liu, B. Synthesis, Crystal Structure and Spectral Properties of the Cadmium(II) Complex with bis(N-allylbenzimidazol-2-ylmethyl)benzylamine. *Bioinorg. Chem.* **2011**, *2011*, 1–9.

(279) Chauhan, M.; Banerjee, K.; Arjmand, F. DNA Binding Studies of Novel Copper(II) Complexes Containing L-Tryptophan as Chiral Auxiliary: In Vitro Antitumor Activity of Cu-Sn_2 Complex in Human Neuroblastoma Cells. *Inorg. Chem*. **2007**, *46*, 3072–3082.

(280) Pillaia, S. I.; Vijayaraghavana, K.; Subramanianb, S. Evaluation of DNA-Binding, Cleavage, BSA Interaction of Zn-Hydroxy Flavone Complex. *Der. Pharma. Chemica* **2014**, *6*, 379–389.

(281) Tabassum, S.; Khan, R. A.; Arjmand, F.; Aziz, M.; Juvekar, A. S.; Zingde, S. M. Carbohydrate-Conjugate Heterobimetallic Complexes: Synthesis, DNA-Binding Studies, Artificial Nuclease Activity and *In Vitro* Cytotoxicity. *Carbohydr. Res.* **2011**, *346*, 2886–2895.

(282) Nath, M.; Pokharia, S.; Song, X.; Eng, G.; Gielen, M.; Kemmer, M.; Biesemans, M.; Willem, R.; De Vos, D. New Organotin(IV) Derivatives of Dipeptides as Models for Metal–Protein Interactions: *In Vitro* Anti-Tumour Activity. *Appl. Organomet. Chem.* **2003**, *17*, 823-839.

(283) Barbieri, R.; Ruisi, G.; Atassi, G. The Antitumour Activity and Structure of Bis(adenoninato-N')diphenyltin(IV). *J. Inorg. Biochem.* **1991**, *41*, 25–30.

(284) Larasati, Y. A.; Putri, D. D. P.; Utomo, R. Y.; Hermawan, A.; Meiyanto, E. Combination of Cisplatin and Cinnamon Essential Oil Inhibits HeLa Cells Proliferation through Cell Cycle Arrest. *J. App. Pharm.* **2014,** *4*, 14–19.

(285) Michael, J.; Thun, S.; Henley, J.; Patrono, C. Nonsteroidal Anti-Inflammatory Drugs as Anticancer Agents: Mechanistic, Pharmacologic, and Clinical Issues. *J. Natl. Cancer Inst*. **2002**, *94*, 252–66.

(286) Elsaman, T.; Ali, M. M. Nonsteroidal Anti-Inflammatory Drugs (NSAIDs) Derivatives with Anti-Cancer Activity. *Am. J. Res. Comm*, **2016**, *4*, 2325–4076.

(287) Endo, H.; Yano, M.; Okumura, Y.; Kido, H. Ibuprofen Enhances the Anticancer Activity of *Cis*-platin in Lung Cancer Cells by Inhibiting the Heat Shock Protein 70. *Cell Death Dis.* **2014**, *5*, e1027.

(288) Qu, X.; Allan, A.; Chui, G.; Hutchings, T. J.; Jiao, P.; Johnson, L.; Leung, W. Y.; Li, P. K.; Steel, G. R.; Thompson, A. S.; Threadgill, M. D.; Woodman, T. J.; Lloyd, M. D. Hydrolysis of Ibuprofenoyl-Coa and Other 2-APA-Coa Esters by Human Acyl-Coa Thioesterases-1 and -2 and their Possible Role in the Chiral Inversion of Profens. *Biochem. Pharmacol.* **2013**, *86*, 1621–1625.

(289) Matos, P.; Jordan P. Beyond Cox-Inhibition: 'Side-Effects' of Ibuprofen on Neoplastic Development and Progression, Current Pharmaceutical Design. **2015**, *21*, 2978–2982.

(290) Husain, M. A.; Sarwar, T.; Rehman, S. Ur; Ishqi, H. M.; Tabish, M.; Ibuprofen Causes Photocleavage through ROS Generation and Intercalates with DNA: A Combined Biophysical and Molecular Docking Approach. *Phys. Chem. Chem. Phys.***2015**, *17*, 13837–13850.

(291) Fiori, A. T. M.; Lustri, W. R.; Magalhães A.; Corbi, P. P.; Chemical, Spectroscopic Characterization and Antibacterial Activities *In Vitro* of a Novel Gold(I)–Ibuprofen Complex. *Inorg. Chem. Comm.* **2011**, *14*, 738–740.

(292) Núñez, C.; Fernández-Lodeiro, A.; Fernández-Lodeiro, J.; Carballo, J.; Capelo, J. L.; Lodeiro, C.; Synthesis, Spectroscopic Studies and *in vitro* Antibacterial Activity of Ibuprofen and its Derived Metal Complexes. *Inorg. Chem. Comm.* **2014**, *45*, 61–65.

(293) Silva, I. M. P.; Profirio, D. de M.; de Paiva, R. E. F.; Lancellotti, M.; Formiga, A. L. B.; Corbi, P. P.; Silver Complex with Ibuprofen: Synthesis, Solid Characterization, DFT Calculations and Antibacterial Assays. *J. Mol. Struct.* **2013**, *1049*, 1–6.

(294) Rico, S. R. A.; Abbasi, A. Z.; Ribeiro, G.; Ahmed, T.; Wu, X. Y.; Silva, D. de O.; Diruthenium(II,III) Metallodrugs of Ibuprofen and Naproxen Encapsulated in Intravenously Injectable Polymer–Lipid Nanoparticles Exhibit Enhanced Activity Against Breast and Prostate Cancer Cells. *Nanoscale* **2017**, *9*, 10701–10714.

(295) Kumar, S.; Garg, S.; Sharma, R. P.; Venugopalan, P.; Tenti, L.; Ferretti, V.; Nivelle, L.; Tarpinc M.; Guillon, E.; Four Monomeric Copper(II) Complexes of Non-Steroidal Anti-Inflammatory Drug Ibuprofen and N-Donor Ligands: Syntheses, Characterization, Crystal Structures and Cytotoxicity Studies. *N. J. Chem.* **2017**, *41*, 8253–8262.

(296) Mao, W.; Bao, K.; Feng, Y.; Wang, Q.; Li, J.; Fan, Z. Synthesis, Crystal Structure, and Fungicidal Activity of Triorganotin(IV) 1-methyl-1*H*-imidazole-4-carboxylates. *Main Group Met. Chem.* **2015**, *38*, 27–30.

(297) Sougoule, A. S.; Xiao, X.; Balde, C. A.; Sakho, A. M.; Zhu D. An Organotin(IV) Carboxylate Based on Amide Carboxylic Acid: Synthesis, Crystal Structure, and Characterizations. *Heteroatom Chem.* **2015**, *26*, 270–276.

(298) Sandhu, G. K.; Sharma, N.; Tiekink, E. R. T. Structural Chemistry of Organotin Carboxylates VIII. Synthesis and Spectroscopic Properties of Diorganotin(IV) Complexes with Thiophenoxyacetic Acid. X-Ray Crystal Structures of [$^{n}Pr_2$ $Sn(O_2CCH_2SPh)_2$] and $\{[R_2Sn(O_2CCH_2SPh)]_2O\}_2$, R = ^{n}Pr, ^{n}Bu. *J. Organomet. Chem.* **1991**, *403*, 119–131.

(299) Amini, M. M.; Azadmeher, A.; Khavasi, H. R.; Ng, S. W. Synthesis, Characterization and Molecular Structures of Di- and Triorganotin(IV) Complexes with 9-Anthracenecarboxylic acid: The Structural Diversity in Organotin 9-Anthracenecarboxylates. *J. Organomet. Chem.* **2007**, *692*, 3922–3930.

(300) Farooq, A.; Kaneez, F.; Shaista, S.; Saqib, Ishtiaq, A.; Noor ud, Q. D. Design, Synthesis, Structure Information and Biochemical Activity of New Fluoro Substituted Organotin(IV) Carboxylates, *J. Photochem. Photobiol. B: Biology* **2016**, *154*, 99–107.

(301) Baul, T. S. B.; Masharing, C.; Basu, S.; Rivarola, E.; Holčapek, M.; Jirásko, R.; Lyčka A.; Vos, D. de; Linden, A. Synthesis, Characterization, Cytotoxic Activity and Crystal Structures of Tri- and Di-Organotin(IV) Complexes Constructed From the β-{[(E)-1-(2-

hydroxyaryl)alkylidene]amino}propionate and β-{[(2Z)-(3-hydroxy-1-methyl-2-butenylidene)]amino}propionate Skeletons. *J. Organomet. Chem.* **2006**, *691*, 952–965.

(302) Kumari, R.; Nath, M. Tri- and Diorganotin(IV) Derivatives of Non-Steroidal Anti-Inflammatory Drug Sulindac: Characterization, Electronic Structures (DFT), DNA Binding and Plasmid Cleavage Studies. *Appl. Organomet. Chem.* **2017**, e3661. doi: 10.1002/aoc.3661

(303) Parulekar, C. S.; Jain, V. K.; Kesavadas, T.; Tiekink E .R. T. Structural Chemistry of Organotin Carboxylates IV. Synthesis and Spectroscopic Properties of Diorganotin(IV) Complexes with *o*-Anisic Acid. The Crystal and Molecular Structure of $\{[^{n}Bu_2Sn(2\text{-}MeOC_6H_4COO)_2O_2\}_2$. *J. Organomet. Chem.* **1990**, *387*, 163-173.

(304) Zhang, Y. Y.; Zhang, R. F.; Zhang, S. L.; Cheng, S.; Lia, Q. Li.; Ma, C. L. Syntheses, Structures And Anti-Tumor Activity Of Four New Organotin(IV) Carboxylates Based on 2-thienylselenoacetic acid, *Dalton Trans.* **2016**, *45*, 8412–8421.

(305) Vatsa, C.; Jain, V. K.; Kesavadas, T.; Tiekink, E .R. T. Structural Chemistry of Organotin Carboxylates X. Synthesis and Characterization Of $\{[R_2Sn(O_2C^{t}Bu)]_2O\}_2$ (R = Me, Et, ^{n}Pr and ^{n}Bu). X-Ray Crystal Structures of $\{[R_2Sn(O_2C^{t}Bu)]_2O\}_22$ (R = Me, Et). *J. Organomet. Chem.* **1991**, *408*, 157–166.

(306) Arjmand, F.; Jamsheera, A. DNA Binding Studies of New Valine Derived Chiral Complexes of Tin(IV) and Zirconium(IV). *Spectrochim. Acta A.* **2011**, *78*, 45–51.

(307) Dey, S.; Sarkar, S.; Paul, H.; Zangrando, E.; Chattopadhyay, P.; Copper(II) Complex With Tridentate N-Donor Ligand: Synthesis, Crystal Structure, Reactivity and DNA Binding Study. Polyhedron **2010**, *29*, 1583–1587.

(308) Nurcahyanti, A. D. R.; Wink, M. L-Canavanine potentiates the cytotoxicity of doxorubicin and cisplatin in arginine deprived human cancer cells, *Peer J.* **2016**, DOI 10.7717/peerj.1542.

(309) Campbell, H.; Smith, W. K.; Roberts, W.; Link, K. P. Studies on the Hemorrhagic Sweet Clover Disease II. The Bioassay of Hemorrhagic Concentrates by Following the Prothrombin Level in The Plasma of Rabbit Blood. *J. Biol. Chem.* **1941,** *138*, 1–20.

(310) Gopalakrishnan, S.; Narayanan, S. Oral Anticoagulants: Current Indian Scenario, **2013**, 410–413.

(311) Kamali, F.; Pirmohamed, M. The Future Prospects of Pharmacogenetics in Oral Anticoagulation Therapy. *Br. J. Clin. Pharmacol.* **2006**, *61*, 746–751.

(312) Pirmohamed, M. Warfarin: Almost 60 Years Old and Still Causing Problems, *Br. J. Clin. Pharmacol.* **2006**, *62*, 509–511.

(313) Zacharski, R.; Henderson, W. G.; Rickles, F. R.; Forman, W. B.; Cornell, C. J.; Forcier, A. J.; Edwards, R. L.; Headley, E.; Kim, S. H.; O'Donnell, J. F.; O'Dell, R.; Tornyos, K.; Kwaan, H. C. Effect of Warfarin Anticoagulation on Survival in Carcinoma of the Lung, Colon, Head and Neck, and Prostate: Final Report of VA Cooperative Study #75. *Cancer* **1984,** *53*, 2046–2052.

(314) Chahinian, A. P; Propert, K. J.; Ware, J. H.; Zimmer, B.; Perry, M. C.; Hirsh, V.; Skarin, A.; Kopel, S.; Holland, J. F.; Comis, R. L. A Randomized Trial of Anticoagulation with Warfarin and of Alternating Chemotherapy in Extensive Small Cell Lung Cancer by the Cancer and Leukemia Group B. *J. Clin. Oncol.* **1989**, *7*, 993–1002.

(315) Maurer, L. H.; Herndon 2nd, J. E.; Hollis, D. R.; Aisner, J.; Carey, R. W.; Skarin, A. T.; Perry, M. C.; Eaton, W. L.; Zacharski, L. L.; Hammond, S.; Green, M. R. Randomized Trial of Chemotherapy and Radiation Therapy with or without Warfarin for Limited Stage Small Cell Lung Cancer: A Cancer and Leukemia Group B Study. *J. Clin. Oncol.* **1997**, *15*, 3378–3387.

(316) Akl, E. A.; Kamath, G.; Kin, S. Y.; Yosuico, V.; Barba, M.; Terrenato, I.; Sperati, F.; Schünemann, H. J. Oral Anticoagulation may Prolong Survival of a Subgroup of Patients with Cancer: A Cochrane Systematic Review. *J. Exp. Cancer Res.* **2007**, *26*, 175–184.

(317) Bobek, V.; Kovarik, J. Antitumor and Antimetastatic Effect of Warfarin and Heparins. *Biomed. Pharmacother.* **2004**, *58*, 213–219.

(318) Smorenburg, S.; Vink, R.; Otten, H.; Swaneveld, F.; Buller, H. The Effect of Vitamin K Antagonists on Survival of Patients With Malignancy: A systematic Analysis. *Thromb. Haemost.* **2001**, *86*, 1586–1587.

(319) Wu, X.; Kang, W.; Zhu, D.; Zhu, C.; Liu, S. Synthesis, Crystal Structure and Biological Activities of Two Novel Organotin(IV) Complexes Constructed from 12-(4-methylbenzoyl)-9,10-dihydro-9,10-ethanoanthracene-11-carboxylic acid. *J. Organomet. Chem.* **2009**, *694*, 2981–2986.

(320) Shah, S. S.; Ashfaq, M.; Waseem, A.; Ahmed, M. M.; Najam, T.; Shaheen, S.; Rivera, G. Synthesis and Biological Activities of Organotin(IV) Complexes as Antitumoral and Antimicrobial Agents, A Review, *Mini Rev. Med. Chem.* **2015**, *15*, 406–426.

(321) Saeed, A.; Channar, P. A.; Larik, F. A.; Jabeen, F.; Muqadar, U.; Saeed, S.; Flörke, U.; Ismail, H.; Dilshad, E.; Mirza, B. Design, Synthesis, Molecular Docking Studies of Organotin-Drug Derivatives as Multi-Target Agents Against Antibacterial, Antifungal, α-amylase, α-glucosidase and Butyrylcholinesterase. *Inorg. Chim. Acta.* **2017**, *464*, 204–213.

(322) KaluCerovi, G. N.; Paschke, R.; Prashar, S.; Gómez-Ruiz, S. Synthesis, Characterization and Biological Studies of 1-D Polymeric Triphenyltin(IV) Carboxylates. *J. Organomet. Chem.* **2010**, *695*, 1883–1890.

(323) Baul, T. S. B.; Paul, A.; Pellerito, L.; Scopelliti, M.; Pellerito, C.; Singh, P.; Verma, P.; Duthie, A.; Vos, D.; Verma, R. P.; Englert, U. Molecular Basis of the Interaction of Novel Tributyltin(IV) 2/4-[(*E*)-2-(aryl)-1-diazenyl]benzoates Endowed with an Improved Cytotoxic Profile: Synthesis, Structure, Biological Efficacy and QSAR Studies. *J. Inorg. Biochem*. **2010**, *104*, 950–966.

(324) Rehman, Z.; Muhammad, N.; Shuja, S.; Ali, S.; Butler, I. S.; Meetsma, A.; Khan, M. New Dimeric, Trimeric and Supramolecular Organotin(IV) Dithiocarboxylates: Synthesis, Structural Characterization and Biocidal Activities. *Polyhedron* **2009**, *28*, 3439–3448.

(325) Jiao, T. Q.; Wu, J. G.; Zeng, F. L.; Fun, Y. L.; Deng, R.W. Synthesis, Characterization and Anticoagulant Action of Lanthanide Complexes of Warfarin. *Synth. React. Inorg. Met.Org. Chem.* **1999**, *29*, 725–735.

(326) Kostova, I.; Momekov, G. New Zirconium (IV) Complexes of Coumarins with Cytotoxic Activity, *E. J. Med. Chem*. **2006**, 41, 717–726.

(327) Kostova, I.; Momekov, G.; Tzanova, T.; Karaivanova, M. Synthesis, Characterization, and Cytotoxic Activity of New Lanthanum(III) Complexes of Bis-Coumarins. *Bioinorg. Chem. Appl*. **2005**, *2006*, 1–9.

(328) T. Mihaylov, T.; Trendafilova. N.; Georgieva, I.; Kostova, I. Coordination Properties of Warfarin Towards Pr(III) Predicted from DFT and FT-IR Studies. *Chem. Phy*. **2010**, 374, 37–45.

(329) Karlsson, B. C. G.; Rosengren, A. M.; Andersson, P. O.; Nicholls, I. A. The Spectrophysics of Warfarin: Implications for Protein Binding. *J. Phys. Chem. B* **2007**, *111*, 10520–10528.

(330) Valente, E. J.; Trager, W. F.; Jensen, L. H. The Crystal and Molecular Structure and Absolute Configuration of (-)-(*S*)-warfarin. *Acta Crystallogr. Sect. B* **1975**, *31*, 954–960.

(331) Kostova, I.; Manolovb, I.; Konstantinov, S.; Karaivanova, M. Synthesis, Physicochemical Characterisation and Cytotoxic Screening of New Complexes of Cerium, Lanthanum and Neodymium with Warfarin and Coumachlor Sodium Salts. *Eur. J. Med. Chem*. **1999**, *34*, 63−68.

(332) Valente, E. J.; Lingafelter, E. C.; Poter, W. R.; Trager, W. F. Structure of Warfarin in Solution. *J. Med. Chem.* **1977**, *20*, 1489–1493.

(333) Giannini, D. D.; Chan, K. K.; Roberts, J. D. Carbon-13 Nuclear Magnetic Resonance Spectroscopy. Structure of the Anticoagulant Warfarin and Related Compounds in Solution. *Proc. Nat. Acad. Sci. USA* **1974**, *71*, 4221–4223.

(334) Valente, E. J.; Poter, W. R.; Trager, W. F. Conformations of Selected 3-Substituted 4-hydroxycoumarins in Solution by Nuclear Magnetic Resonance. Warfarin and Phenprocoumon. *J. Med. Chem.* **1978**, *21*, 231–234.

(335) Kelly, J. M.; Tossi, A. B.; McConnell, D. J.; OhUigin, C. A Study of the Interactions of Some Polypyridylrutheniumn(I) Complexes with DNA using Fluorescence Spectroscopy, Topoisomerisation and Thermal Denaturation. *Nuc. Acids Res.* **1985**, *13*, 6017–6034.

(336) Tabassum, S.; Asim, A.; Arjmand, F.; Afzal, M.; Bagchi, V. Synthesis and Characterization of Copper(II) and Zinc(II)-Based Potential Chemotherapeutic Compounds: Their Biological Evaluation *viz.* DNA Binding Profile, Cleavage and Antimicrobial Activity. *Eur. J. Med. Chem*. **2012**, *58*, 308–316.

(337) Baguley, B. C.; Le Bret, M. Quenching of DNA-Ethidium Fluorescence by Amsacrine and other Antitumor Agents: A Possible Electron-Transfer Effect. *Biochem*. **1984**, *23*, 937–943.

(338) Grueso, E.; Lopez-Pe´rez, G.; Castellano, M.; Prado-Gotor, R. Thermodynamic and Structural Study of Phenanthroline Derivative Ruthenium Complex/DNA Interactions: Probing Partial Intercalation and Binding Properties. *J. Inorg. Biochem.* **2012**, *106*, 1−9.

(339) Ma, Y.; Zhang, G.; Pan, J. Spectroscopic Studies of DNA Interactions with Food Colorant Indigo Carmine with the Use of Ethidium Bromide as a Fluorescence Probe, *J. Agric. Food Chem*. **2012**, *60*, 10867−10875.